



1928

K. N. Toosi University of Technology

**K. N. Toosi University of Technology
Faculty of Electrical Engineering**

**Doctoral Thesis Submitted in Partial
Fulfillment of The Requirements For The
Degree of Doctor of Science in
Control System Engineering**

Passivity Based Control of 3-DOF Underactuated Suspended Cable-Driven Robot

by

Mohammad Reza Jafari Harandi

Supervisor

Dr. Hamid D. Taghirad

Advisor

Dr. Mehrzad Namvar

Summer 2021

Abstract

Underactuated systems (UaSs) are a type of mechanical systems that the number of actuators is fewer than the number of degrees of freedom. Due to this property, well-known methods such as feedback linearization is not usable, and thus, control of UaSs is currently a challenging problem. UaSs have broad applications such as unmanned aerial vehicles, marine and submarine systems, cranes, etc. Recently, underactuated cable-driven robots are the focus of attention of some researchers since they inherit the advantage of both underactuated and cable-driven systems. This thesis is devoted to controller design for 3-DOF underactuated cable-driven robots. For this purpose, interconnection and damping assignment passivity-based control (IDA-PBC) is utilized to stabilize the system at a desired equilibrium point. IDA-PBC is a general method to stabilize the port Hamiltonian systems by assigning the desired interconnection and damping matrices together with desired Hamiltonian to the closed-loop system. In the cases of underactuated systems, the applicability of IDA-PBC is restricted to the analytical solution of two partial differential equations (PDEs) related to shaping the potential and kinetic energy which are called matching equations. One of the aims of this thesis is to solve the matching equations arisen in controller design for 3-DOF underactuated cable-driven robots. The corresponding PDEs are transformed to some Pfaffian differential equations, and their solution is derived by some calculations. Since this method is general, the matching equations of some benchmark systems are also solved. Furthermore, a systematic method to solve the nonlinear PDE related to kinetic energy shaping for systems with underactuation degree one and constant input mapping matrix is proposed. The potential energy shaping of a general underactuated parallel robot is another contribution of this thesis. Another challenging problem is ensuring positive tension in cables since cables can only apply tensile forces. Two different strategy is introduced to address this issue. A method is the analysis of IDA-PBC's control law term by term so that the bounds of the controller are derived. Another method is based on optimization of control law with respect to the free part of the interconnection matrix to minimize the bounds of the controller in the systems with at least two actuators. Incorporation of both methods that results in a more robust controller without conservative gains for a class of UaSs is also proposed. Some other developments of IDA-PBC such as adaptive IDA-PBC, IDA-PBC with desired gravity compensation, etc. are also introduced in this thesis. The proposed methods are verified through some simulations and experiments on different systems such as some underactuated cable-driven robots, 2D SpiderCrane, etc.

Keywords: Underactuated mechanical systems, Cable-driven robot, Passivity-based control, Partial differential equations, Bounded input

بِسْمِ اللَّهِ الرَّحْمَنِ الرَّحِيمِ

In The Name of God

Dedicate

This thesis is dedicated to my parents, who have always loved me unconditionally and have been a constant source of support and encouragement during the challenges of life. I am truly thankful for having you in my life.



1928
K. N. Toosi University of Technology


Faculty of Electrical Engineering

Defence Statement Form for Doctoral Thesis

The defence session for Doctoral Thesis performed by Mr **Mohammad Reza Jafari Harandi** with student ID: 9500346 in Control System Engineering specialisation Control of Nonlinear Systems, on Summer 2021 at K. N. Toosi University of Technology entitled **Passivity Based Control of 3-DOF Underactuated Suspended Cable-Driven Robot.**

We hereby approve the thesis.

1. Supervisor: **Dr. Hamid D. Taghirad** 

2. Advisor: **Dr. Mehrzad Namvar**  signature

3. Internal examiner 1: **Dr. Ali Akbar Moosavian** signature

4. Internal examiner 2: **Dr. Mahsan Tavakoli Kakhki** signature

5. External examiner 1: **Dr. Mohammad Reza Jahed Motlagh** signature

6. External examiner 2: **Dr. Mohammad Azam Khosravi** signature

7. Agent of graduate studies: **Dr. Mohammad Reza Toulabi** signature

Affidavit

I, **Mohammad Reza Jafari Harandi**, hereby declare that this PhD thesis entitled:
**Passivity Based Control of 3-DOF Underactuated Suspended Cable Driven
Robot**

contains only my original works except the sources indicated in the thesis itself.

I have not, in its entirety or in part, submitted it at any other university for a degree.

Mohammad Reza Jafari Harandi

Summer 2021



1928

K. N. Toosi University of Technology

K. N. Toosi University of Technology

Copyright

Copyright in this work rests with the author. Please ensure that any reproduction or re-use is done in accordance with K. N. Toosi University of Technology policies:

- Can be used in any form and any work for everyone without any special license.
- Can be used only by official letter from the advisor and proper citation.
- Can not be used until in any documentation.

Supervisor: **Dr. Hamid D. Taghirad**

Acknowledgement

I would like to thank my thesis advisor Dr. Hamid D. Taghirad at K. N. Toosi University of Technology. The door to Dr. Taghirad office was always open whenever I ran into a trouble spot or had a question about my research or writing. He consistently allowed this research to be my own work, but steered me in the right direction whenever he thought I needed it.

I wish to give my very special thanks to Dr. Mehrzad Namvar from Sharif University of Technology who have been a constant source of support and encouragement for me from the beginning of my studies. His unique view of control theory and his mathematical discipline taught me to see nonlinear control from a new perspective that enhanced my understanding of what constitutes an acceptable solution for certain fundamental problems in control theory.

I would like to thank my colleagues in ARAS laboratory especially Dr. Ahmad Khalilpour for our exciting discussions during the group meetings and for helping me to implement the proposed methods on the robots. Furthermore, I appreciate Mr. Hosseini, Mr. Khodadadi, Mr. Khorrambakht, Mr. Hassani and Mr. Kalantari for their collaborations in experiments.

Contents

List of Figures	c
Symbols and Abbreviations	e
1 Introduction	1
1.1 Cable-Driven Robots	1
1.2 Applications of Underactuated Cable-Driven Robots	3
1.3 Underactuated Systems	4
1.4 Underactuated Cable-Driven Robots	6
1.5 Contributions of This Thesis	6
2 Literature Review	8
2.1 Cable-Driven Robots	8
2.2 Control of Cable-Driven Robots	9
2.3 Control of Underactuated Systems	10
2.4 Underactuated Cable-Driven Robots	16
2.5 Conclusion	17
3 Systems Models	19
3.1 Planar Robot	19
3.2 Spatial Robot	23
3.3 Spidercam	25
3.4 ARAS Cable-Driven Robot	26
3.5 Conclusion	29
4 Solution of Matching Equations	30
4.1 Pfaffian Differential Equations	30
4.2 Potential Energy Shaping of Underactuated Parallel Robots	38
4.3 Solution to Kinetic Energy PDE	40
4.4 Comparison of IDA-PBC to Simultaneous IDA-PBC	45
4.5 Conclusion	48
5 IDA-PBC with Bounded Input	49
5.1 Bounded Input IDA-PBC for Mechanical Systems	49
5.2 IDA-PBC with Prescribed Bounds	55
5.3 Conclusion	63

6	Other Developments of IDA-PBC	64
6.1	IDA-PBC with Position Feedback	64
6.2	Adaptive IDA-PBC	66
6.3	Robust IDA-PBC	71
6.4	IDA-PBC with Desired Gravity Compensation	74
6.5	Conclusion	75
7	Simulation and Experimental Results	76
7.1	Simulation Results	76
7.2	Experimental Results	94
8	Conclusion and Future Works	101
A	Solving the Matching Equations of Benchmark Systems by Pfaffian Differential Equations	103
A.1	Magnetic Levitation System	103
A.2	Micro Electro–Mechanical Optical Switch	106
A.3	Third Order Food-Chain System	107
A.4	Pendubot	109
B	Solving the Matching Equation of Kinetic Energy Shaping by the Pro- posed Procedure in Section 4.3	111
B.1	Pendubot	111
B.2	VTOL Aircraft	113
B.3	2D SpiderCrane	114
	Bibliography	116

List of Figures

1.1	A typical parallel robot	2
1.2	A typical cable-driven robot	2
1.3	Typical fully-constraint and under-constrain CDRs	3
1.4	A CDR during transportation of a load.	4
1.5	A spidercam during imaging.	5
1.6	An example of underactuated cable-driven robot.	6
2.1	An underactuated cable driven robot	17
2.2	Planar underactuated cable-driven robot	18
3.1	The schematic of the planar UCDR.	20
3.2	Feasible equilibrium points of the planar UCDR with $a = 0.25, b = 8$	22
3.3	Schematic of the spatial underactuated cable-driven robot.	23
3.4	Schematic of a 6-DOF underactuated cable-driven robot with four actuators.	25
3.5	Different components of ARAS underactuated cable-driven robot	27
3.6	Schematic of a 3-DOF suspended CDR.	28
3.7	ARAS cable driven robot.	28
4.1	The procedure of solving the kinetic energy PDE based on the proposed method.	44
7.2	Simulation results of potential energy shaping with V_d as (7.3) on planar UCDR.	78
7.3	Simulation results of sliding mode controller on planar UCDR.	79
7.4	Simulation results of Proposition 3 on planar UCDR.	80
7.5	Simulation results of Proposition 6 with V_d as (7.3) on planar UCDR.	80
7.6	Simulation results of potential energy shaping on spatial UCDR.	82
7.7	Simulation results of total energy shaping with $m = 0.1$ on spatial UCDR.	82
7.8	Simulation results of total energy shaping with $m = 0.4$ on spatial UCDR.	83
7.9	Simulation results of total energy shaping with configuration-dependent M_d on spatial UCDR.	83
7.10	Simulation results of sliding mode controller on spatial UCDR.	84
7.11	Simulation results of IDA-PBC in the presence of uncertain parameters.	85
7.12	Simulation results of adaptive IDA-PBC in the presence of uncertain parameters.	85
7.13	Simulation results of IDA-PBC on spidercam.	86
7.14	Control efforts and cables' length of spidercam.	86
7.15	Ball and beam system.	87
7.16	Simulation results of the ball and beam system.	89

7.17	Configuration variables of the VTOL aircraft.	90
7.18	Control efforts of the VTOL aircraft.	90
7.19	Simulation results with total energy shaping without optimization.	93
7.20	Simulation results with total energy shaping and optimized inputs.	93
7.21	Simulation results of IDA-PBC with desired gravity compensation on pendubot.	94
7.22	Configuration variables of ARAS UCDR with IDA-PBC.	95
7.23	Control efforts of ARAS UCDR with IDA-PBC.	96
7.24	Configuration variables of ARAS UCDR with adaptive IDA-PBC.	96
7.25	Control efforts of ARAS UCDR with adaptive IDA-PBC.	97
7.26	Configuration variables of ARAS UCDR with PD controller.	97
7.27	Control efforts of ARAS UCDR with PD controller.	98
7.28	Configuration variables of ARAS UCDR with a controller in joint space.	98
7.29	Control efforts of ARAS UCDR with a controller in joint space.	99
7.30	Experimental results based on Theorem 4 on the 3-DOF ARAS CDR.	100
A.1	Schematic of magnetic levitation system ($y = \theta$).	104
A.2	Schematic of Pendubot. Merely the first joint is actuated.	108
B.1	VTOL aircraft.	112
B.2	Schematic of 2D SpiderCrane system.	113

Symbols, Abbreviations and Notations

SYMBOLS

\mathbf{q}	Generalized position/configuration variable	–
\mathbf{p}	Momentum	
\mathbf{u}	Control input	
H	Hamiltonian	
H_d	Desired Hamiltonian	
\mathbf{J}	Interconnection matrix	
\mathbf{J}_d	Desired interconnection matrix	
\mathbf{R}	Damping matrix	
\mathbf{R}_d	Desired damping matrix	
\mathbf{G}	Input mapping matrix	
\mathbf{y}	Passive output	
\mathbf{y}_d	Closed-loop passive output	
\mathbf{q}^*	Desired equilibrium point	
\mathbf{G}^\perp	Left annihilator of \mathbf{G}	
\mathbf{M}	Inertia matrix	
\mathbf{M}_d	Desired inertia matrix	
V	Potential function	
V_d	Desired potential function	
K	Kinetic energy	
K_d	Desired kinetic energy	
\mathbf{J}_2	Free skew-symmetric matrix	
\mathbf{R}_2	Closed-loop damping matrix in mechanical systems	
\mathbf{K}_v	Damping gain	
s	Degree of underactuation	
\mathbf{X}	Configuration variable in parallel robot	
l_i	Length of i th cable	
\mathbf{J}_a	Jacobian matrix	
\mathbf{C}	Coriolis and Centrifugal terms	
\mathcal{G}	Gravity force/torque	
\mathbf{I}	Inertia matrix	
\mathbf{R}_m	Rotation matrix	
$\boldsymbol{\omega}$	Angular velocity	
V_{dh}	Homogeneous part of V_d	
V_{nh}	Non-homogeneous part of V_d	

ϕ	Arbitrary function
\mathfrak{C}	Dissipative force
λ_{min}	Minimum eigenvalue
λ_{max}	Maximum eigenvalue
\mathbf{u}_m	Lower bound of actuators
\mathbf{u}_M	Upper bound of actuators
\mathbf{J}_u	Free skew-symmetric matrix
$\tilde{\mathbf{J}}$	Vector representation of \mathbf{J}_u
\mathcal{Y}	Matrix representation of \mathbf{y}_d
\mathcal{V}	Lyapunov function
ν	Estimation of velocity

ABBREVIATIONS

DOF	Degree of freedom
CDR	Cable-driven robot
UCDR	Underactuated cable-driven robot
UaS	Underactuated system
PBC	Passivity-based control
IDA-PBC	Interconnection and damping assignment passivity-based control
PH	Port Hamiltonian
EL	Euler-Lagrange
PDE	Partial differential equation
ODE	Ordinary differential equation
SIDA-PBC	Simultaneous IDA-PBC
I&I	Immersion and invariance
MRAS	model reference adaptive system

NOTATIONS

\mathbf{I}_n denotes $n \times n$ identity matrix, $\mathbf{0}_{m \times n}$ is $m \times n$ zero matrix. x_i and ξ_{ij} with $\mathbf{x} \in \mathbb{R}^n$, $\boldsymbol{\xi} \in \mathbb{R}^{m \times n}$ denote i th and (i, j) th element of \mathbf{x} and $\boldsymbol{\xi}$, respectively. $\boldsymbol{\xi}(i, \cdot)$ and $\boldsymbol{\xi}(\cdot, j)$ are i th row and j th column of $\boldsymbol{\xi}$, respectively. $\boldsymbol{\xi}_e(i, j)$ is obtained by elimination of the i th row and j th column of $\boldsymbol{\xi}$. Gradient of a scalar function $f(\mathbf{x})$ which is denoted by $\nabla_{\mathbf{x}} f$ is a column vector as $\nabla_{\mathbf{x}} f = [\frac{\partial f(\mathbf{x})}{\partial x_1}, \dots, \frac{\partial f(\mathbf{x})}{\partial x_n}]^T$. For a square matrix $\mathbf{\Lambda} \in \mathbb{R}^{n \times n}$, $\mathbf{\Lambda} > 0$ means this matrix is positive definite.

Chapter 1

Introduction

In this section, first, different types of cable-driven robots and their applications are presented. Then, underactuated mechanical systems and their properties, as the main topic of this thesis, are introduced. Furthermore, underactuated cable-driven robots as a newly introduced type of cable-driven robots are discussed. Finally, the aims and contributions of this thesis are given.

1.1 Cable-Driven Robots

Parallel robots are a closed-loop mechanism that the end-effector is attached to the base through some kinematic chains. Generally, parallel robots have some advantages compared with serial robots such as high precision, stiffness, and fast speed. Furthermore, since the end-effector is connected to the base by several limbs, they can carry heavy loads. Due to these features, parallel robots have different applications such as simulators, remote handling, medical robots, etc [1]. However, limited workspace is the most essential disadvantage of parallel robots that restricts their application in industry [2]. Fig. 1.1 shows a typical parallel robot.

In order to rectify this issue, a new version of parallel robots has been introduced such that the solid limbs are replaced by cables¹. By this means, the robot's workspace is arbitrarily enlarged such that it is possible to set up the robot in a stadium. Additionally, the movement of the end-effector is faster compared with parallel and serial robots. Due to the fact that the robot's arms are made of cable, the ability to carry a large load compared to the low weight of the robot is another feature that can be enumerated for such robots [3]. Fig. 1.2 illustrates a typical cable-driven robots.

The desirable features of cable-driven robots (CDRs) make it possible to use these robots in various fields. However, CDRs have some stringent limitations such as the cables can only pull and not push. Hence, the design of the robot should be accomplished to ensure that tensile forces are applied on the cables for all maneuvers. To comply with such constraint, most of the CDRs are redundantly actuated. Generally, one may argue that for a n degree of freedom (DOF) CDR, $n + 1$ actuators or even more are required to keep the cables in tension. Cable-driven robots are called fully constrained, if the position of end-effector is fixed then the length of cables is constant. Under-constraint robots are another type of CDRs that positive tension is ensured in the presence of an external passive force such as gravity that can be interpreted as an imaginary cable. In these robots, it is possible to change the position of the end-effector even though the length of

¹Note that serial cable-driven robots are another type of cable-driven robots, but they are out of scope of this thesis.

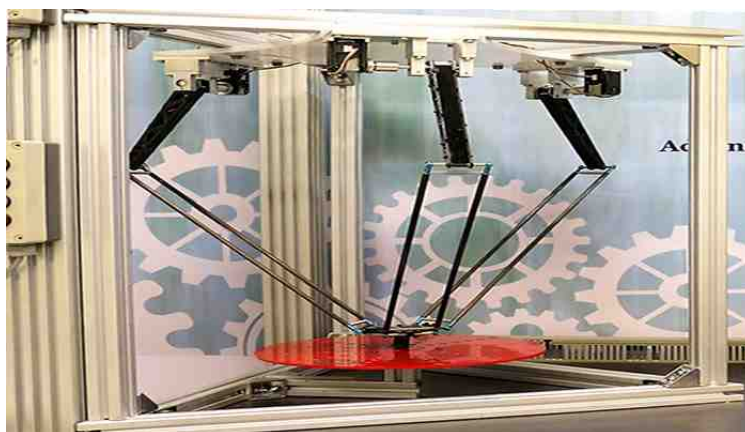


Figure 1.1: A typical parallel robot.

cables are fixed. Note that in contrast to fully-constraint robots, under-constraint robots are not necessarily redundant. Fig. 1.3 illustrates a typical example of both types of CDRs. In this thesis, we only concentrate on under-constraint CDRs. A special version of under-constraint robots has been developed such that the number of cables is fewer than the number of degrees of freedom which are called underactuated cable-driven robots (UCDRs). As explained before, cables can only apply tensile forces. Thus, it is common to use more actuators than the number of degrees of freedom. However, in UCDRs, not only there are no additional actuators to ensure the cables are stretched, but also by using fewer actuators, control of the robot is much more difficult. Although several papers have been reported on the control of benchmark underactuated systems, less attention has been paid to UCDRs due to the complexity and novelty of the problem.

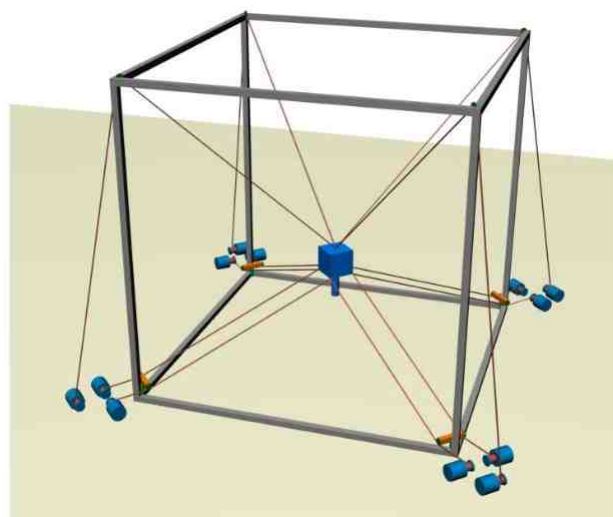


Figure 1.2: A typical cable-driven robot [4].

It should be noted that some of the under-constraint CDRs used in industry are basically UCDRs. However, to reduce the complexity in kinematics and dynamics of the robot and also no requirement to high accuracy, they are modeled as a fully actuated robot. For example, in under-constraint suspended CDRs, it is common to only model the position of end-effector and thus, orientation is neglected. On the other hand, implementation of some tools such as gimbal stabilizer on the end-effector compensate the effects of unmod-

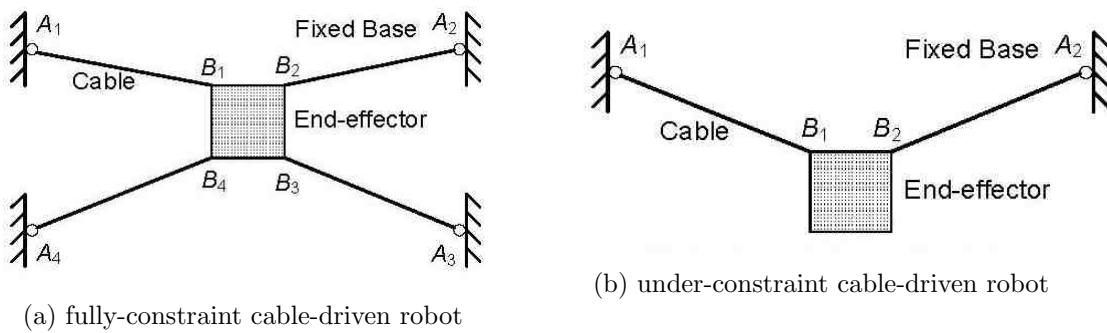


Figure 1.3: Typical fully-constraint and under-constrain CDRs [5].

eled terms and reduce the undesirable fluctuations. Since the main focus of this thesis is underactuated cable-driven robots, in the following, some applications of these robots are presented.

1.2 Applications of Underactuated Cable-Driven Robots

As explained before, UCDRs are a subset of under-constraint robots. Hence, alteration of an UCDR to an under-constraint one and vice versa is quite easy by adding or removing extra cables. For example, one of the most important applications of under-constraint CDRs is transportation of heavy loads which are mostly used in ports and ships. The ratio of the load to the moving weight of the robot makes them unrivaled in the transportation of objects. Fig. 1.4 shows a 6-DOF CDR with six cables during transport of a load. It is clear that it is possible to increase the number of cables to build a redundant robot. Additionally, by reducing one, two, or three cables, it is possible to construct an UCDR. The advantage of the resulted robot is fewer cost of creation with the expense of more complex control. Hence, development of a new control strategy is a stringent requirement.

Another common application of under-constraint CDRs is aerial imaging. This mechanism is called spidercam, and is used in different stadiums. The end-effector of this robot is equipped with a camera that can cover the whole stadium area due to its very large workspace. Fig. 1.5 depicts a spidercam. The unique features of this robot have made it a well-known tool in the aerial imaging industry. The end-effector of this robot is controlled through four cables connected to actuators. Due to the fact that the cables in this robot do not necessarily connect to a unique point; therefore, the spidercam has six degrees of freedom from a theoretical point of view. But since the dimensions of the end-effector are much smaller than that of the stadium, the spidercam is usually modeled as a three degrees of freedom robot. In other words, it is assumed that all the cables are connected to a unique point and the end-effector has only a transient motion, and its rotational motion is neglected. Therefore, it seems that control of the robot is simple. However, this simplification in practice leads to slight oscillations, especially in fast motions. Researchers usually ignore studying these oscillations, or try to reduce them by modification of the mechanism by adding stabilizing gimbals such as reported in [7]. This problem provides the main incentive of our research to focus on underactuated cable-driven robots. By this means, by considering the full dynamic model of the robot, we will develop control algorithms in the field of underactuated systems to reduce undesirable oscillations in the end-effector. In the following, an introduction of underactuated systems and their control methods is



Figure 1.4: A CDR during transportation of a load [6].

proposed. Then how to develop these methods and adapt them to the characteristics of UCDRs will be discussed.

1.3 Underactuated Systems

Underactuated systems (UaSs) are an important and widespread class of mechanical systems such that the number of actuators is fewer than the number of degrees of freedom. UaSs are found in a wide range of applications including robotics, aerospace systems, marine systems, flexible robots, mobile robots, etc [9]. The underactuation property of these systems is due to four reasons. 1- The dynamics of the systems (e.g. aerial, marine, and submarine systems). 2- Reduction of the cost (e.g. satellite). 3- Failure in actuator(s). 4- Intentionally designing a low-order UaS to obtain insights on how to control a high-order UaS (e.g. Pendubot). Thus, research on efficient control methods for these systems, which are found in many applications, has received much attention from researchers in the last two decades. However, control of UaSs is a challenging problem since in contrast to fully actuated systems, they have fewer actuators than degrees of freedom. Thus, it is not possible to use the methods developed based on feedback linearization. Furthermore, several elements such as parameter uncertainties, unmodeled dynamics, external disturbance, actuators saturation, etc. make controller design more challenging. Additionally, UaSs can not track every desired trajectory. However, it is possible to stabilize them in the equilibrium points [10]. Hence, the control formulation of these systems is mostly in the form of regulation or point-to-point control.

Although UaSs cannot be linearized, it is possible to linearize only actuated or unactuated configurations which are called collocated feedback linearization and non-collocated feedback linearization [11]. By this means, the equations of the system are divided into a



Figure 1.5: A spidercam during imaging [8].

linear and a nonlinear subsystem as follows

$$\begin{aligned}\ddot{\mathbf{q}}_1 &= \mathbf{f}(\mathbf{q}, \dot{\mathbf{q}}) + \mathbf{g}(\mathbf{q}, \dot{\mathbf{q}})\mathbf{u} \\ \ddot{\mathbf{q}}_2 &= \mathbf{u},\end{aligned}$$

in which $\mathbf{q} = [\mathbf{q}_1, \mathbf{q}_2]^T$ denotes the configuration variables and \mathbf{u} is the control input. The problem that makes it challenging to design a controller is the presence of a control law in both of the subsystems. Thus, using merely this method cannot control an UaS, and as a result, most of the proposed controllers in the literature are innovative and system-based.

Based on the structure and physical nature of UaSs, one of the most common control methods for such systems is passivity-based control [12]. Ortega et al. developed this method and further modified to interconnection and damping assignment passivity-based control (IDA-PBC) [13,14]. The main goal of this method is to transform the dynamical equations of a system in closed-loop to the following port Hamiltonian (PH) form

$$\dot{\mathbf{x}} = [\mathbf{J}_d(\mathbf{x}) - \mathbf{R}_d(\mathbf{x})]\nabla H_d,$$

in which H_d denotes total energy of closed-loop, $\mathbf{J}_d, \mathbf{R}_d$ are desired interconnection and damping matrices respectively, and ∇H_d is a row vector representing the gradient of H_d . For this means, the system is represented in PH form which is based on network modeling of energy-conserving physical systems with lumped parameters and strictly contains the systems represented by Euler-Lagrange model. The main advantage of the PH modeling is its inherent passivity; thus, its stability is guaranteed. Furthermore, the PH structure of the system is preserved, the storage function is exactly the total energy of the system, and $\mathbf{J}_d, \mathbf{R}_d$ are design matrices that may be assigned based on the nature of the system. IDA-PBC is based on the solution of some partial differential equations (PDEs) without boundary conditions which shall be solved analytically. For mechanical systems, two sets of PDEs arise that are related to shaping of the kinetic and potential energy. In the next chapters this method will be explained in details.

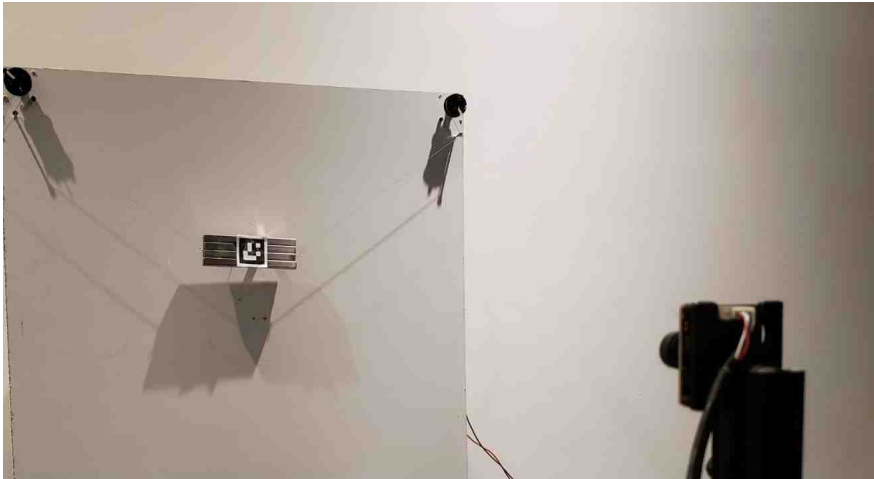


Figure 1.6: An example of underactuated cable-driven robot.

1.4 Underactuated Cable-Driven Robots

As explained before, there exists a class of cable-driven robots that are basically underactuated. A 3-DOF UCDR with two actuators is shown in Fig. 1.6. For example, in spidercam and similar applications, it is not recommended to use more actuators to control the robot, due to the high cost of construction and maintenance. So far, these robots have been modeled as fully actuated ones to avoid computational complexity. These types of suspended cable-driven robots are very useful because of their potential applications, but the issue of underactuation is less taken into account. UCDRs have the positive features of CDRs and UaSs include agility, high speed, simplicity of mechanism with fewer actuators, and large workspace [15]. But the expense of these features is complexity of controller design. On the other hand, the presence of a closed kinematic chain in CDRs creates unique features that are different from what is seen in the literature of URs. The combination of these two issues together leads to more complexity in the problem that has been less addressed. However, recently a number of studies in this field have been reported in the literature, see for example [16–18].

In this thesis, due to the complexity of the 6-DOF UCDR, we first focus on two 3-DOF cases with two actuators, and then a simple general method to stabilize underactuated parallel robots will be proposed. In these robots, since the number of actuators is less than that of the the degrees of freedom of the robot, an arbitrary desired trajectory may not be tracked, but instead, movement from any desired point to any other point inside the robot’s controllable workspace, without determination of the trajectory is accessible. Therefore, the regulation problem for the UCDRs will be investigated using the generalized passivity-based method. As mentioned, the applications of UCDRs can be found in the ports of loading and unloading, construction, warehousing, entertainment, and interaction of human and robot where due to the ability of point-to-point movement, the most important application of these robots is pick and place [15].

1.5 Contributions of This Thesis

The goals and achievements of this thesis are as follows:

- In this thesis, the formulation of underactuated cable-driven robots is done in order

to solve the regulation problem. The main focus is, but not limited to; two 3-DOF suspended UCDRs with two actuators. One of the robots is planar and can rotate in a vertical plane while the other has out-of-plane oscillations. However, since some of the proposed controllers are general, several UaSs such as spidercam will be analyzed.

- Design a controller based on IDA-PBC approach for UCDRs. Since IDA-PBC relies on the solution of some PDEs, we will concentrate on deriving the solution of these equations. For this purpose, some methods will be introduced. A systematic procedure to solve the PDE of kinetic energy shaping for UaSs with underactuation degree one is proposed. By this means, a particular structure for the desired inertia matrix is considered that simplifies the kinetic energy PDE by also using a free sub-block of desired interconnection matrix. Furthermore, invoking the method proposed in [19], it is possible to transform a single PDE to a set of Pfaffian differential equations. Although computing the solution of Pfaffian equations is not trivial, in some cases, it is much easier than the corresponding PDE. Another method is related to the potential energy shaping of underactuated parallel robots. It will be shown that due to the special structure of parallel robots, the solution of potential energy PDE is derived quite easy. The proposed methods will be applied to several benchmark UaSs and UCDRs.
- Design a bounded input IDA-PBC. Since cable-driven robots can only apply tensile forces, positiveness of control law should be taken into account in controller design. Since actuator saturation is a common problem in all practical implementations, in order to address this issue, two different general methods will be introduced. One of the methods is based on the term by term analysis of IDA-PBC's control law. By suitable definition of desired potential energy and computing the upper bound of velocity, the upper bound of the control law is derived. In the other method, it is tried to minimize the control law by the free design matrices in IDA-PBC such that the limitations of actuators are satisfied. For this purpose, UaSs with at least two actuators are considered, and a minimization based on the free sub-block of desired interconnection matrix is solved analytically.
- Design an adaptive IDA-PBC. Since the parameters of a system are uncertain, one suitable approach is to design an adaptive controller to address this issue. However, since IDA-PBC is based on satisfaction of some PDE, it is not trivial to derive a general adaptation law to ensure the stability of the system without the assumption that the parameters are converging. In this thesis, adaptive IDA-PBC for some case studies is proposed.
- Design some developed versions of IDA-PBC. By this means, IDA-PBC with position feedback, IDA-PBC without non-homogeneous solution of potential energy PDE, and IDA-PBC with desired gravity compensation are introduced.
- Implementation of the controllers. In order to test the performance of the proposed controllers in practice, they are implemented on some CDR. By this means, it is shown that the proposed controllers are sufficiently robust to deal with various unavoidable challenges in practice such as external disturbance, measurement noise, unmodeled dynamics, etc.

Chapter 2

Literature Review

Controller design has been a challenging issue for researchers in recent decades. In this chapter, first, the literature about cable-driven robots and their control methods is reviewed. Then, underactuated systems are considered, and the proposed control strategies, especially interconnection and damping assignment passivity-based control, are investigated. Finally, the research gap in this field is presented.

2.1 Cable-Driven Robots

The published articles about CDRs cover various aspects such as robot design, workspace, modeling and control. In the sequel, the related works to this thesis are reviewed.

2.1.1 Positive Tension in Cables

One of the most important features of CDRs is cables can only apply tensile forces. According to this constraint, researchers usually calculate the robot's workspace so that if the end-effector is placed inside it, all the cables are stretched. By this means, researchers have proposed four types of workspace for CDRs.

1. Reachable workspace. This workspace is defined based on physical and practical constraints. These constraints include the maximum and minimum applicable force to the cables to exert the computed forces to the end-effector. Reachable workspace is also named as wrench feasible workspace [20] and force feasible workspace [21]. Note that the applicability of this workspace is restricted due to high complexity.
2. Controllable workspace. One of the most common definitions of CDRs' workspace is controllable workspace which is also named wrench closure workspace [22] and force closure workspace [23]. In this workspace, it is possible to apply force to the end-effector in any direction with any magnitude, while the cables remain stretched. The important point in examining this type of workspace is redundancy requirement in the number of cables, so it cannot be defined for an underactuated cable-driven robot.
3. Statically reachable workspace. To define this type of workspace, gravity is considered as a constant force. In other words, gravity plays the role of an extra artificial cable. This type of workspace can be defined for all suspended robots such as UC-DRs. [24] and [25] have analyzed statically reachable workspace for suspended CDRs. In the aforementioned papers, static workspace refers to a set of points where, if the robot is placed, the positive tension is ensured.

4. Dynamic workspace. Linear and angular velocity are used to define this workspace. In fact, this workspace is a subset of the static workspace that external force is resulted from the applied accelerations. Researchers have defined this workspace for planar CDRs in [26]. Furthermore, [27] has examined the robot's dynamic workspace for the amount of acceleration applied by the cables.

Therefore, it is clear that a method to ensure cables are stretched is to analyze the robot's workspace. The advantage of this method is that it can be performed offline; thus, it is possible to compute the above workspace for a CDR. But these evaluations are not sufficient, and the controller should be designed such that the robot stays within the workspace.

In [28] force distribution in redundant cable-driven robots has been examined. In redundant robots, infinite force distribution is possible, and thus, positive tension may be ensured. [29] has proposed a similar approach for planar CDRs. It should be noted that this method is only applicable for redundant CDRs.

Another method is online trajectory planning. [30] has focused on a 2-DOF suspended CDR with two actuators. The constraint of cable tension is replaced by a restriction on the speed and acceleration of the end-effector. The method to move the robot along a line is to use the dynamic model of the robot and design a trajectory for the length of the cables in the form of time polynomials. In [31] and [32] for the same robot and in a similar way, the desired trajectory for the length of cables has been designed as a sum of some sinusoidal terms by calculating the natural frequency of the system. The problem of this method is numerical solution of equations of motion. Additionally, stability analysis has not been reported in this method. It should be noted that this method is applicable to UCDRs; see section 2.4 for more details. In the following, the proposed controllers for CDRs are reviewed.

2.2 Control of Cable-Driven Robots

Some papers have proposed controller for CDRs by considering cables as a rigid body, e.g. PD and adaptive controllers proposed in [33] and [34–36], respectively. By this means, positive tension in cables has not been considered which may lead to poor performance or malfunction of the system. In most papers, cables have not been modeled. As an example, a robust PID for the same system has been proposed in [37]. Babaghassabha et al. in [38] have proposed an adaptive robust controller for a fully-constraint CDR. Positive tension in cables has been ensured in the two aforementioned papers simply since the system is fully-constraint. A robust cascade controller for a deployable under-constraint CDR has been introduced in [3]. By assigning a suitable value to the null space of the input mapping matrix when one of the elements of the controller reaches zero, tensile forces in cables have been considered. An adaptive controller with respect to kinematic and dynamic uncertainties for parallel robots has been proposed in [39] and positive tension for the case of CDRs has been considered by projection algorithm for adapted parameters. Note that the last three mentioned papers are some of the representatives of sliding mode controllers designed for CDRs. A controller by considering the elasticity of the cables has been designed in [40].

Passivity-based control has also been utilized for the systems that are based on a cable-driven part. [41,42] have used PBC to design a controller for a suspended mass from some cables attached to quadrotors. Caverly et al. in [43–45] have concentrated on exact modeling of CDRs. Each cable is modeled as a sum of masses, springs and dampers, and then, using PBC, the desired trajectory is tracked, and the results are verified through

simulation. In these studies, the robot is a planar CDR such that the gravity is not applied to the end-effector. [46–49] are representatives of recent works on CDRs.

In most of the aforementioned papers, the robot is redundant, and by force distribution, the cables are stretched. For fully actuated non-redundant CDRs, the analysis of robot’s workspace has been used. As a result, ensuring positive tension in UCDRs requires innovations.

2.3 Control of Underactuated Systems

As explained before, UaSs have several applications in different aspects. On the other hand, due to the fewer actuators compared to the degrees of freedom of the robot, control of UaSs is a challenging problem. Due to this property, most of the proposed papers have focused on the stabilization of the system. In the following, the existing works in this field are reviewed.

One of the common methods to stabilize UaSs is using partial feedback linearization to bring the states near the desired point and then apply a linear controller such as linear quadratic regulator to stabilize the system. This idea has been applied to Acrobot in [11]. Energy shaping is another method that is a suitable choice for underactuated serial robots. In this method, which is based on the passive nature of the system, the energy of the system at the desired point is firstly derived. Then, by adding energy to the system, the energy level of the system reaches the energy level of the desired equilibrium point. Finally, similar to the previous method, by applying a linear controller, the system is stabilized, see for example [50] and [51]. Poor performance in transient response is the disadvantage of the two mentioned methods. In general, hybrid control in [52,53] are used to stabilize an underactuated system. The usual problem of hybrid controllers is that there is no assurance of convergence to the desired point. In other words, the states of the system are not necessarily closer to the equilibrium point after switching the control law. Another method developed by Olfati-Saber in [9] is relied on the classification of systems based on actuated configuration variables and also the inertia matrix. The variables that appear in the inertia matrix are called shape variables, and other variables are called external variables. Depending on which variables are actuated, eight classes are defined, and a method is proposed for each class. The advantage of this method is the uniqueness of control law and proof of stability, and its disadvantage is inefficiency in controlling many robots such as UCDRs. Other methods which are mostly case study include sliding mode control [54,55], linear matrix inequality control [56], model predictive control [57], etc. The general method developed by Ortega is a new version of passivity-based method. Since this method is the basis of this thesis, invoking [58], in the following, it is explained in details.

Passivity-based control is a general method firstly proposed in [59] to stabilize a system. The basic of the method is to show that the system is passive with respect to a desired storage function and an output. Generally, PBC is categorized into two classes. In classical PBC, the storage function, which is mainly a quadratic function, is selected priorly, and then, control law is designed such that the storage function would not increase. This method is suitable to stabilize mechanical systems in which merely potential energy shaping is required. By this means, the closed-loop system has an Euler-Lagrange (EL) representation, and the storage function is equal to the difference between the stored energy and the supplied energy to the system. This method is called energy balancing in [60]. Furthermore, classical PBC, which is similar to Lyapunov method, has been successfully applied to many EL systems including mechanical, electrical and electrome-

chanical systems. The reader is referred to [61] to see several examples. Unfortunately, for the applications that require total energy shaping, although the closed-loop system is passive, it does not have an EL representation, and the storage function is not necessarily equal to the total energy of the system.

The second type of passivity is more general than the classical one and it is applicable to a larger class of systems through total energy shaping. In this method, the storage function is not assigned priorly, but instead, the desired structure of the closed-loop system is chosen and then all storage functions compatible with this structure are derived. These functions are the solution of some partial differential equations. ‘‘Control Lagrangian’’ [62, 63] and ‘‘interconnection and damping assignment’’ [13, 64] are the examples of this method. Since PH modeling is more general than EL, and Control Lagrangian is a special form of IDA [65], in this thesis, IDA-PBC is considered. As explained before, IDA-PBC is designed based on the solution of some PDEs that consists of three parameters including the interconnection between subsystems, damping matrix and null space of input mapping matrix. Many interpretations may be presented for these matrices. From a computational point of view, they can be assigned such that the resulting PDE is simplified. From a theoretic viewpoint, they may be chosen to enforce the required passivity property, or from a dynamic viewpoint that may lead to the propagation of dissipation. So far, the concept and general characteristics of IDA-PBC methodology have been stated. The reader is referred to [66–69] and references therein to see some of the applications of this method. In the following, the mathematics of this method will be introduced in details.

2.3.1 IDA-PBC Methodology

IDA-PBC introduces a systematic method to control a system in PH form as follows [13]

$$\begin{aligned}\dot{\mathbf{x}} &= [\mathbf{J}(\mathbf{x}) - \mathbf{R}(\mathbf{x})]\nabla H + \mathbf{G}(\mathbf{x})\mathbf{u} \\ \mathbf{y} &= \mathbf{G}^T(\mathbf{x})\nabla H,\end{aligned}\tag{2.1}$$

in which $\mathbf{x} \in \mathbb{R}^n$ denotes the states, $\mathbf{u} \in \mathbb{R}^m$ is the control input, $H(\mathbf{x}) \in \mathbb{R}$ is the open-loop storage function, ∇H denotes gradient of H , $\mathbf{G}(\mathbf{x}) \in \mathbb{R}^{n \times m}$ is input mapping matrix, $\mathbf{J}(\mathbf{x}) = -\mathbf{J}^T(\mathbf{x}) \in \mathbb{R}^{n \times n}$ and $0 \leq \mathbf{R}(\mathbf{x}) = \mathbf{R}^T(\mathbf{x}) \in \mathbb{R}^{n \times n}$ are interconnection and damping matrices, respectively, and $\mathbf{y} \in \mathbb{R}^m$ is the passive output. Although PH modeling includes most of the physical systems, in some cases representation of a system in PH form is difficult. In the following, a general form is considered and then IDA-PBC is applied to it.

Proposition (Proposition 1 of [58]). Consider the following system

$$\dot{\mathbf{x}} = \mathbf{f}(\mathbf{x}) + \mathbf{g}(\mathbf{x})\mathbf{u}.\tag{2.2}$$

Assume that there exist the matrices $\mathbf{g}^\perp(\mathbf{x})$, $\mathbf{J}_d(\mathbf{x}) = -\mathbf{J}_d^T(\mathbf{x})$, $\mathbf{R}_d(\mathbf{x}) = \mathbf{R}_d^T(\mathbf{x}) \geq 0$ and the function $H_d(\mathbf{x})$ that satisfy the following PDE

$$\mathbf{g}^\perp \mathbf{f}(\mathbf{x}) = \mathbf{g}^\perp [\mathbf{J}_d(\mathbf{x}) - \mathbf{R}_d(\mathbf{x})]\nabla H_d(\mathbf{x}),\tag{2.3}$$

where \mathbf{g}^\perp is the left annihilator of \mathbf{g} (i.e. $\mathbf{g}^\perp \mathbf{g} = 0$), and H_d satisfies

$$\mathbf{x}^* = \arg \min H_d(\mathbf{x}),\tag{2.4}$$

with \mathbf{x}^* as the desired equilibrium point. Then system (2.2) with the following control

law

$$\mathbf{u} = [\mathbf{g}^T \mathbf{g}]^{-1} \mathbf{g}^T \{[\mathbf{J}_d - \mathbf{R}_d] \nabla H_d - \mathbf{f}\} \quad (2.5)$$

takes the following form

$$\dot{\mathbf{x}} = [\mathbf{J}_d(\mathbf{x}) - \mathbf{R}_d(\mathbf{x})] \nabla H_d, \quad (2.6)$$

such that \mathbf{x}^* is (locally) stable. If \mathbf{x}^* is a separated minimum of H_d and also the largest invariant set of

$$\{\mathbf{x} \in \mathbb{R}^n | (\nabla H_d)^T \mathbf{R}_d(\mathbf{x}) \nabla H_d = 0\}, \quad (2.7)$$

is equal to \mathbf{x}^* , then it is asymptotic stable. An estimate of region of attraction is the largest bounded level set of $\mathbf{x} \in \mathbb{R}^n | H_d(\mathbf{x}) \leq c$ for an arbitrary positive c . ■

Note that by considering H_d as a Lyapunov candidate, its derivative is

$$\dot{H}_d(\mathbf{x}) = -(\nabla H_d)^T \mathbf{R}_d(\mathbf{x}) \nabla H_d \leq 0. \quad (2.8)$$

Hence, \mathbf{x}^* is stable.

As it turns out, the advantage of this method is that the Lyapunov function is apparent, so unlike Lyapunov method, there is no need to search to find a suitable candidate. Notice that since PDE (2.3) equalize system (2.2) with (2.6), it is also called matching equation. Note that if the open-loop system itself has a PH structure, it has been shown in [13] that IDA-PBC generates all the stabilizing controllers.

In order to solve the PDE (2.3), three different methods may be utilized.

- Non-Parameterized IDA. In this method the matrices $\mathbf{J}_d, \mathbf{R}_d$ and \mathbf{g}^\perp are priority selected. Then PDE (2.3) is solved respect to H_d .
- Algebraic IDA. In this method H_d is priority selected and (2.3) is solved respect to $\mathbf{J}_d, \mathbf{R}_d$ and \mathbf{g}^\perp . An example of this method has been proposed in [70].
- Parameterized IDA. In some special cases, it is possible to consider a special form for H_d . For example, in mechanical systems, it is equal to the summation of desired kinetic and potential energies. Furthermore, the matrices $\mathbf{J}_d, \mathbf{R}_d$ may also be determined based on the structure of the system.

In the following, IDA-PBC for (simple) mechanical systems is reviewed.

2.3.2 IDA-PBC for Mechanical Systems

Here, stabilization of underactuated mechanical systems using parameterized IDA-PBC is discussed [14]. The equations of an UaS without modeling natural damping terms in PH form is as follows

$$\begin{bmatrix} \dot{\mathbf{q}} \\ \dot{\mathbf{p}} \end{bmatrix} = \begin{bmatrix} \mathbf{0} & \mathbf{I}_n \\ -\mathbf{I}_n & \mathbf{0} \end{bmatrix} \begin{bmatrix} \nabla_{\mathbf{q}} H \\ \nabla_{\mathbf{p}} H \end{bmatrix} + \begin{bmatrix} \mathbf{0} \\ \mathbf{G}(\mathbf{q}) \end{bmatrix} \mathbf{u}, \quad (2.9)$$

in which $\mathbf{q}, \mathbf{p} \in \mathbb{R}^n$ are generalized position and momentum, respectively, $H(\mathbf{q}, \mathbf{p}) = \frac{1}{2} \mathbf{p}^T \mathbf{M}^{-1}(\mathbf{q}) \mathbf{p} + V(\mathbf{q})$ is the summation of kinetic and potential energy, $\mathbf{M}(\mathbf{q}) = \mathbf{M}^T(\mathbf{q}) > 0$

is inertia matrix, and rank $\mathbf{G}(\mathbf{q}) \in \mathbb{R}^{n \times m}$ is equal to m . The desired Hamiltonian is considered in the following form

$$H_d(\mathbf{q}, \mathbf{p}) = \frac{1}{2} \mathbf{p}^T \mathbf{M}_d^{-1}(\mathbf{q}) \mathbf{p} + V_d(\mathbf{q}), \quad (2.10)$$

in which $\mathbf{M}_d(\mathbf{q})$ and V_d are desired inertia matrix and potential function, respectively and V_d should satisfy

$$\mathbf{q}^* = \arg \min V_d(\mathbf{q}). \quad (2.11)$$

By considering H_d in the form of (2.10), the desired interconnection matrix is in the following form

$$\mathbf{J}_d(\mathbf{q}, \mathbf{p}) = \begin{bmatrix} \mathbf{0} & \mathbf{M}^{-1}(\mathbf{q}) \mathbf{M}_d(\mathbf{q}) \\ -\mathbf{M}_d(\mathbf{q}) \mathbf{M}^{-1}(\mathbf{q}) & \mathbf{J}_2(\mathbf{q}, \mathbf{p}) \end{bmatrix} = -\mathbf{J}_d^T(\mathbf{q}, \mathbf{p}), \quad (2.12)$$

where \mathbf{J}_2 is a skew-symmetric matrix. Additionally, the desired damping matrix is

$$\mathbf{R}_d(\mathbf{q}) = \begin{bmatrix} \mathbf{0} & \mathbf{0} \\ \mathbf{0} & \mathbf{G}(\mathbf{q}) \mathbf{K}_v \mathbf{G}^T(\mathbf{q}) \end{bmatrix}, \quad (2.13)$$

with $0 < \mathbf{K}_v \in \mathbb{R}^{m \times m}$. Therefore, the desired structure of closed-loop system is

$$\begin{bmatrix} \dot{\mathbf{q}} \\ \dot{\mathbf{p}} \end{bmatrix} = \begin{bmatrix} \mathbf{0} & \mathbf{M}^{-1}(\mathbf{q}) \mathbf{M}_d(\mathbf{q}) \\ -\mathbf{M}_d(\mathbf{q}) \mathbf{M}^{-1}(\mathbf{q}) & \mathbf{J}_2(\mathbf{q}, \mathbf{p}) - \mathbf{G}(\mathbf{q}) \mathbf{K}_v \mathbf{G}^T(\mathbf{q}) \end{bmatrix} \begin{bmatrix} \nabla_{\mathbf{q}} H_d \\ \nabla_{\mathbf{p}} H_d \end{bmatrix} \quad (2.14)$$

By setting (2.9) equal to (2.14), and multiplying to \mathbf{G}^T , the control law is derived as follows

$$\begin{aligned} \mathbf{u} &= \mathbf{u}_{es}(\mathbf{q}, \mathbf{p}) + \mathbf{u}_{di}(\mathbf{q}, \mathbf{p}) \\ \mathbf{u}_{es} &= (\mathbf{G}^T \mathbf{G})^{-1} \mathbf{G}^T (\nabla_{\mathbf{q}} H - \mathbf{M}_d \mathbf{M}^{-1} \nabla_{\mathbf{q}} H_d + \mathbf{J}_2 \mathbf{M}_d^{-1} \mathbf{p}) \\ \mathbf{u}_{di} &= -\mathbf{K}_v \mathbf{G}^T \nabla_{\mathbf{p}} H_d, \end{aligned} \quad (2.15)$$

where \mathbf{u}_{es} and \mathbf{u}_{di} are energy shaping and damping injection parts, respectively. By multiplying to \mathbf{G}^\perp and separating \mathbf{p} dependent and independent equations, the following PDEs are resulted

$$\mathbf{G}^\perp \{ \nabla_{\mathbf{q}} (\mathbf{p}^T \mathbf{M}^{-1} \mathbf{p}) - \mathbf{M}_d \mathbf{M}^{-1} \nabla_{\mathbf{q}} (\mathbf{p}^T \mathbf{M}_d^{-1} \mathbf{p}) + 2 \mathbf{J}_2 \mathbf{M}_d^{-1} \mathbf{p} \} = 0, \quad (2.16)$$

$$\mathbf{G}^\perp \{ \nabla_{\mathbf{q}} V - \mathbf{M}_d \mathbf{M}^{-1} \nabla_{\mathbf{q}} V_d \} = 0. \quad (2.17)$$

The PDE (2.16) and (2.17) are related to kinetic and potential energy shaping, respectively. First the kinetic energy PDE shall be solved and then using \mathbf{M}_d , the potential energy PDE is solved. The following points are related to the matching equations (2.16) and (2.17).

- The dimensions of $\mathbf{G}^\perp(\mathbf{q})$ is the most important point in the matching equations. If $n = m + 1$ (i.e. the system is underactuation degree one), $\mathbf{G}^\perp(\mathbf{q})$ is a vector results in a nonlinear PDE in (2.16) and a linear PDE in (2.17). Otherwise, both equations are a set of PDEs that they are very difficult to solve.
- Solving the equation (2.16) is very complicated in the general case, since it is a set of nonlinear PDEs that its solution should be positive definite. However, if $\mathbf{G}^\perp(\mathbf{q}) \nabla_{\mathbf{q}} (\mathbf{p}^T \mathbf{M}^{-1}(\mathbf{q}) \mathbf{p}) = 0$, then it is possible to solve (2.16) by a constant \mathbf{M}_d .

- $M_d(\mathbf{q}) = M(\mathbf{q})$ is a trivial solution of (2.16). By this means, the PDE (2.17) is $\mathbf{G}^\perp \{\nabla_{\mathbf{q}} V - \nabla_{\mathbf{q}} V_d\} = 0$. However, it has been shown in [71] and Remark 4.3.18 in [72] that if \mathbf{q}^* is unstable equilibrium point, then total energy shaping is required (i.e. $M_d \neq M$).
- Unfortunately, it is not possible to solve them numerically because the numerical solution requires a boundary condition, but there is no boundary condition here. Furthermore, the condition $\mathbf{q}^* = \arg \min V_d(\mathbf{q})$ should be satisfied. Therefore, homogeneous and non-homogeneous solutions should be derived separately.

In the above formulation, IDA-PBC for mechanical systems without modeling natural damping terms was proposed. However, in some applications, they should be considered. In the following, invoking [73], IDA-PBC for mechanical systems with natural damping terms is proposed. Note that in this thesis, unless indicated, the model (2.9) is used.

The equations of an UaS with natural damping such as friction is as follows

$$\begin{bmatrix} \dot{\mathbf{q}} \\ \dot{\mathbf{p}} \end{bmatrix} = \begin{bmatrix} \mathbf{0} & \mathbf{I}_n \\ -\mathbf{I}_n & -\mathbf{R}(\mathbf{q}) \end{bmatrix} \begin{bmatrix} \nabla_{\mathbf{q}} H \\ \nabla_{\mathbf{p}} H \end{bmatrix} + \begin{bmatrix} \mathbf{0} \\ \mathbf{G}(\mathbf{q}) \end{bmatrix} \mathbf{u}, \quad (2.18)$$

where $\mathbf{R}(\mathbf{q}) \in \mathbb{R}^{n \times n}$ is positive semi-definite physical damping matrix. The structure of closed-loop system is

$$\begin{bmatrix} \dot{\mathbf{q}} \\ \dot{\mathbf{p}} \end{bmatrix} = \begin{bmatrix} \mathbf{0} & \mathbf{M}^{-1} \mathbf{M}_d \\ -\mathbf{M}_d \mathbf{M}^{-1} & \mathbf{J}_2 - \mathbf{R}_2 \end{bmatrix} \begin{bmatrix} \nabla_{\mathbf{q}} H_d \\ \nabla_{\mathbf{p}} H_d \end{bmatrix} \quad (2.19)$$

with the closed-loop damping matrix

$$\mathbf{R}_2 = \frac{1}{2} (\mathbf{R} \mathbf{M}^{-1} \mathbf{M}_d + \mathbf{M}_d \mathbf{M}^{-1} \mathbf{R}) + \mathbf{G} \mathbf{K}_v \mathbf{G}^T. \quad (2.20)$$

The control law and matching equations are similar to previous case. However, \mathbf{R}_2 is positive definite under the following constraint

$$\mathbf{G}^\perp (\mathbf{R} \mathbf{M}^{-1} \mathbf{M}_d + \mathbf{M}_d \mathbf{M}^{-1} \mathbf{R}) (\mathbf{G}^\perp)^T > 0. \quad (2.21)$$

This property is useful in the boundedness of inputs that will be discussed in the next chapters.

In the sequel, the previous works on IDA-PBC for UaSs are reviewed.

Solution of matching equations

In [74] an analytic solution of the matching equations is proposed for the systems with underactuation degree one. Six assumptions are considered, and the matching equations of systems that satisfy these assumptions are reformulated by ordinary differential equations (ODEs). Practically, only a few UaSs satisfy these assumptions. Since these PDEs are challenging, a number of researchers have looked for an alternative method instead of directly solve them. Astolfi et al. in [75] replaced the PDEs by the problem of finding an appropriate Lyapunov candidate. Actually, it has been shown that the classical PBC is related to this formulation. Unfortunately, finding a suitable Lyapunov candidate is as hard as solving a PDE. A similar method by replacing the PDEs with algebraic inequalities has been introduced in [76]. Simplification of kinetic energy PDE via coordinate change has been proposed in [77]. [78] has proposed a method for 2-DOF underactuated systems to

solve potential energy PDE. References [79–82] have proposed a similar method to overcome solving the matching equations under some restrictive assumptions on the dynamical parameters of the system. [83–85] are other papers in this area, that focus on a specific system.

Notice that simultaneous interconnection and damping assignment passivity-based control (SIDA-PBC) is another method proposed to simplify the matching equations. In the general form of IDA-PBC proposed in section 2.3.1, it is common to select \mathbf{R}_d in the range space of \mathbf{G} . This point is clearly verified in mechanical systems as indicated in section 2.3.2. However, in [86] it has been shown that this procedure is not applicable to induction machine since the PDEs are not involutive (i.e. they are not integrable). However, by simultaneously shaping the energy and damping injection, it is possible to design an IDA-PBC for that system. This idea was considered in [87] for mechanical systems and it has been shown that the kinetic energy PDE can be replaced by some algebraic equations for large scale systems. However, this idea was argued in [88] and it is proved that the number of PDEs of kinetic energy shaping that should be solved is $s(s+1)(s+2)/6$ for both IDA-PBC and SIDA-PBC with $s = n - m$ being the degree of underactuation. In [89] it has been asserted that although the number of PDEs are equal in both methods, SIDA-PBC simplifies the resulted matching equations. A claim that has not been proven.

Based on the reviewed literature, the proposed methods may be categorized into two classes. Some methods provide a general method to solve the matching equations. However, finding their solution is as hard as solving the corresponding PDE. Other methods target a particular class of systems in which the matching equations can be easily solved. Unfortunately, it seems that none of the reviewed methods are not capable to solve the matching equations of UCDRs. This gap in the literature, is examined in detail, and properly filled in this thesis.

Other challenging problems in IDA-PBC

Actuator saturation is a common limitation in all the practical systems that should be taken into consideration during the controller design. Otherwise, poor performance or even instability may be resulted [90]. For this purpose, several researchers have focused on controller design with bounded inputs. For fully actuated serial robots, it has been proved that if the actuators are capable to compensate for the gravity in the workspace, see for example [91–93]. Furthermore, different controllers for stabilization of UaSS with input constraints have been reported in literature. However, less attention has been paid to design IDA-PBC for mechanical systems with bounded inputs. This is due to the fact that the desired potential energy cannot be selected arbitrarily, and also the kinetic energy shaping terms are quadratic with respect to velocity. To the best of authors knowledge, [94] is the only bounded input IDA-PBC reported in literature, which is specifically designing controller for Inertia wheel pendulum. This case study does not suffer from two aforementioned problems since the solution of potential energy PDE (2.17) is sinusoid-like functions and also \mathbf{M}, \mathbf{M}_d are constant matrices results in vanishing kinetic energy shaping terms in the control law. On the other hand, in our specific application, namely UCDRs, the robot can merely apply tensile forces, and therefore, designing bounded input IDA-PBC for mechanical systems is the other aim in this thesis.

Robust IDA-PBC with respect to external disturbance is another topic of recent research works. Invoking [95], in [96] a robust IDA-PBC for mechanical systems subject to matched disturbance has been proposed. In these works, three different controllers based on nontrivial change of coordinate has been designed such that the constant disturbance is rejected. In [97] a general method for rejection of matched disturbance for

a PH system with constant input mapping matrix has been introduced. The idea is to design an adaptation law to estimate the external disturbance and add a nonlinear PI term to the control law. The results of this paper are generalized in [98] to a PH system with state-dependent input mapping matrix. Robust IDA-PBC with respect to matched and unmatched disturbance has been given attention in [99]. However, the mathematical proofs of the mentioned paper have been totally rejected in [100]. [101,102] are other robust IDA-PBC papers that are based on [99] and thus, they are technically not correct. as it can be seen, robust IDA-PBC with respect to matched disturbance is sufficiently studied in the literature. However, as indicated in [100], it seems that unmatched disturbance rejection is very complex and less worked out.

Parameter uncertainties is another common problem in applied mechanical systems. Researchers mostly design adaptive controllers to tackle this problem. However, adaptive IDA-PBC is not routine since the matching equations should be satisfied. To the best of our knowledge, [103,104] are the only published works that design adaptation law with respect to friction coefficients in this field. Hence, adaptation of dynamical parameters (i.e. the parameters in the inertia matrix and potential energy) is an open problem. Due to the gap in the literature in this field and also difficulty of the subject, design of adaptive IDA-PBC for some case studies of our interest, is another aim of this thesis.

Another practical problem in the implementation of controllers on mechanical systems is inaccurate velocity measurement. Several observers have been designed in literature to facilitate the implementation of a controller without requirement of velocity measurement. Although asymptotic trajectory tracking of fully actuated robots has not been proved in most cases, it is easy to ensure stability for the regulation problem. The positive characteristics of some observers, such as the observer proposed in [105] which is called dirty derivative of velocity, is its applicability in a class of UaSs. By this means, IDA-PBC with position feedback has been designed for Inertia wheel pendulum using the dirty derivative observer. Immersion and invariance (I&I) observer is an intense observer designed by introducing an attractive invariant manifold [106]. In [74], IDA-PBC with I&I observer has been designed for a class of mechanical systems with a constant inertia matrix. Generalization of this method has been studied in [107] where two sets of PDEs should be solved to design the observer. In this thesis, some of the proposed controllers are designed with an observer in order to simplify its implementation process.

In the following, we will review the previous works on UCDRs and identify the gap of research in this field.

2.4 Underactuated Cable-Driven Robots

Recently, a number of researchers have concentrated on the analysis and control of UCDRs. In [108] point-to-point trajectory planning for a serial UCDR using natural frequency analysis of the system by considering sinusoidal functions for the desired length of the cables has been performed. Design and stabilization of another serial UCDR by feedback linearization has been studied in [109]. Similar to [108], the method has been implemented on a 3-DOF planar UCDR in [15]. Trajectory planning for the same robot has been studied in [16] by considering time polynomial for the length of the cables. The results of the mentioned paper have been generalized in [17] for a general UCDR shown in Fig. 2.1, and rest to rest trajectory planning has been performed by numerical solving of a boundary value problem. Other papers based on trajectory planning of UCDRs can be seen in [110–114]. The advantage of controller design in joint space is that cables' tension can be verified simply. However, the common problem of the proposed works is that the

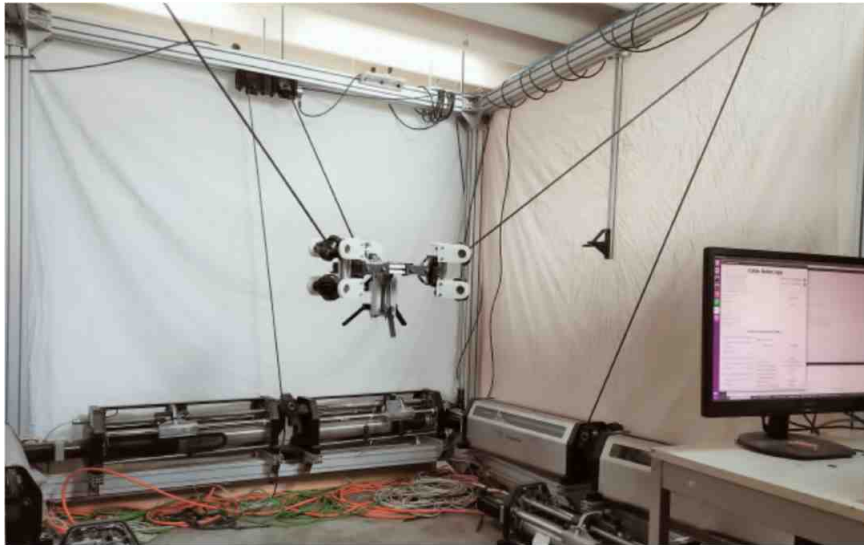


Figure 2.1: The underactuated cable driven robot reported in [17].

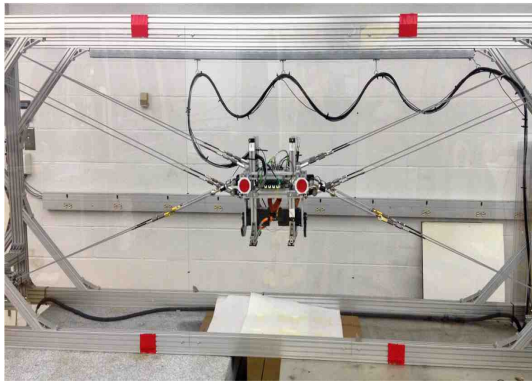
controller is designed in the joint space. Since forward kinematic in UCDRs has infinite solution, stability of desired equilibrium point is not ensured. Furthermore, generally, design a controller for the length of the cables leads to the oscillatory performance of the end-effector.

In [115], analysis, classification, and design of mechanisms that are designed by cables have been studied. In [116], static and dynamic analysis of an UDCR has been performed. The human's leg in which the lower joint is unactuated has been modeled in [117] by cable and pulley. In [18] design and optimal control of a micro-macro robot consisting of a fully actuated CDR attached to an underactuated serial robot has been considered. Since the underactuated part of the robot is in the serial structure, the main focus of the mentioned paper is on the serial robot. Out-of-plane oscillation control of a fully-constraint CDR has been considered in [118]. The studied robot generally has five degrees of freedom and two actuators. However, it is assumed that the lengths of the cables are constant, and only the out-of-plane motion of end-effector is controlled by two operators connected to it. Hence, similar to the previous case, this case is not an underactuated cable-driven robot. It should be noted that some papers have focused on other issues of UCDRs, for example geometrico-static problem in [119,120], stability analysis in [121], self-calibration in [122], etc.

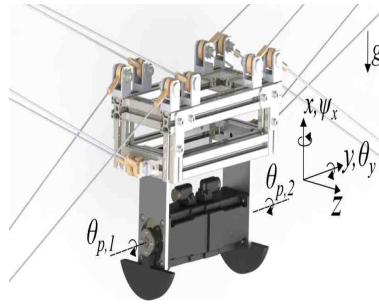
As it was shown, some papers have analyzed, designed and controlled UCDRs. The papers focused on the regulation problem of UCDRs are based on trajectory planning in joint space which requires accurate system equations, powerful software, and numerical forward solution of system's equations. Furthermore, in these papers, only desired length of cables are designed and control law is not proposed. Hence, in this thesis, some controllers based on IDA-PBC method with bounded inputs will be designed and implemented to cover the gap of research in the literature.

2.5 Conclusion

In this chapter, the literature on cable-driven robots, the types of workspace, and the various control methods was reviewed. After this, the control methods provided for underactuated systems and their disadvantages were discussed. Then, IDA-PBC method



(a) Overall view of the robot



(b) The end-effector

Figure 2.2: Planar underactuated cable-driven robot with two actuators on the end-effector [118]. The length of cables are fixed and out-of-plane oscillations are controlled.

as a general version of classical PBC was introduced and its formulation together with the open problems of this method, was proposed. Finally, the literature of underactuated cable-driven robot was reviewed. Due to the gap in controller design for UCDRs, in the next chapters, we will concentrate on this topic.

Chapter 3

Systems Models

In this chapter, the equations of UCDRs that are the subject of this thesis are given. The systems include a 3-DOF planar UCDR with two actuators, a 3-DOF spatial UCDR suspended from two cables, and a 6-DOF robot with four actuators. For each robot, inverse kinematic, Jacobian matrix, and dynamic equations neglecting the cable dynamics are given. Furthermore, the equilibrium points of the robots are also derived.

3.1 Planar Robot

This mechanism, which has been considered in [15, 16], consists of a payload suspended from two cables. The schematic of the robot is depicted in Fig. 3.1. The mechanism has two translational and one rotational motion in a vertical plane. The motion of the end-effector is provided via the length of the cables controlled by the actuators. As indicated in Fig. 3.1, the center of coordinate is located on one of the anchor points such that the X axis is in the direction of the two anchor points with the distance b , while the Y axis is upward (in the opposite direction of gravity). The position of the center of mass of the end-effector is denoted by $\mathbf{p} = [x, y]^T$, and the angle of its rotation relative to the horizon is denoted by θ . The length and the direction of the cables are denoted by l_1, l_2 and $\hat{\mathbf{s}}_1, \hat{\mathbf{s}}_2$, respectively. α_1 and α_2 denote the angles of the cables with the horizon.

3.1.1 Kinematic Analysis

The loop-closure equation may be written in the following form

$$\mathbf{p} = l_1 \hat{\mathbf{s}}_1 - \mathbf{E}_1 = \mathbf{B} + l_2 \hat{\mathbf{s}}_2 - \mathbf{E}_2, \quad (3.1)$$

in which \mathbf{E}_1 and \mathbf{E}_2 are the vectors from the center of mass of end-effector to the connection point of cables to the end-effector, and $\mathbf{B} = [b, 0]^T$. Equation (3.1) may be rewritten in the following form

$$\begin{aligned} x &= l_1 \cos(\alpha_1) + a \cos(\theta) = b + l_2 \cos(\alpha_2) - a \cos(\theta) \\ y &= l_1 \sin(\alpha_1) + a \sin(\theta) = l_2 \sin(\alpha_2) - a \sin(\theta), \end{aligned} \quad (3.2)$$

with $2a$ as the length of the end-effector. From this equation, the inverse kinematics can be easily solved. In other words, if x, y, θ are specified, the cables' length can be easily

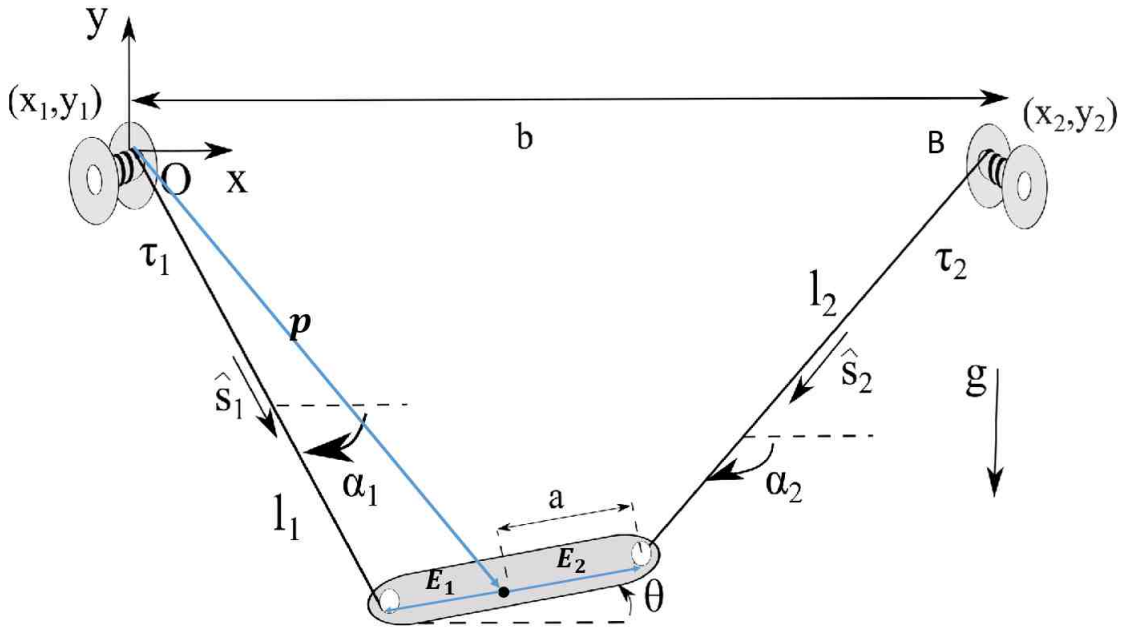


Figure 3.1: The schematic of the planar UCDR. The mechanism has two translational and one rotational motion. The center of mass is on the middle of the end-effector

calculated as follows

$$\begin{aligned} l_1 &= \sqrt{(x - a \cos(\theta))^2 + (y - a \sin(\theta))^2} \\ l_2 &= \sqrt{(x - b + a \cos(\theta))^2 + (y + a \sin(\theta))^2} \end{aligned} \quad (3.3)$$

Furthermore, the other parameters are derived as follows

$$\begin{aligned} \cos(\alpha_1) &= \frac{x - a \cos(\theta)}{l_1}, & \sin(\alpha_1) &= \frac{y - a \sin(\theta)}{l_1}, & \hat{s}_1 &= \begin{bmatrix} \cos(\alpha_1) \\ \sin(\alpha_1) \end{bmatrix}, \\ \cos(\alpha_2) &= \frac{x - b + a \cos(\theta)}{l_2}, & \sin(\alpha_2) &= \frac{y + a \sin(\theta)}{l_2}, & \hat{s}_2 &= \begin{bmatrix} \cos(\alpha_2) \\ \sin(\alpha_2) \end{bmatrix}. \end{aligned} \quad (3.4)$$

In order to solve the forward kinematic problem, it is clear that two variables (l_1, l_2) are known and three variables (x, y, θ) should be determined. This problem has infinite solution since, as indicated in (3.3), the number of unknown variables is more than the number of equations. Actually, the reason why the robot is underactuated is due to this point, since it may seem that the robot has two actuators with two cables and thus, it is possible to control the cables' length and guide the end-effector to the desired position. However, since forward kinematic has infinite solution, it is not possible to guarantee convergence to the desired position, and an oscillating response may be achieved. This is the fact reported in [121] and can be seen in the results of [17].

3.1.2 Jacobian and Dynamic Analysis

In CDRs, the relation between the velocity of end-effector and joints is expressed by $\dot{\mathbf{L}} = \mathbf{J}_a(\mathbf{X})\dot{\mathbf{X}}$ in which $\mathbf{J}_a(\mathbf{X})$ is the Jacobian matrix of the robot, and $\mathbf{L} = [l_1, \dots, l_m]^T$ denotes the cables' length. To compute the Jacobian matrix, we should differentiate the

inverse kinematic with respect to time. Dynamic equations are simply derived via Newton-Euler formula by this assumption that the cables are mass-less infinite stiff.

Time derivative of (3.1) is

$$\dot{\mathbf{p}} = \mathbf{v} = l_1 \dot{\hat{\mathbf{s}}}_1 + \dot{l}_1 \hat{\mathbf{s}}_1 - \dot{\mathbf{E}}_1 = l_2 \dot{\hat{\mathbf{s}}}_2 + \dot{l}_2 \hat{\mathbf{s}}_2 - \dot{\mathbf{E}}_2, \quad (3.5)$$

in which $\dot{\hat{\mathbf{s}}}_i$ is proportional to $\dot{\alpha}_i$ with the direction $\hat{\mathbf{k}} = [0, 0, 1]^T$. Similarly, $\dot{\hat{\mathbf{s}}}_i$ is proportional to $\dot{\theta}$ with the direction $\hat{\mathbf{k}} \times \mathbf{E}_i$. Thus, (3.5) is rewritten in the following form

$$\begin{aligned} \dot{l}_1 \hat{\mathbf{s}}_1 &= \mathbf{v} - l_1 \dot{\alpha}_1 \hat{\mathbf{k}} + \dot{\theta} (\hat{\mathbf{k}} \times \mathbf{E}_1) \\ \dot{l}_2 \hat{\mathbf{s}}_2 &= \mathbf{v} - l_2 \dot{\alpha}_2 \hat{\mathbf{k}} + \dot{\theta} (\hat{\mathbf{k}} \times \mathbf{E}_2) \end{aligned} \quad (3.6)$$

Now dot product the above equations in $\hat{\mathbf{s}}_1$ and $\hat{\mathbf{s}}_2$, respectively. it yields

$$\begin{aligned} \dot{l}_1 &= \mathbf{v} \cdot \hat{\mathbf{s}}_1 + \dot{\theta} \hat{\mathbf{k}} \cdot (\mathbf{E}_1 \times \hat{\mathbf{s}}_1) \\ \dot{l}_2 &= \mathbf{v} \cdot \hat{\mathbf{s}}_2 + \dot{\theta} \hat{\mathbf{k}} \cdot (\mathbf{E}_2 \times \hat{\mathbf{s}}_2) \end{aligned} \quad (3.7)$$

This equation can be represented in the following form

$$\begin{aligned} \begin{bmatrix} \dot{l}_1 \\ \dot{l}_2 \end{bmatrix} &= \mathbf{J}_a(\mathbf{X}) \dot{\mathbf{X}}, \quad \mathbf{X} = \begin{bmatrix} x \\ y \\ \theta \end{bmatrix}, \\ \mathbf{J}_a(\mathbf{X}) &= \begin{bmatrix} \frac{x-a \cos(\theta)}{l_1} & \frac{y-a \sin(\theta)}{l_1} & -\cos(\theta) \frac{y-a \sin(\theta)}{l_1} + \sin(\theta) \frac{x-a \cos(\theta)}{l_1} \\ \frac{x-b+a \cos(\theta)}{l_2} & \frac{y+a \sin(\theta)}{l_2} & \cos(\theta) \frac{y+a \sin(\theta)}{l_2} - \sin(\theta) \frac{x-b+a \cos(\theta)}{l_2} \end{bmatrix} \end{aligned} \quad (3.8)$$

Dynamic equations of parallel robots in Euler-Lagrange formulation are as follows [2]

$$\mathbf{M}(\mathbf{X}) \ddot{\mathbf{X}} + \mathbf{C}(\mathbf{X}, \dot{\mathbf{X}}) \dot{\mathbf{X}} + \mathcal{G}(\mathbf{X}) = \mathbf{F} = -\mathbf{J}_a^T(\mathbf{X}) \boldsymbol{\tau} \quad (3.9)$$

Invoking [15], the dynamic parameters are

$$\mathbf{M} = \begin{bmatrix} m & 0 & 0 \\ 0 & m & 0 \\ 0 & 0 & I \end{bmatrix}, \quad \mathbf{C} = \mathbf{0}, \quad \mathcal{G} = \begin{bmatrix} 0 \\ mg \\ 0 \end{bmatrix}, \quad (3.10)$$

in which \mathbf{C} denotes the Coriolis and Centrifugal terms, $\mathcal{G} = \nabla_{\mathbf{q}} V$ is the gravity force/torque, and m and I are mass and moment of inertia of the end-effector¹. Furthermore, it is possible to represent the dynamic equations in PH form (2.9) with the following parameters

$$H = \frac{1}{2} \mathbf{p}^T \mathbf{M}^{-1} \mathbf{p} + mgy, \quad \mathbf{G} = -\mathbf{J}_a^T, \quad \mathbf{q} = \mathbf{X}, \quad \mathbf{p} = \mathbf{M} \dot{\mathbf{X}}. \quad (3.11)$$

3.1.3 Equilibrium Points

First, the method of calculating equilibrium points is explained. Then, the equilibrium points of the system are calculated.

For a general system with the equations

$$\dot{\mathbf{x}} = \mathbf{f}(\mathbf{x}) + \mathbf{g}(\mathbf{x}) \mathbf{u},$$

¹Note that in this thesis the input mapping matrix and gravity force/torque are shown by \mathbf{G} and \mathcal{G} , respectively.

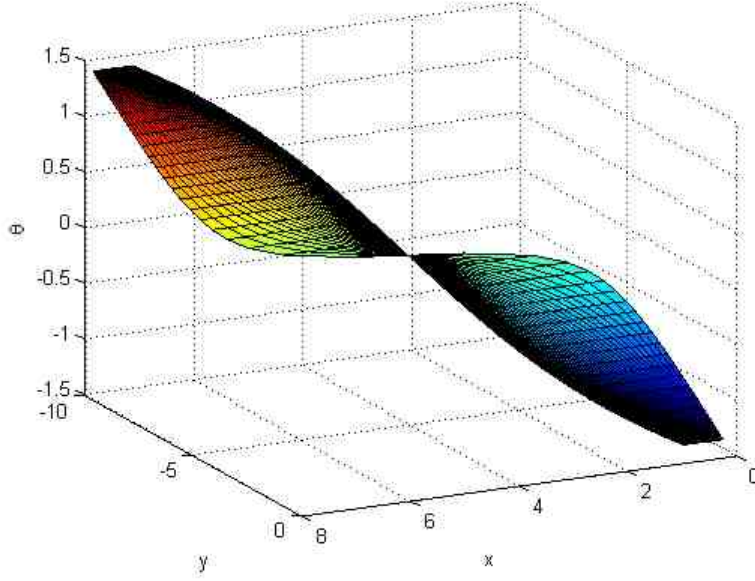


Figure 3.2: Feasible equilibrium points of the planar UCDR with $a = 0.25, b = 8$.

the equilibrium points are derived from $\mathbf{g}^\perp(\mathbf{x})\mathbf{f}(\mathbf{x}) = 0$ with \mathbf{g}^\perp as the left annihilator of \mathbf{g} . Note that $\mathbf{f}(\mathbf{x}) = 0$ denotes equilibrium points with $\mathbf{u} = 0$. The other points required a constant input.

In mechanical systems, $\mathbf{f}(\mathbf{x})$ includes position and velocity-dependent terms. Velocity is equal to zero in equilibrium points. Based on this explanations, equilibrium points of a mechanical system with dynamic equations (2.9) and (3.9) are derived from the following equation

$$\mathbf{G}^\perp \nabla_q H = \mathbf{G}^\perp \nabla_q V = \mathbf{G}^\perp \mathcal{G} = 0 \quad (3.12)$$

Since in CDRs the gravity force \mathcal{G} is constant, they have not an equilibrium point with $\mathbf{u} = 0$. This is compatible with the nature of CDRs since the robot falls without the input due to gravity.

Now the equilibrium points of the robot with dynamic parameters (3.11) are calculated. Since the dimension of \mathbf{G} is 3×2 , \mathbf{G}^\perp is a vector computed by cross product of the columns of \mathbf{G} as follows

$$\mathbf{G}^{\perp T} = \begin{bmatrix} 2 \cos(\theta)y^2 - 2 \sin(\theta)xy + by \sin(\theta) - ab \sin^2(\theta) \\ -2xy \cos(\theta) + by \cos(\theta) + ab \sin(\theta) \cos(\theta) + 2x^2 \sin(\theta) - 2bx \sin(\theta) \\ 2ax \sin(\theta) - 2ay \cos(\theta) + by - ab \sin(\theta) \end{bmatrix} \quad (3.13)$$

The equilibrium points based on $\mathcal{G}(\mathbf{X})$ given in (3.10) are on the following manifold

$$-2xy \cos(\theta) + by \cos(\theta) + ab \sin(\theta) \cos(\theta) + 2x^2 \sin(\theta) - 2bx \sin(\theta) = 0. \quad (3.14)$$

This manifold is shown in Fig. 3.2 with $a = 0.25, b = 8$. Note that all of the points in (3.14) are not feasible since due to the nature of the system, the static workspace of the robot is restricted to $0 < x < 8, y < 0$ and $-\frac{\pi}{2} < \theta < \frac{\pi}{2}$. Thus, Fig. 3.2 shows the feasible workspace of the robot which is equivalent with static workspace of the robot. As indicated in this figure, if the robot is close to the anchor points (i.e. $x \approx 0$ or $x \approx b$), θ is also close to its

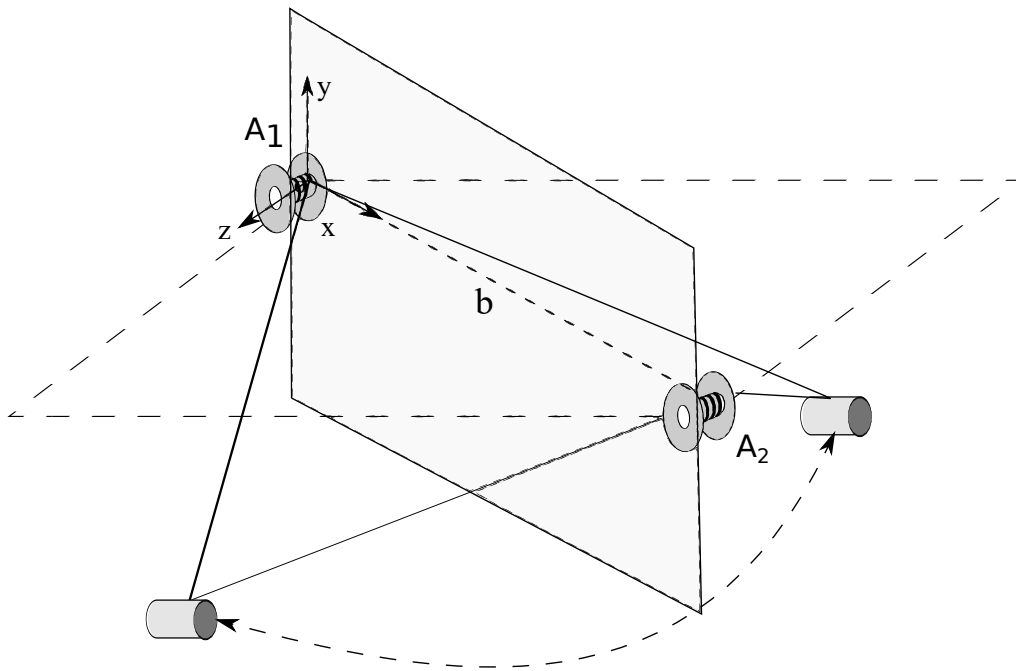


Figure 3.3: Schematic of the spatial underactuated cable-driven robot.

boundary values (i.e. $\theta \approx -\frac{\pi}{2}$ or $\theta \approx \frac{\theta}{2}$). Furthermore, if $x = \frac{b}{2}$, then θ is equal to zero and y is arbitrary. These are verified through a physical point of view to the system. Note that in [123] the equilibrium points of the robot are computed based on a geometric point of view that coincides with (3.14).

3.2 Spatial Robot

Similar to the previous case, the robot consists of a mass suspended from two cables. However, the cables are attached to a unique point of the end-effector; thus, its rotation is negligible. But instead, the end-effector has out-of-plane motion. Hence, the robot is underactuated with three translational degrees of freedom and two actuators. The schematic of the mechanism is depicted in Fig. 3.3. The center of coordinate is located on one of the anchor points, X axis is in the direction of the anchor points, and Y axis is upward. $[x, y, \theta]^T$ denotes the position of end-effector, and l_1 and l_2 are the cables' length. It is common in planar suspended CDRs to use a vertical platform to prevent out-of-plane motions. Therefore, prevention from this oscillations by controller design is the aim. Furthermore, the proposed controller is suitable for a 3-DOF spatial CDR to stabilize it when a failure occurs in an actuator, or one of the cables is torn out.

3.2.1 Kinematic Analysis

The loop-closure equation is

$$\mathbf{X} = l_1 \hat{\mathbf{s}}_1 = b\hat{\mathbf{i}} + l_2 \hat{\mathbf{s}}_2, \quad (3.15)$$

in which $\mathbf{X} = [x, y, z]^T$, $\hat{\mathbf{s}}_1$ and $\hat{\mathbf{s}}_2$ denote the direction of the cables, and $\hat{\mathbf{i}} = [1, 0, 0]^T$. Inverse kinematic is derived from (3.15) as follows

$$l_1 = \sqrt{x^2 + y^2 + z^2}, \quad l_2 = \sqrt{(x-b)^2 + y^2 + z^2}, \quad (3.16)$$

and the direction of cables are

$$\hat{\mathbf{s}}_1 = \frac{1}{l_1} \mathbf{X} = \begin{bmatrix} \frac{x}{l_1} \\ \frac{y}{l_1} \\ \frac{z}{l_1} \end{bmatrix}, \quad \hat{\mathbf{s}}_2 = \frac{1}{l_2} (\mathbf{X} - b\hat{\mathbf{i}}) = \begin{bmatrix} \frac{x-b}{l_2} \\ \frac{y}{l_2} \\ \frac{z}{l_2} \end{bmatrix}, \quad (3.17)$$

with b as the distance between anchor points. Forward kinematic has infinite solution due to fewer number of equations than the number of unknowns.

3.2.2 Jacobian and Dynamic Analysis

In order to derive the Jacobian matrix, it is required to differentiate (3.15) respect to time

$$\dot{\mathbf{X}} = \dot{l}_1 \hat{\mathbf{s}}_1 + l_1 \dot{\hat{\mathbf{s}}}_1 = \dot{l}_2 \hat{\mathbf{s}}_2 + l_2 \dot{\hat{\mathbf{s}}}_2 \quad (3.18)$$

Dot product (3.18) in $\hat{\mathbf{s}}_1$ and $\hat{\mathbf{s}}_2$, yields

$$\dot{l}_1 = \hat{\mathbf{s}}_1 \cdot \dot{\mathbf{X}}, \quad \dot{l}_2 = \hat{\mathbf{s}}_2 \cdot \dot{\mathbf{X}}, \quad (3.19)$$

where $\hat{\mathbf{s}}_1 \cdot \dot{\hat{\mathbf{s}}}_1 = \hat{\mathbf{s}}_2 \cdot \dot{\hat{\mathbf{s}}}_2 = 0$ was used. Therefore, the Jacobian matrix is

$$\mathbf{J}_a(\mathbf{X}) = \begin{bmatrix} \frac{x}{l_1} & \frac{y}{l_1} & \frac{z}{l_1} \\ \frac{x-b}{l_2} & \frac{y}{l_2} & \frac{z}{l_2} \end{bmatrix}. \quad (3.20)$$

Dynamic equations of the robot is in the form (3.9) with the following parameters

$$\mathbf{M} = \begin{bmatrix} m & 0 & 0 \\ 0 & m & 0 \\ 0 & 0 & m \end{bmatrix} \quad \mathbf{C} = \mathbf{0} \quad \mathcal{G} = \begin{bmatrix} 0 \\ mg \\ 0 \end{bmatrix}, \quad (3.21)$$

with m as the mass of end-effector. Note that it is also possible to represent it in PH form (2.9) with the following parameters

$$H = \frac{1}{2} \mathbf{p}^T \mathbf{M}^{-1} \mathbf{p} + mgy, \quad \mathbf{G} = -\mathbf{J}_a^T, \quad \mathbf{q} = \mathbf{X}, \quad \mathbf{p} = \mathbf{M} \dot{\mathbf{X}}. \quad (3.22)$$

3.2.3 Equilibrium Points

Based on the explanations in section 3.1.3, we should calculate $\mathbf{G}^\perp \mathcal{G} = 0$. Since the dimension of \mathbf{G} is 3×2 , \mathbf{G}^\perp is derived easily as follows

$$\mathbf{G}^\perp(\mathbf{X}) = [0 \quad -bz \quad by] \quad (3.23)$$

The equilibrium points of the robot are a subset of the following manifold

$$\mathbf{G}^\perp \mathcal{G} = -mgbz. \quad (3.24)$$

Therefore, the feasible equilibrium points are in the plane $z = 0$ with $0 < x < b$ and $y < 0$ which is equivalent to static workspace of the robot. This coincides with the nature of the

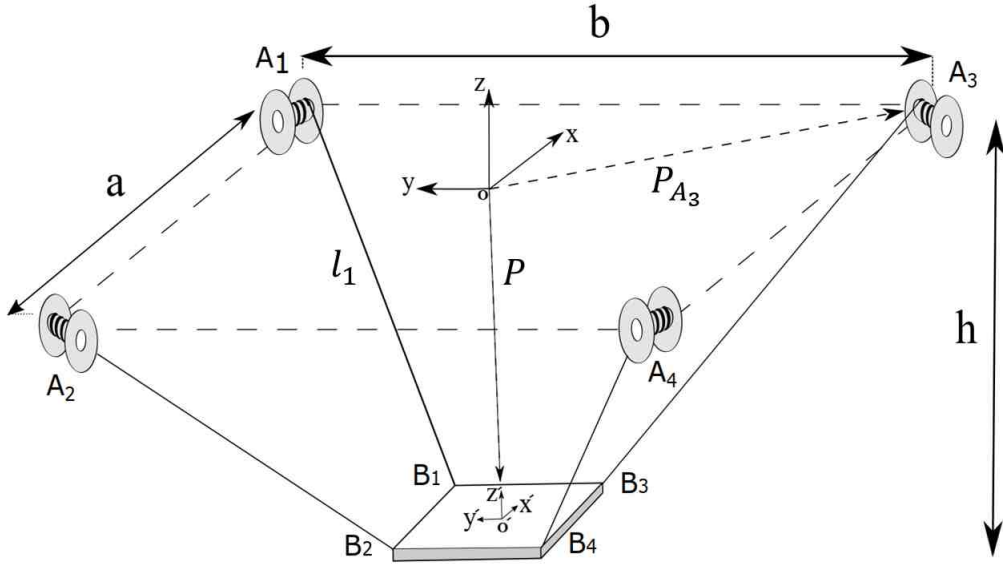


Figure 3.4: Schematic of a 6-DOF underactuated cable-driven robot with four actuators.

robot since a mass is suspended from two anchor points.

3.3 Spidercam

As explained in detail in chapter 1, spidercam is an UCDR with four actuators and 6-DOF. The robot consists of a suspended mass from four cables that the position and orientation of the end-effector are controlled via the cables' length. Fig. 3.4 shows a schematic of a spidercam. In addition to the fixed frame, a frame is attached to the center of mass of the end-effector. \mathbf{P}_{A_i} s and \mathbf{P}_{B_i} s denote the position of anchor points and attachment of cables to the end-effector represented in fixed frame and moving frame, respectively. By this means, the position of \mathbf{B}_i s are constant in the moving frame and can be represented in the fixed frame using rotation matrix \mathbf{R}_m .

3.3.1 Kinematic Analysis

The loop-closure equation of this robot is

$$\mathbf{P} = \mathbf{P}_{A_i} + l_i \hat{\mathbf{s}}_i - \mathbf{R}_m \mathbf{B}_i, \quad \text{for } i = 1, \dots, 4 \quad (3.25)$$

in which $\mathbf{P} = [x, y, z]^T$ denotes the position of center of mass of the end-effector, l_i s are the cables' length and $\hat{\mathbf{s}}_i$ s are unit vectors denoting the direction of the cables. In order to compute inverse kinematic, (3.25) is rewritten in the following form

$$l_i \hat{\mathbf{s}}_i = \mathbf{P} - \mathbf{P}_{A_i} + \mathbf{R}_m \mathbf{B}_i, \quad \text{for } i = 1, \dots, 4 \quad (3.26)$$

Now by multiplying both sides to its transpose, the following equation is derived

$$\begin{aligned} l_i^2 \hat{\mathbf{s}}_i^T \hat{\mathbf{s}}_i = l_i^2 &= (\mathbf{P} - \mathbf{P}_{A_i} + \mathbf{R}_m \mathbf{P}_{B_i})^T (\mathbf{P} - \mathbf{P}_{A_i} + \mathbf{R}_m \mathbf{P}_{B_i}) = \mathbf{P}^T \mathbf{P} - 2\mathbf{P}^T \mathbf{P}_{A_i} \\ &+ 2\mathbf{P}^T \mathbf{R}_m \mathbf{P}_{B_i} + \mathbf{P}_{A_i}^T \mathbf{P}_{A_i} - \mathbf{P}_{A_i}^T \mathbf{R}_m \mathbf{P}_{B_i} + \mathbf{P}_{B_i}^T \mathbf{P}_{B_i}, \quad \text{for } i = 1, \dots, 4 \end{aligned}$$

Therefore, inverse kinematic is

$$l_i = \sqrt{\mathbf{P}^T \mathbf{P} - 2\mathbf{P}^T \mathbf{P}_{A_i} + 2\mathbf{P}^T \mathbf{R}_m \mathbf{P}_{B_i} + \mathbf{P}_{A_i}^T \mathbf{P}_{A_i} - \mathbf{P}_{A_i}^T \mathbf{R}_m \mathbf{P}_{B_i} + \mathbf{P}_{B_i}^T \mathbf{P}_{B_i}} \quad \text{for } i = 1, \dots, 4 \quad (3.27)$$

in which the relation $\mathbf{R}_m^T = \mathbf{R}_m^{-1}$ was used. Note that the rotation matrix can be represented based on different methods such as Euler angles, screw axis, etc. [2]. Similar to previous cases, forward kinematic is not solvable due to fewer number of equations than unknowns.

3.3.2 Jacobian and Dynamic Analysis

In order to derive the Jacobian matrix, we should differentiate (3.26) with respect to time. It yields

$$\dot{l}_i \hat{\mathbf{s}}_i + l_i \dot{\hat{\mathbf{s}}}_i = \dot{\mathbf{P}} + \dot{\mathbf{R}}_m \mathbf{B}_i, \quad \text{for } i = 1, \dots, 4 \quad (3.28)$$

Dot product of (3.28) to $\hat{\mathbf{s}}_i$ yields

$$\dot{l}_i = \hat{\mathbf{s}}_i \cdot \dot{\mathbf{P}} + \hat{\mathbf{s}}_i \cdot \boldsymbol{\omega}_\times \mathbf{R}_m \mathbf{B}_i, \quad \text{for } i = 1, \dots, 4 \quad (3.29)$$

in which $\boldsymbol{\omega}$ denotes angular velocity and $\boldsymbol{\omega}_\times$ is matrix representation of the vector $\boldsymbol{\omega}$ as follows

$$\boldsymbol{\omega}_\times = \begin{bmatrix} 0 & -\omega_3 & \omega_2 \\ \omega_3 & 0 & -\omega_1 \\ -\omega_2 & \omega_1 & 0 \end{bmatrix}, \quad \boldsymbol{\omega} = [\omega_1, \omega_2, \omega_3]^T.$$

Finally, the Jacobian matrix is derived as follows

$$\mathbf{J}_a(\mathbf{X}) = \begin{bmatrix} \hat{\mathbf{s}}_1 & \hat{\mathbf{s}}_2 & \hat{\mathbf{s}}_3 & \hat{\mathbf{s}}_4 \\ \mathbf{R}_m \mathbf{B}_1 \times \hat{\mathbf{s}}_1 & \mathbf{R}_m \mathbf{B}_2 \times \hat{\mathbf{s}}_2 & \mathbf{R}_m \mathbf{B}_3 \times \hat{\mathbf{s}}_3 & \mathbf{R}_m \mathbf{B}_4 \times \hat{\mathbf{s}}_4 \end{bmatrix}^T \quad (3.30)$$

where we used this fact that $a \cdot (b \times c) = b \cdot (c \times a)$.

Invoking [124], dynamic parameters of the robot are easily derived in PH form (2.9) as follows

$$\mathbf{M} = \begin{bmatrix} m\mathbf{I}_3 & \mathbf{0}_{3 \times 3} \\ \mathbf{0}_{3 \times 3} & \mathbf{I} \end{bmatrix}, \quad V = mgy, \quad \mathbf{G} = -\mathbf{J}_a^T, \quad \mathbf{q} = \mathbf{X}, \quad \mathbf{p} = \mathbf{M}\dot{\mathbf{X}}, \quad (3.31)$$

with m and \mathbf{I} as the mass and moment of inertia of the end-effector, respectively.

3.3.3 Equilibrium Points

The dimension of \mathbf{G} is 6×4 . Hence, computing \mathbf{G}^\perp is not straightforward. Therefore, it may be derived for a particular case. Here, it should be noted that as explained in [121], the equilibrium points of an UCDR are natural. In other words, they are open-loop stable and the robot has a oscillatory response around them.

3.4 ARAS Cable-Driven Robot

Since in this thesis, the proposed controllers are implemented on some CDRs, the robots are introduced here.

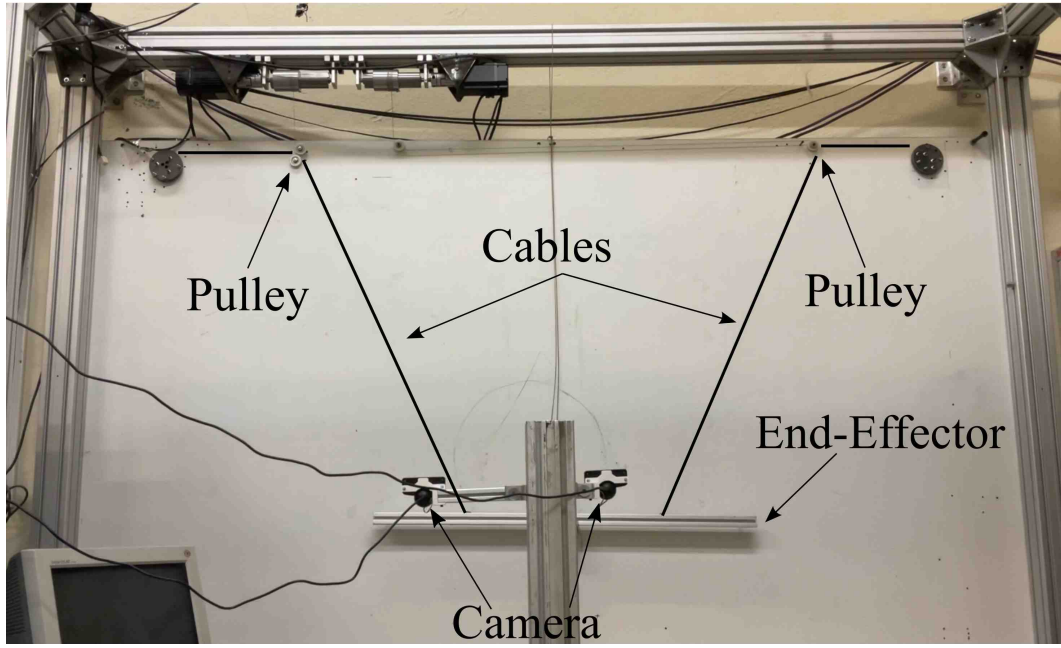


Figure 3.5: Different components of ARAS underactuated cable-driven robot

3.4.1 ARAS Underactuated Cable-Driven Robot

Fig. 3.5 illustrates ARAS planar UCDR. A safety cable is used to confine the workspace of the robot to prevent from dangerous problems. Furthermore, two cameras are used to detect the position of the end-effector. Additionally, the cables' length are measured through incremental encoders and knowing the initial lengths. Using x, y and l_1, l_2 , the value of θ should be calculated analytically. For this purpose, define the following auxiliary variables

$$\begin{aligned}
 \gamma_1 &= x^2 + y^2 + a^2 - l_2^2, & \gamma_2 &= l_1^2 - x^2 - b^2 - y^2 - a^2 + 2bx, \\
 \alpha_1 &= \alpha_2 = 2ay, & \beta_1 &= 2ax, & \beta_2 &= 2ax - 2ab, \\
 A_1 &= \alpha_1^2 + \beta_1^2, & B_1 &= -2\alpha_1\gamma_1, & C_1 &= \gamma_1^2 - \beta_1^2, \\
 A_2 &= \alpha_2^2 + \beta_2^2, & B_2 &= -2\alpha_2\gamma_2, & C_2 &= \gamma_2^2 - \beta_2^2.
 \end{aligned}$$

θ is derived from

$$\theta = \frac{\arcsin\left(\frac{-B_1 + \sqrt{B_1^2 - 4A_1C_1}}{2A_1}\right) + \arcsin\left(\frac{-B_2 - \sqrt{B_2^2 - 4A_2C_2}}{2A_2}\right)}{2} \quad (3.32)$$

The distance between anchor points is $b = 1.49$, the length of end-effector is $2a = 0.48$ and its mass is $1.6Kg$. Implementation results on this robot are proposed in Section 7.2.

3.4.2 ARAS Cam

ARAS cam is generally a 6-DOF CDR with four cables. Since the attachment point of the cables to end-effector is a point, usually it is modeled as a 3-DOF robot by neglecting the rotational variables. In this thesis, we merely utilize three cables of the robot that leads to a fully actuated CRD. The schematic of the setup is shown in Fig. 3.6. Furthermore, a picture of the robot is depicted in Fig. 3.7.

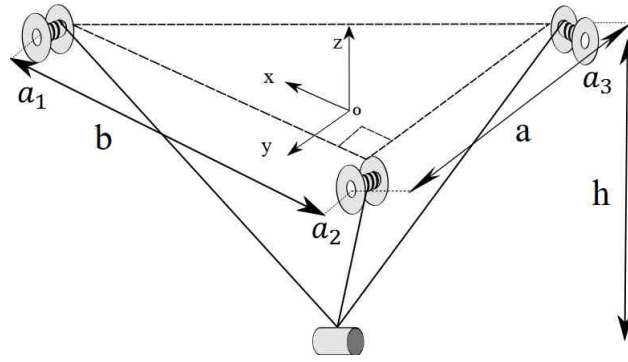


Figure 3.6: Schematic of a 3-DOF suspended CDR.

Dynamic formulation of the robot is represented by equation (2.9) with [125],

$$\mathbf{M} = m\mathbf{I}_3, \quad V = mgz, \quad \mathbf{q} = [x, y, z]^T, \quad \mathbf{G} = \begin{bmatrix} \frac{x_{a1}-x}{l_1} & \frac{y_{a1}-y}{l_1} & \frac{z_{a1}-z}{l_1} \\ \frac{x_{a2}-x}{l_2} & \frac{y_{a2}-y}{l_2} & \frac{z_{a2}-z}{l_2} \\ \frac{x_{a3}-x}{l_3} & \frac{y_{a3}-y}{l_3} & \frac{z_{a3}-z}{l_3} \end{bmatrix}^T$$

Here, \mathbf{q} denotes the position of end-effector and l_i s are the length of the cables given by

$$l_1 = \sqrt{(x - x_{a1})^2 + (y - y_{a1})^2 + (z - z_{a1})^2}$$

$$l_2 = \sqrt{(x - x_{a2})^2 + (y - y_{a2})^2 + (z - z_{a2})^2}$$

$$l_3 = \sqrt{(x - x_{a3})^2 + (y - y_{a3})^2 + (z - z_{a3})^2}$$

Kinematic parameters of this robot are

$$x_{a1} = x_{a2} = -x_{a3} = b/2 = 3.56/2$$

$$y_{a1} = -y_{a2} = -y_{a3} = a/2 = 7.05/2$$

$$z_{a1} = z_{a2} = z_{a3} = h = 4.26,$$

Mass of end-effector payload is $m = 4.5Kg$. The readers are referred to [39] for further details.

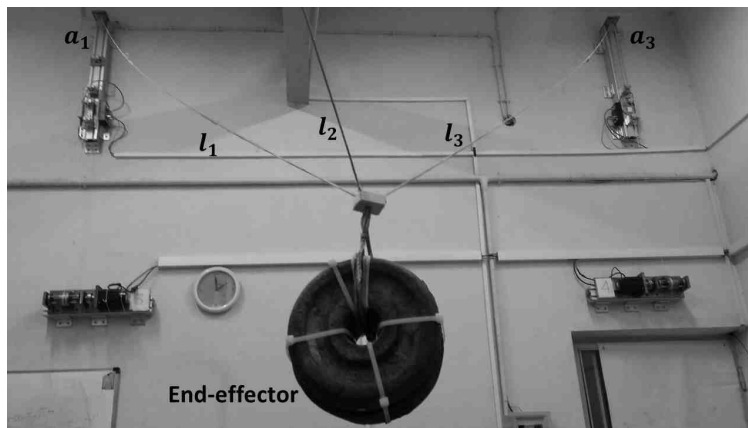


Figure 3.7: ARAS cable driven robot.

3.5 Conclusion

In this chapter, the kinematic, Jacobian, and dynamic equations of three UCDRs were proposed. It should be noted that although the main focus of this thesis is UCDRs, especially the planar and spatial robots, in the following chapters, other benchmark systems are also considered.

Chapter 4

Solution of Matching Equations

In this chapter, we focus on the PDEs arisen from IDA-PBC approach. Three different methods are proposed to solve them. The first method is based on transforming a PDE to some Pfaffian differential equations. By this means, the matching equations of several systems will be solved. Furthermore, the potential energy shaping of underactuated parallel robots will be accomplished. By this means, it is possible to stabilize all of the UCDRs and natural equilibrium points of underactuated parallel robots. Another method is specified to solve kinetic energy PDE of UaSs with underactuation degree one and constant input mapping matrix. Finally, a comment on simultaneous IDA-PBC for mechanical systems is proposed. It will be shown that SIDA-PBC does not simplify the matching equations.

4.1 Pfaffian Differential Equations

Solving the PDEs is the challenging part of IDA-PBC approach that restricts its applications. Although different numerical methods have been proposed to derive an approximate solution of a PDE with boundary condition, here, the matching equations do not have a boundary condition. Furthermore, due to the satisfaction of constraint (2.4) and the fact that an approximate solution may destroy the proof of stability, an exact general solution of the PDEs is required. A method that can derive the general solution of a nonlinear PDE has been proposed in [19]. In this method, a PDE is replaced by some Pfaffian differential equations. Generally, a Pfaffian differential equation is in the following form

$$\sum_{i=1}^n f_i(x_1, \dots, x_n) dx_i = 0.$$

It has been shown that if $\phi_i(x_1, \dots, x_n, z) = c_i, i \in \{1, \dots, n\}$ are independent solutions of the following equations

$$\frac{dx_1}{P_1} = \frac{dx_2}{P_2} = \dots = \frac{dx_n}{P_n} = \frac{dz}{R}, \quad (4.1)$$

then $\Phi(\phi_1, \dots, \phi_n)$ with Φ an arbitrary function forms the general solution of the following (nonlinear) PDE

$$P_1 \frac{\partial z}{\partial x_1} + P_2 \frac{\partial z}{\partial x_2} + \dots + P_n \frac{\partial z}{\partial x_n} = R, \quad (4.2)$$

where P_i s and R are function of independent variables x_1, \dots, x_n and z . Note that since the PDE (4.2) is generally nonlinear, the solution is implicit.

Solving the Pfaffian equations (4.1) is still a cumbersome task while it is easier than that of the corresponding PDE. However, for a Pfaffian differential equation with $n = 3$, i.e.

$$Pdx_1 + Qdx_2 + Rdx_3 = 0, \quad (4.3)$$

it has been shown that if the following condition holds

$$\mathbf{X}^T \text{curl}(\mathbf{X}) = 0, \quad (4.4)$$

with $\mathbf{X} = [P, Q, R]^T$, then the problem turns to an exact differential equation which may be easily solved by direct integration. By this means, in order to solve (4.2) with $n = 3$, one may derive a Pfaffian differential equation such that condition (4.4) holds. Several methods have been proposed to solve a Pfaffian differential equation satisfying (4.4). One of these methods which is proposed in [19, Ch. 1] is summarized here.

Assume that Pfaffian equation (4.3) satisfy condition (4.4).

Stage 1: Assume that x_3 is constant. The solution of

$$Pdx_1 + Qdx_2 = 0$$

is $U(x_1, x_2, x_3) = C$. Define

$$\mu := \frac{1}{P} \frac{\partial U}{\partial x_1} = \frac{1}{Q} \frac{\partial U}{\partial x_2}$$

Stage 2: Define

$$K := \mu R - \frac{\partial U}{\partial x_3}$$

Stage 3: Parameterize K such that $K = K(U, x_3)$.

Stage 4: Solve $dU + Kdx_3 = 0$.

Stage 5: Then the solution is

$$\phi(U, x_3) = \phi(U(x_1, x_2, x_3), x_3) = C.$$

In the following, this method will be used to solve the matching equations of planar and spatial UCDR proposed in the previous chapter. More examples on several benchmark system are presented in Appendix A. Note that since this method is applicable only to a single PDE, it is not possible to solve the matching equations of spidercam. Before solving the PDEs, let us propose the following corollary.

Corollary 1. Consider PDE (4.2) and presume that P_i s and R are merely functions of independent variables x_i s. Then,

a) The functions $z - \phi_i(x_1, \dots, x_n) = c_i, i \in \{1, \dots, n-1\}$ are the homogeneous solutions of this PDE if ϕ_i s are solutions of the first $n-1$ equations (4.1).

b) Non-homogeneous solution is derived by setting the last term in (4.1) equal to other terms.

Proof. a) Presume that $\phi_i(q_1, \dots, q_n) = c_i$ are the solutions of the first $n-1$ equations in (2.1). Since this equations are independent of z ; thus, $z - \phi_i(q_1, \dots, q_n) = c_i$ are also the solutions of Pfaffian differential equations. Notice that they are homogeneous solutions of the PDE, because they satisfy the following equations which are related to homogeneous

part of PDE

$$\frac{dx_1}{P_1(x_1, \dots, x_n)} = \dots = \frac{dx_n}{P_n(x_1, \dots, x_n)} = \frac{dz}{0}$$

b) The proof of this part is clear. Non-homogeneous solution of PDE (2.2) corresponds to its special solution that depends on both the left and right-hand sides of (2.2). Hence, this is derived based on the last term of (4.1). \square

Notice that the results of this section have been published in [126].

4.1.1 Solution of Matching Equations of UCDRs

Here, first, the matching equations of the robots are computed. After this, they will be solved using Pfaffian differential equations. Note that as indicated in [127], to stabilize a natural equilibrium point of a robot, it is sufficient to solve the potential energy PDE.

Planar robot

Since the input mapping matrix \mathbf{G} proposed in (3.11) is a function of all the configuration variables, the available methods in the literature are not applicable to this system. Hence, another approach is required to derive the solution of the PDEs. First, consider kinetic energy PDE (2.16.) The first this PDE is equal to zero due to \mathbf{M} is constant. Thus, it is possible to solve it by considering a constant matrix \mathbf{M}_d . For simplicity, \mathbf{M}_d is considered equal to \mathbf{M} i.e., only potential energy is shaped. This does not limit the stability of the closed-loop system since, as indicated in [121, 123] the equilibrium points of the robot are natural and can be stabilized by only potential shaping. By this means, the potential energy PDE (2.17) yields

$$\begin{aligned} & (-2xy \cos(\theta) + by \cos(\theta) + ab \sin(\theta) \cos(\theta) + 2x^2 \sin(\theta) - 2bx \sin(\theta)) m g a \\ & = a(2 \cos(\theta) y^2 - 2 \sin(\theta) xy + by \sin(\theta) - ab \sin^2(\theta)) \frac{\partial V_d}{\partial x} \\ & + a(-2xy \cos(\theta) + by \cos(\theta) + ab \sin(\theta) \cos(\theta) + 2x^2 \sin(\theta) - 2bx \sin(\theta)) \frac{\partial V_d}{\partial y} \\ & + (2ax \sin(\theta) - 2ay \cos(\theta) + by - ab \sin(\theta)) \frac{\partial V_d}{\partial \theta}. \end{aligned} \quad (4.5)$$

PDE (4.5) is a stumbling block. In order to solve it, the proposed method based on Pfaffian differential equation is used. Hence, the corresponding Pfaffian equations are

$$\frac{dx}{G_1^\perp} = \frac{dy}{G_2^\perp} = \frac{d\theta}{G_3^\perp} = \frac{dV_d}{mgG_2^\perp}, \quad \text{with } \mathbf{G}^\perp = [G_1^\perp, G_2^\perp, G_3^\perp]. \quad (4.6)$$

The solution of linear PDE (4.5) can be separated into homogeneous and non-homogeneous parts. Invoking Corollary 1, the non-homogeneous solution V_{dn} is derived from the second and forth terms in (2.13) as $V_{dn} = mgy$. For the homogeneous solution we should solve the following equations

$$\frac{dx}{G_1^\perp} = \frac{dy}{G_2^\perp} = \frac{d\theta}{G_3^\perp} \quad (4.7)$$

First, it is tried to find a Pfaffian differential equation in the following form:

$$P_1(\theta)dx + P_2(\theta)dy + P_3(x, y, \theta)d\theta = 0, \quad (4.8)$$

such that the condition (2.12) holds. For this purpose, the following simple properties are used.

Assume that $a_1/b_1 = a_2/b_2$. Then:

- For arbitrary values $\alpha, \beta \in \mathbb{R}$ we have:

$$\frac{a_1}{b_1} = \frac{a_2}{b_2} = \frac{\alpha a_1 + \beta a_2}{\alpha b_1 + \beta b_2}.$$

- If α and β are chosen such that $\alpha b_1 + \beta b_2 = 0$, then $\alpha a_1 + \beta a_2 \equiv 0$.

In order to derive a Pfaffian differential equation in the form of (4.8), let us build a new fraction with the aim that the terms $2a \cos(\theta)y^2$ and $2x^2 \sin(\theta)$ are omitted in the denominator. This can be achieved by defining: $\cos(\theta)G_1^\perp + \cos(\theta)yG_3^\perp$ and $\sin(\theta)G_2^\perp - \sin(\theta)xG_3^\perp$, respectively. Therefore

$$\frac{\zeta_1}{\eta_1} = \frac{dx}{G_1^\perp} = \frac{dy}{G_2^\perp} = \frac{d\theta}{G_3^\perp} = \frac{dV_d}{mgG_2^\perp}$$

with

$$\begin{aligned}\zeta_1 &= \cos(\theta)dx + \sin(\theta)dy + (-\sin(\theta)x + \cos(\theta)y)d\theta, \\ \eta_1 &= \cos(\theta)G_1^\perp + \sin(\theta)G_2^\perp + (-\sin(\theta)x + \cos(\theta)y)G_3^\perp \\ &= b \cos(\theta)y^2 - b \sin(\theta)xy - abx \sin^2(\theta) + aby \sin(\theta) \cos(\theta).\end{aligned}$$

To omit $b \cos(\theta)y^2$ the following expression is defined

$$\begin{aligned}\frac{\zeta_2}{\eta_2} &= \frac{\zeta_1}{\eta_1} = \frac{dx}{G_1^\perp} = \frac{dy}{G_2^\perp} = \frac{d\theta}{G_3^\perp} = \frac{dV_d}{mgG_2^\perp} \\ \zeta_2 &= -\frac{b}{2a}dx + \zeta_1 \\ \eta_2 &= -\frac{b}{2a}G_1^\perp + \eta_1 = -\frac{b^2}{2}y \sin(\theta) + \frac{ab^2}{2} \sin^2(\theta) - abx \sin(\theta) + aby \sin(\theta) \cos(\theta).\end{aligned}$$

Finally, by defining new terms $\eta_3 = \frac{b}{2} \sin(\theta)G_3^\perp + \eta_2 = 0$, and $\zeta_3 = \frac{b}{2} \sin(\theta)d\theta + \zeta_2$, the following Pfaffian equation is obtained

$$\zeta_3 = \left(\cos(\theta) - \frac{b}{2a} \right) dx + \sin(\theta)dy + \left(-\sin(\theta)x + \cos(\theta)y + \frac{b}{2} \sin(\theta) \right) d\theta = 0. \quad (4.9)$$

By substituting (4.9) in (4.4), it is clear that this equation is integrable. The solution of (4.9) is derived easily as follows

$$\phi\left((2a \cos(\theta) - b)x + 2a \sin(\theta)y - ab \cos(\theta)\right) = c.$$

Although solving the Pfaffian equation (4.9) is not hard, let us apply the procedure proposed at the beginning of this chapter, to find the solution in a systematic manner. Note that for simplicity, (4.9) is multiplied in $4a$.

$$U\left((4a \cos(\theta) - 2b)x + 4a \sin(\theta)y\right) = C, \quad \mu = 1$$

K is derived as

$$K = R + 4a \sin(\theta)x - 4a \cos(\theta)y = 2ab \sin(\theta).$$

Finally, by using Lemma 1, the solution is given by

$$V_d = \phi\left(U - 2ab \cos(\theta)\right) = \phi\left(\left(4a \cos(\theta) - 2b\right)x + 4a \sin(\theta)y - 2ab \cos(\theta)\right).$$

To derive the other solution of (4.5), it is sufficient to derive a Pfaffian equation in the form:

$$P_1(x)dx + P_2(y)dy + P_3(\theta)d\theta = 0,$$

which is clearly integrable. For this purpose, Consider the following term

$$\begin{aligned} \frac{\xi_1}{\lambda_1} &= \frac{dx}{G_1^1} = \frac{dy}{G_2^1} = \frac{d\theta}{G_3^1} = \frac{dV_d}{mgG_2^1} \\ \xi_1 &= xdx + ydy, \\ \lambda_1 &= -abxy \sin(\theta) - a^2bx \sin^2(\theta) + aby^2 \cos(\theta) + a^2by \sin(\theta) \cos(\theta). \end{aligned}$$

Two terms in λ_1 can be eliminated by defining

$$\begin{aligned} \frac{\xi_2}{\lambda_2} &= \frac{\xi_1}{\lambda_1} = \frac{dx}{G_1^1} = \frac{dy}{G_2^1} = \frac{d\theta}{G_3^1} = \frac{dV_d}{mgG_2^1} \\ \xi_2 &= -\frac{b}{2}dx + \xi_1, \\ \lambda_2 &= -\frac{b}{2}G_1^1 + \lambda_1 = -a^2bx \sin^2(\theta) + a^2by \sin(\theta) \cos(\theta) - \frac{ab^2}{2}y \sin(\theta) + \frac{ab^2}{2} \sin^2(\theta) \end{aligned}$$

Finally, by defining, $\lambda_3 = \frac{ab}{2} \sin(\theta)G_3^1 + \lambda_2 = 0$, the following Pfaffian differential equation is resulted

$$\xi_3 = \left(x - \frac{b}{2}\right)dx + ydy + \frac{ab}{2} \sin(\theta)d\theta = 0.$$

It is a simple equation with the following solution

$$\phi\left(x^2 + y^2 - bx - ab \cos(\theta)\right) = c.$$

Thus, the solution of PDE (4.5) is

$$\begin{aligned} V_d &= V_{dn} + V_{dh} = mgy + \phi\left(\left(2a \cos(\theta) - b\right)x + 2a \sin(\theta)y - ab \cos(\theta), \right. \\ &\quad \left. x^2 + y^2 - bx - ab \cos(\theta)\right), \end{aligned} \tag{4.10}$$

where ϕ is an arbitrary function.

Remark 1. The PDE (4.5) at the first look is seriously a challenging problem. The situation is more crucial when it is seen that neither it is matched with the conditions proposed in the literature in this field nor solvable with the available software. However, by transforming it to the corresponding Pfaffian differential equations, the general solution was derived. Note that although it is not straightforward to derive an equation satisfying (4.4), the structure of equations helps us to facilitate solving this problem.

Spatial robot

The structure of equations of this robot is similar to planar robot since matrix \mathbf{G} is a function of all of the configuration variables. Therefore, the proposed methods in literature are not directly usable. In order to design an IDA-PBC controller, it is possible to shape only the potential energy. By this means, the potential energy PDE (2.17) with the

dynamical parameters (3.22) is in the following form

$$-mgz = -z \frac{\partial V_d}{\partial y} + y \frac{\partial V_d}{\partial z}.$$

This is a simple PDE with the following solution

$$V_d = mgy + \phi(x, y^2 + z^2). \quad (4.11)$$

Unfortunately, as indicated in the simulation results in chapter 7, the response of this controller is prolonged in z direction. In order to rectify this issue, total energy shaping is required. In the following, two controllers based on total energy shaping are presented.

Since the inertia matrix of this robot is constant, a trivial solution of kinetic energy PDE (2.16) is a constant desired inertia matrix. Hence, the structure of \mathbf{M}_d is in the following form

$$\mathbf{M}_d = \begin{bmatrix} m & 0 & 0 \\ 0 & m & 0 \\ 0 & 0 & \mathbf{m} \end{bmatrix} \quad (4.12)$$

with \mathbf{m} being an arbitrary positive constant. The reason why this structure is considered is improving the response in z direction. Replacing (4.12) in potential energy PDE (2.17) yields

$$-mgz = -z \frac{\partial V_d}{\partial y} + y \frac{\partial V_d}{\partial z}.$$

The solution of this PDE is

$$V_d = mgy + \phi(x, y^2 + \frac{m}{\mathbf{m}}z^2). \quad (4.13)$$

Although the response of this controller is better than the previous one, in the sequel IDA-PBC with state-dependent \mathbf{M}_d is proposed. The general form of kinetic energy PDE introduced in (2.16) for this system is

$$\mathbf{G}^\perp \{-m^{-1} \mathbf{M}_d \nabla_{\mathbf{q}} (\mathbf{p}^T \mathbf{M}_d^{-1} \mathbf{p}) + 2 \mathbf{J}_2 \mathbf{M}_d^{-1} \mathbf{p}\} = 0, \quad \mathbf{G}^\perp = [0, -bz, by].$$

As explained in [74], the general solution of kinetic energy PDE is derived from the following equation

$$\sum_{i=1}^n \gamma_i(\mathbf{q}) \frac{d\mathbf{M}_d^{-1}}{dq_i} = -[\mathcal{J}(\mathbf{q}) \mathbf{A}^T(\mathbf{q}) + \mathbf{A}(\mathbf{q}) \mathcal{J}^T(\mathbf{q})]$$

in which

$$\mathbf{J}_2 = \begin{bmatrix} 0 & \tilde{\mathbf{p}}_1^T \boldsymbol{\alpha} & \tilde{\mathbf{p}}_2^T \boldsymbol{\alpha} & \dots & \tilde{\mathbf{p}}_{n-1}^T \boldsymbol{\alpha} \\ -\tilde{\mathbf{p}}_1^T \boldsymbol{\alpha} & 0 & \tilde{\mathbf{p}}_n^T \boldsymbol{\alpha} & \dots & \tilde{\mathbf{p}}_{2n-3}^T \boldsymbol{\alpha} \\ \vdots & \vdots & \vdots & \ddots & \vdots \\ -\tilde{\mathbf{p}}_{n-1}^T \boldsymbol{\alpha} & -\tilde{\mathbf{p}}_{2n-3}^T \boldsymbol{\alpha} & \dots & & 0 \end{bmatrix}, \quad (4.14)$$

$$\tilde{\mathbf{p}} = \mathbf{M}_d^{-1} \mathbf{p}, \quad \mathcal{J} = [\mathbf{1} \boldsymbol{\alpha}; \mathbf{2} \boldsymbol{\alpha}; \dots; \mathbf{n}_0 \boldsymbol{\alpha}] \in \mathbb{R}^{n \times n_0}, \quad \gamma = \mathbf{G}^\perp \mathbf{M}_d \mathbf{M}^{-1},$$

$$\mathbf{A} = -[\mathbf{W}_1 (\mathbf{G}^\perp)^T, \dots, \mathbf{W}_{n_0} (\mathbf{G}^\perp)^T] \in \mathbb{R}^{n_0 \times n}, \quad n_0 = n(n-1)/2.$$

To define \mathbf{W}_i s, first define the (i, j) th element of the matrices $\mathbf{F}^{kl} \in \mathbb{R}^{n \times n}$ with $k, l \in \{1, \dots, n\}$ as follows

$$\mathbf{F}_{ij}^{kl} = \begin{cases} 1 & \text{if } j > i, i = k \text{ and } j = l \\ 0 & \text{otherwise} \end{cases}$$

and set $\mathbf{W}^{kl} = \mathbf{F}^{kl} - (\mathbf{F}^{kl})^T$. The matrices \mathbf{W}_i s are defined as follows

$$\mathbf{W}_1 = \mathbf{W}^{12}, \mathbf{W}_2 = \mathbf{W}^{13}, \dots, \mathbf{W}_{n_0} = \mathbf{W}^{(n-1)n}. \quad (4.15)$$

Hence, the following PDE should be solved

$$\begin{aligned} & (-zM_{d_{22}} + yM_{d_{23}}) \frac{\partial \mathbf{M}_d}{\partial y} + (-zM_{d_{23}} + yM_{d_{33}}) \frac{\partial \mathbf{M}_d}{\partial z} \\ & = m \begin{bmatrix} 2(-z {}_1\alpha_1 + y {}_2\alpha_1) & * & * \\ -z {}_2\alpha_1 + y({}_2\alpha_2 + {}_3\alpha_1) & 2y {}_3\alpha_2 & * \\ y {}_2\alpha_3 + z({}_3\alpha_1 - {}_1\alpha_3) & y {}_3\alpha_3 + z {}_3\alpha_2 & 2z {}_3\alpha_3 \end{bmatrix}, \end{aligned}$$

where ${}_i\alpha_j$ denotes j th element of the vector ${}_i\boldsymbol{\alpha}$ and the up-diagonal elements were not indicated due to symmetry of the matrix. By setting the left and right-hand sides element by element equal to each other, it is clear that $M_{d_{11}}, M_{d_{12}}, M_{d_{13}}$ are defined arbitrarily due to free terms α_{i_j} . The other terms should satisfy the following equations

$$\begin{aligned} & (-zM_{d_{22}} + yM_{d_{23}}) \frac{\partial M_{d_{22}}}{\partial y} + (-zM_{d_{23}} + yM_{d_{33}}) \frac{\partial M_{d_{22}}}{\partial z} = 2my {}_3\alpha_2, \\ & (-zM_{d_{22}} + yM_{d_{23}}) \frac{\partial M_{d_{23}}}{\partial y} + (-zM_{d_{23}} + yM_{d_{33}}) \frac{\partial M_{d_{23}}}{\partial z} = my {}_3\alpha_3 + mz {}_3\alpha_2, \\ & (-zM_{d_{22}} + yM_{d_{23}}) \frac{\partial M_{d_{33}}}{\partial y} + (-zM_{d_{23}} + yM_{d_{33}}) \frac{\partial M_{d_{33}}}{\partial z} = 2mz {}_3\alpha_3. \end{aligned} \quad (4.16)$$

It is a set of PDEs with two arbitrary functions. Thus, it is possible to convert it to a single PDE. However, there is no simple analytical solution to solve it. In the following, the proposed method is used to find the solution of (4.16). With the purpose of converting (4.16) to Pfaffian differential equations, substitute first and third equations of (4.16) in the second equation. This yields to the following equation

$$\frac{dy}{P_1} = \frac{dz}{P_2} = \frac{dM_{d_{23}}}{R} \quad (4.17)$$

with

$$\begin{aligned} P_1 &= -zM_{d_{22}} + yM_{d_{23}}, \\ P_2 &= -zM_{d_{23}} + yM_{d_{33}}, \\ R &= -\left(\frac{y}{2} \frac{\partial M_{d_{33}}}{\partial z} + \frac{z^2}{2y} \frac{\partial M_{d_{22}}}{\partial z} - \frac{y^2}{2z} \frac{\partial M_{d_{33}}}{\partial y} - \frac{z}{2} \frac{\partial M_{d_{22}}}{\partial y}\right) M_{d_{23}} \\ &+ \frac{y}{2z} \left(-zM_{d_{22}} \frac{\partial M_{d_{33}}}{\partial y} + yM_{d_{33}} \frac{\partial M_{d_{33}}}{\partial z}\right) + \frac{z}{2y} \left(-zM_{d_{22}} \frac{\partial M_{d_{22}}}{\partial y} + yM_{d_{33}} \frac{\partial M_{d_{22}}}{\partial z}\right), \end{aligned}$$

in which $M_{d_{22}}$ and $M_{d_{33}}$ are set arbitrarily by suitably defining ${}_3\alpha_2$ and ${}_3\alpha_3$. Equation

(4.17) is equivalent to the following equation

$$\frac{zdy + ydz}{-z^2M_{d22} + y^2M_{d33}} = \frac{dM_{d23}}{R} \quad (4.18)$$

Note that the left-hand side is independent of M_{d23} , while R is summation of two terms including a linear term and an independent term with respect to M_{d23} . Pfaffian equation (4.18) is easier to solve if R is independent of M_{d23} . Notice that the second term in R is fractional and may lead to non-definite M_d since z is in the denominator of the fraction and $z = 0$ is equilibrium point of the system. Hence, a suitable choice for M_{d22} and M_{d33} is

$$M_{d22} = \frac{y^2}{2} + k_1, \quad M_{d33} = \frac{z^2}{2} + k_2,$$

with $k_1, k_2 > 0$ to address the above issues and reduce the complexity of (4.18). Substitute these values in (4.18) yields

$$\frac{zdy + ydz}{k_2y^2 - k_1z^2} = \frac{dM_{d23}}{k_2y^2 - k_1z^2}$$

The solution to this simplified equation is $M_{d23} = \frac{1}{2}yz$, hence, the matrix \mathbf{M}_d is in the following form

$$\mathbf{M}_d = \begin{bmatrix} * & * & * \\ * & \frac{y^2}{2} + k_1 & \frac{1}{2}yz \\ * & \frac{1}{2}yz & \frac{z^2}{2} + k_2 \end{bmatrix} \quad (4.19)$$

in which undefined elements are designed arbitrarily. Note that these elements do not affect on potential energy PDE.

Potential energy PDE (2.17) for this robot is in the following form

$$-bmgz = bm^{-1}(-zM_{d22} + yM_{d23})\frac{\partial V_d}{\partial y} + bm^{-1}(-zM_{d23} + yM_{d33})\frac{\partial V_d}{\partial z}.$$

Replacing (4.19) in this equation, yields

$$-m^2gz = -k_1z\frac{\partial V_d}{\partial y} + k_2y\frac{\partial V_d}{\partial z}$$

This is a simple PDE, that can be solved easily by Corollary 1. The corresponding Pfaffian equations are

$$\frac{dx}{0} = \frac{dy}{-k_1z} = \frac{dz}{k_2y} = \frac{dV_d}{-m^2gz}$$

It is clear that $x = c_1$ and $k_2y^2 + k_1z^2 = c_2$ are the solutions of the first two equalities. Hence, homogeneous solution of the PDE is

$$V_{dh} = \phi(x, k_2y^2 + k_1z^2).$$

From second and fourth terms, non-homogeneous solution is derived as follows

$$V_{dn} = \frac{m^2g}{k_1}y.$$

Hence, $V_d = V_{dh} + V_{dn} = \phi(x, k_2 y^2 + k_1 z^2) + \frac{m^2 g}{k_1} y$.

Remark 2. In this example, total energy shaping for the spatial UCDR has been accomplished by a configuration-dependent desired inertia matrix. Note that none of the proposed articles on this topic, e.g. [74, 77, 79–81] can be utilized to derive a configuration-dependent solution.

4.2 Potential Energy Shaping of Underactuated Parallel Robots

In this section, we focus on the PDE of potential energy in parallel robots. A particular structure of parallel robots is considered to shape the potential energy in a general form. It should be noted that potential energy shaping is sufficient to stabilize a system if the equilibrium point is natural, i.e., similar to downward equilibrium point of a pendulum, it is oscillatory.

As indicated in chapter 3, the input mapping matrix \mathbf{G} in parallel robots is equal to the transpose of the Jacobian matrix. The Jacobian matrix is derived from time derivative of inverse kinematic. Let us consider the inverse kinematic formulation of a general parallel manipulator as

$$l_1 = f_1(\mathbf{X}), \quad \dots \quad l_m = f_m(\mathbf{X}), \quad (4.20)$$

then its derivative is

$$\dot{l}_i = \sum_{j=1}^n \frac{\partial f_i}{\partial X_j} \dot{X}_j, \quad \mathbf{X} = [X_1, \dots, X_n]^T.$$

Therefore, $\mathbf{J}_a(\mathbf{X})$ is in the following form

$$\mathbf{J}_a(\mathbf{X}) = \begin{bmatrix} \nabla_{\mathbf{X}_1} f_1 & \dots & \nabla_{\mathbf{X}_n} f_1 \\ \vdots & \ddots & \vdots \\ \nabla_{\mathbf{X}_1} f_m & \dots & \nabla_{\mathbf{X}_n} f_m \end{bmatrix} \quad (4.21)$$

in which $\nabla_{\mathbf{X}} f_j$ denotes the row vector of gradient of f_j . This structure is a fundamental role in the potential energy shaping of these robots. Although it seems that the equilibrium points of underactuated parallel robots similar to UCDRs are stabilizable by merely potential energy shaping, the following assumption is presented to exclude any particular system.

Assumption 1. The equilibrium point \mathbf{q}^* is a natural equilibrium point of the system. In other words, it is possible to stabilize it by shaping only the potential energy. \square

Theorem 1. Consider an underactuated parallel robot satisfying Assumption 1. The solution of potential energy PDE (2.17) with $\mathbf{M}_d = \mathbf{M}$ is

$$V_d = \phi(f_1, \dots, f_m) + V, \quad (4.22)$$

in which f_i s are introduced in (4.20) and V is potential energy of the system. ■

Proof. Invoking Corollary 1, it is clear that the non-homogeneous solution of (2.17) is $V_{dn} = V$. The homogeneous solution is derived from the following equation

$$\mathbf{G}^\perp \nabla_{\mathbf{q}} V_d = 0, \quad \mathbf{G} = \mathbf{J}_a^T,$$

in which $\mathbf{q} = \mathbf{X}$. This means that the vector $\nabla_{\mathbf{q}} V_d$ should be perpendicular to the rows of \mathbf{G}^\perp . Since the columns of \mathbf{G} are gradient of the f_i s, they are perpendicular to \mathbf{G}^\perp . Hence, the functions f_i s are the homogeneous solutions of the PDE. \square

One of the most important properties of Theorem 1 is that it is possible to apply IDA-PBC to the systems with any degree of underactuation. In the following, the solution of potential energy PDE of the robots presented in chapter 3 is proposed.

Planar robot

Invoking Theorem 1, the solution of potential energy PDE of planar robot with $\mathbf{M}_d = \mathbf{M}$ is as follows

$$V_d = mgy + \phi(l_1(\mathbf{X}), l_2(\mathbf{X})) = mgy + \phi\left(\sqrt{(x - a \cos(\theta))^2 + (y - a \sin(\theta))^2}, \sqrt{(x - b + a \cos(\theta))^2 + (y + a \sin(\theta))^2}\right). \quad (4.23)$$

At the first look, it may seem that the solution (4.10) is different from (4.23). However, after some manipulations, it is shown that a solution can be derived as before by

$$\begin{aligned} (2a \cos(\theta) - b)x + 2a \sin(\theta)y - ab \cos(\theta) &= (l_2^2 - l_1^2)/2, \\ x^2 + y^2 - bx - ab \cos(\theta) &= (l_1^2 + l_2^2)/2. \end{aligned}$$

Note that although Theorem 1 simplifies solving PDE (4.5), it is not applicable if total energy shaping is required.

Spatial robot

In this case, V_d is derived using Theorem 1 as follows

$$V_d = mgy + \phi(l_1(\mathbf{X}), l_2(\mathbf{X})) = mgy + \phi\left(\sqrt{x^2 + y^2 + z^2}, \sqrt{(x - b)^2 + y^2 + z^2}\right). \quad (4.24)$$

Similar to previous case, it is possible to show that (4.11) is equivalent to (4.24) in the following form

$$x = (l_1^2 - l_2^2 + b^2)/2b, \quad y^2 + z^2 = (l_1^2 + l_2^2 - 2x^2 + bx - b^2)/2,$$

where x in the second equation should be replaced from the first equation.

Spidercam

As explained before, the advantage of Theorem 1 is its applicability to the systems with underactuation degree of two or even more. Therefore, stabilization of spidercam via potential energy shaping is possible. By this means, the desired potential energy is derived using Theorem 1 as follows

$$V_d = mgy + \phi(l_1(\mathbf{X}), l_2(\mathbf{X}), l_3(\mathbf{X}), l_4(\mathbf{X})) \quad (4.25)$$

where l_i s are proposed in (3.27). Note that to the best of authors knowledge, this is the first IDA-PBC designed for a system with underactuation degree two.

4.3 Solution to Kinetic Energy PDE

In this section a constructive method to solve the kinetic energy PDE of the UaSS with underactuation degree one is introduced. For this purpose, let us present a necessary condition on the design of \mathbf{M}_d as stated in the following proposition. Note that as explained before, \mathbf{q}^* is a stable equilibrium point if $\left. \frac{\partial V_d}{\partial \mathbf{q}} \right|_{\mathbf{q}=\mathbf{q}^*} = 0$ and also the Hessian matrix $\left. \frac{\partial^2 V_d}{\partial \mathbf{q}^2} \right|_{\mathbf{q}=\mathbf{q}^*}$ should be positive definite. Notice that the results of this section are published in [128].

Proposition 1. Consider PDE (2.17) and assume that $s = n - m = 1$. The following inequality is a necessary condition for $\left. \frac{\partial^2 V_d}{\partial \mathbf{q}^2} \right|_{\mathbf{q}=\mathbf{q}^*}$ to be positive definite

$$\left(\mathbf{G}^\perp \mathbf{M}_d \mathbf{M}^{-1} \frac{\partial(\mathbf{G}^\perp \nabla V)}{\partial \mathbf{q}} \right)_{\mathbf{q}=\mathbf{q}^*} > 0. \quad (4.26)$$

■

Proof. Differentiating the PDE (2.7) with respect to \mathbf{q} yields

$$\frac{\partial(\mathbf{G}^\perp \nabla V)}{\partial \mathbf{q}} = \left(\mathbf{G}^\perp \mathbf{M}_d \mathbf{M}^{-1} \frac{\partial^2 V_d}{\partial \mathbf{q}^2} \right)^T + \frac{\partial(\mathbf{G}^\perp \mathbf{M}_d \mathbf{M}^{-1})}{\partial \mathbf{q}} \nabla V_d. \quad (4.27)$$

Note that $\nabla V_d|_{\mathbf{q}=\mathbf{q}^*} = 0$. Thus, (4.27) at $\mathbf{q} = \mathbf{q}^*$ is

$$\left. \frac{\partial(\mathbf{G}^\perp \nabla V)}{\partial \mathbf{q}} \right|_{\mathbf{q}=\mathbf{q}^*} = \left. \left(\mathbf{G}^\perp \mathbf{M}_d \mathbf{M}^{-1} \frac{\partial^2 V_d}{\partial \mathbf{q}^2} \right)^T \right|_{\mathbf{q}=\mathbf{q}^*} = \left. \left(\frac{\partial^2 V_d}{\partial \mathbf{q}^2} (\mathbf{G}^\perp \mathbf{M}_d \mathbf{M}^{-1})^T \right) \right|_{\mathbf{q}=\mathbf{q}^*}$$

By multiplying the above equation from left side to $(\mathbf{G}^\perp \mathbf{M}_d \mathbf{M}^{-1})|_{\mathbf{q}=\mathbf{q}^*}$, the proof is completed by noticing that an arbitrary matrix \mathbf{A} is positive definite if $\boldsymbol{\xi}^T \mathbf{A} \boldsymbol{\xi} > 0$ for any $\boldsymbol{\xi} \neq 0$. \square

In the sequel, with a minor loss of generality, assume that

$$\mathbf{G} = \mathbf{P} [I_m, 0_{m \times n-m}]^T, \quad (4.28)$$

with \mathbf{P} a permutation matrix that leads to $\mathbf{G}^\perp = \mathbf{e}_k^T$, $k \in \{1, \dots, n\}$ (\mathbf{e}_i is i th Euclidean basis vector). Now we will simplify the kinetic energy PDE (2.16) term by term. The first term is:

$$\mathbf{G}^\perp \nabla_{\mathbf{q}} (\mathbf{p}^T \mathbf{M}^{-1}(\mathbf{q}) \mathbf{p}) = \mathbf{G}^\perp \left[\mathbf{p}^T \frac{\partial \mathbf{M}^{-1}}{\partial q_1} \mathbf{p}, \dots, \mathbf{p}^T \frac{\partial \mathbf{M}^{-1}}{\partial q_n} \mathbf{p} \right]^T = \mathbf{p}^T \frac{\partial \mathbf{M}^{-1}}{\partial q_k} \mathbf{p}.$$

The following matrices are used in the sequel of this section

$$\mathbf{M}^{-1}(\mathbf{q}) = \frac{1}{\det \mathbf{M}} \mathfrak{M}(\mathbf{q}) \quad \implies \quad \frac{\partial \mathbf{M}^{-1}}{\partial q_k} = \frac{1}{(\det \mathbf{M})^2} \mathcal{M}(\mathbf{q}) \quad (4.29)$$

where $\mathfrak{M} \in \mathbb{R}^{n \times n}$ is adjugate matrix of \mathbf{M} and $\mathcal{M} \in \mathbb{R}^{n \times n}$ is a matrix determining the numerator elements of $\frac{\partial \mathbf{M}^{-1}}{\partial q_k}$. Notice that although the most previously works on this topic have presumed that $\mathbf{M}(\mathbf{q})$ is a function of only some specified elements of \mathbf{q} , here $\mathbf{M}(\mathbf{q})$ is an arbitrary matrix. Note that in [88] it has been shown that for the UaSS with

$s = 1$, (2.16) is reduced to a single PDE utilizing free matrix \mathbf{J}_2 . By this means and with regard to second term of (2.16), the following structure for $\mathbf{M}_d^{-1}(\mathbf{q})$ is considered

$$\mathbf{M}_d^{-1} = \begin{bmatrix} a_1 & 0 & \dots & b_1 & 0 & \dots & 0 \\ 0 & a_2 & \dots & b_2 & 0 & \dots & 0 \\ \vdots & \vdots & & \vdots & & & 0 \\ b_1 & b_2 & \dots & a(\mathbf{q}) & b_k & \dots & b_{n-1} \\ 0 & 0 & \dots & b_k & a_k & \dots & 0 \\ \vdots & \vdots & & \vdots & & \ddots & \vdots \\ 0 & 0 & \dots & b_{n-1} & 0 & \dots & a_{n-1} \end{bmatrix} \quad (4.30)$$

in which except diagonal elements, and the k th row and column, the other elements are all zero. Note that $a(\mathbf{q})$ is the only configuration-dependent element. a_i s and b_i s are designed to be constant since our aim is to solve the kinetic energy PDE as simple as possible. By calculation adjugate of \mathbf{M}_d^{-1} , it is inferred that k th row of adjugate matrix of \mathbf{M}_d^{-1} is constant. This is one of the advantage of the proposed structure of (4.30). To streamline second term of (2.16), $\mathbf{G}^\perp \mathbf{M}_d \mathbf{M}^{-1}$ is rewritten in the following form

$$\mathbf{G}^\perp \mathbf{M}_d \mathbf{M}^{-1} = \frac{1}{\det \mathbf{M} \det \mathbf{M}_d^{-1}} \boldsymbol{\gamma} \quad (4.31)$$

where $\boldsymbol{\gamma} \in \mathbb{R}^n$ is a row vector independent of $a(\mathbf{q})$. This point is another advantage of the structure (4.30). The determinant of \mathbf{M}_d^{-1} is

$$\det \mathbf{M}_d^{-1} = \phi_1 a(\mathbf{q}) + \phi_2,$$

with ϕ_1, ϕ_2 being constant parameters that are function of a_i s and b_i s. By this means, the second term of (2.16) is given by

$$\mathbf{G}^\perp \mathbf{M}_d \mathbf{M}^{-1} \nabla_{\mathbf{q}} (\mathbf{p}^T \mathbf{M}_d^{-1}(\mathbf{q}) \mathbf{p}) = \frac{\mathbf{p}^T \sum_{i=1}^n \left(\gamma_i \frac{\partial \mathbf{M}_d^{-1}}{\partial q_i} \right) \mathbf{p}}{\det \mathbf{M} \det \mathbf{M}_d^{-1}} \quad (4.32)$$

where the only non-zero element of $\frac{\partial \mathbf{M}_d^{-1}}{\partial q_i}$ is (k, k) th element. Note that if similar to some of the previous papers such as [74, 129], the matrix \mathbf{M}_d is only a function of q_k , then (4.32) is simplified to the following form

$$\frac{\gamma_k \mathbf{p}^T \frac{\partial \mathbf{M}_d^{-1}}{\partial q_k} \mathbf{p}}{\det \mathbf{M} \det \mathbf{M}_d^{-1}}.$$

Invoking [74], we know that \mathbf{J}_2 is linear with respect to \mathbf{p} . Hence, With the purpose of simplifying the last term of (2.16), \mathbf{J}_2 is represented as follows

$$\mathbf{J}_2(\mathbf{q}, \mathbf{p}) = \frac{1}{\det \mathbf{M}} \begin{bmatrix} 0 & \mathbf{p}^T \boldsymbol{\alpha}(\mathbf{q}) & \dots & \mathbf{p}^T \boldsymbol{\alpha}(\mathbf{q}) \\ \mathbf{p}^T \boldsymbol{\alpha}(\mathbf{q}) & 0 & \dots & \mathbf{p}^T \boldsymbol{\alpha}(\mathbf{q}) \\ \vdots & \vdots & \ddots & \vdots \\ \mathbf{p}^T \boldsymbol{\alpha}(\mathbf{q}) & \mathbf{p}^T \boldsymbol{\alpha}(\mathbf{q}) & \dots & 0 \end{bmatrix} \quad (4.33)$$

with $\boldsymbol{\alpha} \in \mathbb{R}^n, i \in \{1, \dots, n(n-1)\}$. This is not necessarily the structure of a skew-symmetric matrix. However, in the sequel we will consider only the k th row of this matrix. Hence, the k th column can be determined such that $\mathbf{J}_2 = -\mathbf{J}_2^T$. Note that other elements of

this matrix can be determined arbitrarily. It is possible to express (4.33) in the following compact form

$$\mathbf{J}_2 = \frac{1}{\det \mathbf{M}} \sum_{i=1}^{n_0} \mathbf{p}^T \mathbf{i} \boldsymbol{\alpha} \mathbf{W}_i, \quad n_0 = n(n-1),$$

where \mathbf{W}_i s are defined as follows

$$\mathbf{W}_1 = \mathbf{W}^{1,2}, \mathbf{W}_2 = \mathbf{W}^{1,3}, \dots, \mathbf{W}_{n-1} = \mathbf{W}^{1,n}, \mathbf{W}_n = \mathbf{W}^{2,1}, \dots, \mathbf{W}_{n_0} = \mathbf{W}^{n,n-1},$$

where $\mathbf{W}^{i,j}$ is matrix of zeros except (i, j) element which is equal to 1. Notice that this structure is general version of (4.15). Furthermore, $\mathbf{G}^\perp \mathbf{J}_2$ can be expressed as follows

$$\begin{aligned} \mathbf{G}^\perp(\mathbf{q}) \mathbf{J}_2(\mathbf{p}, \mathbf{q}) &= \frac{1}{\det \mathbf{M}} \mathbf{p}^T \mathcal{J}(\mathbf{q}) \mathbf{A}, \quad \mathcal{J} = [\mathbf{1} \boldsymbol{\alpha} \quad \dots \quad \mathbf{n}_0 \boldsymbol{\alpha}] \in \mathbb{R}^{n \times n_0}, \\ \mathbf{A} &= [(\mathbf{G}^\perp \mathbf{W}_1)^T \quad \dots \quad (\mathbf{G}^\perp \mathbf{W}_{n_0})^T]^T \in \mathbb{R}^{n_0 \times n}. \end{aligned}$$

Thus, $\mathcal{J} \mathbf{A}$ is in the following form

$$\mathcal{J} \mathbf{A} = [{}_{(k-1)n-k+2} \boldsymbol{\alpha}, \dots, {}_{(k-1)n} \boldsymbol{\alpha}, 0_n, {}_{(k-1)n+1} \boldsymbol{\alpha}, \dots, {}_{kn-k} \boldsymbol{\alpha}] \triangleq \mathbf{B}(\mathbf{q}) \in \mathbb{R}^{n \times n}. \quad (4.34)$$

It is clear that only one of the rows of \mathbf{J}_2 appears in this equation.

Finally, third term in PDE (2.6) is

$$\mathbf{G}^\perp \mathbf{J}_2(\mathbf{q}, \mathbf{p}) \mathbf{M}_d^{-1}(\mathbf{q}) \mathbf{p} = \frac{1}{\det \mathbf{M}} \mathbf{p}^T \mathbf{B} \mathbf{M}_d^{-1} \mathbf{p}, \quad (4.35)$$

with $\mathbf{B}(\mathbf{q})$ defined in (4.34). All terms in (2.16) are quadratic with respect to \mathbf{p} and shall be symmetric. Substituting (4.29), (4.32) and (4.35) in (2.16) leads to the following equation

$$\frac{\mathcal{M}}{\det \mathbf{M}} - \frac{\sum_{i=1}^n \gamma_i \frac{\partial \mathbf{M}_d^{-1}}{\partial q_i}}{\det \mathbf{M}_d^{-1}} + (\mathbf{B} \mathbf{M}_d^{-1} + \mathbf{M}_d^{-1} \mathbf{B}^T) = 0. \quad (4.36)$$

By considering the diagonal and up-diagonal elements, there are $\frac{n(n+1)}{2}$ equations and $n(n-1)$ design parameters. For $n \geq 3$, the number of design parameters are more than the number of unknowns. Hence, it may seem that it is possible to satisfy it without solving a PDE. However, based on Lemma2 of [74], the rank of $(\mathbf{B} \mathbf{M}_d^{-1} + \mathbf{M}_d^{-1} \mathbf{B}^T)$ is always $n-1$. Note that as explained before, we should solve $s=1$ PDE [88]. Hence, (4.36) is replaced by $\frac{n(n+1)}{2} - 1$ algebraic equations and a PDE with respect to $a(\mathbf{q})$. Note that due to the proposed structure of \mathbf{M}_d^{-1} , (k, k) th element of (4.36) lead to a PDE. By setting the other elements equal to other elements-wise, some algebraic equations in the following form shall be solved

$$\begin{aligned} &\frac{1}{\det \mathbf{M}} [\mathcal{M}_{11}, \mathcal{M}_{12}, \dots, \mathcal{M}_{1n}, \mathcal{M}_{22}, \dots, \mathcal{M}_{k(k+1)}, \dots, \mathcal{M}_{nn}]^T \\ &= -\boldsymbol{\Psi} [{}_{(k-1)n-k+2} \alpha_1, {}_{(k-1)n-k+2} \alpha_2 \dots, {}_{(k-1)n-k+2} \alpha_n, {}_{(k-1)n-k+3} \alpha_1, \dots, \\ &({}_{(k-1)n-k+3} \alpha_n, \dots, {}_{kn-k} \alpha_1, \dots, {}_{kn-k} \alpha_n)]^T, \end{aligned} \quad (4.37)$$

with

$$\Psi = [\psi_1 \quad \dots \quad \psi_{n(n-1)}] \in \mathbb{R}^{\frac{n(n+1)-2}{2} \times n(n-1)}$$

$$\begin{aligned} \psi_1 &= [2a_1, \mathbf{0}_{k-2}^T, b_1, \mathbf{0}_{\frac{n(n+1)}{2}-k-1}^T]^T, & \psi_2 &= [0, a_1, \mathbf{0}_{n+k-4}^T, b_1, \mathbf{0}_{\frac{n(n+1)}{2}-n-k}^T]^T, & \dots \\ \psi_{n+1} &= [0, a_2, \mathbf{0}_{k-3}^T, b_1, \mathbf{0}_{\frac{n(n+1)}{2}-k-1}^T]^T, & \dots & \psi_{n(n-1)} = [\mathbf{0}_{\frac{k(2n-k-1)}{2}-1}^T, b_{n-1}, \mathbf{0}_{\frac{n(n+1)-k(2n-k-1)}{2}-1}^T]^T, \end{aligned}$$

in which, ${}_i\alpha_j$ denotes j th element of ${}_i\alpha$, and 0_n is a column vector of zeros with n elements. The matrix Ψ is generally full rank; thus, equation (4.37) has at least one solution. The remaining PDE is in the following form

$$\frac{\sum_{i=1}^n \gamma_i \frac{\partial a(\mathbf{q})}{\partial q_i}}{\det \mathbf{M}_d^{-1}} - \frac{\mathcal{M}_{kk}}{\det \mathbf{M}} - 2 \sum_{i=1}^{n-1} b_i {}_{(k-1)n-k+1+i}\alpha_k = 0. \quad (4.38)$$

Notice that a_i s and b_i s should be designed such that Proposition 1 is satisfied, the inertia matrix (or equivalently its inverse) should be positive definite, and the matrix Ψ has right pseudo-inverse. The PDE (4.38) has the following cases.

case1: If similar to [129], the inertia matrix \mathbf{M} merely depends on unactuated coordinate q_k , then the first term of (4.38) is equal to $\frac{\gamma_k \frac{\partial \mathbf{M}_d^{-1}}{\partial q_k}}{\det \mathbf{M}_d^{-1}}$. Hence, (4.38) is replaced by the following ODE

$$\frac{\gamma_k \frac{da(q_k)}{dq_k}}{\phi_1 a(q_k) + \phi_2} = \frac{\mathcal{M}_{kk}}{\det \mathbf{M}} + 2 \sum_{i=1}^{k-1} b_i {}_{(k-1)n-k+1+i}\alpha_k \triangleq f(q_k) \quad (4.39)$$

whose solution is

$$a(q_k) = \frac{\lambda e^{\phi_1 F(q_k)} - \phi_2}{\phi_1} \quad (4.40)$$

in which, λ is an arbitrary constant and $F = \int \frac{f}{\gamma_k} dq_k$. Notice that the proposed method is more applicable than the one in [129] where a set of ODEs are derived that are analytically solvable only if $n = 2$. The systems satisfy this case are not restricted, but include ball and beam system [14], cart-pole [74], pendubot [84] and some types of cranes [130, 131].

case2: If \mathcal{M}_{kk} is zero, the second term of (4.38) is also zero. By this means, it is trivial to design $a(\mathbf{q})$ with respect to parameters in the last term. A particular state of this case is reported in [74], where $a(\mathbf{q})$ is designed analytically under this assumption that it is a function of only one of the configurations. Here, since our goal is deriving the simplest solution, a constant \mathbf{M}_d with respect to Proposition 1 is considered. By this means, we get rid of solving (4.38). Note that if \mathbf{M} is constant; this case is satisfied without paying attention to the structure of $\mathbf{G}(\mathbf{q})$. Hence, UCDRs are one of the subjects of this case. The proposed controller for acrobot in [83], VTOL aircraft in [74] and inertia wheel pendulum in [14, 94] are other application examples within this case..

case3: In this case, a PDE shall be solved. It is possible to use the methods in the literature to solve it. Furthermore, the proposed method in section 4.1 based on Pfaffian

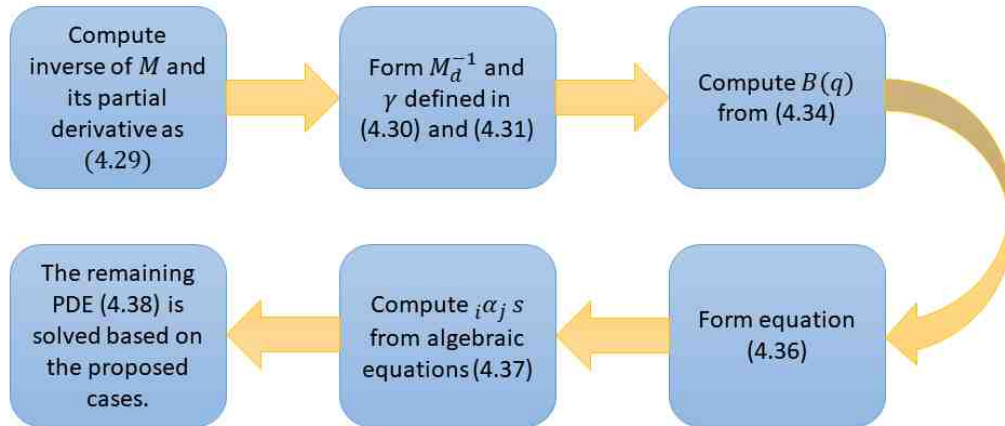


Figure 4.1: The procedure of solving the kinetic energy PDE based on the proposed method.

differential equations is another powerful tool. By this means, the PDE (4.38) is equivalent to

$$\frac{\det \mathbf{M}_d^{-1} dq_1}{\gamma_1} = \dots = \frac{\det \mathbf{M}_d^{-1} dq_n}{\gamma_n} = \frac{da}{\frac{\mathcal{M}_{kk}}{\det \mathbf{M}} + 2 \sum_{i=1}^{n-1} b_i (k-1)n-k+1+i \alpha_k}$$

For ease of readers, the design steps of \mathbf{M}_d are summarized in Fig. 4.1. As seen in this diagram, firstm invers of \mathbf{M} and its partial derivative should be computed. Then, the matrix \mathbf{M}_d^{-1} and the vector γ are formulated as (4.30) and (4.31), respectively. The matrix $\mathbf{B}(\mathbf{q})$ is computed from (4.34). After this, equation (4.36) is fomulated and ${}_i \alpha_j$ is derived from (4.37). At last, the PDE (4.38) should be solved based on the proposed cases. Some examples of this procedure are presented in Appendix B.

During this section, some of the advantages of the structure (4.30) were reported. In the following remark, the motivation why this structure was considered, is presented.

Remark 3. The matching equation (2.16) related to kinetic energy shaping is a nonlinear PDE. Moreover, its solution should be positive definite. According to this condition, a novel structure for \mathbf{M}_d^{-1} was proposed that not only reduces the complexity of kinetic energy PDE but also eases up verification of the positive definiteness of this matrix. Additionally, this structure results in the vector γ defined in (4.31) to be independent of $a(\mathbf{q})$ that reduces the nonlinearity of the PDE, and verification of Proposition 1 is quite simple.

4.4 Comparison of IDA-PBC to Simultaneous IDA-PBC

In this section, IDA-PBC and SIDA-PBC are compared. For this purpose, first, SIDA-PBC is reviewed. Then we focus on the results of [89], where it has been asserted that SIDA-PBC simplify the kinetic energy PDE, and show that practically SIDA-PBC is equivalent to IDA-PBC.

4.4.1 Simultaneous IDA-PBC

In IDA-PBC, we use gyroscopic (workless) forces to simplify the kinetic energy PDE. However, it seems that what is presented in the literature loses the generality of the problem. Considering dissipative forces instead of gyroscopic forces is more general. A typical example has been shown in [132] that the system

$$\begin{aligned} \begin{bmatrix} \dot{x}_1 \\ \dot{x}_2 \end{bmatrix} &= \begin{bmatrix} x_1 \\ -x_2 \end{bmatrix} + \begin{bmatrix} 0 \\ 1 \end{bmatrix} u \\ y &= x_1^2 x_2 \end{aligned} \quad (4.41)$$

is conservative by considering $H = 1/2x_1^2x_2^2$. However, there is not a smooth skew-symmetric matrix $\mathbf{J}(\mathbf{X})$ such that

$$\begin{bmatrix} \dot{x}_1 \\ \dot{x}_2 \end{bmatrix} = \mathbf{J}(\mathbf{X}) \begin{bmatrix} x_1x_2^2 \\ x_1^2x_2 \end{bmatrix} + \begin{bmatrix} 0 \\ 1 \end{bmatrix}$$

However, note that considering $\mathbf{F} = [x_1, -x_2]^T$ as a dissipative force that

$$(\nabla H)^T \mathbf{F} = [x_1x_2^2, x_1^2x_2][x_1, -x_2]^T = 0.$$

It should be noted that it is possible to represent a conservative system using dissipative force, but it may not be possible with gyroscopic forces.

According to this fact, in [87, 89], the target dynamic (2.14) is replaced by

$$\begin{bmatrix} \dot{\mathbf{q}} \\ \dot{\mathbf{p}} \end{bmatrix} = \begin{bmatrix} \mathbf{0} & \mathbf{M}^{-1}(\mathbf{q})\mathbf{M}_d(\mathbf{q}) \\ -\mathbf{M}_d(\mathbf{q})\mathbf{M}^{-1}(\mathbf{q}) & \mathbf{0} \end{bmatrix} \begin{bmatrix} \nabla_{\mathbf{q}}H_d \\ \nabla_{\mathbf{p}}H_d \end{bmatrix} + \begin{bmatrix} \mathbf{0} \\ \mathfrak{C}(\mathbf{q}, \mathbf{p}) \end{bmatrix} \quad (4.42)$$

in which the vector $\mathfrak{C}(\mathbf{q}, \mathbf{p})$ denotes dissipative forces and will be determined later. Based on stability criteria, this vector should satisfy

$$\mathbf{P}^T \mathbf{M}_d^{-1} \mathfrak{C} \leq 0 \quad (4.43)$$

Note that a particular choice of this vector is $\mathfrak{C} = (\mathbf{J}_2 - \mathbf{G}\mathbf{K}_v\mathbf{G}^T)\mathbf{M}_d^{-1}\mathbf{p}$ which coincides with IDA-PBC. This shows that SIDA-PBC is a general version of IDA-PBC.

By setting (4.42) equal to open-loop dynamic (2.9), the kinetic energy PDE (2.16) is replaced by

$$\mathbf{G}^\perp(\mathbf{q})\{\nabla_{\mathbf{q}}(\mathbf{p}^T\mathbf{M}^{-1}(\mathbf{q})\mathbf{p}) - \mathbf{M}_d\mathbf{M}^{-1}\nabla_{\mathbf{q}}(\mathbf{p}^T\mathbf{M}_d^{-1}(\mathbf{q})\mathbf{p}) + 2\mathfrak{C}\} = 0, \quad (4.44)$$

while the potential energy PDE (2.17) does not change. By considering the structure of (4.44), it is inferred that the structure of \mathfrak{C} is in the following form

$$\mathfrak{C}(\mathbf{q}, \mathbf{p}) = \mathbf{\Lambda}(\mathbf{q}, \mathbf{p})\mathbf{M}_d^{-1}\mathbf{p} \quad (4.45)$$

in which the matrix $\mathbf{\Lambda}$ is a free matrix such that its elements should be linear with respect to \mathbf{p} since the other terms in (4.44) are quadratic with respect to \mathbf{p} (note that this constraint is not necessarily applied to the part of \mathfrak{C} which is in range space of \mathbf{G}). By this means, the closed-loop dynamic (4.42) is in the following form

$$\begin{bmatrix} \dot{\mathbf{q}} \\ \dot{\mathbf{p}} \end{bmatrix} = \begin{bmatrix} 0 & \mathbf{M}^{-1}(\mathbf{q})\mathbf{M}_d(\mathbf{q}) \\ -\mathbf{M}_d(\mathbf{q})\mathbf{M}^{-1}(\mathbf{q}) & \mathbf{\Lambda} \end{bmatrix} \begin{bmatrix} \nabla_{\mathbf{q}}H_d \\ \nabla_{\mathbf{p}}H_d \end{bmatrix}, \quad (4.46)$$

and (4.43) yields to

$$\mathbf{p}^T \mathbf{M}_d^{-1} \mathbf{\Lambda} \mathbf{M}_d^{-1} \mathbf{p} \leq 0.$$

A sufficient condition to ensure this inequality is

$$\mathbf{\Lambda} + \mathbf{\Lambda}^T \leq \mathbf{0}. \quad (4.47)$$

By this means, the control law is derived easily as follows

$$\mathbf{u} = (\mathbf{G}^T \mathbf{G})^{-1} \mathbf{G}^T (\nabla_{\mathbf{q}}H - \mathbf{M}_d \mathbf{M}^{-1} \nabla_{\mathbf{q}}H_d + \mathbf{\Lambda} \mathbf{M}_d^{-1} \mathbf{p})$$

Note that in comparison with IDA-PBC that energy shaping and damping injection are performed separately; here it is accomplished simultaneously. In [89], some examples of solving the kinetic energy PDE using this method have been proposed.

4.4.2 Comment on SIDA-PBC

In the previous section, SIDA-PBC was introduced. At first sight, it seems that the kinetic energy PDE is much easier in SIDA-PBC method. In the following, we show that SIDA-PBC is practically equivalent to IDA-PBC.

The first point is the possibility of negative definiteness of $\mathbf{\Lambda}$. Since the elements of this matrix are linear with respect to \mathbf{p} , it is impossible to derive a definite matrix. Hence, the damping term should be added to the system through inputs. By which, the matrix $\mathbf{\Lambda}$ should be in the following form

$$\mathbf{\Lambda} = \mathbf{\Lambda}_n - \mathbf{G} \mathbf{K}_v \mathbf{G}^T, \quad (4.48)$$

in which the first term is lossless part of $\mathbf{\Lambda}$ appears in the PDE (4.42) and the second term is damping injection, which clearly does not affect on (4.42). Note that if similar to (2.18) the natural damping terms are modeled, the first term in (2.20) is added to (4.48). By comparing SIDA-PBC with IDA-PBC, it is inferred that the damping term is equal in both methods. The difference is limited to the skew-symmetric matrix \mathbf{J}_2 and lossless matrix $\mathbf{\Lambda}_n$. Note that both matrices are multiplied to $\mathbf{M}_d^{-1} \mathbf{p}$ from the right side. Although it is clear that the number of free parameters in $\mathbf{\Lambda}_n$ is more than \mathbf{J}_2 , it seems that the reported applications of SIDA-PBC are representable with IDA-PBC. In other words, it is possible to replace $\mathbf{\Lambda}_n$ with the skew-symmetric matrix \mathbf{J}_2 . In the following, it is shown that the examples of SIDA-PBC are equivalent to IDA-PBC.

Cart-pole

In [79] a controller for a class of underactuated mechanical systems based on energy shaping without solving the matching equations that is different from IDA-PBC has been reported. In [89] it is asserted that this controller is in the form of SIDA-PBC with $\mathbf{\Lambda}$ in the following

form

$$\begin{aligned} \mathbf{\Lambda} = & \frac{1}{2} \mathbf{M}_d \begin{bmatrix} 0 & -\frac{2k_a k_u k_k}{ml^3} \sin(q_2) p_2 \\ \frac{k_a k_u k_k}{ml^3} \sin(q_2) p_2 & \frac{k_a k_u k_k}{ml^3} \sin(q_2) p_1 \end{bmatrix} \mathbf{M}_d \\ & - \begin{bmatrix} 1 \\ ml \cos(q_2) \end{bmatrix} k_v \begin{bmatrix} 1 & ml \cos(q_2) \end{bmatrix}. \end{aligned} \quad (4.49)$$

Other matrices have been proposed in [79, 89]. Note that to design this controller, first a partial feedback linearization has been used which results in a system in the form (2.9) with the following new input mapping matrix

$$\mathbf{G} = \begin{bmatrix} 1 \\ ml \cos(q_2) \end{bmatrix}.$$

by this means, the second term of (4.49) is in the form $\mathbf{G} \mathbf{K}_v \mathbf{G}^T$. Hence, (4.49) is in the form of (4.48). As explained before, the matrix $\mathbf{\Lambda}$ is multiplied to $\mathbf{M}_d^{-1} \mathbf{p}$ from right side. Thus, we should find \mathbf{J}_2 such that

$$\frac{1}{2} \mathbf{M}_d \begin{bmatrix} 0 & -\frac{2k_a k_u k_k}{ml^3} \sin(q_2) p_2 \\ \frac{k_a k_u k_k}{ml^3} \sin(q_2) p_2 & \frac{k_a k_u k_k}{ml^3} \sin(q_2) p_1 \end{bmatrix} \begin{bmatrix} p_1 \\ p_2 \end{bmatrix} = \mathbf{J}_2 \mathbf{M}_d^{-1} \mathbf{p}$$

Considering this equation, it is inferred that a suitable choice is $\mathbf{J}_2 = \mathbf{M}_d \mathbf{J}_{2_{new}} \mathbf{M}_d$ with $\mathbf{J}_{2_{new}}^T = -\mathbf{J}_{2_{new}}$. One can easily verify that

$$\mathbf{J}_{2_{new}} = \begin{bmatrix} 0 & -2a \sin(q_2) p_2 \\ 2a \sin(q_2) p_2 & 0 \end{bmatrix} \quad (4.50)$$

Hence, the proposed controller is exactly an IDA-PBC.

Ball and beam

The second example is ball and beam system (see Section 7.1.4 for more details). In [133] a controller based on direct Lyapunov method has been design. In [89] it has been asserted that that controller is a SIDA-PBC. The matrix $\mathbf{\Lambda}$ is in the following

$$\begin{aligned} \mathbf{\Lambda} = & -\frac{1}{2} \mathbf{M}_d \begin{bmatrix} 0 & -\frac{q_1 p_1}{\sqrt{\epsilon + q_1^2}} + \frac{\sqrt{2\epsilon + q_1^2} q_1 p_2}{\epsilon + q_1^2} \\ \frac{q_1 p_1}{\sqrt{\epsilon + q_1^2}} - \frac{\sqrt{2\epsilon + q_1^2} q_1 p_2}{\epsilon + q_1^2} & 0 \end{bmatrix} \mathbf{M}_d - \frac{\delta}{\epsilon} \begin{bmatrix} \sqrt{2\epsilon + q_1^2} & \sqrt{\epsilon + q_1^2} \\ \sqrt{\epsilon + q_1^2} & \sqrt{2\epsilon + q_1^2} \end{bmatrix} \\ & - \begin{bmatrix} k_v & 0 \\ 0 & 0 \end{bmatrix}. \end{aligned}$$

The first term is apparently skew-symmetric. Furthermore, the last term is in the form $\mathbf{G} \mathbf{K}_v \mathbf{G}^T$ with $\mathbf{G} = [1, 0]^T$. The second term is arisen from modeling the natural damping term of the system (i.e., $-\delta p_1$) as discussed in (2.20). Therefore, this case is also representable with IDA-PBC methodology.

At the end of this section, it is necessary to disclose two points. The first one is that the motivator example (4.41) is representable with a skew-symmetric matrix as follows

$$\begin{bmatrix} \dot{x}_1 \\ \dot{x}_2 \end{bmatrix} = \begin{bmatrix} 0 & \frac{1}{x_1 x_2} \\ -\frac{1}{x_1 x_2} & 0 \end{bmatrix} \begin{bmatrix} x_1 x_2^2 \\ x_1^2 x_2 \end{bmatrix} + \begin{bmatrix} 0 \\ 1 \end{bmatrix}$$

Although this matrix is not smooth, it is merely a representation on the paper that may give us some insights into the system. By this means, one may argue that SIDA-PBC prevents this non-smooth structure. The other point is that although we showed the current literature of SIDA-PBC does not differ from IDA-PBC, it may find some cases that it is not representable with IDA-PBC.

4.5 Conclusion

In this section, we concentrated on the matching equations arisen in IDA-PBC method. One method was based on Pfaffian differential equations in which a nonlinear PDE was replaced by some Pfaffian equations. This powerful method has successfully been applied to several systems, such as planar and spatial underactuated cable-driven robots. Potential energy shaping of underactuated parallel robots with application to stabilization of UCDRs was another subject of this chapter. Furthermore, a systematic approach to solve the kinetic energy PDE of UaSs with underactuation degree one. In the end, a comparison between SIDA-PBC and IDA-PBC was performed and it was shown that the current state of SIDA-PBC is not different from IDA-PBC for mechanical systems.

Chapter 5

IDA-PBC with Bounded Input

In this chapter, we concentrate on designing IDA-PBC with bounded inputs. For this purpose, two different methodologies is introduced. The first one is based on analyzing the control law of IDA-PBC term by term. By this means, the upper bound of velocity is calculated, and then the upper bound of all terms is derived. Another method is based on a suitable definition of the free part of the interconnection matrix. An optimization problem with respect to this matrix is formulated and solved analytically for the mechanical systems with at least two actuators.

5.1 Bounded Input IDA-PBC for Mechanical Systems

In this section, the upper bound of IDA-PBC's control law is derived. First, we focus on the terms related to potential energy shaping. A suitable form for the homogeneous solution of potential energy PDE is considered such that limits its derivative. However, the difficulty of computing the upper bound of control law is velocity-dependent terms. Since the upper bound of velocity is generally unknown, computation of the upper bound of velocity-dependent terms is challenging. Here, the upper bound of velocity is analytically computed, and then using this value, the upper bound of velocity-dependent terms are derived. Notice that the results of this section are published in [134].

First, assume that the elements of input mapping matrix \mathbf{G} are only 0 or 1. As indicated in Corollary 1, the solution of potential energy PDE (2.16) is divided to homogeneous (V_{dh}) and non-homogeneous (V_{dn}) parts. The homogeneous solution is computed from the following PDE

$$\mathbf{G}^\perp \mathbf{M}_d \mathbf{M}^{-1} \nabla_{\mathbf{q}} V_{dh} = 0,$$

as follows

$$V_{dh} = \phi(V_{dh_1}, V_{dh_2}, \dots),$$

in which ϕ is an arbitrary function and V_{dh_i} s are the homogeneous solutions. Note that ϕ is chiefly defined in quadratic form to satisfy (2.11). This form leads to very large or even unbounded control law. Hence, the function ϕ should be defined such that the inputs are confined. Invoking [91], it seems that it is possible to confine the homogeneous solution by designing V_{dh} as follows

$$V_{dh} = \sum k_i \int \mathcal{S}(V_{dh_i} - V_{dh_i}^*) dV_{dh_i}, \quad (5.1)$$

where, $V_{dh_i}^* = V_{dh_i}|_{\mathbf{q}=\mathbf{q}^*}$ and $\mathcal{S}(x)$ shall be designed based on the following items

1. $\mathcal{S}(0) = 0$,
2. \mathcal{S} is an increasing function which is bounded with the upper bound $|\mathcal{S}| \leq 1$,
3. $\frac{d^2\mathcal{S}(x)}{dx^2} \neq 0, \quad \forall x \neq 0$.

For example, $S(x) = \tanh(x)$ is a suitable choice. Note that in contrast to fully actuated robots, suitable definition of $S(x)$ does not guarantee boundedness of homogeneous solution of all the UaSs. This problem is related to the physical property of the systems and is confirmed by Brockett's theorem [135]. For example, consider the cart-pole system. It is clear that if the position of the pendulum is close to the horizon, an immense force is required to prevent it from falling. In this case, irrespective of $S(x)$, the functions V_{dh} and V_{dn} may be non-smooth, resulting in unbounded control law. Hence, we consider the following assumption to foster the rest of this section. Note that we will relax this assumption by Remark 6.

Assumption 2. Consider a mechanical system with natural damping represented by the model (2.18). Presume that the input mapping matrix is constant as (4.28). The coefficients k_i s in (5.1) are chosen sufficiently small. Similar to bounded input controllers that have been designed for fully actuated serial robots, the actuators should be capable to compensate the terms related to potential energy shaping. In IDA-PBC, these terms are

$$\mathbf{u}_v = \nabla_{\mathbf{q}}V - \mathbf{M}_d\mathbf{M}^{-1}\nabla_{\mathbf{q}}V_d. \quad (5.2)$$

Hence, it is necessary that the following inequality is satisfied

$$|(\nabla_{\mathbf{q}}V - \mathbf{M}_d\mathbf{M}^{-1}\nabla_{\mathbf{q}}V_d)_i| < u_{M_i}, \quad (5.3)$$

with u_{M_i} being the upper bound of actuators. This means that the actuators can compensate the effects of gravitational force in the workspace. Note that in (5.3), $(\cdot)_i$ denotes the i th element of (\cdot) while i is related to only actuated joints. Based on (5.3), it is also assumed that there exist the constants c_{V_i} s and c_{V_d} such that

$$|(\nabla_{\mathbf{q}}V)_i| \leq c_{V_i}, \quad \|\nabla_{\mathbf{q}}V_d\| \leq c_{V_d}. \quad (5.4)$$

□

Note that this assumption is not restrictive since $\nabla_{\mathbf{q}}V$ is bounded for all the systems in workspace and also it is always possible to find c_{V_d} , see Remark 6 for more details.

Now consider the terms related to kinetic energy shaping which are as follows

$$\nabla_{\mathbf{q}}K - \mathbf{M}_d\mathbf{M}^{-1}\nabla_{\mathbf{q}}K_d. \quad (5.5)$$

Note that it is possible to add the term $\mathbf{J}_2\mathbf{M}_d^{-1}\mathbf{p}$ to (5.5) since it is used to simplify the kinetic energy PDE. Since $K = 1/2\mathbf{p}^T\mathbf{M}^{-1}\mathbf{p}$ and $K_d = 1/2\mathbf{p}^T\mathbf{M}_d^{-1}\mathbf{p}$, it is obvious that the terms in (5.5) are quadratic with respect of \mathbf{p} . Thus, confining the velocity may lead to limitation of the terms related to kinetic energy shaping. The results are proposed in the following theorem. Before that, the following required assumption is stated.

Assumption 3. There exist constants c_{M_i} s, c_{M_d} , c_J and c_{Λ_i} s such that

$$(\nabla_{\mathbf{q}}K)_i \leq c_{M_i}\|\mathbf{p}\|^2, \quad \|\nabla_{\mathbf{q}}K_d\| \leq c_{M_d}\|\mathbf{p}\|^2, \quad \|\mathbf{J}_2(\mathbf{q}, \mathbf{p})\| \leq c_J\|\tilde{\mathbf{p}}\|, \quad \|\boldsymbol{\Lambda}_i\| \leq c_{\Lambda_i} \quad (5.6)$$

where $\tilde{\mathbf{p}} = \mathbf{M}_d^{-1}\mathbf{p}$ and $\mathbf{\Lambda} := \mathbf{M}_d\mathbf{M}^{-1}$. \square

Notice that this assumption is satisfied mathematically for CDRs and the robots with revolute joint, and practically for all the systems in the workspace.

The upper bound of the control law is derived in the following theorem. Note that the particular structure $\mathbf{G} = \mathbf{P}[\mathbf{I}_m, \mathbf{0}_{s \times m}]^T$ will be relaxed in Remark 5.

Theorem 2. Consider a mechanical system represented with the model (2.18) and control law (2.15). Assume that condition (2.21), Assumption 2 and Assumption 3 are satisfied. The the following items are inferred:

a) The upper bounds of $\|\mathbf{p}\|$ and $\|\tilde{\mathbf{p}}\|$ are

$$\|\mathbf{p}\| \leq \sqrt{\frac{H_d(t_0)}{\lambda_{\min}\{\mathbf{M}_d^{-1}\}}} \triangleq c_{p1}, \quad \|\tilde{\mathbf{p}}\| \leq \sqrt{\frac{H_d(t_0)}{\lambda_{\min}\{\mathbf{M}_d\}}} \triangleq c_{\tilde{p}1}. \quad (5.7)$$

b) The ultimate bounds of $\|\mathbf{p}\|$ and $\|\tilde{\mathbf{p}}\|$ are derived as follows

$$\|\mathbf{p}\| \leq \left(\frac{\lambda_{\max}\{\mathbf{M}_d^{-1}\}}{\lambda_{\min}\{\mathbf{M}_d^{-1}\}}\right)^{1/2} \frac{c_{V_d}\lambda_{\max}\{\mathbf{M}_d^{-1}\}}{\lambda_{\min}^2\{\mathbf{M}_d^{-1}\}\lambda_{\min}\{\mathbf{R}_2\} - \mu} \triangleq c_{p2}. \quad (5.8a)$$

$$\|\tilde{\mathbf{p}}\| \leq \left(\frac{\lambda_{\max}\{\mathbf{M}_d\}}{\lambda_{\min}\{\mathbf{M}_d\}}\right)^{1/2} \frac{c_{V_d}}{\lambda_{\min}\{\mathbf{R}_2\} - \mu} \triangleq c_{\tilde{p}2}, \quad (5.8b)$$

where $\lambda_{\min}\{\cdot\}$ and $\lambda_{\max}\{\cdot\}$ denote the maximum and the minimum eigenvalue of $\{\cdot\}$, respectively, and μ is a small positive scalar.

c) The upper bound of $|u_i|$ is

$$c_{V_i} + c_{\Lambda_i}c_{V_d} + (c_{M_i} + c_{\Lambda_i}c_{M_d})c_p^2 + c_Jc_{\tilde{p}}^2 + \lambda_{\max}\{K_v\}c_{\tilde{p}}, \quad (5.9)$$

in which c_p and $c_{\tilde{p}}$ are the upper bounds of $\|\mathbf{p}\|$ and $\|\tilde{\mathbf{p}}\|$, respectively. In general, $c_p = c_{p1}$ and $c_{\tilde{p}} = c_{\tilde{p}1}$, unless $\|\mathbf{p}(t_0)\| \leq c_{p2}$ and $\|\tilde{\mathbf{p}}(t_0)\| \leq c_{\tilde{p}2}$, then

$$c_p = \min\{c_{p1}, c_{p2}\}, \quad c_{\tilde{p}} = \min\{c_{\tilde{p}1}, c_{\tilde{p}2}\}. \quad \blacksquare$$

Proof. a) Consider H_d as a Lyapunov candidate. The trajectory of the system with initial value $H_d(t_0)$ descends to lower level sets because \dot{H}_d is negative semi-definite. Thus, the following inequality is inferred

$$\frac{1}{2}\lambda_{\min}\{\mathbf{M}_d\}\|\tilde{\mathbf{p}}\|^2 \ \& \ \frac{1}{2}\lambda_{\min}\{\mathbf{M}_d^{-1}\}\|\mathbf{p}\|^2 \leq K_d \leq H_d \leq H_d(t_0).$$

Hence, the upper bounds of $\|\tilde{\mathbf{p}}\|$ and $\|\mathbf{p}\|$ are derived easily as indicated in (5.7).

b) Consider the desired kinetic energy K_d as a Lyapunov candidate. Since $H_d = K_d + V_d$, we have the following equation

$$K_d = H_d - V_d. \quad (5.10)$$

Using this equation, time derivative of K_d is

$$\begin{aligned} \dot{K}_d &= -\mathbf{p}^T \mathbf{M}_d^{-1} \mathbf{R}_2 \mathbf{M}_d^{-1} \mathbf{p} - (\nabla_{\mathbf{q}} V_d)^T \mathbf{M}_d^{-1} \mathbf{p} \\ &\leq -\|\mathbf{p}\|^2 \lambda_{\min}^2\{\mathbf{M}_d^{-1}\} \lambda_{\min}\{\mathbf{R}_2\} + \|\nabla_{\mathbf{q}} V_d\| \lambda_{\max}\{\mathbf{M}_d^{-1}\} \|\mathbf{p}\|. \end{aligned} \quad (5.11)$$

Due to the satisfaction of (2.21) that means \mathbf{R}_2 is negative definite, this inequality ensures that $\|\mathbf{p}\|$ is bounded since the first term which is negative is proportional to $\|\mathbf{p}\|^2$ while the other term is proportional to $\|\mathbf{p}\|$. Note that the Lyapunov function (5.10) has the following upper and lower bounds

$$\frac{1}{2}\lambda_{\min}\{\mathbf{M}_d^{-1}\}\|\mathbf{p}\|^2 \leq K_d \leq \frac{1}{2}\lambda_{\max}\{\mathbf{M}_d^{-1}\}\|\mathbf{p}\|^2.$$

On the other hands, the right hand side of (5.11) is less than $-\mu\|\mathbf{p}\|^2$ if:

$$\|\mathbf{p}\| \geq \frac{c_{V_d}\lambda_{\max}\{\mathbf{M}_d^{-1}\}}{\lambda_{\min}^2\{\mathbf{M}_d^{-1}\}\lambda_{\min}\{\mathbf{R}_2\} - \mu},$$

where $\mu \in \mathbb{R} > 0$ is an arbitrary value such that the denominator be positive, while the upper bound of $\nabla_{\mathbf{q}}V_d$ is replaced by c_{V_d} based on Assumption 3. Invoking Theorem 4.18 of [136], the ultimate bound of $\|\mathbf{p}\|$ is derived as (5.8a). Similarly, the ultimate bound of $\tilde{\mathbf{p}}$ is derived as (5.8b). Notice that one may compute the upper bound of $\tilde{\mathbf{p}}$ using (5.8a). However, it is more conservative than (5.8b). Note that by considering (5.8a) and (5.8b), it is obvious that these ultimate bounds are reduced by increasing $\lambda_{\min}\{\mathbf{R}_2\}$. It should be noted that these ultimate bounds are also the upper bounds, if the initial condition of \mathbf{p} and $\tilde{\mathbf{p}}$ are less than c_{p2} and $c_{\tilde{p}2}$, respectively.

c) Considering Assumption 3, the upper bound of i th element of the kinetic energy shaping terms proposed in (5.5) is

$$(c_{M_i} + c_{\Lambda_i}, c_{M_d})c_p^2 \quad (5.12)$$

with the parameters defined in the Assumption 3. Notice that as explained in previous chapter, the elements of \mathbf{J}_2 are linear with respect to velocity. Thus, similar to (4.14), it is given as

$$\mathbf{J}_2(\mathbf{q}, \mathbf{p}) = \sum_{i=1}^{n_0} \tilde{\mathbf{p}}^T \mathbf{i} \boldsymbol{\alpha}(\mathbf{q}) \mathbf{W}_i$$

in which $n_0 = \frac{n(n-1)}{2}$, and \mathbf{W}_i s were introduced in (4.15). Since $\boldsymbol{\alpha}_i$ s are determined based on PDE (2.16), it is inferred that

$$\|\mathbf{J}_2(\mathbf{q}, \mathbf{p})\| \leq c_J \|\tilde{\mathbf{p}}\|. \quad (5.13)$$

Therefore, $\mathbf{J}_2\tilde{\mathbf{p}}$ has also an upper bound proportional to $\|\tilde{\mathbf{p}}\|^2$. The remaining term in control law is the damping term which has the following upper bound

$$\|\mathbf{K}_v \mathbf{G}^T \tilde{\mathbf{p}}\| \leq \lambda_{\max}\{\mathbf{K}_v\}c_{\tilde{p}}. \quad (5.14)$$

Finally, the upper bound of i th element of control law (2.15) is derived through summation of the above terms given in (5.4), (5.6), (5.12), (5.13) and (5.14) as (5.9). \square

Remark 4. The natural damping of a system represented by \mathbf{R} does not depend on whether a configuration is actuated or unactuated. Therefore, it is possible to \mathbf{R} be a positive definite matrix. If all the friction-like terms of a system are modeled, condition (2.21) is certainly satisfied. However, if they are not modeled, or if (2.21) is not satisfied, part *b* of the Theorem 2 is not applicable. Hence, for a system without natural damping terms, the upper bound of the velocity is derived from part *a* of Theorem 2. Furthermore, if the natural damping is included in the model and \mathbf{R}_2 is positive definite, the upper

bound of the velocity will be the minimum of the two upper bounds obtained in parts *a* and *b* of the Theorem 2. \square

In some UaSs like parallel robots [137] and VTOL aircraft [74], the input mapping matrix $\mathbf{G}(\mathbf{q})$ is configuration-dependent. Additionally, in some cases, the bound of the control law is not necessarily symmetric (i.e., $\mathbf{u}_m \neq -\mathbf{u}_M$ with \mathbf{u}_m and \mathbf{u}_M being the lower and upper bounds of actuators, respectively), e.g., in cable-driven robots, the control law shall be positive since cables can only push [138]. In the following remark, these issues are investigated.

Remark 5. Consider $\mathbf{G}(\mathbf{q})$ as a full rank matrix that maps the actuator torques/forces to configuration space torques/forces of the system. Based on a physical and energy-based point of view, it is bounded in the entire workspace. Thus, presume that,

$$\|(\mathbf{G}^T \mathbf{G})^{-1} \mathbf{G}^T\| \leq G_M, \quad \|\mathbf{G}\| \leq G_m.$$

In this case, the upper bound of the control law is derived based on the results of Theorem 2 as follows

$$G_M(c_V + c_{\Lambda_i} c_{V_d} + (c_M + c_{\Lambda_i} c_{M_d})c_p^2 + c_J c_{\bar{p}}^2) + G_m \lambda_{max}\{\mathbf{K}_v\} c_{\bar{p}}, \quad (5.15)$$

with $\|\nabla_{\mathbf{q}} V\| \leq c_V$, which is more conservative than that of (5.9). For the cases in which the bounds of the controller are non-symmetric, the lower bound of the actuators should be calculated separately. In this case, presume that σ denotes the minimum of all elements of the following expression in the workspace of the robot

$$(\mathbf{G}^T \mathbf{G})^{-1} \mathbf{G}^T \left(\nabla_{\mathbf{q}} V - \mathbf{M}_d \mathbf{M}^{-1} \nabla_{\mathbf{q}} V_d \right).$$

Hence, using (5.15) the lower bound of the control law (2.15) is derived as

$$\sigma - G_M((c_{M_i} + c_{\Lambda_i} c_{M_d})c_p^2 + c_J c_{\bar{p}}^2) - G_m \lambda_{max}\{\mathbf{K}_v\} c_{\bar{p}}. \quad (5.16)$$

By this means, if this value is positive, tensile forces in CDRs are ensured. Note that the aforementioned upper and lower bounds are general, but they are very conservative. Hence, for a specific system, one may derive less conservative bounds. \square

One of the main features of the IDA-PBC is that the stability of desired equilibrium is ensured without a switching in the control law. However, it may require high control effort in some cases. This fact is in confirmation of Brockett's theorem [135]. The reason is when the generalized positions of the system are close to a singular region, the control effort will get enormous values. As an example, for the cart-pole system [74], when the pendulum is close to the horizontal configuration, the control effort should get very enormous values to prevent the pendulum from falling. The following remarks are given on this issue.

Remark 6. In the Assumption 2, $\nabla_{\mathbf{q}} V_d$ is presumed to be bounded. However, in some UaSs, $\nabla_{\mathbf{q}} V_d$ is non-smooth. By considering H_d as a Lyapunov candidate, the system trajectory starts on the level set $H_d(t_0)$ and goes to lower level sets. The maximum value of $q_i - q_i^*$, is found by setting $\mathbf{p} = 0$ and $q_j = q_j^*$ for $j = 1, \dots, i-1, i+1, \dots, n$ in H_d and set it equal to $H_d(t_0) = V_d(t_0)$ since

$$V_d(t_0) \leq H_d \leq H_d(t_0).$$

By this means, the upper bound of each element of $\nabla_q V_d$ is derived. Therefore, Assumption 2 is always satisfied. This will be used in the VTOL aircraft example explained in Chapter 7. \square

Remark 7. The maximum torque/force of actuators is practically limited, and it may be lower than the computed upper bound proposed in (5.9), which maybe leads to actuator saturation. Poor performance or even instability are the results of this situation. Furthermore, this may lead to a divergence of the configuration variables from the region of attraction of the controller. As explained in Remark 6, large control efforts might be due to the initial configuration of the system in the vicinity of the singular regions. In order to rectify this problem; it is possible to design a two-phase controller, such that the goal of the first phase is to bring the system into a configuration away from the singular points, and then IDA-PBC, as the second phase, will be applied. The design of the first controller is case-dependent and might be done by prior knowledge of the system and the reported methods in literature such as [139, 140], but usually not a prohibitive task. We assume that the first phase controller is designed suitably such that the closed-loop system is stable and the configuration variables reach to a new configuration far from singular points. The stability of the system is ensured under this assumption since the first phase which is applied in a period of time, brings the system into a new configuration, and then the IDA-PBC, which has a precise stability proof, is applied. Furthermore, since from Theorem 2 and Remark 6, it is inferred that the upper bound of IDA-PBC depends on the initial condition of the system, the first phase aims to bring the system into a new configuration such that in this situation, the upper bound (5.9) is less than the upper bound of actuators (note that the new configuration is the initial condition of IDA-PBC). \square

5.1.1 Discussion

Here, we discuss how the derived upper bound can be used to design a suitable controller to keep the control effort within the actuator's limit. Furthermore, a comparison with similar works in the literature is accomplished to validate the proposed method. Additionally, the applicability of the method to fully actuated systems is also described.

In (5.9), except the upper bound of the gravity (i.e., c_V), the other parameters are either derived from the matching equations or the free gains of the controller (i.e., \mathbf{K}_v and k_i s defined in (5.1)). Thus, derivation of a suitable solution of the PDEs and appropriate selection of the gains lead to a suitable controller with respect to the practical limitation of the actuators. Smaller values for k_i s result to lower control efforts and its bound, with the expense of a slow rate of convergence. On the other hand, the effects of \mathbf{K}_v can be considered twofold. With a larger value of \mathbf{K}_v , it is expected that the control law is augmented. However, it may reduce the upper bound of the velocity. Hence, it is possible to decrease the upper bound of control law by enlarging \mathbf{K}_v . In order to analyze the relation between \mathbf{K}_v and control law, first, its effect on the fully actuated systems is investigated. After this, UaSSs are categorized into two classes, and each case is analyzed in detail. Notice that the proposed upper bound may also be extended to the fully actuated systems without either solving the PDEs or requirement to the condition (2.21). Furthermore, note that in most cases $c_{p1} < c_{p2}$ and it may be inferred that c_{p2} is not useful. However, in total energy shaping of fully actuated systems, it is conceivable to decrease c_{p2} arbitrarily by increasing \mathbf{K}_v . It is due to the fact that in a fully actuated system, enlarging \mathbf{K}_v leads to increasing $\lambda_{min}\{\mathbf{R}_2\}$, while this is not necessarily held in UaSSs. Therefore, with $K_v = \kappa \mathbf{I}_n$ and a large $\kappa \in \mathbb{R} > 0$, the upper bound of the fully

actuated systems is approximated by the following expression:

$$c_{V_i} + c_{\Lambda_i} c_{V_d} + c_{V_d} \left(\frac{\lambda_{\max}\{\mathbf{M}_d\}}{\lambda_{\min}\{\mathbf{M}_d\}} \right)^{1/2}.$$

In UaSSs, suitable selection of \mathbf{K}_v is more complex. If $c_{\tilde{p}} = c_{\tilde{p}2}$, the right hand side of (5.14) is as follows

$$\lambda_{\max}\{\mathbf{K}_v\} c_{\tilde{p}} = \left(\frac{\lambda_{\max}\{\mathbf{M}_d\}}{\lambda_{\min}\{\mathbf{M}_d\}} \right)^{1/2} \frac{c_{V_d} \lambda_{\max}\{\mathbf{K}_v\}}{\lambda_{\min}\{\mathbf{R}_2\} - \mu}$$

By setting μ to be infinitesimal ($\mu \approx 0$), and replacing \mathbf{R}_2 from (2.20), the following equation is derived

$$\frac{\lambda_{\max}\{\mathbf{K}_v\}}{\lambda_{\min}\{\mathbf{R}_2\}} = \frac{\lambda_{\max}\{\mathbf{K}_v\}}{\lambda_{\min}\left\{\frac{1}{2}(\mathbf{R}\mathbf{M}^{-1}\mathbf{M}_d + \mathbf{M}_d\mathbf{M}^{-1}\mathbf{R}) + \mathbf{G}\mathbf{K}_v\mathbf{G}^T\right\}} \quad (5.17)$$

Hence, in order to decrease the upper bound of the damping term, if $\mathbf{R}\mathbf{M}^{-1}\mathbf{M}_d + \mathbf{M}_d\mathbf{M}^{-1}\mathbf{R}$ is positive definite, $\mathbf{K}_v \approx 0$ is a suitable choice. Otherwise, \mathbf{K}_v should be sufficiently large such that $\mathbf{R}_2 > 0$ is satisfied. From (5.8a), it is also inferred that the upper bound of the velocity is reduced by having a larger value for $\lambda_{\min}\{\mathbf{R}_2\}$. In the cases in which $\mathbf{R}\mathbf{M}^{-1}\mathbf{M}_d + \mathbf{M}_d\mathbf{M}^{-1}\mathbf{R} \geq 0$ and $\lambda_{\min}\{\mathbf{R}_2\}$ depends on \mathbf{K}_v , analytical design of \mathbf{K}_v is not facile, and it can be chosen case by case. However, under $\mathbf{R}\mathbf{M}^{-1}\mathbf{M}_d + \mathbf{M}_d\mathbf{M}^{-1}\mathbf{R} > 0$, and $\lambda_{\min}\{\mathbf{R}_2\}$ is independent of $\mathbf{K}_v\mathbf{G}^T\tilde{\mathbf{p}}$, $\mathbf{K}_v = 0$ is the best choice for minimizing (5.9).

In Theorem 2, the upper bound of the control law was computed. Since the control law of IDA-PBC was not modified, the domain of attraction depends on the solutions of potential and kinetic energy PDEs [74]. However, in the cases that the upper bound (5.9) is larger than the upper bound of actuators, Remark 7 is a suitable way to get rid of this problem. Otherwise, the domain of attraction of the controller is shrunk. This is the expense of using a bounded input controller with prescribed bounds.

Another method to address this issue is the modification of IDA-PBC approach. It should be accomplished such that the stability of the closed-loop system is not endangered. This is the main concentration of the next section.

5.2 IDA-PBC with Prescribed Bounds

In this section, we concentrate on the problem of designing an IDA-PBC for a mechanical system such that saturation of the actuators is prevented. Presume that Assumption 2 with V_d defined as (5.1) is satisfied. By virtue of Assumption 2, define \mathbf{u}_m and \mathbf{u}_M as the lower and upper bounds of actuators

$$\mathbf{u}_m \leq \mathbf{u} \leq \mathbf{u}_M. \quad (5.18)$$

In order to satisfy this inequality, the matrix \mathbf{J}_n is added to the target dynamic (2.14) as follows

$$\begin{bmatrix} \dot{\mathbf{q}} \\ \dot{\tilde{\mathbf{p}}} \end{bmatrix} = \begin{bmatrix} \mathbf{0} & \mathbf{M}^{-1}\mathbf{M}_d \\ -\mathbf{M}_d\mathbf{M}^{-1} & \mathbf{J}_2 - \mathbf{G}\mathbf{K}_v\mathbf{G}^T + \mathbf{J}_n \end{bmatrix} \begin{bmatrix} \nabla_{\mathbf{q}} H_d \\ \nabla_{\tilde{\mathbf{p}}} H_d \end{bmatrix}, \quad (5.19)$$

where $\mathbf{J}_n \in \mathbb{R}^{n \times n}$ is a design parameter. Note that adding extra parameters to other elements of the matrix in (5.19) is not straightforward since $\dot{\mathbf{q}} = \mathbf{M}_d^{-1}\tilde{\mathbf{p}}$ should be held in

closed-loop. By this means, the kinetic energy PDE (2.16) is replaced by

$$\mathbf{G}^\perp \{ \nabla_q(\mathbf{p}^T \mathbf{M}^{-1} \mathbf{p}) - \mathbf{M}_d \mathbf{M}^{-1} \nabla_q(\mathbf{p}^T \mathbf{M}_d^{-1} \mathbf{p}) + 2(\mathbf{J}_2 + \mathbf{J}_n) \mathbf{M}_d^{-1} \mathbf{p} \} = 0, \quad (5.20)$$

the potential energy PDE (2.16) does not changed, and the control law is

$$\mathbf{u} = \mathbf{G} \left(\nabla_q H - \mathbf{M}_d \mathbf{M}^{-1} \nabla_q H_d + (\mathbf{J}_2 - \mathbf{G} \mathbf{K}_v \mathbf{G}^T + \mathbf{J}_n) \nabla_p H_d \right), \quad (5.21)$$

in which $\mathbf{G} = (\mathbf{G}^T \mathbf{G})^{-1} \mathbf{G}^T$. Furthermore, the stability condition is in the following form

$$\dot{H}_d = (\nabla_p H_d)^T (-\mathbf{G} \mathbf{K}_v \mathbf{G}^T + \mathbf{J}_n) \nabla_p H_d, \quad (5.22)$$

which should be negative (semi) definite. Considering PDE (5.20), it is clear that the obtained solution of (2.16) does not satisfy (5.20) in general. Therefore, it seems that the proposed solutions for specific systems are not usable here. Additionally, the stability of the closed-loop system is not ensured. With the purpose of remedy these problems, it is reasonable to design \mathbf{J}_n such that it is in range space of input mapping matrix and it is skew-symmetric. This structure leads to vanishing \mathbf{J}_n in PDE (5.20) and its ineffectiveness on stability criteria (5.22). Hence, \mathbf{J}_n is in the following form

$$\mathbf{J}_n = \mathbf{G} \mathbf{J}_u \mathbf{G}^T, \quad (5.23)$$

with $\mathbf{J}_u = -\mathbf{J}_u^T \in \mathbb{R}^{m \times m}$ as a design parameter. Since a skew-symmetric matrix has at least two rows, the following assumption is required.

Assumption 4. The mechanical system has at least two actuators, i.e., $m \geq 2$. \square

The control law (5.21) may be decomposed as follows

$$\mathbf{u} = \mathbf{u}_I + \mathbf{u}_J \quad (5.24)$$

$$\mathbf{u}_I = \mathbf{G} \left(\nabla_q H - \mathbf{M}_d \mathbf{M}^{-1} \nabla_q H_d + (\mathbf{J}_2 - \mathbf{G} \mathbf{K}_v \mathbf{G}^T) \nabla_p H_d \right)$$

$$\mathbf{u}_J = \mathbf{G} \mathbf{J}_n \nabla_p H_d,$$

in which \mathbf{u}_I represent the normal IDA-PBC control law and \mathbf{u}_J is the added design parameter with respect to actuators' bound. Replacing (5.23) in (5.24) results in $\mathbf{u}_J = \mathbf{J}_u \mathbf{G}^T \nabla_p H_d = \mathbf{J}_u \mathbf{y}_d$ with \mathbf{y}_d as follows

$$\mathbf{y}_d := \mathbf{G}^T \nabla_p H_d. \quad (5.25)$$

Incorporation of (5.18) and (5.24) yields

$$\mathbf{u}_m \leq \mathbf{u}_I + \mathbf{u}_J \leq \mathbf{u}_M. \quad (5.26)$$

Adding $-\frac{\mathbf{u}_m + \mathbf{u}_M}{2}$ to all sides of (5.26), results in

$$\left| u_{I_i} + u_{J_i} - \frac{u_{m_i} + u_{M_i}}{2} \right| \leq \frac{u_{M_i} - u_{m_i}}{2}, \quad \text{for } i = 1, \dots, m \quad (5.27)$$

in which the index i denotes the i th element of a vector. With a minor loss of generality, replace (5.27) by the following inequality

$$\|\mathbf{u}_J - \mathbf{b}\|_\infty \leq \rho := \min_i \left\{ \frac{u_{M_i} - u_{m_i}}{2} \right\}, \quad (5.28)$$

with

$$\mathbf{b} = -\mathbf{u}_I + \frac{\mathbf{u}_m + \mathbf{u}_M}{2}. \quad (5.29)$$

Note that (5.28) is derived by calculating the largest and the lowest values of the left and right-hand side of (5.27), respectively. It is clear that if (5.28) is satisfied then (5.27) is satisfied. See the following lemma for more details.

Lemma 1. A sufficient condition for equivalence of the inequality (5.27) to (5.28) is satisfaction of one of the following conditions.

- a) $\mathbf{u}_M - \mathbf{u}_m = \kappa[1, \dots, 1]^T$ with an arbitrary scalar κ ,
- b) $\mathbf{u}_m = \kappa[1, \dots, 1]^T$ and $\mathbf{u}_M = \kappa'[1, \dots, 1]^T$ with arbitrary scalars κ and κ' ,
- c) $\mathbf{u}_m = -\mathbf{u}_M$.

■

Proof. Notice that inequality (5.28) is the worst case of (5.27) in which the maximum value of the left hand side, and the minimum value of the right hand side of (5.27) are replaced. If all elements of the right hand side of (5.27) are equal, i.e.,

$$\frac{u_{M_i} - u_{m_i}}{2} = \frac{u_{M_j} - u_{m_j}}{2} \quad \text{for every } i, j \in \{1, \dots, m\}. \quad (5.30)$$

then it is required to prove that the inequality (5.28) holds. Now the condition (5.30) is verified for the above cases.

a) It is the simplest case that apparently satisfies (5.30).

b) It is clear that if all components of \mathbf{u}_m and \mathbf{u}_M are the same, then (5.30) is held. Note that this case is very fit for parallel robots.

c) If $\mathbf{u}_m = -\mathbf{u}_M$, it is possible to form the new control inputs as $u_{new_i} = u_i/u_{M_i}$. In this case, the upper and lower bounds of all components of \mathbf{u}_{new} are 1 and -1, respectively. Hence, this coincide with case b) and thus, (5.30) is satisfied. This case is fit for serial robots in practice. □

In [125] the inequality (2.18) was replaced by a 2-norm and this conservative problem was solved for the case of fully actuated CDRs. In the following, we focus on the problem (2.18). Since the design parameters are in the matrix \mathbf{J}_u , the inequality (5.28) should be reformulated. Hence, $\mathbf{u}_J = \mathbf{J}_u \mathbf{y}_d$ is represented as follows

$$\mathcal{Y}\mathfrak{J} := \mathbf{J}_u \mathbf{y}_d, \quad (5.31)$$

where $\mathcal{Y}(\mathbf{q}, \mathbf{p}) \in \mathbb{R}^{m \times \frac{m(m-1)}{2}}$ is matrix representation of \mathbf{y}_d and $\mathfrak{J} \in \mathbb{R}^{\frac{m(m-1)}{2}}$ contains the components of \mathbf{J}_u as

$$\mathfrak{J} = [J_{u_{1,2}}, \dots, J_{u_{1,m}}, J_{u_{2,3}}, \dots, J_{u_{m-1,m}}]^T,$$

with \mathbf{J}_u represented in the following form

$$\mathbf{J}_u = \begin{bmatrix} 0 & J_{u_{1,2}} & \dots & J_{u_{1,m}} \\ -J_{u_{1,2}} & 0 & \dots & J_{u_{2,m}} \\ \vdots & \vdots & \ddots & \vdots \\ -J_{u_{1,m}} & -J_{u_{2,m}} & \dots & 0 \end{bmatrix}.$$

The structure of the matrix \mathcal{Y} is defined as follows. Denote the i th column of \mathcal{Y} by $\mathcal{Y}(:, i)$ and (i, j) th element of \mathbf{J}_u as $J_{u_{i,j}}$. Presume that \mathfrak{J}_i is (j, k) th element of matrix \mathbf{J}_u , i.e., $\mathfrak{J}_i = J_{u_{j,k}}$ with $k > j$. Due to skew-symmetric feature of the matrix \mathbf{J}_u , \mathfrak{J}_i is multiplied to two elements of \mathbf{y}_d with different sign since $J_{u_{j,k}} = -J_{u_{k,j}}$. Therefore, in the new representation $\mathcal{Y}\mathfrak{J}$, every column of matrix \mathcal{Y} has only two nonzero elements with different sign. In $\mathcal{Y}(:, i)$, the non-zero elements $\mathcal{Y}_{j,i}$ and $\mathcal{Y}_{k,i}$ are derived as follows

$$\mathcal{Y}_{j,i} = y_{d_k}, \quad \mathcal{Y}_{k,i} = -y_{d_j}.$$

For example, for $m = 2$ and $m = 3$ the matrix \mathcal{Y} is in the following form

$$m = 2: \quad \mathcal{Y} = \begin{bmatrix} y_{d_2} \\ -y_{d_1} \end{bmatrix}, \quad m = 3: \quad \mathcal{Y} = \begin{bmatrix} y_{d_2} & y_{d_3} & 0 \\ -y_{d_1} & 0 & y_{d_3} \\ 0 & -y_{d_1} & -y_{d_2} \end{bmatrix} \quad (5.32)$$

The problem is now designing the vector \mathfrak{J} with respect to

$$\|\mathcal{Y}\mathfrak{J} - \mathbf{b}\|_\infty \leq \rho, \quad (5.33)$$

with ρ as(5.28). As it will be described in the latter theorem, the rank of the matrix \mathcal{Y} has a critical role in solving (5.33). In the following lemma, the rank is computed.

Lemma 2. Under Assumption 4,

$$\text{rank}(\mathcal{Y}) = m - 1. \quad \blacksquare$$

Proof. Since \mathbf{J}_n is skew-symmetric, $(\nabla_{\mathbf{p}} H_d)^T \mathbf{J}_n (\nabla_{\mathbf{p}} H_d) = 0$, from (5.23) and (5.31) it is inferred that $(\mathbf{G}^T \nabla_{\mathbf{p}} H_d)^T \mathbf{J}_u (\mathbf{G}^T \nabla_{\mathbf{p}} H_d) = \mathbf{y}_d^T \mathcal{Y} \mathfrak{J} = 0$. Due to satisfaction of this term for every \mathfrak{J} , the following equation is deduced

$$\mathbf{y}_d^T \mathcal{Y} = 0. \quad (5.34)$$

Based on this equation, the structure of \mathcal{Y} and also the dimension of \mathcal{Y} which is $m \times \frac{m(m-1)}{2}$, it is inferred that

$$\text{rank}(\mathcal{Y}) = \min(m, \frac{m(m-1)}{2}) - 1.$$

Clearly, for $m \geq 3$, it shows that $\text{rank}(\mathcal{Y}) = m - 1$. The remaining case is $m = 2$ that from (5.32) it is apparent its rank is one. Thus, generally it is argued that $\text{rank}(\mathcal{Y}) = m - 1$. \square

Due to rank deficiency of \mathcal{Y} , we should find the best value of \mathcal{J} . The main results of this section are gathered in the next theorem where the following optimization problem is solved

$$\min_{\mathfrak{J}} \|\mathcal{Y}\mathfrak{J} - \mathbf{b}\|_\infty \quad (5.35)$$

Theorem 3. Consider the optimization problem (5.35) and presume that the optimal solution is denoted by \mathfrak{J}^* .

1. Define

$$\begin{aligned} \sigma^* &:= \min_a -\frac{\boldsymbol{\varpi}^T \mathbf{b}}{\boldsymbol{\varpi}^T \mathbf{v}(a)} \\ \text{s.t. } &-\frac{\boldsymbol{\varpi}^T \mathbf{b}}{\boldsymbol{\varpi}^T \mathbf{v}(a)} > 0, \end{aligned} \quad (5.36)$$

in which

$$\mathbf{v}(a) = [(-1)^{a_1}, \dots, (-1)^{a_m}]^T, \quad (5.37)$$

with $a_i \in \{0, 1\}$ for $i \in \{1, \dots, m\}$ and $\boldsymbol{\varpi}$ denotes left kernel of

$$\mathcal{A} := \mathcal{Y}\mathcal{Y}^T \quad (5.38)$$

such that $\boldsymbol{\varpi}^T \mathcal{A} = 0$. Then, σ^* is the minimum value of (5.35).

2. In order to derive the optimal \mathfrak{J} , consider ℓ such that the matrix $\mathcal{A}_e(\ell, \ell)$ is full rank where $\mathcal{A}_e(i, j)$ is obtained by elimination of the i th row and j th column of \mathcal{A} . Then, \mathfrak{J}^* as the optimal \mathfrak{J} is

$$\mathfrak{J}^* = \mathcal{Y}^T \mathbf{x}^*, \quad (5.39)$$

where

$$\begin{aligned} \mathbf{x}^* &= [\theta_1, \dots, \theta_{\ell-1}, 0, \theta_\ell, \dots, \theta_m]^T \\ \boldsymbol{\theta} &:= \mathcal{A}_e^{-1}(\ell, \ell)(\mathbf{b}_e(\ell) + \sigma^* \mathbf{v}_e^*(\ell)) \end{aligned} \quad (5.40)$$

in which $\mathbf{v}^* = \mathbf{v}(a^*)$ and $\mathbf{b}_e(i)$ means i th element of \mathbf{b} is omitted. ■

Invoking Theorem 3, the control law is

$$\mathbf{u} = \mathbf{u}_I + \mathbf{u}_J = \mathbf{G} \left(\nabla_{\mathbf{q}} H - \mathbf{M}_d \mathbf{M}^{-1} \nabla_{\mathbf{q}} H_d + (\mathbf{J}_2 - \mathbf{G} \mathbf{K}_v \mathbf{G}^T) \nabla_{\mathbf{p}} H_d \right) + \mathcal{Y} \mathfrak{J}^*. \quad (5.41)$$

Proof. 1. Since $\text{range}\{\mathcal{Y}\} = \text{range}\{\mathcal{Y}\mathcal{Y}^T\}$, for simplicity $\mathfrak{J} = \mathcal{Y}^T \mathbf{x}$ is set with $\mathbf{x} \in \mathbb{R}^m$ as the new design parameter. By this means, the problem (5.35) is in the following form

$$\min_{\mathbf{x}} \|\mathcal{A}\mathbf{x} - \mathbf{b}\|_\infty \quad (5.42)$$

with \mathcal{A} introduced in (5.38). In order to prove this part, the problem is separated into two cases.

a) Suppose that for any $i \in \{1, \dots, m\}$, the matrix $\mathcal{A}_e(i)$ which is derived from elimination of i th row of \mathcal{A} , is full rank. Then, it is shown by contradiction that the absolute value of all components of $\mathcal{A}\mathbf{x}^* - \mathbf{b}$, with \mathbf{x}^* as optimal solution, are equal. Define the residual vector $\mathbf{r} = \mathcal{A}\mathbf{x} - \mathbf{b}$ and presume that the absolute value of one of the components of $\mathbf{r}^* = \mathcal{A}\mathbf{x}^* - \mathbf{b}$ is smaller than the others, where with out loss of generality, the last element is considered as the smallest value. Hence, The problem (5.42) is reformulated in the following form

$$\begin{bmatrix} \mathcal{A}_e(m) \\ \mathcal{A}(m, \cdot) \end{bmatrix} \mathbf{x}^* - \begin{bmatrix} \mathbf{b}_e(m) \\ b_m \end{bmatrix} = \begin{bmatrix} \mathbf{r}_e^*(m) \\ r_m^* \end{bmatrix},$$

in which $\mathcal{A}(m, \cdot)$ denotes the m th row of \mathcal{A} . Since $\mathcal{A}_e(m)$ is full rank, it is possible to reduce $\mathbf{r}_e^*(m)$ and acquire a new optimal residual vector denoted by \mathbf{r}^{**} such that the largest absolute value of $\mathbf{r}_e^{**}(m)$ is equal to $|\mathbf{r}_m^{**}|$. Thus, a smaller value for (5.42) is derived and this is a contradiction.

b) Suppose that \mathcal{A} and \mathbf{b} are decomposed as follows

$$\mathcal{A} = \begin{bmatrix} \mathcal{A}_1 \\ \mathcal{A}_2 \end{bmatrix}, \quad \mathbf{b} = \begin{bmatrix} \mathbf{b}_1 \\ \mathbf{b}_2 \end{bmatrix},$$

in which rank of the matrix $\mathcal{A}_1 \in \mathbb{R}^{r \times m}$ is $r - 1$ and $\mathcal{A}_2 \in \mathbb{R}^{m-r \times m}$ is full rank. Then absolute value of all components of $\mathcal{A}_1 \mathbf{x}^* - \mathbf{b}_1$ are equal. This claim is easily proven by referring to the case a) because the matrix \mathcal{A}_2 is full rank and the minimization is limited by $\|\mathcal{A}_1 \mathbf{x} - \mathbf{b}_1\|_\infty$ that from the prior case, the absolute value of its components in $\mathbf{x} = \mathbf{x}^*$ are equal. Notice that in this case, it is feasible to set the last $m - r$ components of the residual vector \mathbf{r}^* equal to zero. However, to derive a general solution for \mathbf{x}^* , it is set equal to $\|\mathcal{A}_1 \mathbf{x}^* - \mathbf{b}_1\|_\infty$. Thus, it is asserted that the absolute value of all components of $\mathcal{A} \mathbf{x}^* - \mathbf{b}$ are equal.

According to above statement, the optimal residual vector is in the following form

$$\mathbf{r}^* = \sigma^* \mathbf{v}^*,$$

in which the components of the vector \mathbf{v} are in $\{-1, 1\}$ as determined in (5.37). From $\mathcal{A} \mathbf{x} - \mathbf{b} = \sigma \mathbf{v}$, it is deduced that $-\varpi^T \mathbf{b} = \sigma (\varpi^T \mathbf{v})$ in which ϖ belongs to the left kernel of \mathcal{A} . The optimal σ^* is derived by selecting the optimal sequences of 1 and -1 in \mathbf{v} , as indicated in (5.36).

2. Based on previous part, using σ^* and \mathbf{v}^* , the optimal \mathbf{x} is computed from $\mathcal{A} \mathbf{x}^* - \mathbf{b} = \sigma^* \mathbf{v}^*$. A method is removing the ℓ th equation and also ℓ th column of \mathcal{A} such that $\mathcal{A}_e(\ell, \ell)$ is full rank. By this means, the special solution \mathbf{x}^* is derived directly as (5.40) and then, $\mathfrak{J}^* = \mathcal{Y}^T \mathbf{x}^*$. Note that due to rank deficiency of \mathcal{A} , \mathbf{x}^* is not unique. □

Theorem 3 proposes the best solution of the optimal problem (5.35). However, it does not necessarily satisfy the input constraint (5.33). Therefore, although the results of Theorem 3 minimize the actuators' efforts with respect to \mathbf{J}_u , it is not possible to ensure boundedness of inputs with prescribed bounds using merely a skew-symmetric matrix.

5.2.1 Satisfaction of Prescribed Input Bounds for a Particular Class of Systems

In some cases, such as potential energy shaping of fully actuated serial robots [92] and total energy shaping of inertia wheel pendulum (where the inertia and desired inertia matrices are constant results in vanishing kinetic energy shaping terms) [94], by defining V_d as (5.1) and selection of conservative gains, the desired equilibrium point is stabilized while preventing the actuators from saturation. In this case, full power of the actuators are not used. Here, a methodology is designed for a class of mechanical systems to ensure stability with bounded input.

Assumption 5. Suppose that one of the following states holds.

1. The desired equilibrium point \mathbf{q}^* is natural such that merely potential energy is shaped.

2. The term $\nabla_{\mathbf{q}}(\mathbf{p}^T \mathbf{M}^{-1} \mathbf{p})$ is zero. Thus, total energy shaping is accomplished with a constant \mathbf{M}_d .

□

Notice that a large number of systems such as VTOL aircraft [74], inertia wheel pendulum [94], UCDRs [17, 123] and cranes [141] satisfy Assumption 5. For the case of fully actuated systems, the control law is modified to

$$\begin{aligned} \mathbf{u} &= \mathbf{u}_A + \mathbf{u}_B + \mathbf{u}_J \\ \mathbf{u}_A &= \mathbf{G} \nabla_{\mathbf{q}} V \\ \mathbf{u}_B &= -\bar{k} \mathbf{G} (\nabla_{\mathbf{q}} V_d + \mathbf{G} \mathbf{K}_v \mathbf{G}^T \nabla_{\mathbf{p}} H_d) \\ \mathbf{u}_J &= \mathbf{G} \mathbf{J}_n \nabla_{\mathbf{p}} H_d = \mathcal{Y} \mathfrak{J}, \end{aligned} \quad (5.43)$$

in which $\bar{k} > 0$ is a design parameter determined later, and in this case $\mathbf{G} = \mathbf{G}^{-1}$. For the case of underactuated systems, the control law is modified as follows

$$\begin{aligned} \mathbf{u} &= \mathbf{u}_A + \mathbf{u}_B + \mathbf{u}_J \\ \mathbf{u}_A &= \mathbf{G} (\nabla_{\mathbf{q}} V - \mathbf{M}_d \mathbf{M}^{-1} \nabla_{\mathbf{q}} V_{dn}) \\ \mathbf{u}_B &= -\bar{k} \mathbf{G} (\mathbf{M}_d \mathbf{M}^{-1} \nabla_{\mathbf{q}} V_{dh} + \mathbf{G} \mathbf{K}_v \mathbf{G}^T \nabla_{\mathbf{p}} H_d) \\ \mathbf{u}_J &= \mathbf{G} \mathbf{J}_n \nabla_{\mathbf{p}} H_d = \mathcal{Y} \mathfrak{J}, \end{aligned} \quad (5.44)$$

in which from first case of Assumption 5, $\mathbf{M}_d = \mathbf{M}$ is selected if \mathbf{q}^* is the natural equilibrium point. Under satisfaction of second condition in Assumption 5, \mathbf{M}_d will be a constant matrix. Note that \mathbf{u}_A contains some of the terms of controller related to potential energy shaping and \mathbf{u}_B includes all the terms that depends on the gains, i.e., \mathbf{K}_v and k_i s in (5.1).

Theorem 4. Consider a mechanical system represented as (2.9) with control law (5.43) if it is fully actuated, or (5.44) if it is underactuated. Suppose that Assumptions 2, 4, 5 and Lemma 1 are satisfied. σ^* denotes the solution of (5.35) derived from applying Theorem 1 with $\mathbf{b} = -\mathbf{u}_B$ with $\bar{k} = 1$. Define \bar{k} as

$$\bar{k} = \begin{cases} 1 & \text{if } \sigma^* \leq \rho' \\ \frac{\rho'}{\sigma^*} & \text{otherwise} \end{cases} \quad (5.45)$$

with

$$\rho' := \rho - \left\| \mathbf{u}_A - \frac{\mathbf{u}_m + \mathbf{u}_M}{2} \right\|_{\infty}. \quad (5.46)$$

Then, \mathbf{q}^* is stable while prescribed bounds of actuators are met.

■

The interpretation of this theorem is that at first, Theorem 3 is used. If the control law is not within the prescribed bounds, then \bar{k} is modified as (5.45) such that the input constraints are held. Notice that under Assumption 5, it is feasible to guarantee stabilization with bounded inputs via only modification of the gains in \mathbf{u}_B . However, using \mathbf{J}_u , a better response with less conservative inputs may be achieved.

Proof. Invoking [142], the system is stable by considering the following Lyapunov function candidate,

$$\mathcal{V} = \frac{1}{2} \mathbf{p}^T \mathbf{M}_d^{-1} \mathbf{p} + V_{dn} + \int_0^{q-q^*} \bar{\mathbf{k}} \frac{\partial V_{dh}(\mathbf{r})}{\partial \mathbf{r}} d\mathbf{r},$$

whose time derivative is equal to (2.8). The left hand side of (5.27) in this case is in the following form

$$\|\mathbf{u}_A + \mathbf{u}_B + \mathbf{u}_J - \frac{\mathbf{u}_m + \mathbf{u}_M}{2}\|_\infty \leq \|\mathbf{u}_B + \mathbf{u}_J\|_\infty + \|\mathbf{u}_A - \frac{\mathbf{u}_m + \mathbf{u}_M}{2}\|_\infty$$

where triangle inequality was used. By virtue of Assumption 2 and Lemma 1, it is simply deduced that $\rho' > 0$. Now we should prove that $\|\mathbf{u}_B + \mathbf{u}_J\| \leq \rho'$, or equivalently,

$$\|\mathcal{Y}\mathfrak{J} - \mathbf{b}\| \leq \rho',$$

with $\mathbf{b} = -\mathbf{u}_B$ and $\bar{\mathbf{k}} = 1$. After applying Theorem 1, if $\sigma^* \leq \rho'$ with σ^* as the solution of (5.35), this control law is within the actuators' bound. Otherwise, consider equations (5.36), (5.39) and (5.40). Clearly, \mathfrak{J}^* is linear with respect to \mathbf{b} , which itself is linearly dependent on $\bar{\mathbf{k}}$. Thus, \mathfrak{J}^* is linear with respect to $\bar{\mathbf{k}}$. Hence, \mathfrak{J}^* and \mathbf{b} are both linear with respect to $\bar{\mathbf{k}}$ results in linearity of σ^* to $\bar{\mathbf{k}}$. By this means, $\bar{\mathbf{k}}$ should be reduced such that $\sigma^* = \|\mathcal{Y}\mathfrak{J}^* - \mathbf{b}\|_\infty \leq \rho'$ is satisfied. From linearity of \mathfrak{J}^* and \mathbf{b} to $\bar{\mathbf{k}}$, the control law is modified based on (5.45). Therefore, the control law is within the prescribed bounds of actuators. \square

At the end of this chapter and based on the above theorem, it is possible to propose a simple practical method to confine the control law. The results are presented in the following proposition.

Proposition 2. Consider a mechanical system with dynamic formulation (2.9) under Assumptions 2, 5 with the following control law

$$\mathbf{u} = \text{sat}\left(\mathbf{G}(\nabla_q V - \mathbf{M}_d \mathbf{M}^{-1} \nabla_q V_d - \mathbf{G} \mathbf{K}_v \mathbf{G}^T \nabla_p H_d)\right) \quad (5.47)$$

in which the function $\text{sat}(\cdot)$ is the standard saturation function as follows

$$\text{sat}(u_i) = \begin{cases} u_{max_i} & u_i > u_{max_i} \\ u_i & u_{min_i} \leq u_i \leq u_{max_i} \\ u_{min_i} & u_i < u_{min_i} \end{cases} \quad (5.48)$$

in which \mathbf{u}_{min} and \mathbf{u}_{max} should be chosen such that

$$u_{m_i} \leq u_{min_i}, \quad u_{M_i} \geq u_{max_i}. \quad (5.49)$$

Then \mathbf{q}^* is stable with bounded inputs. \blacksquare

Proof. The boundedness of the inputs in the prescribed bounds is immediately derived from (5.47). Furthermore, the stability proof is similar to the proof of Theorem 4. In other words, we claim that the control law (5.47) is equal to the controller of Theorem 4 with $\mathbf{u}_J = 0$. Note that the terms in control law which are independent of the gains are necessarily inside the bounds of actuators. Hence, if control law is out of the range $[\mathbf{u}_{min}, \mathbf{u}_{max}]$, it is possible to choose the gains such that \mathbf{u} coincides with the edge of the

$[\mathbf{u}_{min}, \mathbf{u}_{max}]$. This means that saturation of the control law is equivalence to a controller with varying gains. This completes the proof since Theorem 4 ensures the stability of a controller with varying gain. \square

5.3 Conclusion

In this section, we focused on the bounded input IDA-PBC for mechanical systems. The problem was examined from two different perspectives. The first approach was based on the calculation of the upper bound of each term in the control law. Based on the suitable definition of V_{dh} and computation of the upper bound of velocity, the upper bound of controller was derived. The effect of non-smooth terms in potential shaping was analyzed, and a two-phase controller was designed to prevent enormous control law. The second method was devised with the purpose of satisfying the prescribed bounds of actuators. Using the free part of the interconnection matrix, the problem was reformulated in an infinite norm optimization, and the analytic solution was computed. Modification of IDA-PBC for a class of mechanical systems such that the control law is within the prescribed bounds was another achievement of this section.

Chapter 6

Other Developments of IDA-PBC

This chapter presents a number of advanced methods of IDA-PBC. First, IDA-PBC with position feedback for a class of underactuated manipulators is designed. Then, we concentrate on the problem of stabilization of UaSs in the presence of parameter uncertainties. It will be shown that generally, this problem does not seem to obviate using an adaptive controller without the requirement of correct estimation of parameters. However, for a class of mechanical systems, it is possible to design an adaptive IDA-PBC such that stability of desired equilibrium point is ensured while the parameters are not necessarily estimated correctly. Another achievement of this chapter is a simplification of potential energy PDE for stabilization of natural equilibrium points such that the non-homogeneous solution is not required. Finally, gravity compensation of actuated joints in the entire workspace is replaced by desired gravity compensation. By this means, only the gravity term in the desired pose is needed.

6.1 IDA-PBC with Position Feedback

As explained in chapter 2, using immersion and invariance (I&I) observer, it is possible to design IDA-PBC by merely position feedback [107]. However, I&I is designed based on the solution of two sets of PDEs that restrict its applicability. Here, a simple well-known velocity observer in mechanical systems which is usually called “dirty derivative” is used to implement IDA-PBC with position feedback on a class of systems including UCDRs. Let us first introduce this observer. Consider a fully actuated serial robot with dynamic formulation

$$M(\mathbf{q})\ddot{\mathbf{q}} + C(\mathbf{q}, \dot{\mathbf{q}})\dot{\mathbf{q}} + \mathcal{G}(\mathbf{q}) = \mathbf{u},$$

in which $M(\mathbf{q})$ is inertia matrix, $C(\mathbf{q}, \dot{\mathbf{q}})$ denotes the centrifugal and Coriolis matrix, $\mathcal{G}(\mathbf{q}) = \nabla_{\mathbf{q}}V$ is the vector of gravity terms. The control law for regulation problem is designed as follows [105, 143]

$$\mathbf{u} = \mathcal{G}(\mathbf{q}) - \mathbf{K}_p(\mathbf{q} - \mathbf{q}^*) - \mathbf{K}_d\boldsymbol{\nu} \quad (6.1a)$$

$$\dot{\boldsymbol{\nu}} = -\mathbf{A}\boldsymbol{\nu} + \mathbf{B}\dot{\mathbf{q}}, \quad (6.1b)$$

with $\mathbf{K}_p, \mathbf{K}_d, \mathbf{A}, \mathbf{B} \in \mathbb{R}^{n \times n}$ being arbitrary positive definite matrix. Note that the control law is the well-known PD with gravity compensation, but $\dot{\mathbf{q}}$ is replaced by its estimate

denoted by $\boldsymbol{\nu}$. Notice that the observer (6.1b) may be represented as follows

$$\begin{aligned}\dot{\boldsymbol{q}}_c &= -\boldsymbol{A}(\boldsymbol{q}_c + \boldsymbol{B}(\boldsymbol{q} - \boldsymbol{q}^*)) \\ \boldsymbol{\nu} &= \boldsymbol{q}_c + \boldsymbol{B}(\boldsymbol{q} - \boldsymbol{q}^*),\end{aligned}\quad (6.2)$$

with \boldsymbol{q}_c being an auxiliary variable. Asymptotic stability of closed-loop system is easily proved by considering

$$\boldsymbol{\nu} = \frac{1}{2}\dot{\boldsymbol{q}}^T \boldsymbol{M}(\boldsymbol{q})\dot{\boldsymbol{q}} + \frac{1}{2}(\boldsymbol{q} - \boldsymbol{q}^*)^T \boldsymbol{K}_p(\boldsymbol{q} - \boldsymbol{q}^*) + \frac{1}{2}\boldsymbol{\nu}^T \boldsymbol{K}_d \boldsymbol{B}^{-1} \boldsymbol{\nu}$$

as a Lyapunov candidate. Note that by integrating (6.1b), it is inferred that $\boldsymbol{\nu}$ is a function of \boldsymbol{q} .

Now consider IDA-PBC methodology. Since the controller (6.1a) is a particular form of potential energy shaping, it seems that the observer (6.1b) is applicable to IDA-PBC when potential energy is shaped, or \boldsymbol{M} and \boldsymbol{M}_d are constant. The results are presented in the following proposition.

Proposition 3. Consider a mechanical system with dynamic formulation (2.9) (or (2.18)) under satisfaction of Assumption 5. Then, the equilibrium \boldsymbol{q}^* is stable with the following control law

$$\begin{aligned}\boldsymbol{u} &= (\boldsymbol{G}^T \boldsymbol{G})^{-1} \boldsymbol{G}^T (\nabla_{\boldsymbol{q}} V - \boldsymbol{M}_d \boldsymbol{M}^{-1} \nabla_{\boldsymbol{q}} V_d) - \boldsymbol{K}_v \boldsymbol{G}^T \boldsymbol{\nu} \\ \dot{\boldsymbol{\nu}} &= -\boldsymbol{A} \boldsymbol{\nu} + \boldsymbol{G} \boldsymbol{K}_v \boldsymbol{G}^T \boldsymbol{M}_d^{-1} \boldsymbol{p},\end{aligned}\quad (6.3)$$

in which V_d satisfy PDE (2.17). ■

Recall that Assumption 5 contains a number of UaSs including UCDRs.

Proof. Replacing (6.3) in (2.9), the closed-loop system has a PH structure as follows

$$\begin{bmatrix} \dot{\boldsymbol{q}} \\ \dot{\boldsymbol{p}} \\ \dot{\boldsymbol{\nu}} \end{bmatrix} = \begin{bmatrix} \mathbf{0} & \boldsymbol{M}^{-1} \boldsymbol{M}_d & \mathbf{0} \\ -\boldsymbol{M}_d \boldsymbol{M}^{-1} & \mathbf{0} & -\boldsymbol{G} \boldsymbol{K}_v \boldsymbol{G}^T \\ \mathbf{0} & \boldsymbol{G} \boldsymbol{K}_v \boldsymbol{G}^T & -\boldsymbol{A} \end{bmatrix} \begin{bmatrix} \nabla_{\boldsymbol{q}} H_{d_{new}} \\ \nabla_{\boldsymbol{p}} H_{d_{new}} \\ \nabla_{\boldsymbol{\nu}} H_{d_{new}} \end{bmatrix}\quad (6.4)$$

with

$$H_{d_{new}} = H_d + \frac{1}{2} \boldsymbol{\nu}^T \boldsymbol{\nu}.\quad (6.5)$$

Consider $H_{d_{new}}$ as Lyapunov function. Its derivative is

$$\dot{H}_{d_{new}} = -\boldsymbol{\nu}^T \boldsymbol{A} \boldsymbol{\nu}.$$

Hence, $\boldsymbol{\nu}$ converges to zero. Replacing $\boldsymbol{\nu} = 0$ in the dynamic of observer, it is inferred that $\boldsymbol{G} \boldsymbol{K}_v \boldsymbol{G}^T \nabla_{\boldsymbol{p}} H_{d_{new}}$ converges to zero. Hence, \boldsymbol{q}^* is stable. □

Remark 8. In Proposition 3, it was possible to represent the closed-loop equations with control law (6.3) as PH form (6.4) since $\nabla_{\boldsymbol{q}} H_{d_{new}} = \nabla_{\boldsymbol{q}} V_d$ or $\boldsymbol{M}_d = \boldsymbol{M}$. In other words, if the kinetic energy shaping terms in control law (2.15) are not omitted, it is not possible to use the dirty derivative observer. In this case, we may design an I&I observer with the

expense of solving two sets of PDEs. Note that although designing I&I observer for the cases satisfy Assumption 5 is straightforward, it is not possible to represent the closed-loop system in PH form. \square

6.2 Adaptive IDA-PBC

In the IDA-PBC approach, it is assumed that the dynamic parameters of the system are known. However, the exact value of the parameters is usually uncertain in practice. Furthermore, in some cases that the input mapping matrix is state-dependent, such as VTOL aircraft and UCDRs, some parameters in \mathbf{G} may be uncertain. A powerful method to address this issue is adaptive control. This method categorizes to some classes, including model reference adaptive system, (MRAS) such that stability is ensured without necessarily correct estimation of parameters. Indirect adaptive control is another method that the parameters are estimated online. Here, the aim is to develop MRAS for IDA-PBC methodology that stability of desired equilibrium point is ensured in the presence of uncertain parameters. In the following, we show that this problem is generally hard to solve.

Due to uncertain parameters in \mathbf{M} and V , presume that we have the following regressors:

$$\nabla_q(\mathbf{p}^T \mathbf{M}^{-1} \mathbf{p}) - \mathbf{M}_d \mathbf{M}^{-1} \nabla_q(\mathbf{p}^T \mathbf{M}_d^{-1} \mathbf{p}) + 2\mathbf{J}_2 \mathbf{M}_d^{-1} \mathbf{p} = [\mathbf{Y}_{11}, \mathbf{Y}_{12}][\boldsymbol{\theta}_{11}^T, \boldsymbol{\theta}_{12}^T]^T = \mathbf{Y}_1 \boldsymbol{\theta}_1 \quad (6.6a)$$

$$\nabla_q V - \mathbf{M}_d \mathbf{M}^{-1} \nabla_q V_d = [\mathbf{Y}_{21}, \mathbf{Y}_{22}][\boldsymbol{\theta}_{21}^T, \boldsymbol{\theta}_{22}^T]^T = \mathbf{Y}_2 \boldsymbol{\theta}_2, \quad (6.6b)$$

where

$$\begin{aligned} \mathbf{Y}_{11} \boldsymbol{\theta}_{11} &= \nabla_q(\mathbf{p}^T \mathbf{M}^{-1} \mathbf{p}), & \mathbf{Y}_{12} \boldsymbol{\theta}_{12} &= -\mathbf{M}_d \mathbf{M}^{-1} \nabla_q(\mathbf{p}^T \mathbf{M}_d^{-1} \mathbf{p}) + 2\mathbf{J}_2 \mathbf{M}_d^{-1} \mathbf{p}, \\ \mathbf{Y}_{21} \boldsymbol{\theta}_{21} &= \nabla_q V, & \mathbf{Y}_{22} \boldsymbol{\theta}_{22} &= -\mathbf{M}_d \mathbf{M}^{-1} \nabla_q V_d. \end{aligned} \quad (6.7)$$

It seems that if the following matching equations are satisfied

$$\mathbf{G}^\perp(\mathbf{Y}_1 \tilde{\boldsymbol{\theta}}_1) = 0, \quad \mathbf{G}^\perp(\mathbf{Y}_2 \tilde{\boldsymbol{\theta}}_2) = 0, \quad (6.8)$$

then by applying the following control law

$$\begin{aligned} \mathbf{u} &= (\mathbf{G}^T \mathbf{G})^{-1} \mathbf{G}^T (\mathbf{Y}_1 \hat{\boldsymbol{\theta}}_1 + \mathbf{Y}_2 \hat{\boldsymbol{\theta}}_2) = (\mathbf{G}^T \mathbf{G})^{-1} \mathbf{G}^T (\mathbf{Y}_1 \boldsymbol{\theta}_1 + \mathbf{Y}_2 \boldsymbol{\theta}_2) \\ &\quad + (\mathbf{G}^T \mathbf{G})^{-1} \mathbf{G}^T (\mathbf{Y}_1 \tilde{\boldsymbol{\theta}}_1 + \mathbf{Y}_2 \tilde{\boldsymbol{\theta}}_2), \end{aligned} \quad (6.9)$$

the following equations are derived for the closed-loop system

$$\begin{bmatrix} \dot{\mathbf{q}} \\ \dot{\mathbf{p}} \end{bmatrix} = \begin{bmatrix} \mathbf{0} & \mathbf{M}^{-1} \mathbf{M}_d \\ -\mathbf{M}_d \mathbf{M}^{-1} & \mathbf{J}_2 - \mathbf{G} \mathbf{K}_v \mathbf{G}^T \end{bmatrix} \begin{bmatrix} \nabla_q H_d \\ \nabla_p H_d \end{bmatrix} + \begin{bmatrix} \mathbf{0} \\ \mathbf{Y}_1 \tilde{\boldsymbol{\theta}}_1 + \mathbf{Y}_2 \tilde{\boldsymbol{\theta}}_2 \end{bmatrix}, \quad (6.10)$$

By considering $\mathcal{V} = H_d + \frac{1}{2} \tilde{\boldsymbol{\theta}}^T \boldsymbol{\Gamma} \tilde{\boldsymbol{\theta}}$ as a Lyapunov function with $\mathbf{Y} = [\mathbf{Y}_1, \mathbf{Y}_2]$, $\boldsymbol{\theta} = [\boldsymbol{\theta}_1^T, \boldsymbol{\theta}_2^T]^T$ and $\boldsymbol{\Gamma}$ a free positive definite matrix, its derivative is

$$\dot{\mathcal{V}} = -\mathbf{p}^T \mathbf{M}_d^{-1} \mathbf{G} \mathbf{K}_v \mathbf{G}^T \mathbf{M}_d^{-1} \mathbf{p} + \mathbf{p}^T \mathbf{M}_d^{-1} \mathbf{Y} \tilde{\boldsymbol{\theta}} + \tilde{\boldsymbol{\theta}}^T \boldsymbol{\Gamma} \dot{\tilde{\boldsymbol{\theta}}}. \quad (6.11)$$

By defining the adaptation law $\dot{\tilde{\boldsymbol{\theta}}} = -\boldsymbol{\Gamma}^{-1} \mathbf{Y}^T \mathbf{M}_d^{-1} \mathbf{p}$, under satisfaction of (6.8), the derivative of Lyapunov function (6.11) is $-\mathbf{p}^T \mathbf{M}_d^{-1} \mathbf{G} \mathbf{K}_v \mathbf{G}^T \mathbf{M}_d^{-1} \mathbf{p}$. It is clear that a sufficient

condition for satisfaction of (6.8), is that $\tilde{\boldsymbol{\theta}}_1 = 0$ and $\tilde{\boldsymbol{\theta}}_2 = 0$. Generally, we should have

$$\tilde{\boldsymbol{\theta}}_1 \in \text{null space}\{\mathbf{G}^\perp \mathbf{Y}_1\}, \quad \tilde{\boldsymbol{\theta}}_2 \in \text{null space}\{\mathbf{G}^\perp \mathbf{Y}_2\},$$

such that (6.8) is held. This is the major problem of designing adaptive IDA-PBC such that ensuring stability of system depends on some conditions on estimated parameters. Furthermore, the proposed adaptation law is not well-defined since it is a function of \mathbf{M}_d which is unknown. Additionally, the expression of the terms in (6.6) in regressor form is doubtful due to the fractional terms. Hence, based on the above shortcoming issues, it is clear why an adaptive IDA-PBC with respect to dynamical parameters has not yet been reported in the literature. In the following, we try to design adaptive IDA-PBC for a class of UaSs. A particular form of the following theorem has been designed for spatial CDR in [144].

6.2.1 Adaptive Potential Energy Shaping of UCDRs

Before presenting the results, we need to the following assumption.

Assumption 6. The natural damping matrix of the robot is positive definite, i.e., there exists the constant σ such that

$$0 < \sigma \leq \min\{r_1, \dots, r_n\} \quad \text{with} \quad \mathbf{R} = \text{diag}[r_1, \dots, r_n] \quad (6.12)$$

where \mathbf{R} was defined in (2.18). \square

Note that not only this assumption is not restrictive due to several elements such as air resistance, but also it lead to a better simulation of real world.

Theorem 5. Consider a general n -DOF UCDR with potential energy $V = mgy$ and the solution of potential energy PDE is derived as (4.22). The control law is designed as follows

$$\mathbf{u} = (\mathbf{G}^T \mathbf{G})^{-1} \mathbf{G}^T (\nabla_{\mathbf{q}} \hat{V} - \nabla_{\mathbf{q}} \hat{V}_d) - \mathbf{K}_v \mathbf{G}^T \tanh(\dot{\mathbf{q}}) \quad (6.13)$$

where

$$\hat{V} = \hat{m}gy, \quad \hat{V}_d = \hat{m}gy + \sum_{i=1}^m \hat{m}c_i \ln \cosh(f_i) + k_i \ln \cosh(f_i - f_i^*),$$

m denotes the number of cables (actuators), \hat{m} is the estimated value of the mass, and $\mathbf{q} = \mathbf{X}$ denotes position and orientation of the end-effector. The constants c_i s are derived from the condition $\nabla_{\mathbf{q}} V_d|_{\mathbf{q}=\mathbf{q}^*}$, and positive gains k_i s are chosen such that $\nabla_{\mathbf{q}}^2 V_d|_{\mathbf{q}=\mathbf{q}^*} > 0$. The adaptation law of \hat{m} is

$$\dot{\hat{m}} = \begin{cases} 0 & \text{if } \mu > 0 \ \& \ \hat{m} = \overline{m} \\ 0 & \text{if } \mu < 0 \ \& \ \hat{m} = \underline{m} \\ \gamma\mu & \text{else} \end{cases} \quad (6.14)$$

$$\mu := -\dot{\mathbf{q}}^T \sum_{i=1}^m c_i \nabla_{\mathbf{q}} \ln \cosh(f_i) - \varkappa \tanh(y - y_d) \left(\sum_{i=1}^m c_i \nabla_{\mathbf{y}} \ln \cosh(f_i) \right)$$

in which $\gamma > 0$ is a free gain, \overline{m} and \underline{m} are the upper and lower bounds of \hat{m} , and \varkappa is an

arbitrary value satisfying

$$0 < \varkappa < \min \left\{ \sqrt{\sum_{i=1}^m \left((1 + \tanh^2(f_i^*)) \left(\frac{\partial f_i}{\partial y} \right)^2 \Big|_{\mathbf{q}=\mathbf{q}^*} + \tanh(f_i^*) \frac{\partial^2 f_i}{\partial y^2} \Big|_{\mathbf{q}=\mathbf{q}^*} \right)} / \bar{m}, \right. \\ \left. \frac{\kappa\sigma}{mn\lambda_{max}^2\{K_v\}}, \frac{\sigma}{\bar{m}}, \frac{4\kappa\sigma^2}{\sigma(\sigma + \sqrt{mn}\lambda_{max}\{K_v\})^2 + \sigma mn\lambda_{max}^2\{K_v\}} \right\}. \quad (6.15)$$

Then \mathbf{q}^* is asymptotically stable with bounded inputs. ■

Proof. Replacing the control law (6.13) in (2.18), yields

$$\begin{bmatrix} \dot{\mathbf{q}} \\ \dot{\mathbf{p}} \end{bmatrix} = \begin{bmatrix} \mathbf{0} & \mathbf{I}_n \\ -\mathbf{I}_n & -\mathbf{R} \end{bmatrix} \begin{bmatrix} \nabla_{\mathbf{q}} H_d \\ \nabla_{\mathbf{p}} H_d \end{bmatrix} - \begin{bmatrix} \mathbf{0} \\ \mathbf{G}\mathbf{K}_v\mathbf{G}^T \tanh(\dot{\mathbf{q}}) \end{bmatrix} + \tilde{m} \begin{bmatrix} \mathbf{0} \\ \sum_{i=1}^m c_i \nabla_{\mathbf{q}} \ln \cosh(f_i) \end{bmatrix} \quad (6.16)$$

Consider the following Lyapunov candidate

$$\mathcal{V} = \frac{1}{2} \mathbf{p}^T \mathbf{M}^{-1} \mathbf{p} + V_d + \varkappa \tanh(y - y_d) p_2 + \frac{1}{2} \gamma^{-1} \tilde{m}^2. \quad (6.17)$$

First it should be shown that the above function is a suitable Lyapunov candidate. For this purpose, the third term in (6.17) together with $\frac{1}{2} m \dot{y}^2$ may be expressed as follows

$$\frac{1}{2} m (\dot{y} + \varkappa \tanh(y - y_d))^2 - \frac{m \varkappa^2}{2} \tanh^2(y - y_d).$$

Hence, all the terms in (6.17) are clearly non-negative except the terms related to y . For this purpose, define

$$\hbar := -\frac{m \varkappa^2}{2} \tanh^2(y - y_d) + mgy + \sum_{i=1}^m mc_i \ln \cosh(f_i)$$

It is simple to show that $\nabla_y \hbar = 0$. Furthermore,

$$\frac{\partial^2 \hbar}{\partial y^2} \Big|_{\mathbf{q}=\mathbf{q}^*} = -m \varkappa^2 + \sum_{i=1}^m \left((1 + \tanh^2(f_i^*)) \left(\frac{\partial f_i}{\partial y} \right)^2 \Big|_{\mathbf{q}=\mathbf{q}^*} + \tanh(f_i^*) \frac{\partial^2 f_i}{\partial y^2} \Big|_{\mathbf{q}=\mathbf{q}^*} \right),$$

which is positive definite with respect to (6.15). Thus, (6.17) is a suitable Lyapunov candidate. Its derivative is

$$\begin{aligned} \dot{\mathcal{V}} &= -\dot{\mathbf{q}}^T \mathbf{R} \dot{\mathbf{q}} - \dot{\mathbf{q}}^T \mathbf{G}\mathbf{K}_v\mathbf{G}^T \tanh(\dot{\mathbf{q}}) + \tilde{m} \dot{\mathbf{q}}^T \sum_{i=1}^m c_i \nabla_{\mathbf{q}} \ln \cosh(f_i) - \varkappa \tanh(y - y_d) (mg \\ &+ \sum_{i=1}^m mc_i \tanh(f_i) \nabla_y f_i + k_i \tanh(f_i - f_i^*) \nabla_y f_i + r_2 \dot{y} + (\mathbf{G}\mathbf{K}_v\mathbf{G}^T \tanh(\dot{\mathbf{q}}))_2 \\ &- \tilde{m} \sum_{i=1}^m c_i \nabla_y \ln \cosh(f_i)) + m \varkappa (1 - \tanh^2(y - y_d)) \dot{y}^2 + \gamma^{-1} \tilde{m} \dot{\tilde{m}}. \end{aligned}$$

Replacing adaptation law (6.14) in the above equation, yields

$$\begin{aligned}\dot{\mathcal{V}} &= -\dot{\mathbf{q}}^T \mathbf{R}\dot{\mathbf{q}} - \dot{\mathbf{q}}^T \mathbf{G}\mathbf{K}_v \mathbf{G}^T \tanh(\dot{\mathbf{q}}) - \varkappa \tanh(y - y_d) \left(mg + \sum_{i=1}^m mc_i \tanh(f_i) \nabla_y f_i \right. \\ &\quad \left. + k_i \tanh(f_i - f_i^*) \nabla_y f_i + r_2 \dot{y} + (\mathbf{G}\mathbf{K}_v \mathbf{G}^T \tanh(\dot{\mathbf{q}}))_2 \right) + m\varkappa (1 - \tanh^2(y - y_d)) \dot{y}^2 \\ &\leq -\dot{\mathbf{q}}^T \mathbf{R}\dot{\mathbf{q}} - \varkappa \kappa \tanh^2(y - y_d) + \varkappa r_2 |\tanh(y - y_d)| |\dot{y}| + \varkappa mn \lambda_{max}\{\mathbf{K}_v\} |\tanh(y - y_d)| \\ &\quad \|\tanh(\dot{\mathbf{q}})\| + m\varkappa \dot{y}^2,\end{aligned}$$

in which $\|\mathbf{G}\|_2 \leq \|\mathbf{G}\|_F \leq \sqrt{mn}$ [145], and based on the structure of f_i s, the following inequality was used

$$mg + \sum_{i=1}^m mc_i \tanh(f_i) \nabla_y f_i + k_i \tanh(f_i - f_i^*) \nabla_y f_i \geq \kappa \tanh(y - y_d), \quad \kappa < \frac{-y_d}{mg}.$$

Hence, by defining $\dot{\mathbf{q}}_{y_\times} \in \mathbb{R}^{n-1}$ as a part of the velocity vector by omitting \dot{y} , $\dot{\mathcal{V}}$ may be represented as follows

$$\dot{\mathcal{V}} \leq -\varkappa \begin{bmatrix} |\tanh(y - y_d)| \\ \|\tanh(\dot{\mathbf{q}}_{y_\times})\| \\ |\dot{y}| \end{bmatrix}^T \begin{bmatrix} \kappa & \frac{mn\lambda_{max}\{K_v\}}{2} & \frac{r_2 + mn\lambda_{max}\{K_v\}}{2} \\ \frac{mn\lambda_{max}\{K_v\}}{2} & \frac{\varkappa}{\varkappa} & 0 \\ \frac{r_2 + mn\lambda_{max}\{K_v\}}{2} & 0 & \frac{r_2}{\varkappa} / -m \end{bmatrix} \begin{bmatrix} |\tanh(y - y_d)| \\ \|\tanh(\dot{\mathbf{q}}_{y_\times})\| \\ |\dot{y}| \end{bmatrix} \quad (6.18)$$

which is negative definite under (6.15). Hence, using Lasalle theorem, \mathbf{q}^* is asymptotic stable. Furthermore, based on Remark 5 and projection algorithm defined in (6.14), the control law is bounded. Positive tension is ensured by suitable selection of the gains with respect to (5.16), or using Proposition 2. \square

The semi-strict Lyapunov candidate (6.17) has a significant role in suitable designing of adaptation law and, as a result, stability analysis. This fact is explained in the following remark.

Remark 9. Consider a general UCDR with control law (6.13) and the following adaptation law

$$\dot{\hat{m}} = -\dot{\mathbf{q}}^T \sum_{i=1}^m c_i \nabla_{\mathbf{q}} \ln \cosh(f_i).$$

By considering

$$\mathcal{V} = \frac{1}{2} \mathbf{p}^T \mathbf{M}^{-1} \mathbf{p} + V_d + \frac{1}{2} \gamma^{-1} \hat{m}^2$$

as Lyapunov candidate, it is simple to verify that $\mathbf{p} \rightarrow 0$. This means that all of the configuration variables of the robot converge to desired values. However, convergence of y to y^* depends on correct estimation of m since the remaining dynamic is

$$mg + \hat{m} \sum_{i=1}^m c_i \nabla_y \ln \cosh(f_i) + \sum_{i=1}^m k_i \nabla_y \ln \cosh(f_i),$$

which is zero in $y = y^*$ if $\hat{m} = m$. \square

In addition to the uncertainty in the dynamic parameters, the parameters in the input mapping matrix may also be unknown. However, as discussed at the beginning of this

section, since in general, these parameters appear in the PDEs, it is difficult to design a suitable adaptive IDA-PBC controller. However, in some cases, the structure of \mathbf{G} is such that \mathbf{G}^\perp is independent of the parameters of \mathbf{G} . Thus, it seems that it is possible to design an adaptive IDA-PBC concerning unknown parameters in \mathbf{G} . Invoking the novel idea developed in our articles [39, 146], in the following proposition, an adaptive IDA-PBC with respect to kinematics and dynamics parameters is designed for 3-DOF spatial UCDR.

Proposition 4. Consider the spatial UCDR with dynamic formulation (3.22) satisfying Assumption 6. The control law is designed based on (4.13) as

$$\begin{aligned} \mathbf{u} &= (\hat{\mathbf{G}}^T \hat{\mathbf{G}})^{-1} \hat{\mathbf{G}}^T (\nabla_{\mathbf{q}} \hat{V} - \nabla_{\mathbf{q}} \hat{V}_d) - \mathbf{K}_v \hat{\mathbf{G}}^T \tanh(\boldsymbol{\nu}) \\ \dot{\boldsymbol{\nu}} &= -\mathbf{A} \tanh(\boldsymbol{\nu}) + \hat{\mathbf{G}} \mathbf{K}_v \hat{\mathbf{G}}^T [\dot{x}, \dot{y}, \beta \dot{z}]^T, \end{aligned} \quad (6.19)$$

with

$$\nabla_{\mathbf{q}} \hat{V}_d = \begin{bmatrix} k_1 \tanh(x - x_d) \\ 2\hat{m}ck_2y \tanh(k_2(y^2 + \beta z^2)) \\ 2\hat{m}ck_2\beta z \tanh(k_2(y^2 + \beta z^2)) \end{bmatrix}, \quad \hat{\mathbf{G}}^T = \begin{bmatrix} \frac{x}{l_1} & \frac{y}{l_1} & \frac{z}{l_1} \\ \frac{x-b}{l_2} & \frac{y}{l_2} & \frac{z}{l_2} \end{bmatrix},$$

where k_1, k_2 are positive gains and it is presumed that the length of cables are known. The constants c and β are

$$\beta := \frac{m}{\underline{m}} = \frac{\hat{m}}{\hat{m}}, \quad c := \frac{-g}{2k_2y_d \tanh(k_2y_d^2)}. \quad (6.20)$$

The adaptation laws are

$$\dot{\hat{m}} = \begin{cases} 0 & \text{if } \mu > 0 \ \& \ \hat{m} = \bar{m} \\ 0 & \text{if } \mu < 0 \ \& \ \hat{m} = \underline{m} \\ \gamma_1 \mu & \text{else} \end{cases} \quad (6.21)$$

$$\begin{aligned} \mu &:= -[\dot{y}, \beta \dot{z}] [2ck_2y \tanh(k_2(y^2 + \beta z^2)), 2ck_2\beta z \tanh(k_2(y^2 + \beta z^2))]^T \\ &\quad - 2ck_2\aleph y \tanh(y - y_d) \tanh(k_2(y^2 + \beta z^2)), \end{aligned}$$

$$\dot{\hat{b}} = \begin{cases} 0 & \text{if } \dot{x}\xi_2 > 0 \ \& \ \hat{b} = \bar{b} \\ 0 & \text{if } \dot{x}\xi_2 < 0 \ \& \ \hat{b} = \underline{b} \\ \gamma_2 \dot{x} \frac{u_2}{l_2} & \text{else} \end{cases} \quad (6.22)$$

with $\bar{m}, \underline{m}, \bar{b}, \underline{b}$ being the bounds of \hat{m}, \hat{b} , while \aleph should be chosen with respect to the following inequality

$$\begin{aligned} \aleph &\leq \min \left\{ \sqrt{-g/y_d + 4\underline{m}ck_2^2y_d^2 / \cosh^2(k_2y_d^2)}, 4\kappa\sigma / (4\kappa\bar{m} - \sigma^2), \right. \\ &\quad \left. \kappa\lambda_{\min}\{A\} / (9\lambda_{\max}^2\{\mathbf{K}_v\} + r_2\lambda_{\min}\{A\}) \right\}, \end{aligned} \quad (6.23)$$

with $0 < \kappa \leq \frac{-y_d}{mg}$. Then \mathbf{q}^* is asymptotic stable with bounded inputs. ■

Proof. The closed-loop dynamic of the robot is

$$\begin{bmatrix} \dot{q} \\ \dot{p} \end{bmatrix} = \begin{bmatrix} 0 & \mathbf{M}^{-1}\mathbf{M}_d \\ -\mathbf{M}_d\mathbf{M}^{-1} & \mathbf{R}_2 \end{bmatrix} \begin{bmatrix} \nabla_q H_d \\ \nabla_p H_d \end{bmatrix} - \begin{bmatrix} 0 \\ \hat{\mathbf{G}}\mathbf{K}_v\hat{\mathbf{G}}^T \tanh(\boldsymbol{\nu}) \end{bmatrix} + \tilde{m} \begin{bmatrix} 0 \\ \boldsymbol{\xi}_1 \end{bmatrix} + \tilde{b} \begin{bmatrix} 0 \\ \boldsymbol{\xi}_2 \end{bmatrix} \quad (6.24)$$

with the following parameters

$$\boldsymbol{\xi}_1 := \begin{bmatrix} 0 \\ 2ck_2y \tanh(k_2(y^2 + \beta z^2)) \\ 2ck_2\beta z \tanh(k_2(y^2 + \beta z^2)) \end{bmatrix}, \boldsymbol{\xi}_2 = \begin{bmatrix} \frac{u_2}{l_2} \\ 0 \\ 0 \end{bmatrix}, \mathbf{R}_2 = \text{diag}[r_1, r_2, \frac{r_3}{\beta}], \mathbf{M}_d = \text{diag}[m, m, \mathbf{m}].$$

Note that (6.24) is derived by replacing $\mathbf{G} = \hat{\mathbf{G}} - \tilde{\mathbf{G}}$ in the dynamic of the system. Now, consider the following Lyapunov candidate

$$\mathcal{V} = \frac{1}{2}\mathbf{p}^T \mathbf{M}_d^{-1}\mathbf{p} + V_d + \varkappa \tanh(y - y_d)p_2 + \frac{1}{2}\gamma_1^{-1}\tilde{m}^2 + \frac{1}{2}\gamma_2^{-1}\tilde{b}^2 + \sum_{i=1}^3 \ln \cosh(v_i). \quad (6.25)$$

Similar to Theorem 5, one may verify that under (6.23), it is a suitable Lyapunov function. Its derivative is

$$\begin{aligned} \dot{\mathcal{V}} &= -r_1\dot{x}^2 - r_2\dot{y}^2 - \frac{r_3}{\beta}\dot{z}^2 - [\dot{x}, \dot{y}, \beta\dot{z}]\hat{\mathbf{G}}\mathbf{K}_v\hat{\mathbf{G}}^T \tanh(\boldsymbol{\nu}) + \tilde{m}[\dot{y}, \beta\dot{z}][\boldsymbol{\xi}_2, \boldsymbol{\xi}_3]^T + \tilde{b}\dot{x}\boldsymbol{\xi}_2 \\ &\quad - \varkappa \tanh(y - y_d)(mg + 2mck_2y \tanh(k_2(y^2 + \beta z^2))) - \varkappa r_2 \tanh(y - y_d)\dot{y} \\ &\quad - \varkappa \tanh(y - y_d)(\hat{\mathbf{G}}\mathbf{K}_v\hat{\mathbf{G}}^T \tanh(\boldsymbol{\nu}))_2 + \varkappa \tilde{m} \tanh(y - y_d)2ck_2y \tanh(k_2(y^2 + \beta z^2)) \\ &\quad + \frac{\varkappa m \dot{y}^2}{\cosh^2(y - y_d)} + \frac{\tilde{m}}{\gamma_1}\dot{\tilde{m}} + \frac{\tilde{b}}{\gamma_2}\dot{\tilde{b}} + \sum_{i=1}^3 \tanh(v_i)\dot{v}_i \leq -r_1\dot{x}^2 - r_2\dot{y}^2 - \frac{r_3}{\beta}\dot{z}^2 \\ &\quad + \varkappa r_2 |\tanh(y - y_d)| |\dot{y}| + \varkappa m \dot{y}^2 + mn\varkappa \lambda_{\max}\{\mathbf{K}_v\} |\tanh(y - y_d)| \|\tanh(\boldsymbol{\nu})\| \\ &\quad - \varkappa \kappa |\tanh(y - y_d)|^2 - \tanh(\boldsymbol{\nu})^T \mathbf{A} \tanh(\boldsymbol{\nu}), \end{aligned}$$

hence, $\dot{\mathcal{V}}$ is rewritten in the following form

$$\begin{aligned} \dot{\mathcal{V}} &\leq -r_1\dot{x}^2 - \frac{r_3}{\beta}\dot{z}^2 \\ &\quad - \varkappa \begin{bmatrix} |\tanh(y - y_d)| \\ |\dot{y}| \\ \|\tanh(\boldsymbol{\nu})\| \end{bmatrix}^T \begin{bmatrix} \kappa & \frac{r_2}{2} & \frac{mn\lambda_{\max}\{\mathbf{K}_v\}}{2} \\ \frac{r_2}{2} & \frac{r_2}{\varkappa} - m & 0 \\ \frac{mn\lambda_{\max}\{\mathbf{K}_v\}}{2} & 0 & \frac{\lambda_{\min}\{\mathbf{A}\}}{\varkappa} \end{bmatrix} \begin{bmatrix} |\tanh(y - y_d)| \\ |\dot{y}| \\ \|\tanh(\boldsymbol{\nu})\| \end{bmatrix}, \end{aligned} \quad (6.26)$$

which is negative definite due to (6.23). Boundedness of inputs is derived from Remark 5, or Proposition 2. \square

6.3 Robust IDA-PBC

as discussed in Chapter 2, designing robust IDA-PBC with matched disturbance has attracted more attention from researchers rather than adaptive IDA-PBC. In [96], nonlinear PI and nonlinear PID terms have been added to IDA-PBC to design a robust controller with respect to constant matched disturbance. The method, which is applicable to the mechanical systems with constant input mapping matrix is based on non-trivial change of

coordinate. A robust IDA-PBC controller for PH systems with constant \mathbf{G} has been reported in [97] where the matched disturbance, which is derived from another PH structure, is rejected. The results of the last-mentioned paper were generalized in [98] to include the systems with configuration-dependent input mapping matrix. [99, 101, 102] are the works that design robust IDA-PBC with respect to unmatched disturbance. Unfortunately, as indicated in [100], the results of these papers are not correct. Thus, it is inferred that rejection of matched disturbance is well studied. Furthermore, robust IDA-PBC with respect to unmatched disturbance is still an open problem due to the following reasons:

1) The damping term $\mathbf{G}\mathbf{K}_v\mathbf{G}^T$ is not negative definite. In other words, it is not possible to inject damping to unactuated coordinates.

2) The unmatched disturbance appears in the matching equations.

Due to these problems, It is very challenging to design a robust IDA-PBC with respect to unmatched disturbance. In the following, we analyze some particular cases. Let us first introduce the following simple but practical proposition in which has been published for a particular case in [147].

Proposition 5. Consider a mechanical system subject to matched disturbance as follows

$$\begin{bmatrix} \dot{\mathbf{q}} \\ \dot{\mathbf{p}} \end{bmatrix} = \begin{bmatrix} \mathbf{0} & \mathbf{I}_n \\ -\mathbf{I}_n & \mathbf{0} \end{bmatrix} \begin{bmatrix} \nabla_{\mathbf{q}} H \\ \nabla_{\mathbf{p}} H \end{bmatrix} + \begin{bmatrix} \mathbf{0} \\ \mathbf{G}(\mathbf{q}) \end{bmatrix} (\mathbf{u} + \mathbf{d}), \quad (6.27)$$

1) The equilibrium \mathbf{q}^* is stable with the following control law

$$\mathbf{u} = \mathbf{u}_{es} + \mathbf{u}_{di} - \mathbf{K} \text{sign}(\mathbf{G}^T \mathbf{M}_d^{-1} \mathbf{p}), \quad (6.28)$$

in the presence of bounded disturbance $\|\mathbf{d}\| \leq \varpi$ where $\mathbf{u}_{es} + \mathbf{u}_{di}$ was defined in (2.15) and $\mathbf{K} \in \mathbb{R}^{m \times m}$ is such that $\lambda_{\min}\{\mathbf{K}\} \geq \varpi$.

2) The equilibrium \mathbf{q}^* is stable with $\mathbf{u} = \mathbf{u}_{es} + \mathbf{u}_{di}$ as (2.15) if

$$\int_0^\infty \|\mathbf{d}\|^2 dt < \infty. \quad (6.29)$$

Proof. 1) By considering H_d as a Lyapunov function, its derivative is

$$\begin{aligned} \dot{H}_d &= -\mathbf{p}^T \mathbf{M}_d^{-1} \mathbf{G} \mathbf{K}_v \mathbf{G}^T \mathbf{M}_d^{-1} \mathbf{p} + \mathbf{p}^T \mathbf{M}_d^{-1} \mathbf{G} \mathbf{d} - \mathbf{p}^T \mathbf{M}_d^{-1} \mathbf{G} \mathbf{K} \text{sign}(\mathbf{G}^T \mathbf{M}_d^{-1} \mathbf{p}) \\ &\leq -\mathbf{p}^T \mathbf{M}_d^{-1} \mathbf{G} \mathbf{K}_v \mathbf{G}^T \mathbf{M}_d^{-1} \mathbf{p} + \|\mathbf{p}^T \mathbf{M}_d^{-1} \mathbf{G}\| \|\mathbf{d}\| - \lambda_{\min}\{\mathbf{K}\} \|\mathbf{p}^T \mathbf{M}_d^{-1} \mathbf{G}\| \\ &\leq -\lambda_{\min}\{\mathbf{K}_v\} \|\mathbf{p}^T \mathbf{M}_d^{-1} \mathbf{G}\|^2, \end{aligned}$$

which prove that \mathbf{q}^* is stable.

2) Similar to previous part, time derivative of Lyapunov function H_d is

$$\begin{aligned} \dot{H}_d &= -\mathbf{p}^T \mathbf{M}_d^{-1} \mathbf{G} \mathbf{K}_v \mathbf{G}^T \mathbf{M}_d^{-1} \mathbf{p} + \mathbf{p}^T \mathbf{M}_d^{-1} \mathbf{G} \mathbf{d} \\ &\leq -\lambda_{\min}\{\mathbf{K}_v\} \|\mathbf{p}^T \mathbf{M}_d^{-1} \mathbf{G}\| + \|\mathbf{p}^T \mathbf{M}_d^{-1} \mathbf{G}\| \|\mathbf{d}\| \end{aligned}$$

Using the young inequality:

$$xy \leq kx^2 + \frac{y^2}{4k}, \quad x, y \in \mathbb{R}, k \in \mathbb{R} > 0,$$

\dot{H}_d is as follows

$$\dot{H}_d \leq -\lambda_{\min}\{\mathbf{K}_v\} \|\mathbf{p}^T \mathbf{M}_d^{-1} \mathbf{G}\| + k \|\mathbf{p}^T \mathbf{M}_d^{-1} \mathbf{G}\| + \|\mathbf{p}^T \mathbf{M}_d^{-1} \mathbf{G}\|^2 + \frac{\|\mathbf{d}\|^2}{4k}.$$

Integrating both sides of above inequality yields

$$H_d(t) - H_d(t_0) \leq - \int_{t_0}^t \lambda_{\min}\{\mathbf{K}_v\} \|\mathbf{p}^T \mathbf{M}_d^{-1} \mathbf{G}\|^2 dt + \int_{t_0}^t k \|\mathbf{p}^T \mathbf{M}_d^{-1} \mathbf{G}\|^2 dt + \int_{t_0}^t \frac{\|\mathbf{d}\|^2}{4k} dt.$$

Rearranging the terms yields

$$\int_{t_0}^t (\lambda_{\min}\{\mathbf{K}_v\} - k) \|\mathbf{p}^T \mathbf{M}_d^{-1} \mathbf{G}\|^2 dt \leq H_d(t_0) + \int_{t_0}^t \frac{\|\mathbf{d}\|^2}{4k} dt.$$

The left hand side is positive if k is chosen such that $\lambda_{\min}\{\mathbf{K}_v\} > k$. By limiting $t \rightarrow \infty$ and considering the constraint (6.29), it is inferred that integral of a positive value is bounded. Hence, based on Barbalat's lemma [136], $\|\mathbf{p}^T \mathbf{M}_d^{-1} \mathbf{G}\|$ converges to zero. Thus, it is deduced that \mathbf{q}^* is stable. \square

Notice that the term $\mathbf{K} \text{sign}(\mathbf{G}^T \mathbf{M}_d^{-1} \mathbf{p})$ may lead to chattering phenomena [137] that degrade the performance in practice. Replacing “sign” function with a smooth function like “tanh” may rectify this problem with the expense of an ultimate bound for the error.

As explained before, the solution of potential energy PDE is separated to homogeneous and non-homogeneous parts. In some cases, derivation of non-homogeneous solution is difficult. Furthermore, in potential energy shaping of underactuated parallel robots, it is desirable to set $V_d = V_{dh}$ since based on Theorem 1, $V_{dh} = \phi(l_1, \dots, l_m)$ and the function ϕ may be defined easily. In other words, satisfaction of $\mathbf{q}^* = \arg \min V_d(\mathbf{q})$ with $V_d = mgy + V_{dh}$ needs some calculations while $V_d = V_{dh} = \sum_{i=1}^m k_i (l_i - l_{id})^2$ has a nice physical interpretation that the minimum value of V_d is the pose that the cables' length are equal to their desired values. The results are proposed in the following proposition.

Proposition 6. Consider a mechanical system with IDA-PBC controller such that $V_d = V_{dh}$ is designed suitably. Then \mathbf{q}^* is stable if the following inequality is satisfied

$$\left. \frac{\partial^2 \mathcal{V}_n}{\partial \mathbf{q}^2} \right|_{\mathbf{q}=\mathbf{q}^*} > 0, \quad (6.30)$$

in which

$$\mathcal{V}_n = V_d + \int \frac{(\mathbf{G}^\perp \nabla V) \mathbf{G}^\perp}{\|\mathbf{G}^\perp\|^2} \mathbf{M}_d^{-1} \mathbf{M} d\mathbf{q},$$

should be integrable. \blacksquare

Proof. By defining $V_d = V_{dh}$, it means that instead of potential energy PDE (2.17), the following PDE has been solved

$$\mathbf{G}^\perp \mathbf{M}_d \mathbf{M}^{-1} \nabla_{\mathbf{q}} V_d = 0.$$

this means that the gravity vector $\nabla_{\mathbf{q}} V$ has not been compensated in unactuated coordinates. Hence, the closed-loop dynamics of the system is

$$\begin{bmatrix} \dot{\mathbf{q}} \\ \dot{\mathbf{p}} \end{bmatrix} = \begin{bmatrix} \mathbf{0} & \mathbf{M}^{-1} \mathbf{M}_d \\ -\mathbf{M}_d \mathbf{M}^{-1} & \mathbf{J}_2 - \mathbf{G} \mathbf{K}_v \mathbf{G}^T \end{bmatrix} \begin{bmatrix} \nabla_{\mathbf{q}} H_d \\ \nabla_{\mathbf{p}} H_d \end{bmatrix} - \begin{bmatrix} \mathbf{0} \\ \frac{(\mathbf{G}^\perp \nabla V) \mathbf{G}^{\perp T}}{\|\mathbf{G}^\perp\|^2} \end{bmatrix}, \quad (6.31)$$

where the last term indicates the gravity terms related to unactuated coordinates. Now, if

$$\mathcal{V} = K_d + V_d + \int \frac{(\mathbf{G}^\perp \nabla V) \mathbf{G}^\perp}{\|\mathbf{G}^\perp\|^2} \mathbf{M}_d^{-1} \mathbf{M} d\mathbf{q} = K_d + \mathcal{V}_n, \quad (6.32)$$

is a suitable Lyapunov function, its derivative yields $-\mathbf{p}^T \mathbf{M}_d^{-1} \mathbf{G} \mathbf{K}_v \mathbf{G}^T \mathbf{M}_d^{-1} \mathbf{p}$ which shows that \mathbf{q}^* is stable. \mathcal{V} exists since \mathcal{V}_n is integrable. Note that \mathcal{V}_n is merely a function of \mathbf{q} ; thus, we should have

$$1) \left. \frac{\partial \mathcal{V}_n}{\partial \mathbf{q}} \right|_{\mathbf{q}=\mathbf{q}^*} = 0, \quad 2) \left. \frac{\partial^2 \mathcal{V}_n}{\partial \mathbf{q}^2} \right|_{\mathbf{q}=\mathbf{q}^*} > 0. \quad (6.33)$$

Notice that the first condition of (6.33) is trivially satisfied since

$$\left. \frac{\partial V_n}{\partial \mathbf{q}} \right|_{\mathbf{q}=\mathbf{q}^*} = \left. \frac{\partial V_d}{\partial \mathbf{q}} \right|_{\mathbf{q}=\mathbf{q}^*} + \left. \frac{(\mathbf{G}^\perp \nabla V) \mathbf{G}^\perp}{\|\mathbf{G}^\perp\|^2} \mathbf{M}_d^{-1} \mathbf{M} \right|_{\mathbf{q}=\mathbf{q}^*} = \left. \frac{\partial V_d}{\partial \mathbf{q}} \right|_{\mathbf{q}=\mathbf{q}^*} = 0$$

Recall that $\mathbf{q} = \mathbf{q}^*$ is an equilibrium point if $\mathbf{G}^\perp \nabla V|_{\mathbf{q}=\mathbf{q}^*} = 0$. Hence, it is sufficient to check the second condition of (6.33). \square

Note that Proposition 6 is related to stability of \mathbf{q}^* in open-loop. By this means, if it is stable, then this proposition is certainly applicable.

6.4 IDA-PBC with Desired Gravity Compensation

Proportional derivative with gravity compensation (PD-GC) is a well-known controller to stabilize fully actuated robotic systems in the desired pose. This controller is based on compensation of gravity at the current position of the robot. A simpler version of PD-DG has been introduced that the gravity is compensated merely at desired pose. This controller which is called PD with desired gravity compensation (PD-DGC) has been successfully applied to serial robots with revolute joints [148]. The control law of PD-DGC is as follows

$$\mathbf{u} = \mathcal{G}(\mathbf{q}^*) - \mathbf{K}_p(\mathbf{q} - \mathbf{q}^*) - \mathbf{K}_d \dot{\mathbf{q}},$$

with $\mathbf{K}_p, \mathbf{K}_d$ being positive definite matrices. The stability of closed-loop system is guaranteed by the following Lyapunov function

$$\mathcal{V} = H + \frac{1}{2}(\mathbf{q} - \mathbf{q}^*)^T \mathbf{K}_p(\mathbf{q} - \mathbf{q}^*) - (\mathbf{q} - \mathbf{q}^*)^T \mathcal{G}(\mathbf{q}^*),$$

under this constraint

$$\lambda_{\min}\{\mathbf{K}_p\} > \kappa_g,$$

where κ_g is a constant satisfies the following inequality

$$\|\mathcal{G}(\mathbf{q}_1) - \mathcal{G}(\mathbf{q}_2)\| \leq \kappa_g \|\mathbf{q}_1 - \mathbf{q}_2\|, \quad \text{for every } \mathbf{q}_1, \mathbf{q}_2 \text{ in the workspace of the robot.} \quad (6.34)$$

In this section, we aim to merge PD-DGC with IDA-PBC to derive a simpler controller. For simplicity, we focus on the systems with constant input mapping matrix as (4.28).

Proposition 7. Consider a mechanical system with input mapping matrix as (4.28) and the following control law

$$\mathbf{u} = \mathbf{u}_{es} + \mathbf{u}_{di} - \nabla_{\mathbf{q}_a} V(\mathbf{q}) + \left(\nabla_{\mathbf{q}_a} V(\mathbf{q}) \right) \Big|_{\mathbf{q}=\mathbf{q}^*}, \quad (6.35)$$

where V_d, \mathbf{M}_d are derived from the matching equations and $\mathbf{q} = [\mathbf{q}_a, \mathbf{q}_u]^T$ with $\mathbf{q}_a \in \mathbb{R}^m$ and $\mathbf{q}_u \in \mathbb{R}^{n-m}$ denote the actuated and unactuated coordinates, respectively. The gains of V_d should be chosen such that the following inequality is held

$$\left(\frac{\partial^2 V_d}{\partial \mathbf{q}^2} + \mathbf{M} \mathbf{M}_d^{-1} \mathbf{G} \left(\frac{\partial \nabla_{\mathbf{q}_a} V(\mathbf{q})}{\partial \mathbf{q}} \right) \right) \Big|_{\mathbf{q}=\mathbf{q}^*} > 0 \quad (6.36)$$

Then, under the integrability condition of the following expression, \mathbf{q}^* is stable

$$\int \dot{\mathbf{q}}^T \mathbf{M} \mathbf{M}_d^{-1} \mathbf{G} \nabla_{\mathbf{q}_a} V(\mathbf{q}) dt - \int \dot{\mathbf{q}}^T \mathbf{M} \mathbf{M}_d^{-1} \mathbf{G} \left(\nabla_{\mathbf{q}_a} V(\mathbf{q}) \right) \Big|_{\mathbf{q}=\mathbf{q}^*} dt.$$

■

Note that the control law (6.35) is similar to IDA-PBC's control law and merely the gravity compensation in actuated coordinate is replaced by desired gravity compensation. Hence, the matching equations do not change.

Proof. Under the integrability condition, consider the following Lyapunov candidate

$$\mathcal{V} = H_d + \int \dot{\mathbf{q}}^T \mathbf{M} \mathbf{M}_d^{-1} \mathbf{G} \nabla_{\mathbf{q}_a} V(\mathbf{q}) dt - \int \dot{\mathbf{q}}^T \mathbf{M} \mathbf{M}_d^{-1} \mathbf{G} \left(\nabla_{\mathbf{q}_a} V(\mathbf{q}) \right) \Big|_{\mathbf{q}=\mathbf{q}^*} dt$$

Note that it is a suitable Lyapunov function since

$$\frac{\partial \mathcal{V}}{\partial \mathbf{q}} = \nabla_{\mathbf{q}} V_d + \mathbf{M} \mathbf{M}_d^{-1} \mathbf{G} \nabla_{\mathbf{q}_a} V(\mathbf{q}) - \mathbf{M} \mathbf{M}_d^{-1} \mathbf{G} \left(\nabla_{\mathbf{q}_a} V(\mathbf{q}) \right) \Big|_{\mathbf{q}=\mathbf{q}^*},$$

and thus, $\frac{\partial \mathcal{V}}{\partial \mathbf{q}} \Big|_{\mathbf{q}=\mathbf{q}^*} = 0$ and $\frac{\partial^2 \mathcal{V}}{\partial \mathbf{q}^2} \Big|_{\mathbf{q}=\mathbf{q}^*} > 0$ due to (6.36). One may easily verify that

$$\dot{\mathcal{V}} = -\mathbf{p}^T \mathbf{M}_d^{-1} \mathbf{G} \mathbf{K}_v \mathbf{G}^T \mathbf{M}_d^{-1} \mathbf{p}.$$

Hence, \mathbf{q}^* is stable. □

6.5 Conclusion

In this chapter, some developments of IDA-PBC were introduced. First, we concentrated on IDA-PBC with position feedback, and it was shown that dirty derivative of velocity might be employed to address this topic for a case of UaSs. Adaptive and robust IDA-PBC were other subjects of this chapter. By this means, adaptive IDA-PBC for potential energy shaping of UCDRs with unknown mass and also total energy shaping of spatial UCDR with kinematic and dynamic uncertainties were proposed. Furthermore, simplification of solving potential energy PDE that leads to the elimination of non-homogeneous solution was analyzed. Finally, IDA-PBC with desired gravity compensation for actuated coordinates of mechanical systems with constant input mapping matrix was designed.

Chapter 7

Simulation and Experimental Results

In this chapter, the proposed controllers are applied to some different systems to evaluate the performance. By this means, some simulations and experiments are presented. In the following, first, simulation results are exhibited and then, experimental results are introduced.

7.1 Simulation Results

In this section, the results of previous chapters are verified through several simulations. For this purpose, first, using the solution of matching equations proposed in Chapter 4 together with the results of Chapter 5 and Chapter 6, some controllers are implemented on the UCDRs. Furthermore, some benchmark systems are utilized to show the effectiveness of the proposed methods in detail. Note that despite analyzing the controllers via some experiments, the simulations are also presented to test the performance of the controllers in accordance with the conditions of the theorems/propositions.

7.1.1 Planar Underactuated Cable-Driven Robot

In this section, some controllers are applied to planar UCDR introduced in Section 3.1. For this purpose, the results of Section 4.1.1 are utilized to design some controllers based on potential energy shaping. A common method to define the function ϕ in (4.10) is quadratic form. Hence,

$$V_d = mgy + \alpha\chi + \beta\psi + k_3(\chi - \chi_d)^2 + k_4(\psi - \psi_d)^2, \quad (7.1)$$

with

$$\chi = (2a \cos(\theta) - b)x + 2a \sin(\theta)y - ab \cos(\theta), \quad \psi = x^2 + y^2 - bx - ab \cos(\theta). \quad (7.2)$$

Defining V_d as (7.1) leads to appearance of the terms including y^3 and x^3 in the control law. A better definition of V_d which is proposed in (5.1) is as follows

$$V_d = mgy + \alpha\chi + \beta\psi + k_3 \ln \cosh(\chi - \chi_d) + k_4 \ln \cosh(\psi - \psi_d). \quad (7.3)$$

By this means, $\nabla_{\mathbf{q}} V_d$ is a function of x and y . The positive gains k_3 and k_4 should be chosen concerning $\frac{\partial^2 V_d}{\partial \mathbf{q}^2} \Big|_{\mathbf{q}=\mathbf{q}^*} > 0$ while the constants α and β are derived from $\frac{\partial V_d}{\partial \mathbf{q}} \Big|_{\mathbf{q}=\mathbf{q}^*} = 0$

as follows

$$\begin{bmatrix} \alpha \\ \beta \end{bmatrix} = \begin{bmatrix} 2a \cos(\theta_d) - b & 2x_d - b \\ 2a \sin(\theta_d) & 2y_d \end{bmatrix}^{-1} \begin{bmatrix} 0 \\ -mg \end{bmatrix}, \quad (7.4)$$

The gains k_3 and k_4 together with \mathbf{K}_v shall be chosen based on Remark 5 such that positive tension in cables are ensured. Since $\nabla_q V_d$ is a function of x^3, y^3 and x, y , respectively, we should use the method proposed in Remark 2.2 to compute the upper bounds of potential energy shaping terms in the control law. However, this method leads to conservative gains. Note that for simplicity, we merely concentrate on assurance of tensile force in cables.

In order to compare the results, the sliding mode controller proposed in [123] is also simulated. The control law is [123]

$$\begin{aligned} \mathbf{u} = & \begin{bmatrix} \frac{x-a \cos(\theta)}{l_1} & \frac{y-a \sin(\theta)}{l_1} \\ \frac{x-b+a \cos(\theta)}{l_2} & \frac{y+a \sin(\theta)}{l_2} \end{bmatrix}^{-T} \begin{bmatrix} -\gamma \dot{x} \\ 0 \end{bmatrix} + \begin{bmatrix} \frac{y-a \sin(\theta)}{l_1} & \frac{-\cos(\theta)(y-a \sin(\theta))}{l_1} + \frac{\sin(\theta)(x-a \cos(\theta))}{l_1} \\ \frac{y+a \sin(\theta)}{l_2} & \frac{\cos(\theta)(y+a \sin(\theta))}{l_2} - \frac{\sin(\theta)(x-b+a \cos(\theta))}{l_2} \end{bmatrix}^{-T} \\ & \left(\begin{bmatrix} m & 0 \\ 0 & I \end{bmatrix} \dot{\boldsymbol{\nu}} + \begin{bmatrix} mg \\ 0 \end{bmatrix} - \mathbf{K} \mathbf{s} - \kappa \text{sgn}(\mathbf{s}) \right) \end{aligned} \quad (7.5)$$

with $\mathbf{K}, \mathbf{\Gamma}, \gamma > 0$ and

$$\begin{aligned} \kappa = & |f(\mathbf{X}, \dot{\mathbf{X}}) \gamma \dot{x}| = \left| \mathbf{J}^T(3, :) \begin{bmatrix} \frac{x-a \cos(\theta)}{l_1} & \frac{y-a \sin(\theta)}{l_1} \\ \frac{x-b+a \cos(\theta)}{l_2} & \frac{y+a \sin(\theta)}{l_2} \end{bmatrix}^{-T} \begin{bmatrix} -\gamma \dot{x} \\ 0 \end{bmatrix} \right| \\ = & \left| \frac{2y^2 \cos(\theta) - 2xy \sin(\theta) + by \sin(\theta) - ab \sin^2(\theta)}{2ax \sin(\theta) - 2ay \cos(\theta) + by - ab \sin(\theta)} \gamma \dot{x} \right| \end{aligned}$$

and

$$\boldsymbol{\nu} = -\mathbf{\Gamma} \tilde{\mathbf{X}}', \quad \tilde{\mathbf{X}}' = \mathbf{X}' - \mathbf{X}'^*, \quad \mathbf{s} = \dot{\mathbf{X}}' - \boldsymbol{\nu} = \dot{\mathbf{X}}' + \mathbf{\Gamma} \mathbf{X}', \quad \mathbf{X}' = [y, \theta]^T.$$

The parameters of the robot are $a = 0.5m, b = 8m$ and $m = 2Kg$. Based on the above explanations, it is deduced that $k_3 = k_4 = 0.01, \mathbf{K}_v = \mathbf{I}_2$ and $k_3 = k_4 = 0.1, \mathbf{K}_v = 3\mathbf{I}_2$ are suitable gains for IDA-PBC with desired potential energy given in (7.1) and (7.3), respectively. The gains of sliding mode controller are $\mathbf{K} = \mathbf{\Gamma} = 2\mathbf{I}_2$ and $\gamma = 3$. Note that it is tried to choose the gains of (7.4) such that the settling time is close to settling time of the other controllers. The results are proposed in Fig. 7.1-7.3. Fig. 7.1 and Fig. 7.2 show the results of IDA-PBC with desired potential energy (7.1) and (7.3), respectively, while the results of sliding mode controller (7.5) are presented in Fig. 6.4. It is clear that all the configuration variables converge to their desired values. More precisely, the best performance is related to the IDA-PBC with V_d as (7.3). However, the control efforts are quite different. The lower value of control effort of the controllers based on energy shaping is about $5N$ while it is less than $-5N$ with sliding mode controller since positive tension has not been considered in this controller. Clearly, negative control law leads to poor performance or even instability of the system. Furthermore, a transient chattering in inputs is apparent due to the ‘‘sign’’ term. Another disadvantage of this controller in comparison with energy shaping controllers is its dependency on the full dynamic parameters of the system. In other words, the potential shaping controllers merely require the mass of the system while the other controller needs mass and inertia

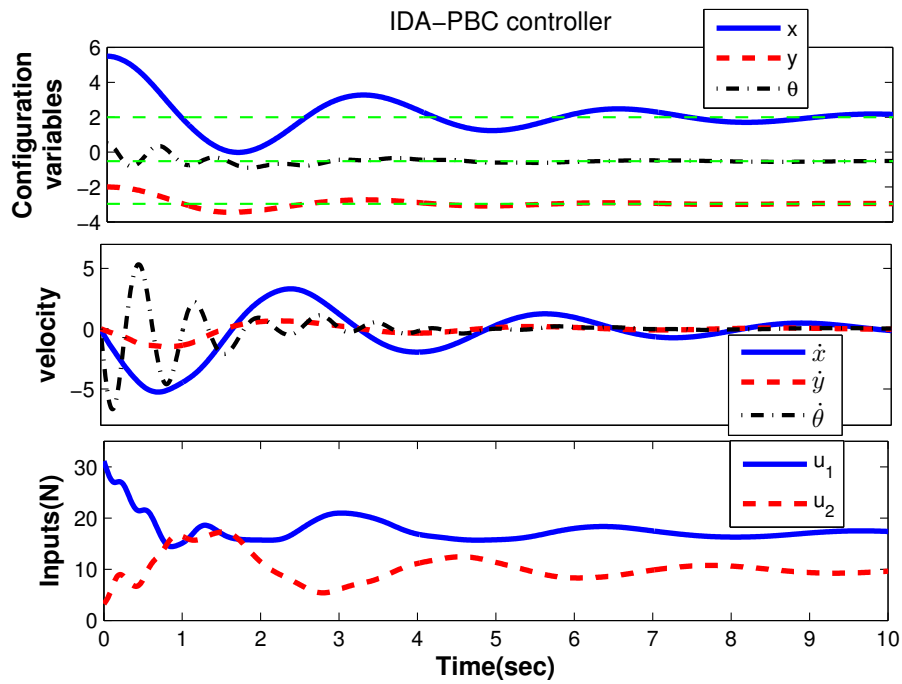


Figure 7.1: Simulation results of potential energy shaping with V_d as (7.1) on planar UCDR.

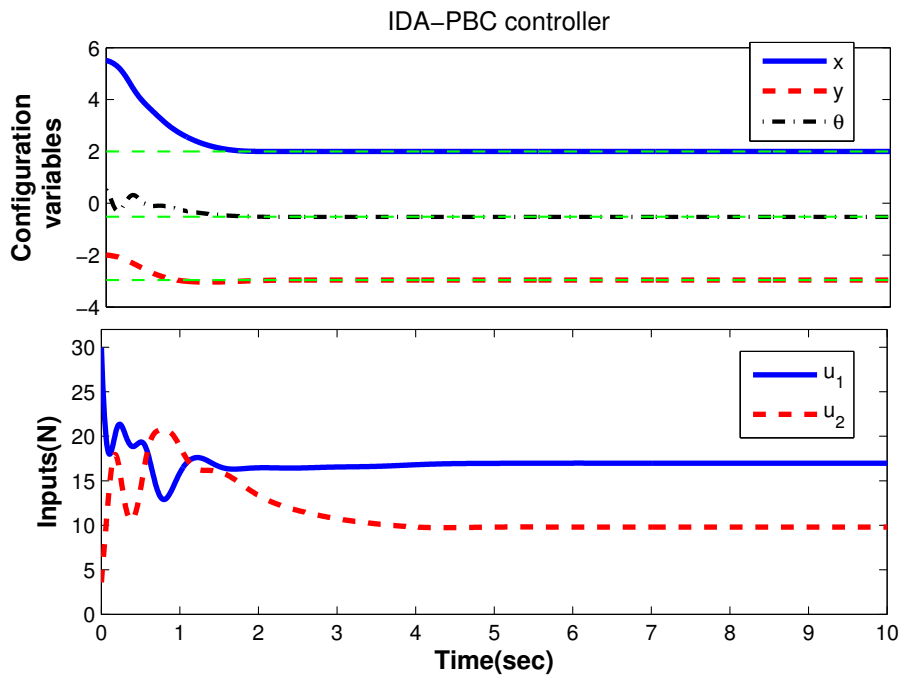


Figure 7.2: Simulation results of potential energy shaping with V_d as (7.3) on planar UCDR.

of the end-effector.

In order to examine some of the results of Chapter 6, Proposition 3 and Proposition 6 are also simulated on this robot. Proposition 3 is applied with V_d as (7.3) and $\mathbf{A} = 10$. In Proposition 6, $V_d = V_{dh}$ is designed based on Theorem 1 as follows

$$V_d = k_1 \ln \cosh(l_1 - l_{1d}) + k_2 \ln \cosh(l_2 - l_{2d}), \quad (7.6)$$

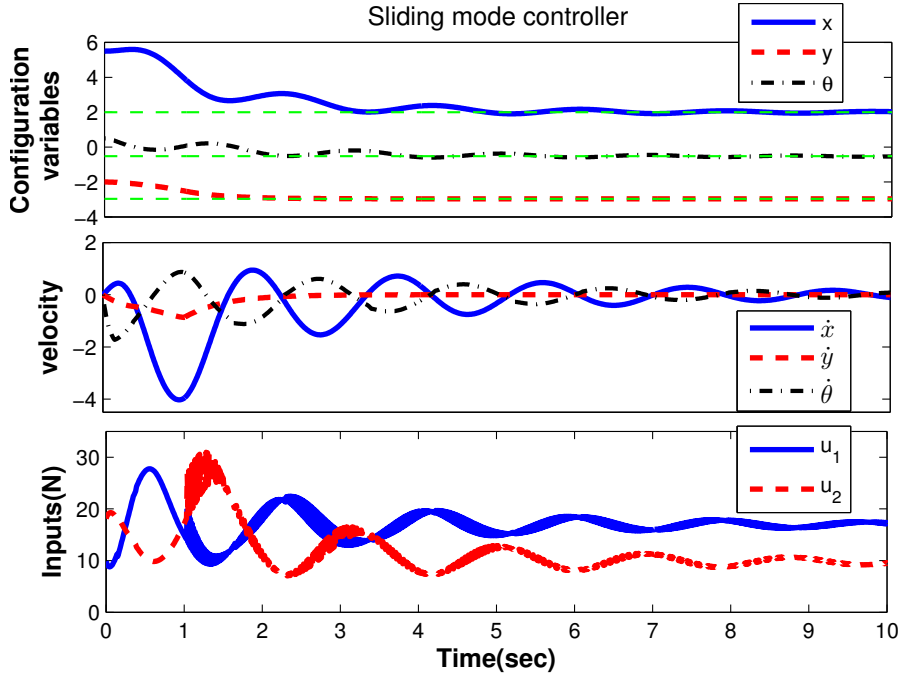


Figure 7.3: Simulation results of sliding mode controller [123] on planar UCDR.

where $k_1 = k_2 = 1$ are chosen. Simulation results are illustrated in Fig. 7.4 and Fig. 7.5. Fig. 7.4 shows the results of Proposition 6. It is clear that replacing $\dot{\mathbf{q}}$ with ν does not affect on the stability of the closed-loop system. Comparison of this figure with Fig. 7.2 shows that the performance of this controller is similar to original IDA-PBC with a bit more oscillation in the initial times of control effort. The results of Proposition 7.5 are depicted in Fig. 7.5. Although V_{dn} is eliminated in control law, all the configuration variables converge to their desired values. Comparison between (7.3) and (5.25) show that Proposition 7.5 simplify controller design for UCDRs. Additionally, the control efforts are far from zero in the initial times that is another superiority of this controller since in regulation, inputs have usually the largest value at the beginning.

7.1.2 Spatial Underactuated Cable-Driven Robot

In this section, the proposed controllers are applied to the spatial UCDR proposed in Section 3.2. First, some controllers including potential energy shaping, total energy shaping and sliding mode are implemented on the robot. For this purpose, a controller relied on potential energy shaping is designed based on (4.11) with the following desired potential energy

$$V_d = k_1 \ln \cosh(x - x^*) + k_2 \ln \cosh(y^2 + z^2 - \alpha) + mgy \quad (7.7)$$

where k_1, k_2 are free positive gains and the constant α is derived from $\nabla V_d|_{\mathbf{q}=\mathbf{q}^*} = 0$ as follows

$$\alpha = y^{*2} - 0.5 \ln\left(\frac{1+a}{1-a}\right), \quad a = -\frac{mg}{2k_2 y^*}.$$

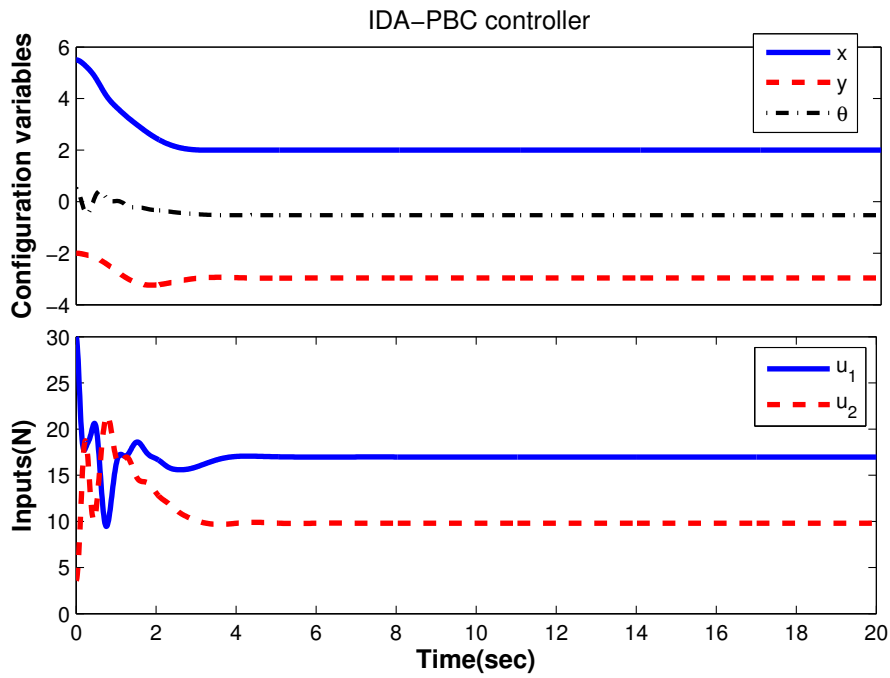
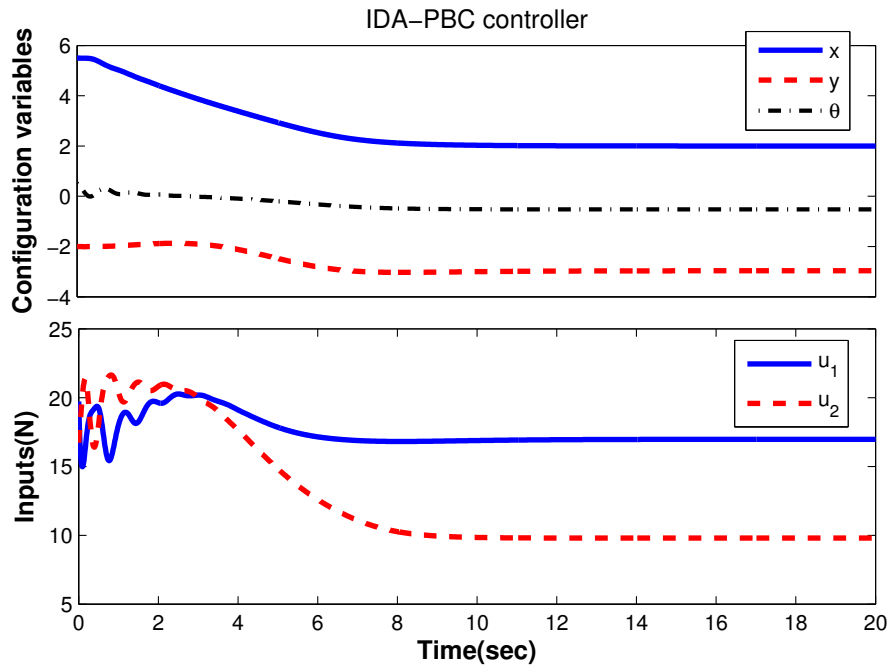


Figure 7.4: Simulation results of Proposition 3 on planar UCDR.

Figure 7.5: Simulation results of Proposition 6 with V_d as (7.3) on planar UCDR.

The other controller is based on total energy shaping with \mathbf{M}_d as (4.12) and desired potential energy (4.13) which is designed as follows

$$V_d = k_1 \ln \cosh(x - x^*) + c_1 \ln \cosh\left(y^2 + \frac{m}{m} z^2\right) + mgy, \quad (7.8)$$

with $k_1 \in \mathbb{R}^+$ a free parameter and the constant c_1 is derived as follows

$$c_1 = -\frac{mg}{2y^* \tanh(y^{*2})}.$$

Note that c_1 is a positive constant since $y^* < 0$. Furthermore, we simulate the controller based on total energy shaping with configuration-dependent \mathbf{M}_d . For this purpose, the desired inertia matrix given in (4.19) is

$$\mathbf{M}_d = \begin{bmatrix} m & 0 & 0 \\ 0 & \frac{y^2}{2} + k_1 & \frac{1}{2}yz \\ 0 & \frac{1}{2}yz & \frac{z^2}{2} + k_2 \end{bmatrix}, \quad (7.9)$$

α_i s are

$${}_1\alpha = [0, 0, 0]^T, \quad {}_2\alpha = [0, 0, 0]^T, \quad {}_3\alpha = \left[0, -\frac{k_1 z}{2m}, \frac{k_2 y}{2m}\right]^T, \quad (7.10)$$

and the desired potential energy is designed as follows

$$V_d = k_3 \ln \cosh(x - x^*) + k_4 \ln \cosh(k_2 y^2 + k_1 z^2 - \alpha) + \frac{m^2 g}{k_1} (y - y^*), \quad (7.11)$$

in which α is

$$\alpha = k_2 y^{*2} - 0.5 \ln\left(\frac{1+a}{1-a}\right), \quad a = -\frac{m^2 g}{2k_1 k_4 y^*}.$$

In order to compare the results, we invoke to the controller designed for planar UCDR [123] and develop it for this case. The control law is as follows

$$\mathbf{u} = \begin{bmatrix} \frac{x}{l_1} & \frac{x-b}{l_2} \\ \frac{y}{l_1} & \frac{y}{l_2} \end{bmatrix}^{-1} \left(m\dot{\boldsymbol{\nu}} + [0, mg]^T - \mathbf{K}\mathbf{s} - \kappa \text{sign}(\mathbf{s}) \right) - \begin{bmatrix} \gamma \text{sign}(z) \dot{z} \\ \gamma \text{sign}(z) \dot{z} \end{bmatrix} \quad (7.12)$$

with the following parameters

$$\boldsymbol{\nu} = \boldsymbol{\Gamma} \begin{bmatrix} x - x^* \\ y - y^* \end{bmatrix}, \quad \mathbf{s} = \begin{bmatrix} \dot{x} \\ \dot{y} \end{bmatrix} - \boldsymbol{\nu}, \quad \kappa = \frac{\gamma |z \dot{z}|}{l_1} + \frac{\gamma |z \dot{z}|}{l_2},$$

with $0 < \mathbf{K}, \boldsymbol{\Gamma} \in \mathbb{R}^{2 \times 2}$ and $\gamma > 0$ as free parameters. Simulation results are proposed in Fig. 7.6-7.10. The gains of the energy shaping controllers are chosen based on the results of Section 5.1 to ensure positive tension in cables. Note that for simplicity, only the lower bound of actuators is considered. The parameters of the robot are $m = 3Kg$ and $b = 3m$. The results of potential energy shaping are proposed in Fig. 7.6. the gains of the controller are $k_1 = 2, k_2 = 3$ and $\mathbf{K}_v = 5\mathbf{I}_2$. It is clear that $x - x^*$ and $y - y^*$ converge to zero while the inputs are positive. However, the rate of convergence of z is very slow. In order to improve the results, total energy shaping controllers are designed and simulated. The results of the controller with constant \mathbf{M}_d as (4.12) and V_d as (7.8) are depicted in Fig. 7.7 and Fig. 7.8 with $m = 0.1$ and $m = 0.4$, respectively. The convergence rate of z is faster than the potential energy shaping controller. Lower values of m lead to faster response with the expense of more oscillations in the control efforts. Fig. 7.9 shows the results of total energy shaping with \mathbf{M}_d as (7.9) and V_d as (7.11) with the gains $k_1 = 2, k_2 = 0.5, k_3 = 8, k_4 = 24$. The results show that the convergence rate of z is suitable while other configuration variables converge to their desired values in a short time. Note that the initial value of u_1 is very large in

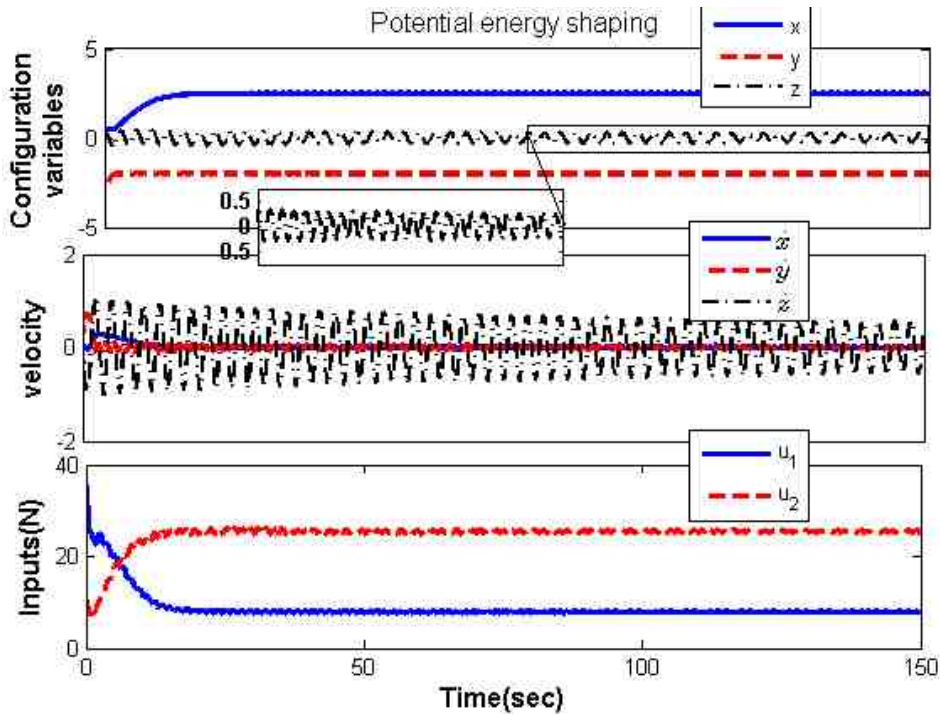


Figure 7.6: Simulation results of potential energy shaping on spatial UCDR.

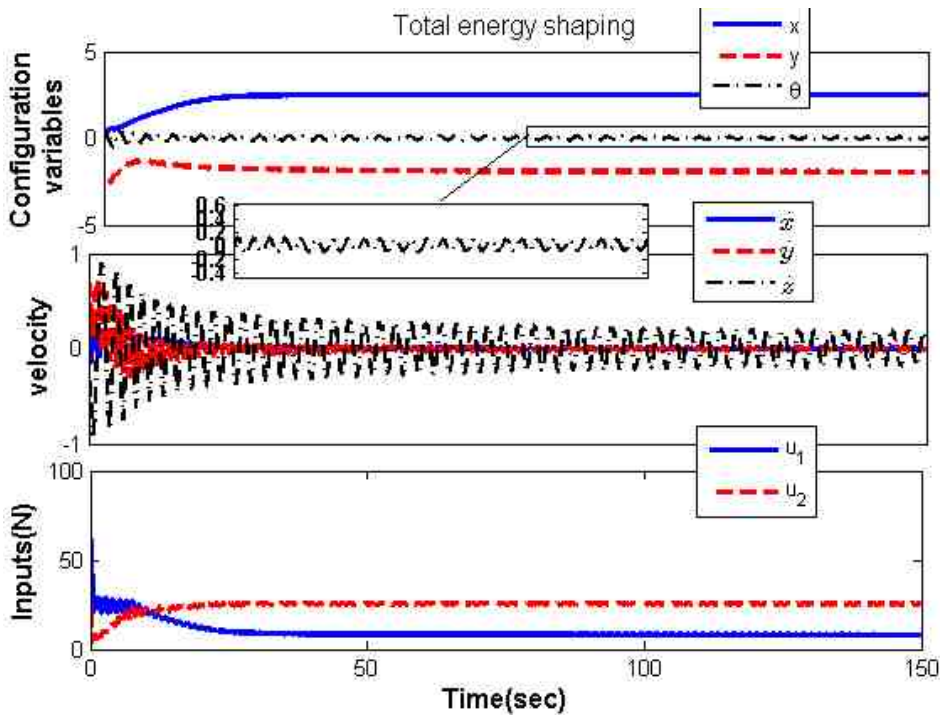


Figure 7.7: Simulation results of total energy shaping with $m = 0.1$ on spatial UCDR.

this controller due to the term $M_d M^{-1} \nabla_q V_d$ since at $t \approx 0$ the velocity is almost zero and the term related to \mathbf{p} are negligible. Thus, invoking the results of Theorem 3 may not improve the control efforts. Note that it may seem that the control effort is non-smooth in initial times; however, it is due to long simulation time and u is smooth. The results of sliding mode controller are depicted in Fig. 7.10 with the gains $\mathbf{K} = 0.5\mathbf{I}_2, \mathbf{\Gamma} = 3\mathbf{I}_2, \gamma = 2$.

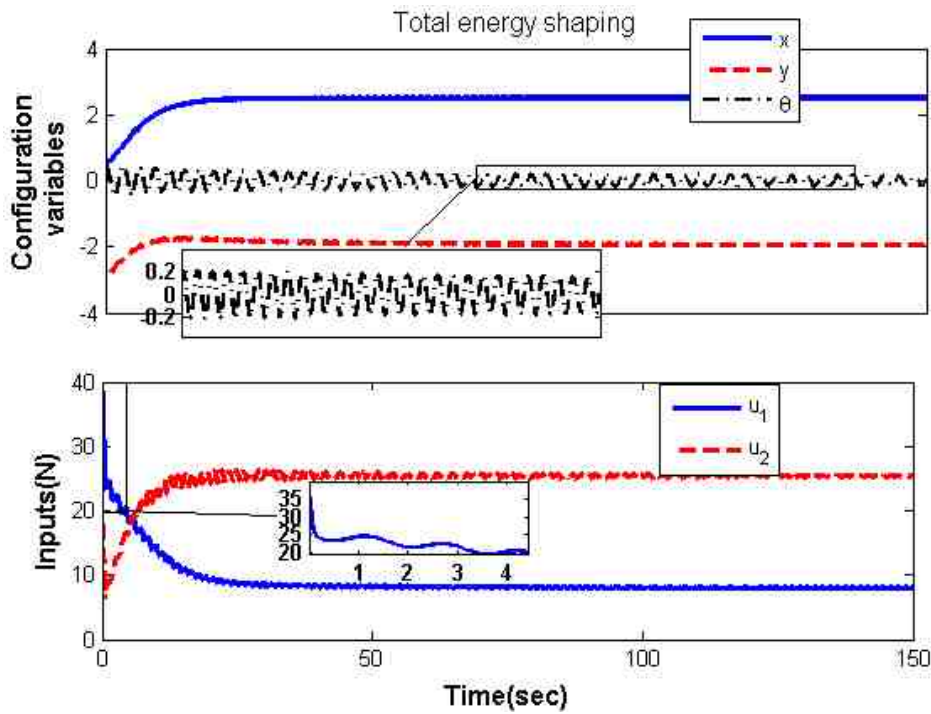


Figure 7.8: Simulation results of total energy shaping with $m = 0.4$ on spatial UCDR.

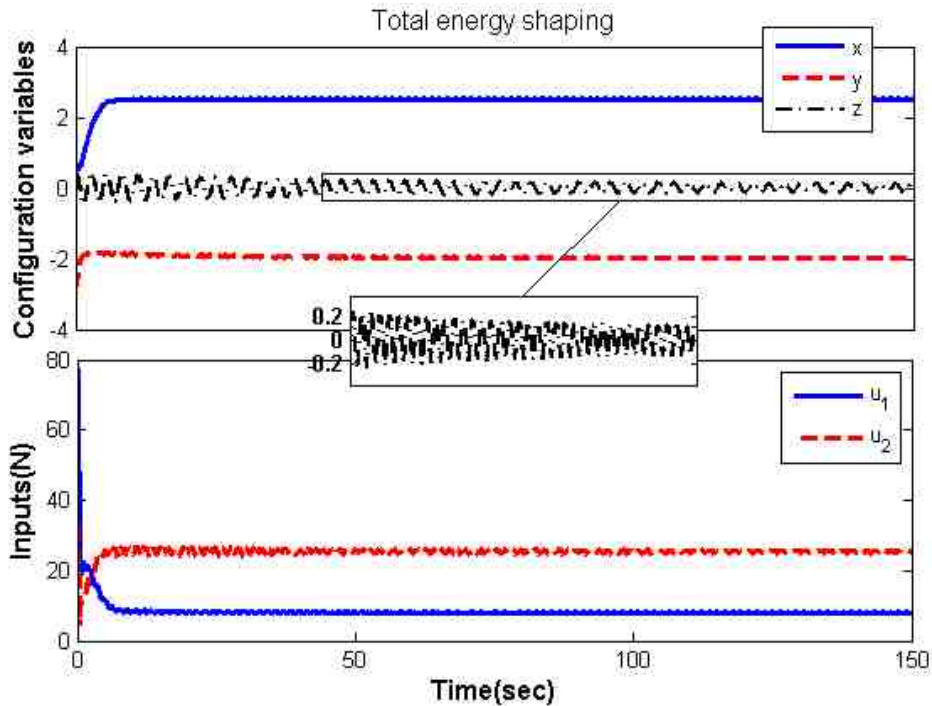


Figure 7.9: Simulation results of total energy shaping with configuration-dependent M_d on spatial UCDR.

Although the convergence rate of z is appropriate, the inputs' oscillations may worsen the performance in practice. Furthermore, assurance of tensile forces in cables is not straightforward.

With the purpose of analyzing uncertainty in parameters, Proposition 4 is also simu-

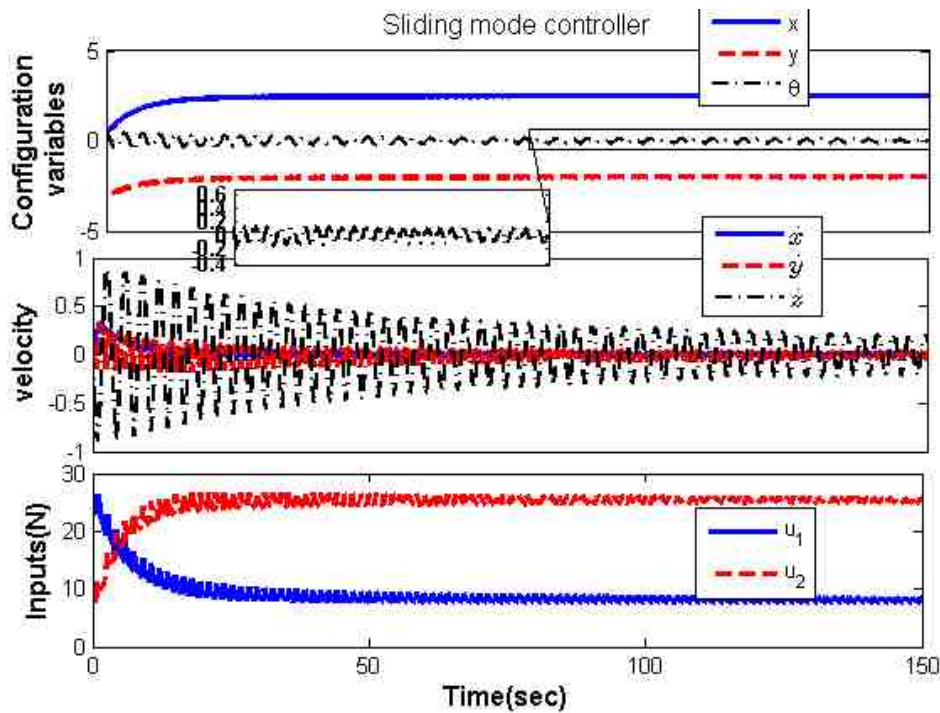


Figure 7.10: Simulation results of sliding mode controller on spatial UCDR.

lated. For this purpose, the end-effector's mass and the distance between anchor points which are $m = 2Kg$ and $b = 3m$, respectively, are perturbed about 10% and 1%, respectively. The gains/parameters of Proposition 4 are

$$r_1 = r_2 = r_3 = 0.005, \quad m = 0.02, \quad k_1 = 0.1, \quad k_2 = 0.01, \quad \gamma_1 = \gamma_2 = 0.1, \quad \varkappa = 0.05$$

The results of simple IDA-PBC and adaptive IDA-PBC are illustrated in Fig. 7.11 and Fig. 7.12. As it is seen, simple IDA-PBC leads to a steady-state error in y direction while using adaptive IDA-PBC, all the errors of stabilization converge to zero. This is the superiority of Proposition 4 that uncertainties in kinematic and dynamic parameters do not destroy the stability of the closed-loop system.

7.1.3 Spidercam

The robot was introduced in Section 3.3. Since the degrees of underactuation of the robot is two, calculation of equilibrium points is not straightforward. Furthermore, finding the solution of matching equations is very complex since a set of PDEs shall be solved. Fortunately, based on Theorem 1, it is possible to shape the potential energy of the robot. Furthermore, Proposition 6 simplifies suitable design of V_d . Hence, it is possible to propose a simulation on a spidercam. The parameters of the robot are

$$m = 3Kg, \quad I = 0.2I_3, \quad A_1 = \begin{bmatrix} 3.56/2 \\ 7.05/2 \\ 4.06 \end{bmatrix}, \quad A_2 = \begin{bmatrix} -3.56/2 \\ 7.05/2 \\ 4.06 \end{bmatrix}, \quad A_3 = \begin{bmatrix} 3.56/2 \\ -7.05/2 \\ 4.06 \end{bmatrix},$$

$$A_4 = \begin{bmatrix} -3.56/2 \\ -7.05/2 \\ 4.06 \end{bmatrix}, \quad B_1 = \begin{bmatrix} 0.2 \\ 0.4 \\ 0 \end{bmatrix}, \quad B_2 = \begin{bmatrix} -0.2 \\ 0.4 \\ 0 \end{bmatrix}, \quad B_3 = \begin{bmatrix} 0.2 \\ -0.4 \\ 0 \end{bmatrix}, \quad B_4 = \begin{bmatrix} -0.2 \\ -0.4 \\ 0 \end{bmatrix}.$$

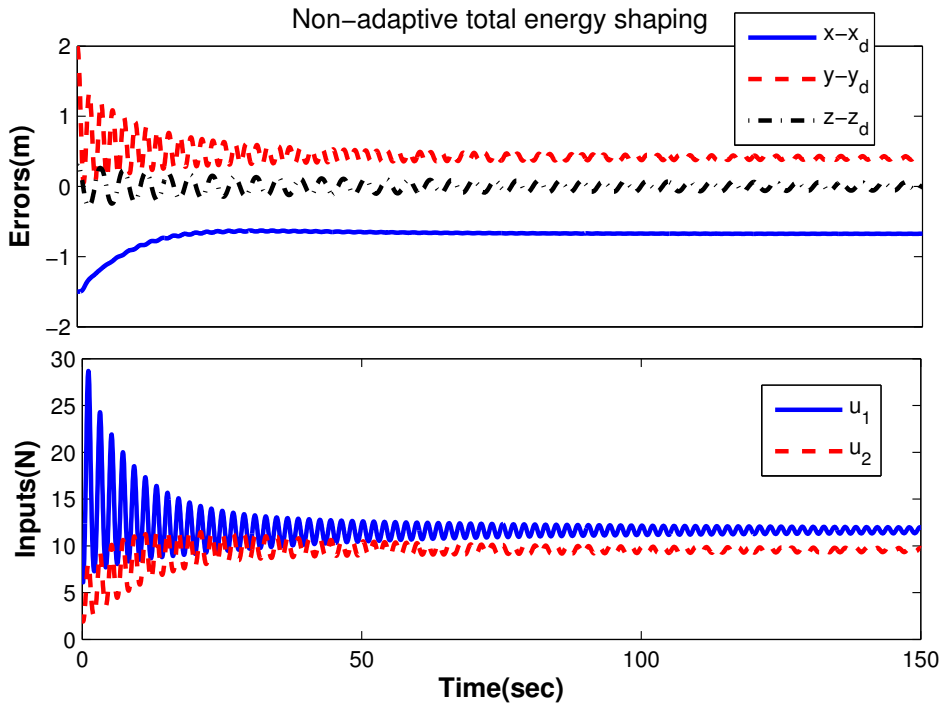


Figure 7.11: Simulation results of IDA-PBC in the presence of uncertain parameters.

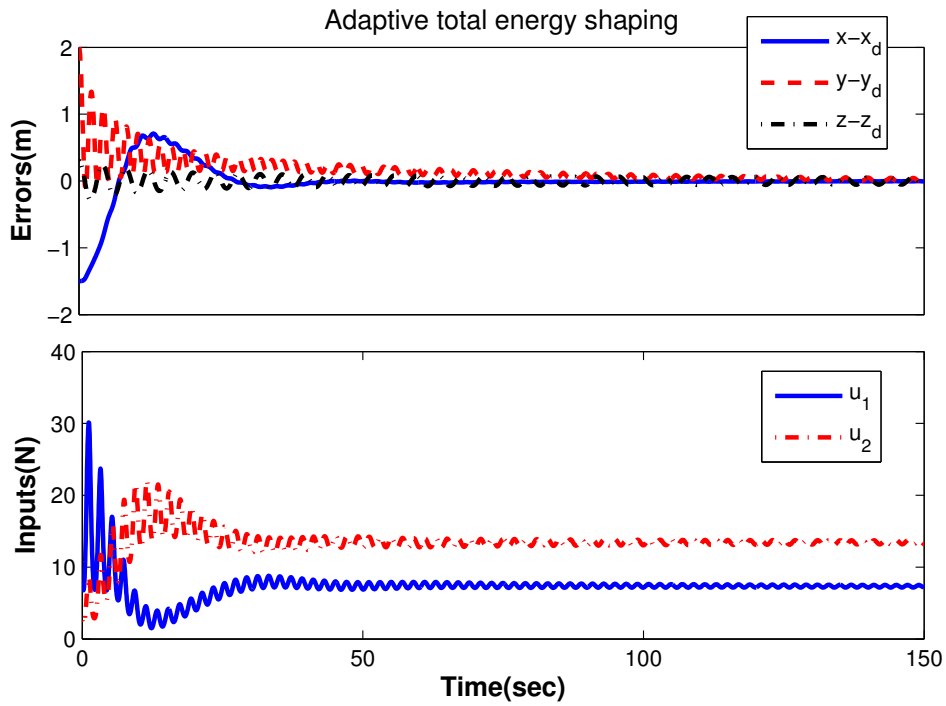


Figure 7.12: Simulation results of adaptive IDA-PBC in the presence of uncertain parameters.

V_d given in (4.25) is redesigned based on Proposition 6 as follows

$$V_d = k_1 \ln \cosh(l_1 - l_{1d}) + k_2 \ln \cosh(l_2 - l_{2d}) + k_3 \ln \cosh(l_3 - l_{3d}) + k_4 \ln \cosh(l_4 - l_{4d}).$$

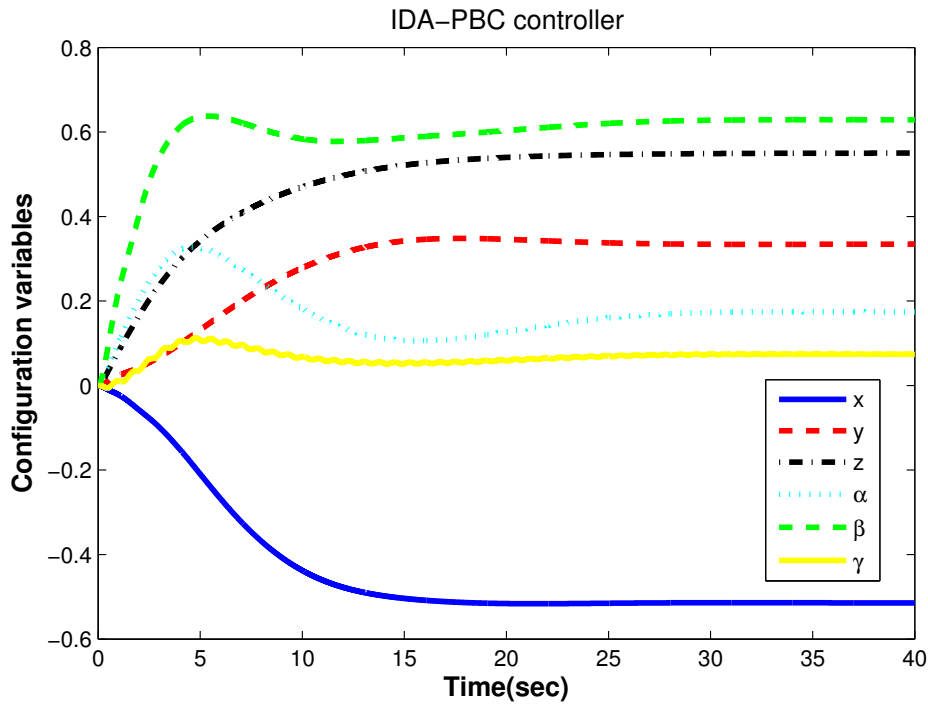


Figure 7.13: Simulation results of IDA-PBC on spidercam. All the configuration variables converge to their desired values.

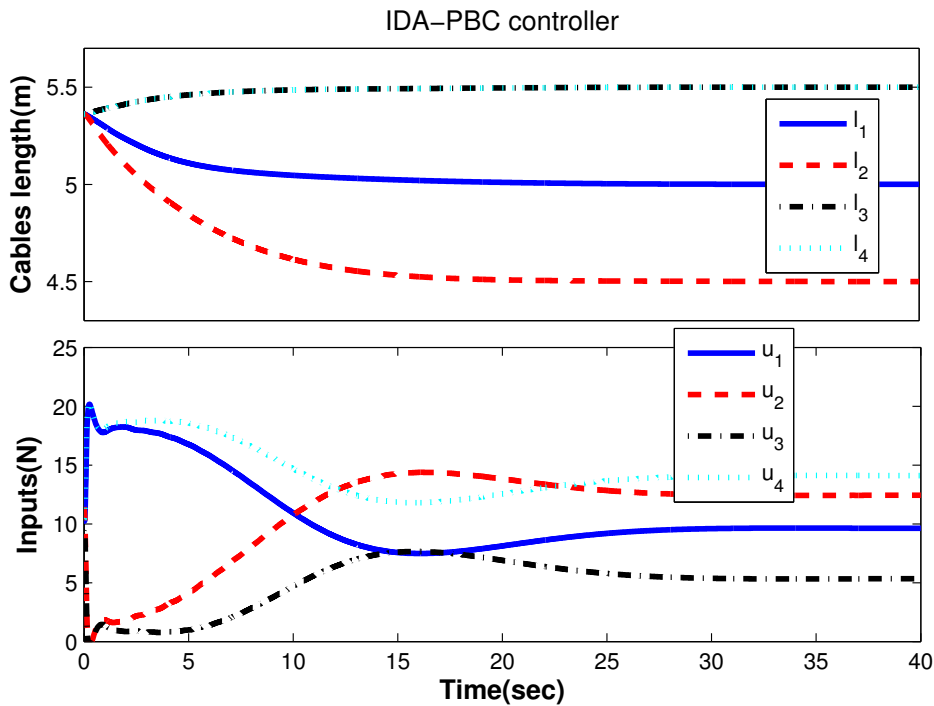


Figure 7.14: Control efforts and cables' length of spidercam.

The gains of the controller are

$$k_1 = k_2 = k_3 = k_4 = 5, \quad K_v = 5I.$$

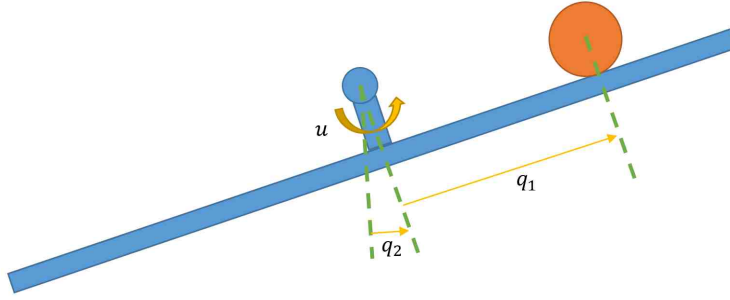


Figure 7.15: Ball and beam system.

To choose a desired equilibrium point, a method is calculation of $\mathbf{G}^\perp \nabla_{\mathbf{q}} V = 0$. Another way which is fit to the structure of V_d , is selection of the l_{id} s and the computation of \mathbf{q}^* from four forward kinematic equations and two equations $\mathbf{G}^\perp \nabla_{\mathbf{q}} V = 0$. By this means, presume that

$$l_{1d} = 5, \quad l_{2d} = 4.5, \quad l_{3d} = 5.5, \quad l_{4d} = 5.$$

Thus, the feasible equilibrium point of the robot is

$$x_d = -0.51, \quad y_d = 0.33, \quad z_d = 0.55, \quad \alpha = 0.17, \quad \beta = 0.63, \quad \gamma = 0.07$$

Note that the orientation of the end-effector is displayed by pitch–roll–yaw Euler angles. By this means, α denotes the rotation about x axis, β and γ denote the rotation about y and z axes of fixed frame, respectively. Notice that in this case this representation is singular free since due to structure of the robot, $-\pi/2 < \alpha, \beta, \gamma < \pi/2$. Additionally, to verify Proposition 5, the following matched disturbance is applied to the robot

$$\mathbf{d} = [e^{-t}, 1/(t^2 + 1), t/(t^3 + 1), e^{-2t} \sin(t)]^T.$$

To ensure tensile forces in cables, Proposition 2 is utilized. The results are depicted in Fig. 7.13 and Fig. 7.14. It is clear that all the configuration variables and cables' length converge to their desired values. This shows the applicability of Theorem 1, Proposition 6 that simplify controller design for a complex UCDR. Additionally, positive tension in cables are ensured easily using Proposition 2. Note that in this case, the gains are chosen more than the required values derived from Remark 5 to reduce the convergence rate.

7.1.4 Benchmark Systems

In this section, we verify the results of previous sections on some benchmark systems. The first two examples are introduced to verify the results of Section 5.1. Third and the last examples are related to Section 5.2 and Proposition 7, respectively.

Ball and beam system

The system consists of a ball moving along a beam whose angle is controlled. The schematic of the system is depicted in Fig. 7.15. The position of the ball with respect to the pivot point of the beam is denoted by q_1 , and the angle of the beam with respect to the vertical line is given by $\theta = q_2$. The dynamic parameters of the system are chosen

based on the model given in [14],

$$\mathbf{M} = \begin{bmatrix} 1 & 0 \\ 0 & L^2 + q_1^2 \end{bmatrix}, \quad V = gq_1 \sin(\theta),$$

where L is the half length of the beam, θ is the beam angle. For the control law, we utilize the proposed controller in [14] with the desired parameters of the closed-loop system, given by:

$$\begin{aligned} \mathbf{M}_d &= \begin{bmatrix} \sqrt{2}(L^2 + q_1^2)^{1/2} & L^2 + q_1^2 \\ L^2 + q_1^2 & \sqrt{2}(L^2 + q_1^2)^{3/2} \end{bmatrix} \\ V_d &= g[1 - \cos(q_2)] + \frac{k_p}{2} \left[q_2 - \frac{1}{\sqrt{2}} \operatorname{arcsinh}\left(\frac{q_1}{L}\right) \right]^2 \\ \mathbf{J}_2 &= \begin{bmatrix} 0 & j \\ -j & 0 \end{bmatrix}, \quad j = q_1 [p_1 - \sqrt{2}(L^2 + q_1^2)^{-1/2} p_2], \end{aligned}$$

in which $L = 2m$, $\mathbf{R} = \operatorname{diag}\{0.2, 0.1\}$, and the gains of the controller are $k_p = 5$ and $k_v = 5$ based on analysis proposed in [73]. The initial condition of the robot is considered to be $[\mathbf{q}^T(0), \mathbf{p}^T(0)] = [0.5, -0.1, 0.1, 0]$ based on *Proposition 5* of [14] and the controller is supposed to position the ball at the equilibrium point $[\mathbf{q}^T(0), \mathbf{p}^T(0)] = [0, 0, 0, 0]$. With the given parameters, $H_d(0) = 0.24$ is less than 0.31 derived from *Proposition 5* of [14], which ensures that the ball is always on the beam. Note that we do not modify the homogeneous solution of V_d to utilize the analysis proposed in [14]. The parameters in Theorem 2 are derived after some calculations as follows:

$$\begin{aligned} c_{V_2} &= 10.4, & c_{V_d} &= 2.4, & c_{\gamma_2} &= 6, & \lambda_{\max}\{M_d^{-1}\} &= 0.82, \\ c_{M_2} &= 0, & c_{M_d} &= 0.9, & c_J &= 10.4, & \lambda_{\min}\{M_d^{-1}\} &= 0.06 \end{aligned}$$

Using (5.7), one can simply compute $c_p = 2$ and $c_{\bar{p}} = 0.44$. Simulation results are depicted in Fig. 7.16. The control effort is less than 15 which is clearly less than the upper bound obtained from (5.9) with the above parameters. The upper bound of $\|\mathbf{p}\|$ and $\|\tilde{\mathbf{p}}\|$ are about 1.6 and 0.3 which are less than c_P and $c_{\bar{p}}$, respectively. Notice that the reason of difference between the actual and the computed upper bound is that in (5.9) we consider the worst-case scenario in obtaining the upper bounds. Note that in this case, it is possible to confine $\nabla_{\mathbf{q}} V_d$ using (5.1) as by considering $V_{dn} = g[1 - \cos(q_2)]$ and $v_{dh} = q_2 - \frac{1}{\sqrt{2}} \operatorname{arcsinh}\left(\frac{q_1}{L}\right)$, their partial derivative would be as:

$$\nabla_{\mathbf{q}} V_{dn} = [0, g \sin(q_2)]^T, \quad \nabla_{\mathbf{q}} V_{dh} = \left[\frac{1}{L\sqrt{2}\sqrt{1 + \left(\frac{q_1}{L}\right)^2}}, 1 \right]^T,$$

that are clearly bounded.

VTOL aircraft

In the previous example, the effects of velocity-dependent terms were investigated. Through this example we aim to analyze the Remarks 5, 6 and 7. Hence, we consider an UaS with strongly coupled dynamics, referred to as VTOL aircraft, which is introduced in Section B.2. First, a non-smooth control law is derived, and the tracking performance of the system and the magnitude of the control effort is analyzed. Secondly, we propose a two-phase controller to compensate for the effects of the non-smooth control law. Finally,

for the comparison purpose, the performance of smooth control law is also investigated. The dynamic parameters are given in equation (B.6). The purpose is to stabilize the unstable equilibrium point $[x^*, y^*, 0]$ with bounded input IDA-PBC controller. In [74], an IDA-PBC controller with configuration-dependent \mathbf{M}_d and smooth V_d has been designed. Here, in order to analyze the effects of non-smooth terms, intentionally a locally stabilizing controller with constant \mathbf{M}_d and non-smooth $\nabla_{\mathbf{q}} V_d$ is applied. The controller's parameters which are derived in Section B.2 are as follows

$$\begin{aligned} \mathbf{M}_d &= \begin{bmatrix} 20\epsilon^2 & 0 & \epsilon \\ 0 & 1 & 0 \\ \epsilon & 0 & 0.1 \end{bmatrix}, \quad \mathbf{J}_2 = \mathbf{0}_{3 \times 3}, \quad V_d = k_1 \ln \cosh(\epsilon(y - y^*) + \ln(\epsilon \cos(\theta) - 0.1\epsilon)) \\ &+ k_2 \ln \cosh\left(\frac{1}{20\epsilon}(x - x^*) - \theta - 0.1 \operatorname{arctanh}\left(1.1055 \tan\left(\frac{\theta}{2}\right)\right)\right) \\ &- k_1 \epsilon \tanh \ln(0.9\epsilon)(y - y^*) - \frac{g + k_1 \epsilon \tanh \ln(0.9\epsilon)}{\epsilon} \ln(\epsilon \cos(\theta) - 0.1\epsilon) - \rho, \end{aligned}$$

with $k_1, k_2 > 0$ being the free parameters and the constant ρ is determined such that $V_d(t_0) = 0$. It is clear that the terms $\operatorname{arctanh}\left(1.1055 \tan\left(\frac{\theta}{2}\right)\right)$ and $\ln(\epsilon \cos(\theta) - 0.1\epsilon)$ confine θ in a region inside the workspace and lead to non-smooth terms in $\nabla_{\mathbf{q}} V_d$. Hence, we invoke the results of Remark 6 and 7. Note that due to the simple structure of \mathbf{G} , it is possible to derive better upper bounds with respect to the conservative upper bound proposed in (5.15) by the following matrices,

$$\begin{aligned} (\mathbf{G}^T \mathbf{G})^{-1} \mathbf{G}^T &= \begin{bmatrix} -\sin(\theta) & \cos(\theta) & 0 \\ \frac{\epsilon \cos(\theta)}{1+\epsilon} & \frac{\epsilon \sin(\theta)}{1+\epsilon} & \frac{1}{1+\epsilon} \end{bmatrix} \\ (\mathbf{G}^T \mathbf{G})^{-1} \mathbf{G}^T \mathbf{M}_d \mathbf{M}^{-1} &= \begin{bmatrix} -20\epsilon^2 \sin(\theta) & \cos(\theta) & -\epsilon \sin(\theta) \\ \frac{20\epsilon^3 \cos(\theta) + \epsilon}{1+\epsilon} & \frac{\epsilon \sin(\theta)}{1+\epsilon} & \frac{\epsilon^2 \cos(\theta) + 0.1}{1+\epsilon} \end{bmatrix} \end{aligned}$$

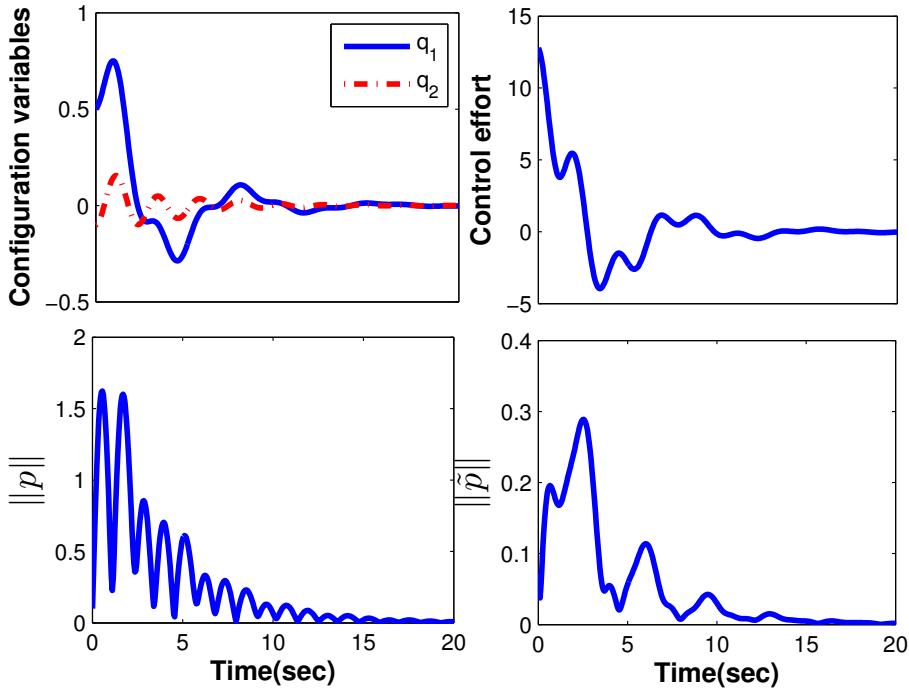


Figure 7.16: Simulation results of the ball and beam system.

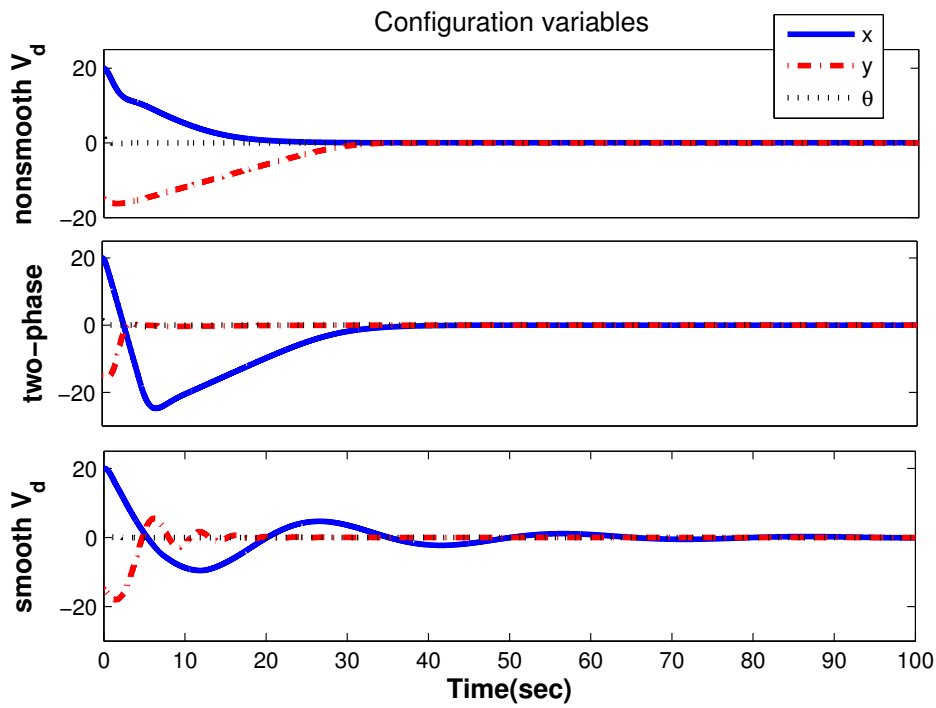


Figure 7.17: Configuration variables of the VTOL aircraft.

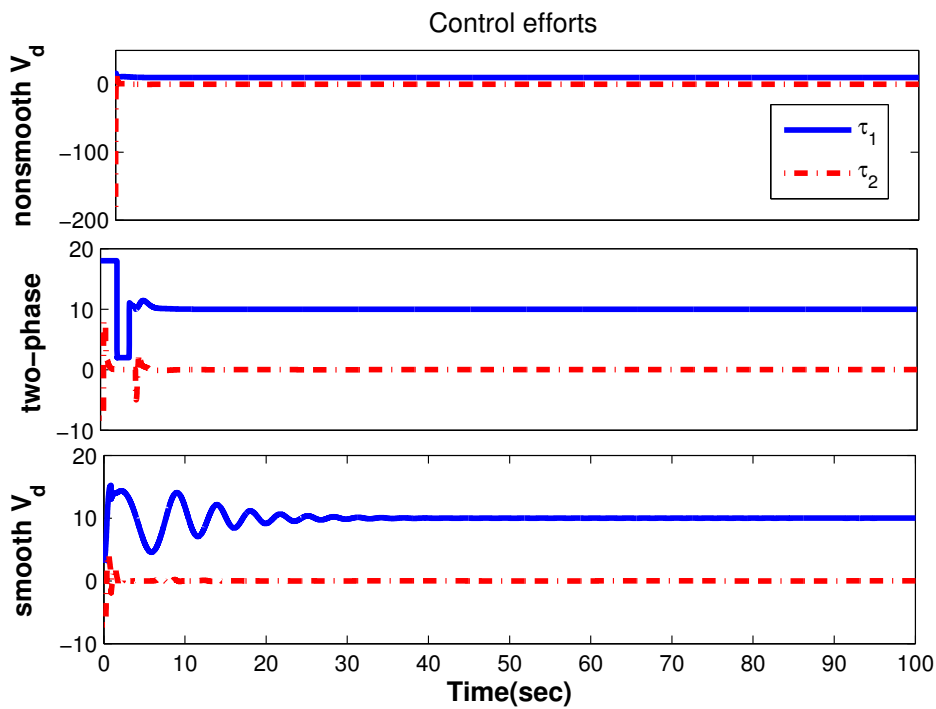


Figure 7.18: Control efforts of the VTOL aircraft.

Note that a constant gravity is applied to the y direction of the system. Thus, the bounds

of controller are in the following form:

$$\begin{aligned} |u_1 - g| &\leq \max_q \{|g - ((\mathbf{G}^T \mathbf{G})^{-1} \mathbf{G}^T \nabla_q V)_1|\} + \max_q \{\|(\mathbf{G}^T \mathbf{G})^{-1} \mathbf{G}^T \mathbf{M}_d \mathbf{M}^{-1}\|\} c_{V_d} + \lambda_{max}\{\mathbf{K}_v\}, \\ |u_2| &\leq \max_q \{|((\mathbf{G}^T \mathbf{G})^{-1} \mathbf{G}^T \nabla_q V)_2|\} + \max_q \{\|(\mathbf{G}^T \mathbf{G})^{-1} \mathbf{G}^T \mathbf{M}_d \mathbf{M}^{-1}\|\} c_{V_d} + \lambda_{max}\{\mathbf{K}_v\}, \end{aligned} \quad (7.13)$$

where the damping term is modified to be $\mathbf{K}_v \mathcal{S}(\mathbf{G}^T \dot{\mathbf{p}})$ with \mathcal{S} defined in (5.1). The initial condition of the system is $[20, -15, 1.3]^T$ with zero velocity and the desired position is the equilibrium point of the system at $[0, 0, 0]^T$. Since the initial value of θ is close to singularity, it results into high values for the control effort. Invoking Remark 6, one can compute the upper bound of $\theta = 1.33$ by considering $k_1 = 4$ and $k_2 = 5$. By this means, the following upper bounds are derived after some calculations,

$$\begin{aligned} |((\mathbf{G}^T \mathbf{G})^{-1} \mathbf{G}^T \nabla_q V)_1| &\leq 10, & |((\mathbf{G}^T \mathbf{G})^{-1} \mathbf{G}^T \nabla_q V)_2| &\leq 2.25, \\ \|(\mathbf{G}^T \mathbf{G})^{-1} \mathbf{G}^T \mathbf{M}_d \mathbf{M}^{-1}\| &\leq 1.75, & c_{V_d} &= 170. \end{aligned}$$

Simulation results with $\mathbf{K}_v = \mathbf{I}_2$ and $\mathcal{S} = \tanh$ is depicted in Fig. 7.17 and Fig. 7.18, denoted by ‘nonsmooth V_d ’ in both figures. The simulation results of the two-phase controller and the smooth control law are also demonstrated in figures identified with the label ‘two-phase’ and ‘smooth V_d ’, respectively. In Fig. 7.17 the performance of the controllers is shown, and Fig. 7.18 shows the control efforts. As it is clear from the figures, for the non-smooth control law, the configuration variables converge to zero, but the upper bound of the control effort is about 200, which is not even close to being applicable. To rectify this problem, a two-phase controller based on Remark 7 is designed. Additionally, the controller proposed in [74] is simulated. In the two-phase controller, the primary controller is used in the first phase to converge θ to zero. Hence, for a small value of the θ , the dynamic of the system can be represented in the following form:

$$\ddot{x} \approx 0, \quad \ddot{y} \approx u_1 - g,$$

which is obtained by replacing $\theta \approx 0, u_2 \approx 0$ in the dynamic of the system. Considering the simplified dynamic, then a secondary controller is designed using IDA-PBC approach such that $y - y^*$ converges to zero. Although with this controller $|x|$ will increase with a constant speed, it is possible to reduce $H_d(t_0)$ arbitrary by increasing M_{d11} or decreasing k_2 in which t_0 denotes the initial time of applying the secondary controller. In the two-phase controller, the primary controller is given by:

$$\begin{aligned} u_1 &= g - \vartheta_1 \mathcal{S}(\kappa_1 y + \kappa_2 \dot{y}) \\ u_2 &= -\vartheta_2 \mathcal{S}(\kappa_3 \theta + \kappa_4 \dot{\theta}) \end{aligned}$$

with the following parameters:

$$\vartheta_1 = \vartheta_2 = 8, \quad \kappa_1 = 30, \quad \kappa_2 = 20, \quad \kappa_3 = 80, \quad \kappa_4 = 30$$

with this aim that $|u_1 - g| \leq 10$ and $|u_2| \leq 10$ are satisfied. Referring to the simulation results in Fig. 7.17 and Fig. 7.18, it is clear that after applying the two-phase controller, the control efforts are in the bounds, and configuration variables converge to their desired values. This shows the superiority of this method. Note that one may design a better controller for the first phase to prevent the increase of $|x|$, but this is out of the scope of this thesis. We have also investigated the controller proposed in [74] which is based on a smooth V_d . The

parameters of that controller are $\mathbf{P} = \text{diag}\{0.003, 0.005\}$ and $\mathbf{K}_v = 0.2\mathbf{I}_2$. It should be noted that in this case, we have set smaller gains rather than the gains considered in [74] for the controller such that the calculated upper bound meets the saturation requirement, with the expense of a slow convergence rate. The simulation results show that as expected, $|u_1 - g|$ and $|u_2|$ lie in the predefined range. In other words, the non-smooth two-phase controller and the smooth one proposed in [74] satisfy the practical constraint of the actuators while the non-smooth controller has enormous control effort. This study confirms that the suitable solution for the PDEs is an essential part of the controller design while considering bounded input control problems. If the derived solution of V_d is not a smooth function, it is recommended to design a two-phase controller to meet the actuators' bounds. Note that as discussed in the paragraph before Remark 6, in some cases, V_d is necessarily non-smooth. Furthermore, generally, the matching equations are complicated to obtain, and hence, it may not be possible to derive a smooth solution. Thus, the applicability of a two-phase controller is preferred while it may also result in a faster response in comparison with a smooth controller with small conservative gains.

2D SpiderCranr

To examine the proposed method in Section 5.2, consider 2D SpiderCrane introduced in [127]. The schematic of this system is depicted in Fig. B.2, while its dynamic formulation are given in Section B.3. $[F_x, F_y]^T$ are considered as the control inputs. In [131], a controller based on total energy shaping was proposed while in [127], potential energy shaping was employed to design the controller. Here, we modify the controller introduced in [131] through our proposed method in Theorem 3. The reader is referred to [131] for details of the controller design.

First, by using partial feedback linearization, the system dynamics is transformed into the normal form. Then, \mathbf{M}_d is designed by

$$\mathbf{M}_d = \begin{bmatrix} -k_1 l_3 \cos^2(\theta) + k_3 & -k_1 l_3 \cos(\theta) \sin(\theta) & k_1 \cos(\theta) \\ -k_1 l_3 \cos(\theta) \sin(\theta) & k_1 l_3 \cos^2(\theta) + k_3 & k_1 \sin(\theta) \\ k_1 \cos(\theta) & k_1 \sin(\theta) & k_2 \end{bmatrix}$$

while, V_d , proposed in [131], is modified to

$$V_d = 0.2 \ln \cosh 10 \left(x - x_d - \frac{k_3}{k_1 + l_3 k_2} (1 - \cos(\theta)) \right) + 0.2 \ln \cosh 10 \left(y - y_d - \frac{k_3 + l_3 k_1}{k_1 + l_3 k_2} (1 - \cos(\theta)) \right) - \frac{g}{k_1 + l_3 k_2} \cos(\theta).$$

Note that with this control law, Assumption 5 is not satisfied; thus, we will apply the proposed method based on the optimization given by Theorem 3. The controller gains are chosen by

$$k_1 = 0.05, \quad k_2 = 10, \quad k_3 = 3, \quad \mathbf{K}_v = 6\mathbf{I}_2,$$

while the initial and desired positions are set $[x_r(0), y_r(0), \theta(0)]^T = [-1, 3, 0.5]^T$, $[\dot{x}_r(0), \dot{y}_r(0), \dot{\theta}(0)]^T = [0.1, 0, 0]^T$ and $[x_{rd}, y_{rd}, \theta_d]^T = [0.5, 1, 0]^T$, respectively. The inputs are set to be bounded by $\mathbf{u}_m = [-3, 22]^T$ and $\mathbf{u}_M = [3, 28]^T$.

Simulation results are shown in Fig. 7.19 and Fig. 7.20. Fig. 7.19 illustrates system response using the IDA-PBC's control law given in (2.15). As it is observed, the input bounds are not satisfied in both control inputs. Fig. 7.20 illustrates the simulation results with the control law (5.41) which is based on the optimization proposed in Theorem 3.

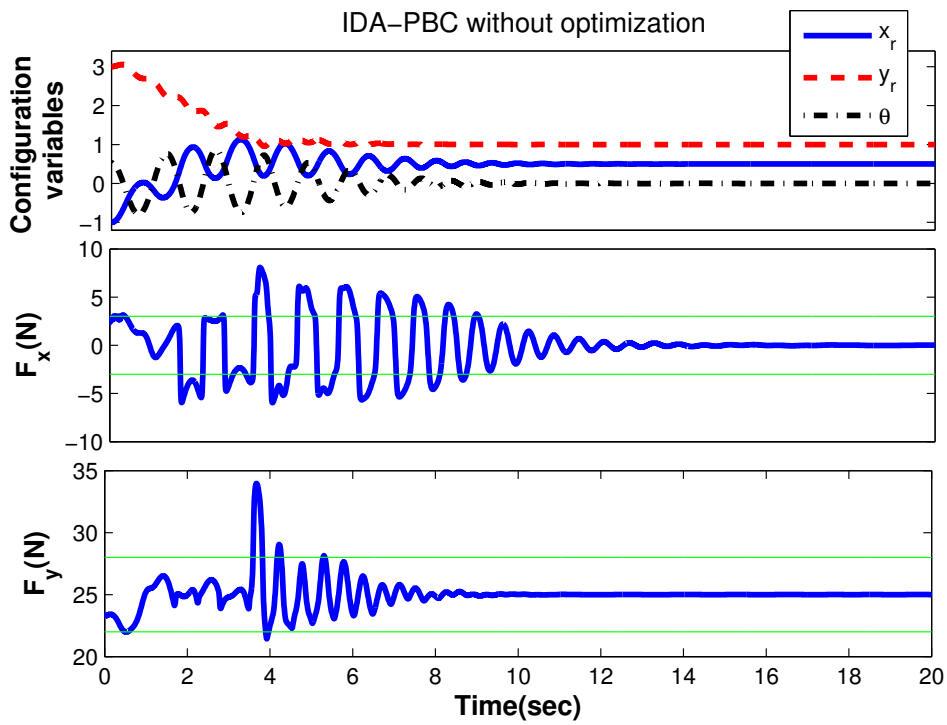


Figure 7.19: Simulation results with total energy shaping without optimization.

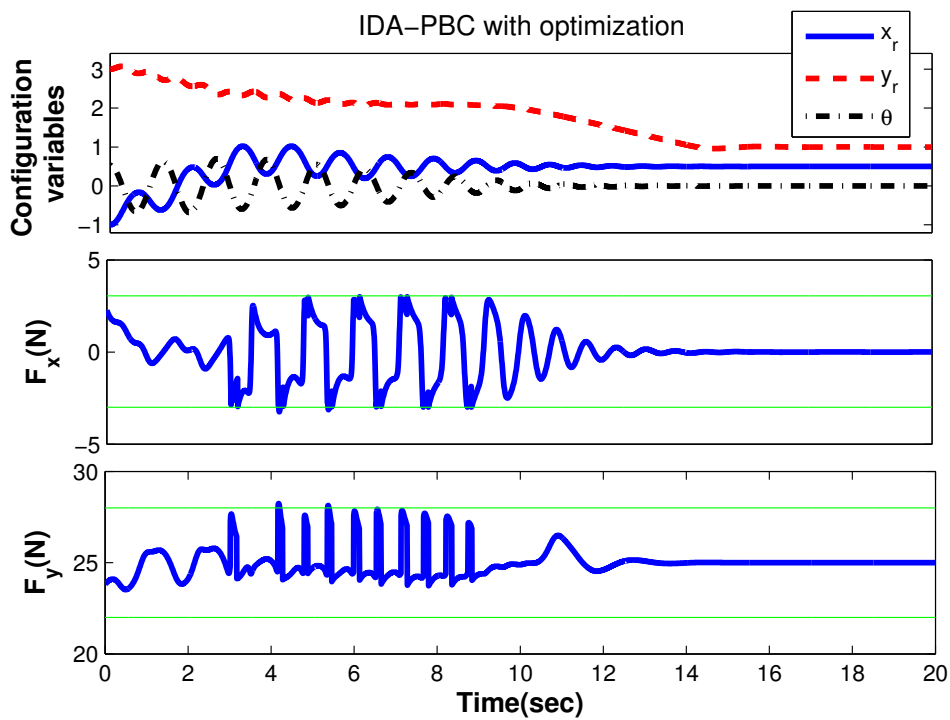


Figure 7.20: Simulation results with total energy shaping and optimized inputs.

Comparison of these figures shows significant improvement in restricting the control efforts within the assigned bounds while all the configuration variables converge to their desired values, in expense of slightly slower convergence.

Pendubot

Here, the aim is analyzing Proposition 7. For this purpose, the proposed controller for pendubot in Section A.4 is considered. The designed controller in that section with desired gravity compensation is implemented. Since in $\mathbf{q}^* = [\pi, 0]^T$ the gravity term is zero, the term $\nabla_{\mathbf{q}}V$ is omitted in control law based on Proposition 7. The parameters of the robot and the gains of the controller are similar to [84]. The initial condition is $\mathbf{q}(0) = [\pi - 0.7, 0.8]^T$ with zero velocity. The results are depicted in Fig. 7.21. It is clear that the configuration variables converge to their desired values. This shows that in some scenarios, it is possible to design a simplified version of IDA-PBC by removing the gravity compensation term.

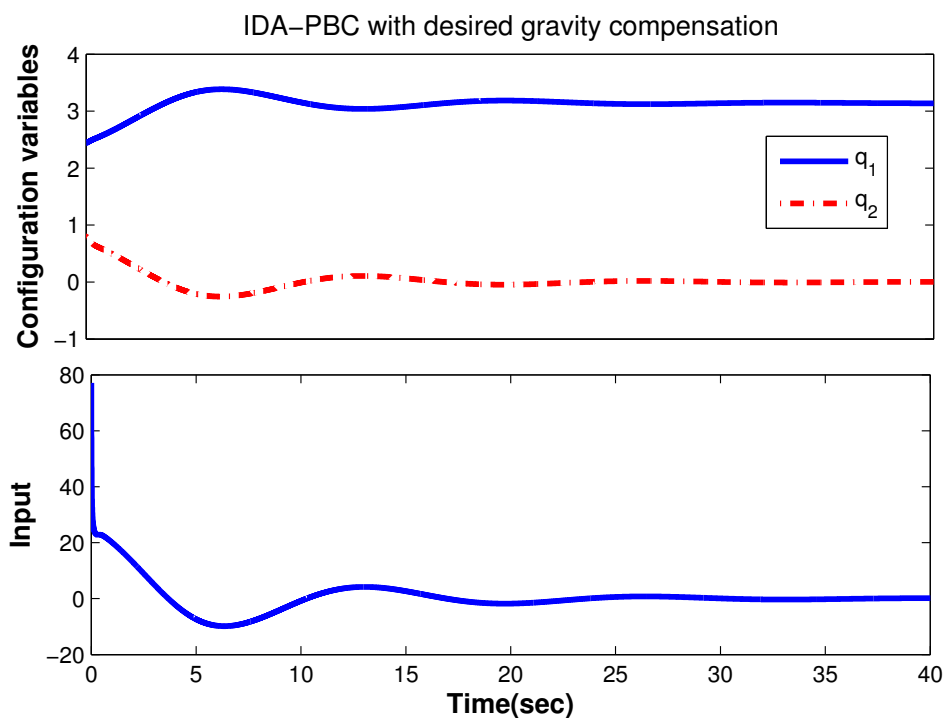


Figure 7.21: Simulation results of IDA-PBC with desired gravity compensation on pendubot.

7.2 Experimental Results

Here, some of the proposed controllers are implemented on cable-driven robots to analyze the performance in practice.

7.2.1 ARAS Underactuated Cable-Driven Robot

The robot was introduced in Section 3.4. Here, some of the results of this thesis are implemented on the robot. For this purpose, IDA-PBC controller based on potential energy shaping with V_d as (7.3) is applied to the robot. To ensure positive tension in cables, we utilize the results of simple Proposition 2 which was simply derived from Theorem 4.

The gains of the controller are

$$k_3 = 20 \quad k_4 = 20 \quad \mathbf{K}_v = 10\mathbf{I}_2. \quad (7.14)$$

The robot starts from $\mathbf{q}(0) = [0.73, -1.04, 0]^T$ and moves toward $\mathbf{q}^* = [0.58, -0.914, -0.392]^T$

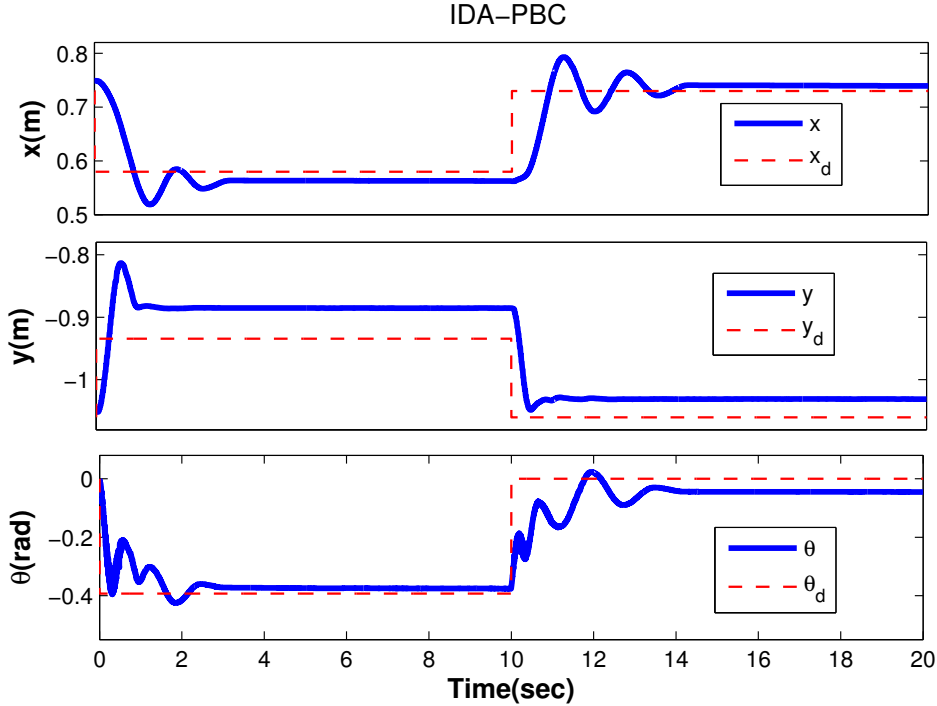


Figure 7.22: Configuration variables of ARAS UCDR with IDA-PBC.

and then comes back to the initial position. Note that these points are on the manifold of equilibrium points. The bounds of actuators are $\mathbf{u}_{min} = [0.5, 0.5]^T$ and $\mathbf{u}_{max} = [20, 20]^T$. The results are illustrated in Fig. 7.22 and Fig. 7.23. As indicated in Fig. 7.22, the configuration variables are settled after about four seconds. The error of x and θ is negligible while $y - y^*$ is about 4cm. The reason may be arisen from imprecise value of the mass of the end-effector. The control efforts are depicted in Fig. 7.23. It is clear that the control efforts are in the predefined bounds while the system is stable. This shows the applicability of the proposed method in Proposition 2.

In order to improve the results, adaptive IDA-PBC proposed in Theorem 5 is also implemented on the robot. The results are shown in Fig. 7.24 and Fig. 7.25. It is clear that using an adaptation law, the error of y is essentially reduced. The reason is this fact that the gravity force which is proportional to m is directly affects on y . Note that since equilibrium points of the robot are on a complex manifold and also the matrix \mathbf{G} is configuration-dependent, improvement of $y - y^*$ leads to reduction of $x - x^*$ and $\theta - \theta^*$.

For the sake of comparison, a PD with gravity compensation is executed on the system. It is designed such that merely x and y are controlled. The results are illustrated in Fig. 7.26 and Fig. 7.27. It is seen that in the first movement, the configuration variables converge to their desired values after about 18 second. However, in the latter relocation, the response is oscillatory with large domain. In this phase, the robot goes out of scope of the cameras, results in unknown defined value of θ . Furthermore, as indicated in Fig. 7.26, although the gains of the controller are selected suitably, they are not always positive. Note that the results of this controller are oscillatory in simulation, but in practice, due

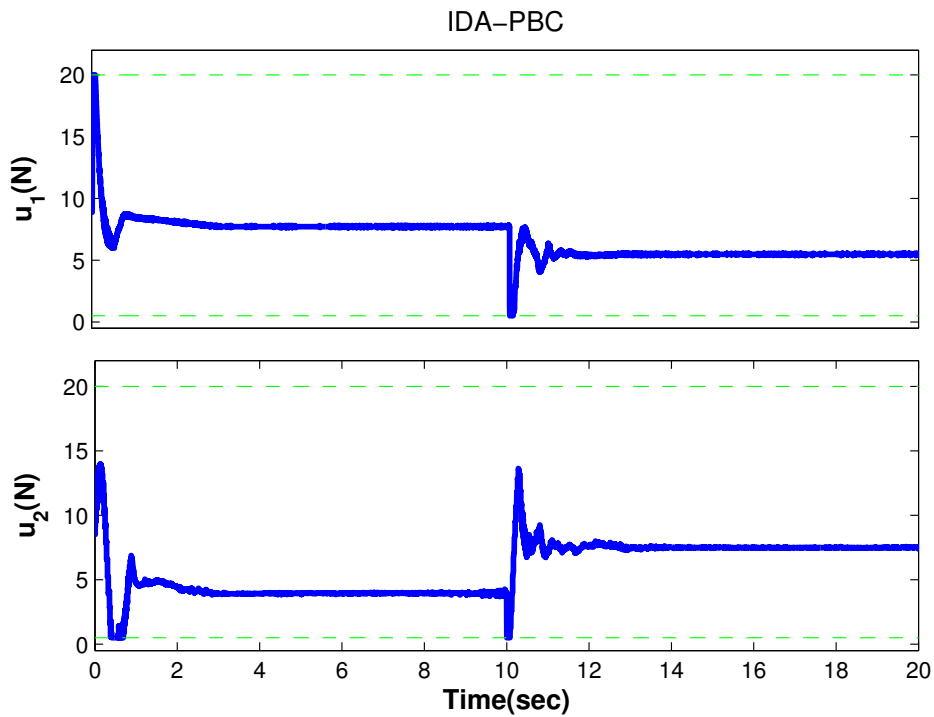


Figure 7.23: Control efforts of ARAS UCDR with IDA-PBC.

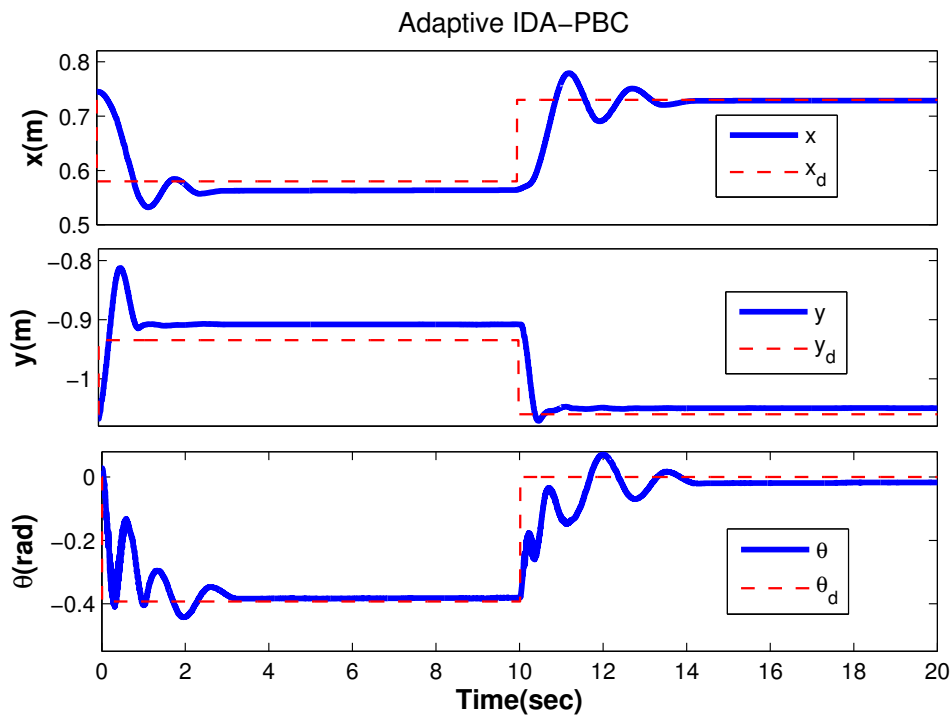


Figure 7.24: Configuration variables of ARAS UCDR with adaptive IDA-PBC.

to friction, the oscillations may be damped. By comparing the results, it is deduced that the performance of IDA-PBC is much better than a traditional controller.

Furthermore, a simple controller in joint space (i.e. the cables' length) is implemented on the robot. The results are shown in Fig. 7.28 and Fig. 7.29. As indicated in these

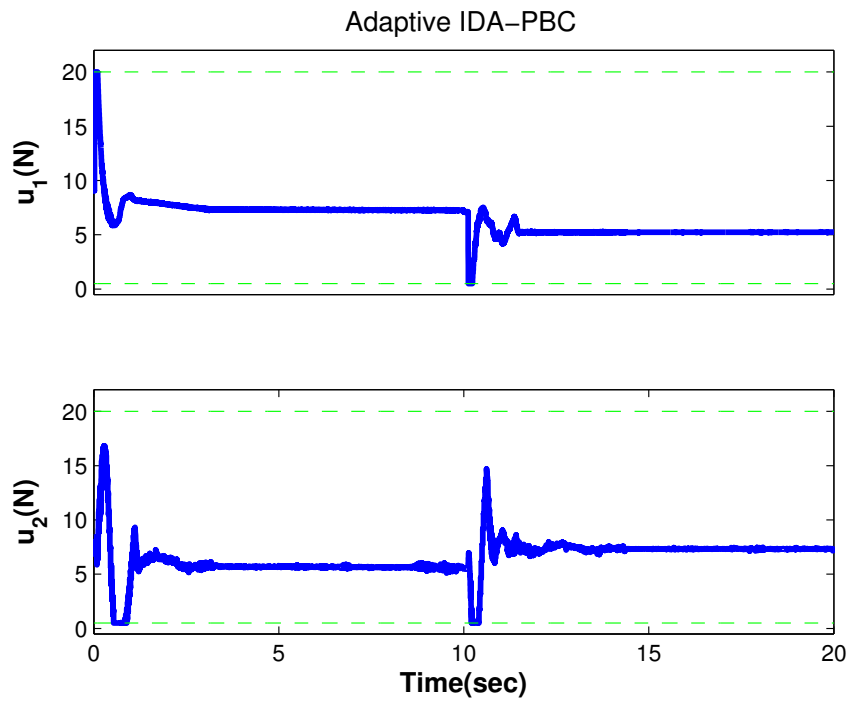


Figure 7.25: Control efforts of ARAS UCDR with adaptive IDA-PBC.

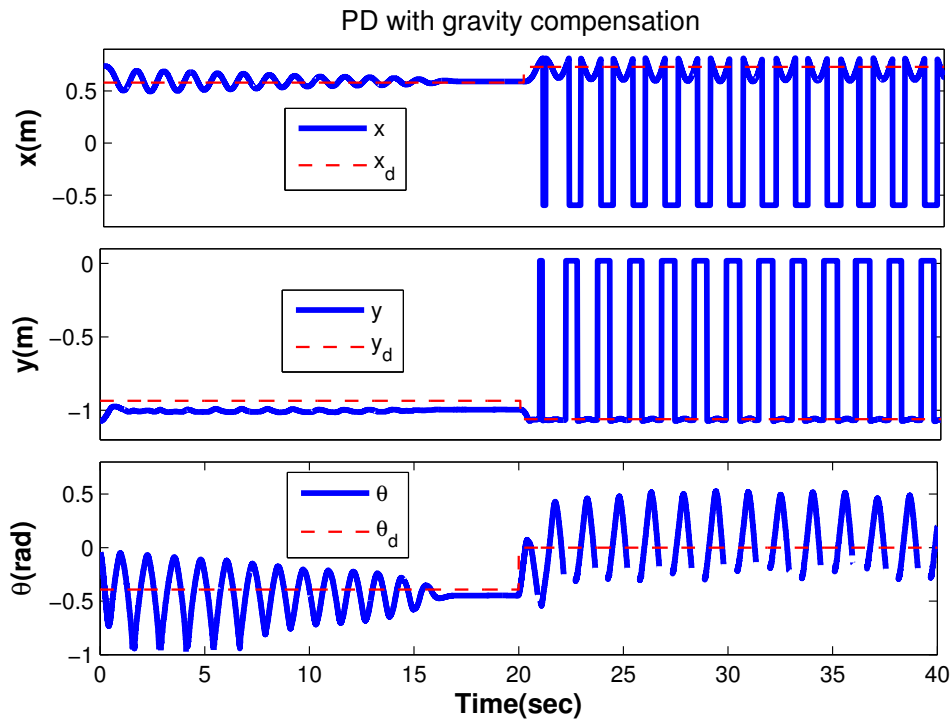


Figure 7.26: Configuration variables of ARAS UCDR with PD controller.

figures, the performance and steady state error is much worse than IDA-PBC controller. It is in concurrence with the results of [149] in which it is proven that a controller in task space leads to better response compared to that in the joint space for parallel robots. Additionally, the performance of a controller in joint space for UCDRs depends hugely

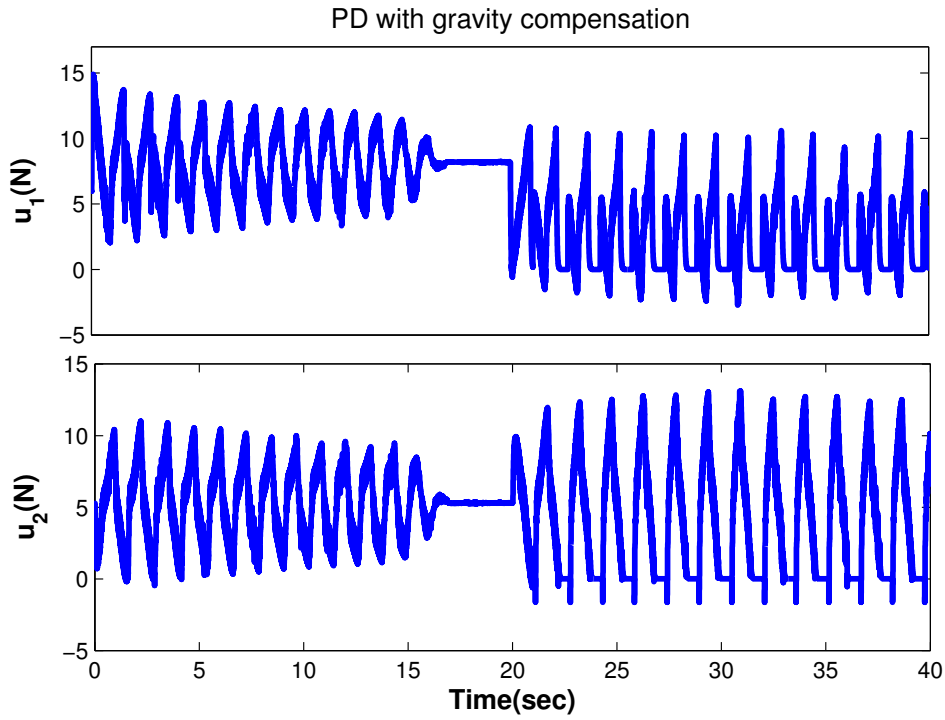


Figure 7.27: Control efforts of ARAS UCDR with PD controller.

to the friction of the system in such a way that asymptotic stability is not achieved in simulation without modeling natural damping terms.

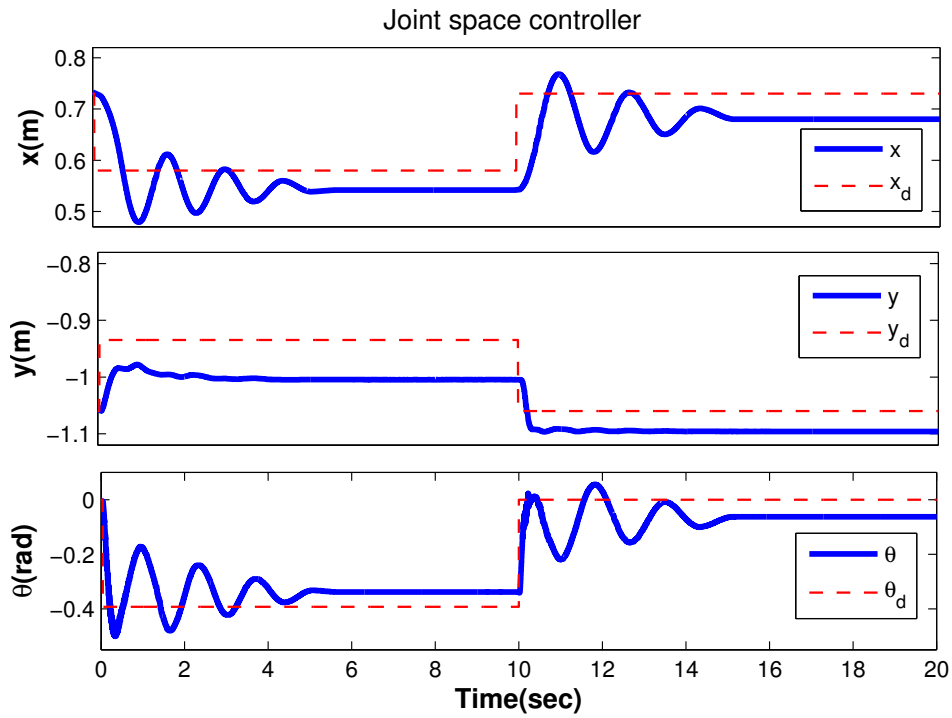


Figure 7.28: Configuration variables of ARAS UCDR with a controller in joint space.

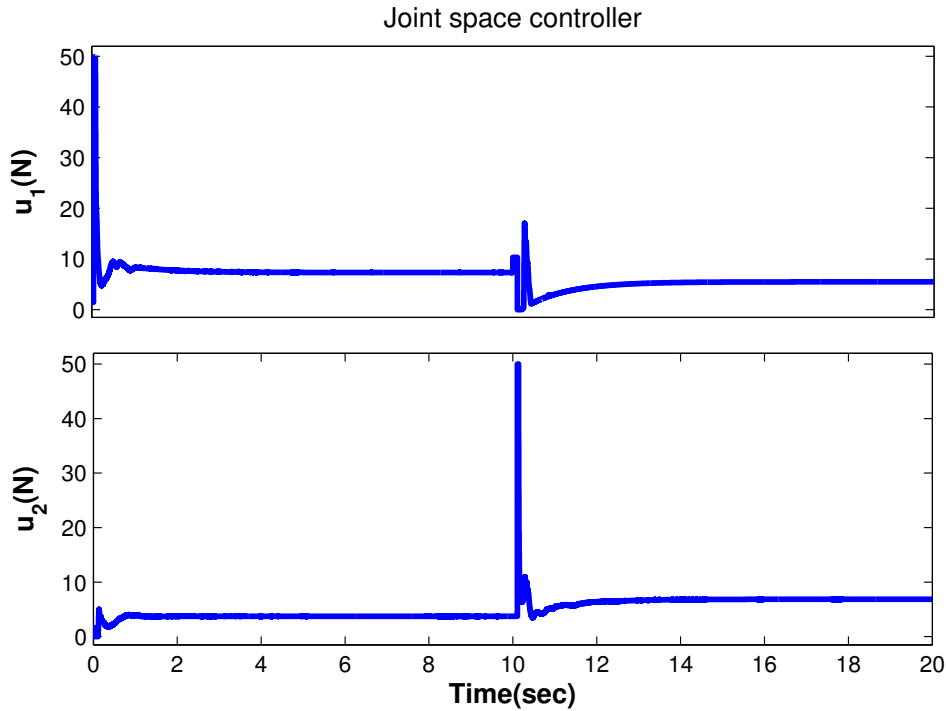


Figure 7.29: Control efforts of ARAS UCDR with a controller in joint space.

7.2.2 ARAS Cam

The proposed method in Theorem 4 is implemented on the fully actuated 3-DOF cable-driven robot introduced in Section 3.4. The initial and desired position of the CDR are $[x(0), y(0), z(0)]^T = [1.23, -0.6, 1.41]^T$ and $[x^*, y^*, z^*]^T = [1.11, -0.72, 1.28]^T$, respectively. Controller parameters and gains are as follows

$$M_d = M, \quad V_d = (\mathbf{q} - \mathbf{q}^*)^T \mathbf{K}_p (\mathbf{q} - \mathbf{q}^*), \quad \mathbf{K}_p = 1100 \mathbf{I}_3, \quad \mathbf{K}_v = 100 \mathbf{I}_3.$$

The bounds of actuators are given by $\mathbf{u}_m = [0.5, 0.5, 0.5]^T$ and $\mathbf{u}_M = [60, 60, 60]^T$ to prevent loosening of the cables and their over stretching.

Fig. 7.30 illustrates the stabilization errors together with the control efforts with their limits by using Theorem 4. Due to high gains of the controller, if \mathbf{J}_u and $\bar{\mathbf{k}}$ are not used, the cable forces become negative, resulting in loosening of the cables. However, with the proposed method, the cable forces remain within the desired bounds, while the robot end-effector position converges to the desired value. It is observed that adjustment of $\bar{\mathbf{k}}$ has been merely done at the beginning of the experiment.

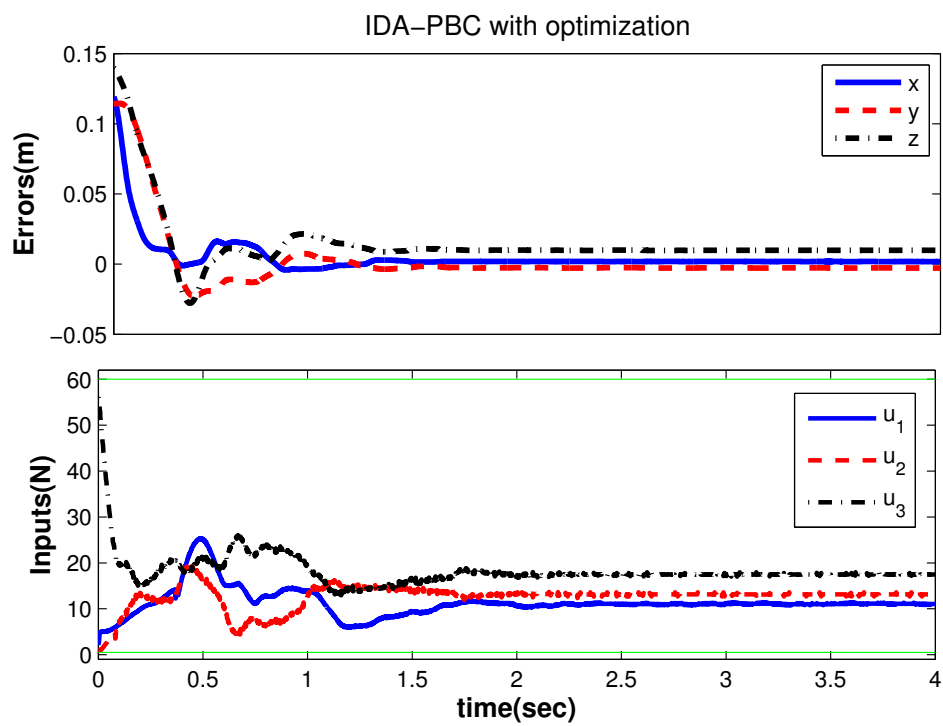


Figure 7.30: Experimental results based on Theorem 4 on the 3-DOF ARAS CDR. Positive tensions are achieved with the proposed controller.

Chapter 8

Conclusion and Future Works

In this thesis, controller design for underactuated systems and particularly, 3-DOF underactuated cable-driven robots were studied. For this purpose, interconnection and damping assignment passivity-based control was utilized to stabilize the mechanical system at the desired equilibrium point. Since IDA-PBC is based on the solution of some partial differential equations, it is required to solve these matching equations analytically. In order to address this stumbling block, three methods were proposed in this thesis. Replacing a first-order PDE by some Pfaffian differential equations was one of the methods in which it was shown that under the satisfaction of a condition for a Pfaffian equation with three variables, it is straightforward to derive its solution. Using this method, the matching equations of some UaSs, including magnetic levitation system, pendubot, underactuated planar and spatial cable-driven robots were solved. Another method was proposed to solve the matching equation of potential energy shaping in underactuated parallel robots. By this means, it was possible to design IDA-PBC for the systems with underactuation degrees of more than one, such as spidercam. Simplification of the nonlinear PDE of kinetic energy shaping for a class of UaSs was another achievement of this thesis regards to the matching equations. Furthermore, since the amplitude of actuators is limited in practice, the design of IDA-PBC with bounded input for mechanical systems was another topic of interest in this thesis. For this purpose, two strategies were employed. Computing the upper bound of control law in IDA-PBC approach was accomplished via calculation of the upper bound of velocity and some of the parameters of the controller. Since, in some cases, the desired potential energy is non-smooth and thus, it is unbounded, a two-phase controller was proposed to confine the control efforts while the stability of the desired pose is guaranteed. Design of IDA-PBC with prescribed bounds of actuators was another aim of this thesis. For this purpose, the free part of a sub-block of the interconnection matrix was considered, and an optimization problem based on minimization of control law was solved analytically. Although it does not necessarily lead to satisfaction of the bounds of the actuators, a modified version of it for a class of manipulators was presented to ensure boundedness of inputs inside the prescribed bounds. IDA-PBC with position feedback for a class of mechanical systems was also introduced to simplify its implementation in practice. Since parameters' uncertainty is inevitable in practice, an adaptive version of IDA-PBC was suggested. It was shown that generally, the parameters should be estimated correctly to ensure the stability of the closed-loop system. However, in some cases, such as the potential energy shaping of UCDRs, it is possible to design a suitable adaptive IDA-PBC for the mass of the end-effector. Additionally, robust IDA-PBC with respect to matched external disturbance was analyzed. It was shown that the system is stable with simple IDA-PBC if the disturbance satisfies a condition. IDA-PBC with desired gravity

compensation and IDA-PBC with merely homogeneous part of desired potential energy for a class of manipulators were other simplified versions of IDA-PBC that were introduced in this thesis. Finally, the proposed controllers are verified through several simulations on different UCDRs and underactuated benchmark systems. Furthermore, some of the controllers are implemented on ARAS underactuated planar cable-driven robot and ARAS cam to examine the performance in practice.

In future, several works in compliment of the accomplished studies will be performed. Some of them are listed as follows:

- Implementation of the controllers to analyze their performance in practice.
- Analysis of feasible trajectory tracking with IDA-PBC especially for underactuated spatial cable-driven robot.
- Total energy shaping of UCDRs.
- Extension of the results to port-Hamiltonian systems.

Appendix A

Solving the Matching Equations of Benchmark Systems by Pfaffian Differential Equations

Here, some examples of finding the solution of matching equations by Pfaffian differential equations are proposed. First, let us introduce a special form of (2.2-2.7) for PH systems. Consider a PH system with dynamic formulation of the following form

$$\dot{\mathbf{x}} = (\mathbf{J}(\mathbf{x}) - \mathbf{R}(\mathbf{x}))\nabla_{\mathbf{x}}H(\mathbf{x}) + \mathbf{g}(\mathbf{x})\mathbf{u}, \quad (\text{A.1})$$

where $\mathbf{x} \in \mathbb{R}^n$ denotes the states of the system, $\mathbf{u} \in \mathbb{R}^m$ denotes the input, $\mathbf{J}(\mathbf{x}) = -\mathbf{J}^T(\mathbf{x}) \in \mathbb{R}^{n \times n}$ and $0 \leq \mathbf{R}(\mathbf{x}) = \mathbf{R}^T(\mathbf{x}) \in \mathbb{R}^{n \times n}$ are the interconnection and damping matrices respectively, $H(\mathbf{x}) \in \mathbb{R}$ denotes the total stored energy in the system and $\mathbf{g}(\mathbf{x}) \in \mathbb{R}^{n \times m}$ is full rank input mapping matrix. The IDA-PBC method relies on matching the system (A.1) with the generalized Hamiltonian structure

$$\dot{\mathbf{x}} = (\mathbf{J}_d(\mathbf{x}) - \mathbf{R}_d(\mathbf{x}))\nabla_{\mathbf{x}}H_d(\mathbf{x}), \quad (\text{A.2})$$

in which $H_d(\mathbf{x})$ is continuously differentiable desired storage function which is (locally) minimum at the desired equilibrium point \mathbf{x}^* , while $0 \leq \mathbf{R}_d(\mathbf{x}) = \mathbf{R}_d^T(\mathbf{x}) \in \mathbb{R}^{n \times n}$ and $\mathbf{J}_d(\mathbf{x}) = -\mathbf{J}_d^T(\mathbf{x}) \in \mathbb{R}^{n \times n}$ represent desired interconnection and damping matrices, respectively. Assume that the matrices $\mathbf{J}_d, \mathbf{R}_d$ together with H_d are chosen such that the following equation is satisfied

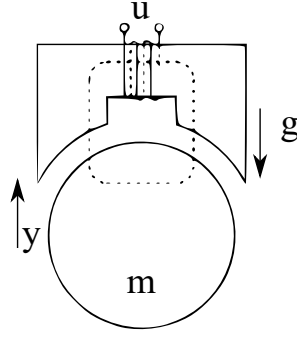
$$\mathbf{g}^\perp(\mathbf{J} - \mathbf{R})\nabla_{\mathbf{x}}H(\mathbf{x}) = \mathbf{g}^\perp(\mathbf{J}_d - \mathbf{R}_d)\nabla_{\mathbf{x}}H_d(\mathbf{x}), \quad (\text{A.3})$$

where matrix $\mathbf{g}^\perp(\mathbf{x}) \in \mathbb{R}^{n-m \times n}$ is left annihilator of $\mathbf{g}(\mathbf{x})$ such that $\mathbf{g}^\perp \mathbf{g} = 0$. This equation results from matching the systems (A.1) and (A.2). The control law is derived as follows

$$\mathbf{u}(\mathbf{x}) = (\mathbf{g}^T \mathbf{g})^{-1} \mathbf{g}^T \left((\mathbf{J}_d(\mathbf{x}) - \mathbf{R}_d(\mathbf{x}))\nabla_{\mathbf{x}}H_d(\mathbf{x}) - (\mathbf{J}(\mathbf{x}) - \mathbf{R}(\mathbf{x}))\nabla_{\mathbf{x}}H(\mathbf{x}) \right).$$

A.1 Magnetic Levitation System

This system consists of a ferric ball hovered under a magnetic field created by an electromagnet. The schematic of the system is illustrated in Fig. A.1. Consider λ as the flux

Figure A.1: Schematic of magnetic levitation system ($y = \theta$).

generated by the magnet and θ as the distance of the center of mass of the ball to its nominal position. It is shown in [60] that the system may be represented in PH form as follows:

$$\dot{\mathbf{x}} = \begin{bmatrix} -r & 0 & 0 \\ 0 & 0 & 1 \\ 0 & -1 & 0 \end{bmatrix} \frac{\partial H}{\partial \mathbf{x}} + \begin{bmatrix} 1 \\ 0 \\ 0 \end{bmatrix} u,$$

in which, $\mathbf{x} = [\lambda, \theta, m\dot{\theta}]^T$ and r represents coil resistance while the Hamiltonian function is given by [60]

$$H(\mathbf{x}) = \frac{1}{2k}(1 - x_2)x_1^2 + \frac{1}{2m}x_3^2 + mgx_2,$$

where k is a constant. Let us consider stabilization of the equilibrium point $\mathbf{x}^* = [\sqrt{2kmg}, x_2^*, 0]^T$. It is shown in [60] that without modification of interconnection matrix, it is not possible to stabilize \mathbf{x}^* . Hence, the following interconnection matrix is considered

$$\begin{bmatrix} 0 & 0 & -\alpha \\ 0 & 0 & 1 \\ \alpha & -1 & 0 \end{bmatrix}.$$

Furthermore, with $\mathbf{R}_d = \mathbf{R}$, the matching equation (A.3) yields to

$$K_3(\mathbf{x}) = 0, \quad \alpha K_1(\mathbf{x}) - K_2(\mathbf{x}) = -\frac{\alpha}{k}(1 - x_2)x_1, \quad (\text{A.4})$$

where it is assumed that $H_d = H + H_a$ and

$$[K_1, K_2, K_3]^T := \frac{\partial H_a}{\partial \mathbf{x}} = \left[\frac{\partial H_a}{\partial x_1}, \frac{\partial H_a}{\partial x_2}, \frac{\partial H_a}{\partial x_3} \right]^T. \quad (\text{A.5})$$

The PDE represented by (A.4) shows that H_a is independent of x_3 . If $\alpha \neq 0$, using the proposed method, the PDE (A.4) is equivalent to the following Pfaffian equations

$$\frac{dx_1}{1} = \frac{dx_2}{-\beta} = \frac{dH_a}{-\frac{1}{k}(1 - x_2)x_1} \quad (\text{A.6})$$

with $\beta = 1/\alpha$. Assume that $\beta = -c_1x_1 - c_2x_2 - c_3$ with c_i s as arbitrary constants, and substitute it in (A.6), results in

$$\frac{dx_1}{1} = \frac{dx_2}{c_1x_1 + c_2x_2 + c_3} = \frac{dH_a}{-\frac{1}{k}(1-x_2)x_1} \quad (\text{A.7})$$

First, non-homogeneous solution is calculated by using Corollary 1. The strategy is to derive a Pfaffian equation satisfying (4.4). With some manipulation one may show that equation (A.7) is equal to the following equations

$$\frac{dH_a - \frac{x_1}{c_2k}dx_2}{-\frac{x_1}{k} - \frac{c_1x_1^2}{c_2k} - \frac{c_3x_1}{c_2k}} = \frac{dH_a - \frac{x_1}{c_2k}dx_2 - \frac{x_2}{c_2k}dx_1}{-\frac{x_1}{k} - \frac{c_1x_1^2}{c_2k} - \frac{c_3x_1}{c_2k} - \frac{x_2}{c_2k}}$$

In this representation, the term $\frac{x_1x_2}{k}$ was omitted in the left-hand side, and then the term $-\frac{x_2}{c_2k}dx_1$ was added with respect to condition (4.4). In order to eliminate $\frac{x_2}{c_2k}$ from right-hand side of this equation, let us add it with $\frac{1}{c_2^2k}dx_2$. One may verify that the denominator of the new expression depends only to x_1 . Hence, using the first term of (A.7), it is possible to omit the remaining terms. By this means, the following Pfaffian differential equation is derived:

$$dH_a - \frac{x_1}{c_2k}dx_2 - \frac{x_2}{c_2k}dx_1 + \frac{1}{c_2^2k}dx_2 + \frac{x_1}{k}dx_1 + \frac{c_1x_1^2}{c_2k}dx_1 + \frac{c_3x_1}{c_2k}dx_1 - \frac{c_1x_1}{c_2^2k}dx_1 - \frac{c_3}{c_2^2k}dx_1 = 0.$$

This equation satisfies condition (4.4), and is separable in the following form:

$$(dH_a) - \left(\frac{x_1}{c_2k}dx_2 + \frac{x_2}{c_2k}dx_1 \right) + \left(\frac{1}{c_2^2k}dx_2 \right) + \left(\frac{x_1}{k}dx_1 + \frac{c_1x_1^2}{c_2k}dx_1 + \frac{c_3x_1}{c_2k}dx_1 - \frac{c_1x_1}{c_2^2k}dx_1 - \frac{c_3}{c_2^2k}dx_1 \right) = 0.$$

Therefore, one may find the following solution

$$H_a = \frac{x_1x_2}{c_2k} - \frac{x_2}{c_2^2k} - \frac{x_1^2}{2k} - \frac{c_1x_1^3}{3c_2k} - \frac{c_3x_1^2}{2c_2k} + \frac{c_1x_1^2}{2c_2^2k} - \frac{c_3x_1}{c_2^2k}.$$

Furthermore, by using Corollary 1, the homogeneous solution is derived from the following equation

$$(c_1x_1 + c_2x_2 + c_3)dx_1 - dx_2 = 0. \quad (\text{A.8})$$

This equation need an integration factor μ which satisfies the following relation

$$\frac{\partial\mu}{\partial x_1} + (c_1x_1 + c_2x_2 + c_3)\frac{\partial\mu}{\partial x_2} = -c_2\mu.$$

Hence, using the proposed method, it is equivalent to

$$\frac{dx_1}{1} = \frac{dx_2}{c_1x_1 + c_2x_2 + c_3} = \frac{d\mu}{-c_2\mu}.$$

By considering the first and last terms, the solution may be given as $\mu = e^{-c_2x_1}$. Hence, homogeneous solution of (A.7) is derived from multiplying (A.8) to μ and then integration

as follows

$$H_a = \phi\left(\left(\frac{c_1}{c_2}x_1 + x_2 + \frac{c_3}{c_2} + \frac{c_1}{c_2^2}\right)e^{-c_2x_1}\right),$$

in which, the function ϕ and the constants c_i s shall be determined such that \mathbf{x}^* becomes stable.

Remark 10. References [60,76], state that θ shall remain in the interval of $(-1, \infty)$ while this limitation is released in our proposed solution. Note that using the method proposed in [150] based on control barrier functions, one may define c_i s such that this constraint is satisfied. For example, set $c_1 = 0$ and $c_3 = -c_2$ results in $\alpha = -1/(c_2x_2 - c_2)$ that ensures $\theta \in (-1, \infty)$. Furthermore, for the solution given in [60] it is assumed that α is a constant. This limiting assumption is also released in the proposed solution given in this paper. Therefore, based on the proposed method, a solution with suitable property was derived.

A.2 Micro Electro–Mechanical Optical Switch

Another benchmark example is the optical switching system with the following PH model [80, 151]:

$$\dot{\mathbf{x}} = \begin{bmatrix} 0 & 1 & 0 \\ -1 & -b & 0 \\ 0 & 0 & -\frac{1}{r} \end{bmatrix} \nabla H(\mathbf{x}) + \begin{bmatrix} 0 \\ 0 \\ \frac{1}{r} \end{bmatrix} u, \quad (\text{A.9})$$

whose energy function is given by [80]:

$$H(\mathbf{x}) = \frac{1}{2m}x_2^2 + \frac{1}{2}a_1x_1^2 + \frac{1}{4}a_2x_1^4 + \frac{x_3^2}{2c_1(x_1 + c_0)}, \quad (\text{A.10})$$

where $b, r > 0$ are resistive constants, $a_1, a_2 > 0$ are spring terms, $c_0, c_1 > 0$ are capacitive elements and m denotes the mass of actuator. The physical constraint to consider is $x_1 > 0$, while the equilibrium points of the system are [80]

$$x_2^* = 0, \quad x_3^* = (c_0 + x_1^*)\sqrt{2c_1x_1^*(a_1 + a_2x_1^{*2})}, \quad (\text{A.11})$$

The aim of controller design in this example is to stabilize the system in $x_1^* > 0$. Hence, let us consider the following desired interconnection matrix

$$\mathbf{J}_d = \begin{bmatrix} 0 & 1 & 0 \\ -1 & 0 & \alpha(\mathbf{x}) \\ 0 & -\alpha(\mathbf{x}) & 0 \end{bmatrix},$$

where α is a design parameter and $\mathbf{R}_d = \mathbf{R}$. For simplicity and due to physical constraint, consider $\alpha = \frac{\beta(x_1 + c_0)}{x_1}$. By this means, the following Pfaffian differential equations should be solved

$$\frac{dx_1}{-x_1} = \frac{dx_3}{\beta(x_1 + c_0)} = \frac{dH_a}{-\frac{\beta x_3}{c_1}}. \quad (\text{A.12})$$

In the sequel, it is shown that

$$H_a = \phi\left(\beta x_1 + \beta c_0 \ln(x_1) + x_3, x_2\right) - \frac{1}{2c_0c_1}x_3^2 - \frac{\beta}{c_0c_1}x_1x_3 - \frac{\beta}{2c_0c_1}x_1^2 - \frac{\beta}{c_1}x_1, \quad (\text{A.13})$$

is the solution of Pfaffian differential equations (A.12). In order to derive non-homogeneous solution, the following equation is derived

$$\frac{dx_3}{\beta(x_1 + c_0)} = \frac{dH_a}{-\frac{\beta x_3}{c_1}} = \frac{\frac{x_3}{c_0c_1}dx_3 + dH_a}{\frac{\beta x_1 x_3}{c_0c_1}} = \frac{\frac{x_3}{c_0c_1}dx_3 + dH_a + \frac{\beta x_3}{c_0c_1}dx_1}{0}. \quad (\text{A.14})$$

Unfortunately, the last equation does not satisfy condition (4.4). To rectify this, let us add the term $\frac{\beta x_1}{c_0c_1}dx_3$ to it. Finally, one may reach to the following Pfaffian differential equation

$$\frac{x_3 + \beta x_1}{c_0c_1}dx_3 + dH_a + \frac{\beta x_3}{c_0c_1}dx_1 + \frac{\beta x_1}{c_0c_1}dx_1 + \frac{\beta}{c_1}dx_1 = 0,$$

which has the following solution

$$H_a = -\frac{1}{2c_0c_1}x_3^2 - \frac{\beta}{c_0c_1}x_1x_3 - \frac{\beta}{2c_0c_1}x_1^2 - \frac{\beta}{c_1}x_1. \quad (\text{A.15})$$

The homogeneous solution of (A.12) is derived easily as follows

$$H_a = \phi(\beta x_1 + \beta c_0 \ln(x_1) + x_3, x_2).$$

Thus, one can suitably define the constants and function ϕ such that \mathbf{x}^* becomes a stable equilibrium point while based on definition of α , the constraint $x_1 > 0$ is satisfied [150].

A.3 Third Order Food-Chain System

Consider the following model for third order food-chain system based on [76] in PH form (A.1) with the following values

$$\mathbf{J} = \begin{bmatrix} 0 & x_1x_2 & 0 \\ -x_1x_2 & 0 & x_2x_3 \\ 0 & -x_2x_3 & 0 \end{bmatrix}, \quad \mathbf{R} = \begin{bmatrix} x_1 & 0 & 0 \\ 0 & x_2 & 0 \\ 0 & 0 & x_3 \end{bmatrix}$$

$$\mathbf{g} = [0, 0, 1]^T, \quad H = x_1 + x_2 + x_3, \quad (\text{A.16})$$

where x_i denotes the population of i -th species. In [152] it is shown that the PDE (A.3) is not solvable with $\mathbf{J}_d = \mathbf{J}$ and $\mathbf{R}_d > 0$ since the span of the first 2 rows of $\mathbf{J}_d - \mathbf{R}_d$ is not involutive (i.e., its Lie bracket is not in the span of the first 2 rows of $\mathbf{J}_d - \mathbf{R}_d$, see [136] for more information). The matching equation with the following matrices

$$\mathbf{J}_d = \begin{bmatrix} 0 & J_1 & J_2 \\ -J_1 & 0 & J_3 \\ -J_2 & -J_3 & 0 \end{bmatrix}, \quad \mathbf{R}_d = \begin{bmatrix} R_1 & 0 & 0 \\ 0 & R_2 & 0 \\ 0 & 0 & R_3 \end{bmatrix}, \quad H_d = H + H_a,$$

is in the following form

$$\begin{aligned} -x_1 + x_1x_2 &= -R_1(1 + K_1) + J_1(1 + K_2) + J_2(1 + K_3), \\ -x_2 - x_1x_2 + x_2 + x_3 &= -J_1(1 + K_1) - R_2(1 + K_2) + J_3(1 + K_3), \end{aligned}$$

in which K_i s are defined in (A.5). If we set $\mathbf{R}_d = \mathbf{I}$ as the simplest choice, it is inferred that with $J_1 = 0, J_2 = f(x_1), J_3 = g(x_2)$ where f, g are arbitrary functions, the PDEs are involutive. This means that homogeneous part of PDEs has a solution. The overall of PDEs has also a solution if non-homogeneous solution of a PDE satisfies the other PDE in above equations. The corresponding Pfaffian differential equations are

$$\begin{aligned} \frac{dx_1}{-1} &= \frac{dx_2}{0} = \frac{dx_3}{f(x_1)} = \frac{dH_a}{-x_1 + x_1x_2 + 1 - f(x_1)}, \\ \frac{dx_1}{0} &= \frac{dx_2}{-1} = \frac{dx_3}{g(x_3)} = \frac{dH_a}{-x_2 - x_1x_2 + x_2x_3 + 1}. \end{aligned}$$

The solution of these equations using the explained methods is

$$\begin{aligned} H_a &= \phi_1(x_2, \int f(x_1)dx_1 + x_3) + \frac{1}{2}x_1^2 - \frac{1}{2}x_1^2x_2 - x_1 + \int f(x_1)dx_1, \\ H_a &= \phi_2(x_1, x_2 + \int \frac{1}{g(x_3)}dx_3) + \frac{1}{2}x_2^2 + \frac{1}{2}x_1x_2^2 - x_2 \\ &+ \int (\alpha(x_2, x_3) + \beta(x_2, x_3)g(x_3)), \quad \text{s. to } \alpha + \beta g = -x_2x_3, \end{aligned}$$

where the functions α and β should be defined such that the last term is integrable. Now we should define $f(x_1)$ and $g(x_2)$ such that the non-homogeneous solution of a PDE lies in the homogeneous solution of other PDE. Hence, by defining $f(x_1) = -1$ and $g(x_3) = 0$, the solution of PDEs is

$$H_a = \phi(x_1 - x_3) + \frac{1}{2}x_2^2 + \frac{1}{2}x_2^2(x_1 - x_3) - x_2. \tag{A.17}$$

Hence, although the proposed method is based on a PDE, it might be utilized to solve a set of PDEs.

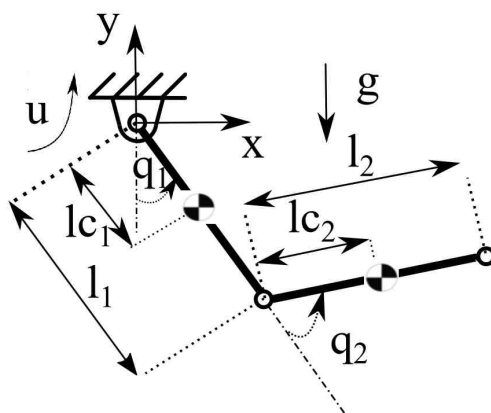


Figure A.2: Schematic of Pendubot. Merely the first joint is actuated.

A.4 Pendubot

Here, the IDA-PBC method is applied to pendubot system in which it is not matched to the proposed papers based on total energy shaping without solving matching equations [79–82,153]. The robot consists of two revolute joints in which merely the first one is actuated. The schematic of this system is shown in Fig. A.2. The dynamic model of the robot may be expressed in the form of (2.9) with the following matrices [84]

$$\mathbf{M} = \begin{bmatrix} c_1 + c_2 + 2c_3 \cos(q_2) & c_2 + c_3 \cos(q_2) \\ c_2 + c_3 \cos(q_2) & c_2 \end{bmatrix}$$

$$\mathbf{G} = [1, 0]^T, \quad V = -c_4 g \cos(q_1) - c_5 g \cos(q_1 + q_2),$$

where the constants c_i s are given as follows

$$\begin{aligned} c_1 &= m_1 l_{c1}^2 + m_2 l_1^2 + I_1, & c_2 &= m_2 l_{c2}^2 + I_2, \\ c_3 &= m_2 l_1 l_{c2}, & c_4 &= m_1 l_{c1} + m_2 l_1, & c_5 &= m_2 l_{c2}. \end{aligned} \quad (\text{A.18})$$

In [84], it is shown that the corresponding kinetic energy PDE given in (2.16) is simplified to the following equation

$$2c_3 \sin(q_2)(\lambda_3^2 + \lambda_3 \lambda_4) + \lambda_4 \frac{d}{dq_2} (\lambda_3 (c_2 + c_3 \cos(q_2)) + \lambda_4 c_2) = 0, \quad (\text{A.19})$$

in which

$$\mathbf{M}_d \mathbf{M}^{-1} := \begin{bmatrix} \lambda_1 & \lambda_2 \\ \lambda_3 & \lambda_4 \end{bmatrix}.$$

Note that two other PDEs generated from kinetic energy PDE (2.16) may be solved by suitable definition of the matrix \mathbf{J}_2 in (2.14). The potential energy PDE (2.17) for this system is

$$\lambda_3 \nabla_{q_1} V_d + \lambda_4 \nabla_{q_2} V_d = c_5 g \sin(q_1 + q_2). \quad (\text{A.20})$$

Since, PDE (A.19) has two unknown variables, for simplicity, assume that $\lambda_4 = k\lambda_3$, and reduce it to the following Pfaffian differential equations:

$$\frac{dq_1}{0} = \frac{dq_2}{k\lambda_3(c_2 + c_3 \cos(q_2) + kc_2)} = \frac{d\lambda_3}{-c_3 \lambda_3^2 \sin(q_2)(2+k)}$$

Let us define $k = -1$ to simplify these equations. The non-homogeneous solution is derived from the following equation

$$\frac{d\lambda_3}{\lambda_3} = \tan(q_2) dq_2,$$

which has the solution $\lambda_3 = \frac{\kappa}{\cos(q_2)}$ with $\kappa > 0$ an arbitrary value since $M_{d_{22}} = \kappa c_3$ should be positive. Note that the homogeneous solution is trivially found to be $\phi(q_1)$. The corresponding Pfaffian equations to PDE (A.20) are given as follows

$$\frac{dq_1}{\kappa} = \frac{dq_2}{-\kappa} = \frac{dV_d}{c_5 g \cos(q_2) \sin(q_1 + q_2)}$$

The homogeneous solution is $V_d = \phi(q_1 + q_2)$. In order to compute the non-homogeneous solution, we should derive an equation in the form of

$$f_1(q_1, q_2)dq_1 + f_2(q_1, q_2)dq_2 + dV_d = 0, \quad (\text{A.21})$$

in which,

$$\kappa f_1 - \kappa f_2 + c_5 g \cos(q_2) \sin(q_1 + q_2) = 0,$$

and the following constraint resulted from (4.4) shall be satisfied

$$\frac{\partial f_2}{\partial q_1} = \frac{\partial f_1}{\partial q_2}.$$

Combination of the two above equations yields to the following equation

$$\kappa \frac{\partial f_2}{\partial q_1} - \kappa \frac{\partial f_2}{\partial q_2} = -c_5 g \cos(q_1 + 2q_2).$$

The solution of this equation is

$$f_2 = \frac{c_5 g}{\kappa} \sin(q_1 + 2q_2).$$

Therefore, the Pfaffian equation (A.21) yields to

$$\left(c_5 g \sin(q_1 + 2q_2) - c_5 g \cos(q_2) \sin(q_1 + q_2) \right) dq_1 + c_5 g \sin(q_1 + 2q_2) dq_2 - \kappa dV_d = 0.$$

In order to derive its solution, rewrite it in the following form

$$c_5 g \sin(q_2) \cos(q_1 + q_2) dq_1 + \left(c_5 g \sin(q_2) \cos(q_1 + q_2) + c_5 g \cos(q_2) \sin(q_1 + q_2) \right) dq_2 - \kappa dV_d = 0,$$

whose solution may be found easily as

$$V_d = \frac{c_5 g}{\kappa} \sin(q_1 + q_2) \sin(q_2). \quad (\text{A.22})$$

Remark 11. In [84], the simplest solution of (A.19) is reported, in which λ_3 and λ_4 are set to be constant values. Here, a nontrivial solution with enlarged domain of attraction is derived. In [84], $M_{d_{22}} \propto -c_2 + c_3 \cos(q_2)$ that ensures M_d is positive definite if $q_2 \in (-\epsilon, \epsilon)$ with $\epsilon = \arccos(\frac{c_2}{c_3})$. This limitation is also released in the proposed solution, where $M_{d_{22}} = \kappa c_3$ and $M_{d_{21}} = \kappa c_1 / \cos(q_2) + \kappa c_3$ and the condition $\det(\mathbf{M}_d) > 0$ confines q_2 inside a subset of the interval $(-\frac{\pi}{2}, \frac{\pi}{2})$ which can be enhanced by enlarging arbitrary value $M_{d_{11}}$.

Appendix B

Solving the Matching Equation of Kinetic Energy Shaping by the Proposed Procedure in Section 4.3

In the following, three case studies are proposed to apply the proposed method in Section 4.3 on them. The first example is Pendubot, in which its matching equation is replaced by an ODE. The second example is VTOL aircraft where the corresponding PDE is solved easily by a constant M_d . The last example is 2D SpiderCrane in which, its matching equation is solved by Pfaffian differential equations.

B.1 Pendubot

The robot was defined in Section A.4. After some manipulation, the following expressions are derived

$$\begin{aligned}
 \det \mathbf{M} &= c_1 c_2 - c_3^2 \cos^2(q_2), & \mathfrak{M} &= \begin{bmatrix} c_2 & -c_2 - c_3 \cos(q_2) \\ -c_2 - c_3 \cos(q_2) & c_1 + c_2 + 2c_3 \cos(q_2) \end{bmatrix}, \\
 \mathcal{M} &= \begin{bmatrix} -2c_2 c_3^2 \sin(q_2) \cos(q_2) & c_1 c_2 c_3 \sin(q_2) + c_3^3 \sin(q_2) \cos^2(q_2) \\ c_1 c_2 c_3 \sin(q_2) + c_3^3 \sin(q_2) \cos^2(q_2) & -2c_1 c_2 c_3 \sin(q_2) - 2c_3^3 \sin(q_2) \cos^2(q_2) \\ +2c_2 c_3^2 \sin(q_2) \cos(q_2) & -2c_3^2 (c_1 + c_2) \sin(q_2) \cos(q_2) \end{bmatrix}, \\
 \mathbf{M}_d^{-1} &= \begin{bmatrix} a_1 & b_1 \\ b_1 & a(q_2) \end{bmatrix}, & \mathbf{J}_2 &= \begin{bmatrix} 0 & \mathbf{p}_1^T \boldsymbol{\alpha} \\ \mathbf{p}_2^T \boldsymbol{\alpha} & 0 \end{bmatrix}, \\
 \boldsymbol{\gamma}^T &= \begin{bmatrix} -c_2 b_1 - c_2 a_1 - c_3 a_1 \cos(q_2) \\ a_1 c_1 + a_1 c_2 + b_1 c_2 + b_1 c_3 \cos(q_2) + 2a_1 c_3 \cos(q_2) \end{bmatrix}
 \end{aligned} \tag{B.1}$$

Note that in the following ${}_2 \boldsymbol{\alpha}$ will be determined and ${}_1 \boldsymbol{\alpha} = -{}_2 \boldsymbol{\alpha}$ will be set. Equation (4.36) for this case is derived as follows

$$\frac{\gamma_2}{\det \mathbf{M}_d^{-1}} \begin{bmatrix} 0 & 0 \\ 0 & \frac{\partial a}{\partial q_2} \end{bmatrix} = \frac{1}{\det \mathbf{M}} \mathcal{M} + \begin{bmatrix} {}_2 \alpha_1 a_1 & {}_2 \alpha_2 a_1 + {}_2 \alpha_1 b_1 \\ {}_2 \alpha_2 a_1 + {}_2 \alpha_1 b_1 & {}_2 \alpha_2 b_1 \end{bmatrix} \tag{B.2}$$

By solving two algebraic equations, α_2 is obtained as follows

$$\begin{aligned} {}_2\alpha_1 &= -\frac{\mathcal{M}_{11}}{2a_1 \det \mathbf{M}} = \frac{c_2 c_3^2 \sin(q_2) \cos(q_2)}{a_1 (c_1 c_2 - c_3^2 \cos^2(q_2))}, \\ {}_2\alpha_2 &= -\frac{\mathcal{M}_{21}}{a_1 \det \mathbf{M}} - \frac{{}_2\alpha_1 b_1}{a_1} = -\frac{c_1 c_2 c_3 \sin(q_2) + c_3^3 \sin(q_2) \cos^2(q_2) + 2c_2 c_3^2 \sin(q_2) \cos(q_2)}{a_1 (c_1 c_2 - c_3^2 \cos^2(q_2))} \\ &\quad - \frac{b_1 c_2 c_3^2 \sin(q_2) \cos(q_2)}{a_1^2 (c_1 c_2 - c_3^2 \cos^2(q_2))} \end{aligned} \quad (\text{B.3})$$

Finally, the following ODE should be solved

$$\frac{1}{a_1 a(q_2) - b_1^2} \frac{da}{dq_2} = \frac{1}{\gamma_2} \det \mathbf{M} \left(\mathcal{M}_{22} - \frac{-2b_1 \mathcal{M}_{21}}{a_1} + \frac{b_1^2 \mathcal{M}_{11}}{a_1^2} \right) \quad (\text{B.4})$$

This ODE is in the form of (4.39) and its solution is derived from (4.40) with

$$\phi_1 = b_1, \quad \phi_2 = -b_1^2, \quad F(q_2) = \int \frac{1}{\gamma_2 \det \mathbf{M}} \left(\mathcal{M}_{22} - \frac{-2b_1 \mathcal{M}_{21}}{a_1} + \frac{b_1^2 \mathcal{M}_{11}}{a_1^2} \right) dq_2.$$

For example, assume that $c_1 = 4$, $c_2 = 1$ and $c_3 = 1.5$. By some manipulation, $a(q_2)$ is obtained as follows

$$a(q_2) = \cos(q_2)^{-7/3} + (4 - 3 \cos(q_2))^{49/6} - (4 + 3 \cos(q_2))^{-7/2}, \quad (\text{B.5})$$

in which, $a_1 = 1$, $b_1 = -5$, $\lambda = 1$ are chosen to simplify the ODE (B.4) and also the necessary condition (4.26) is satisfied.

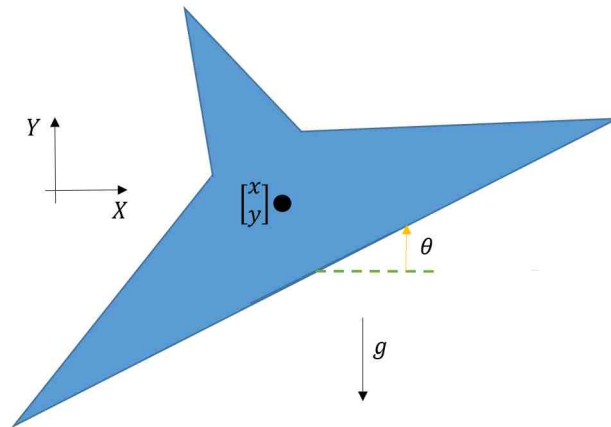


Figure B.1: VTOL aircraft.

B.2 VTOL Aircraft

Dynamic model of VTOL in PH form (2.9) is given as follows

$$\mathbf{G}(\mathbf{q}) = \begin{bmatrix} -\sin(\theta) & \epsilon \cos(\theta) \\ \cos(\theta) & \epsilon \sin(\theta) \\ 0 & 1 \end{bmatrix}, \quad \mathbf{M} = \mathbf{I}, \quad V = gy, \quad \mathbf{q} = \begin{bmatrix} x \\ y \\ \theta \end{bmatrix} \quad (\text{B.6})$$

in which, x and y denote the position of center of mass, θ is the roll angle and ϵ models the effect of the slopped wings. The desired equilibrium point of the system is $[x_*, y_*, 0]^T$. In [74] a controller with state-dependent \mathbf{M}_d by defining new inputs is derived. Notice that although the matrix $\mathbf{G}(\mathbf{q})$ does not have the form $\mathbf{P}[\mathbf{I}_m, \mathbf{0}_{m \times n-m}]^T$, based on case2, it is possible to solve the PDE of kinetic energy with a constant \mathbf{M}_d , represented by:

$$\mathbf{M}_d = \begin{bmatrix} a & d & e \\ d & b & f \\ e & f & c \end{bmatrix}$$

Necessary condition (4.26) in this case leads to following inequality

$$\left(g \cos(\theta)(\epsilon \cos(\theta) + f \sin(\theta) - c\epsilon) \right) \Big|_{\theta=0} > 0.$$

A suitable choice for \mathbf{M}_d is

$$a = \kappa\epsilon^2, \quad b = 1, \quad c = \kappa', \quad d = 0, \quad e = \epsilon, \quad f = 0,$$

in which, the constants $\kappa, \kappa' > 0$ should be selected such that $\kappa\kappa' > 1$. Note that $\mathbf{M}_d = \mathbf{I}$ does not satisfy the necessary condition (4.26) which is in line with our prior knowledge that it is not possible to stabilize the system with merely potential energy shaping. The solution of potential energy PDE (2.17) with $\kappa = 20$ and $\kappa' = 0.1$ is derived easily as follows

$$\begin{aligned} V_d = & \left(\epsilon(y - y^*) + \ln(\epsilon \cos(\theta) - 0.1\epsilon) \right)^2 + \left(\frac{1}{20\epsilon}(x - x^*) - (\theta - \theta^*) \right. \\ & \left. - 0.1 \operatorname{arctanh}\left(1.1055 \tan\left(\frac{\theta}{2}\right)\right) \right)^2 - 2\epsilon \ln(0.9\epsilon)(y - y^*) - \frac{g - 2\epsilon \ln(0.9\epsilon)}{g\epsilon} \ln(\epsilon \cos(\theta) - 0.1\epsilon). \end{aligned}$$

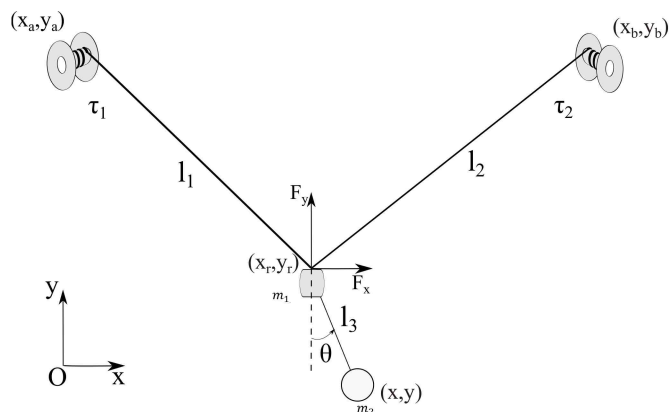


Figure B.2: Schematic of 2D SpiderCrane system.

B.3 2D SpiderCrane

This system consists of a load suspended from a ring which is controlled by two cables. The schematic of this system is depicted in Fig. B.2. The position of the ring and the mass are denoted by (x_r, y_r) and (x, y) , respectively, and their mass is denoted by m_1 and m_2 , respectively. The length of the controlled cables is denoted by l_1 and l_2 , while l_3 denotes the fixed length of the cable between ring and the mass. Dynamic equation of the system is represented in the form (2.9) with following parameters

$$\mathbf{q} = \begin{bmatrix} x_r \\ y_r \\ \theta \end{bmatrix}, \quad \mathbf{G} = \begin{bmatrix} 1 & 0 \\ 0 & 1 \\ 0 & 0 \end{bmatrix}^T, \quad V = (m_1 + m_2)gy_r - m_2gl_3 \cos(\theta),$$

$$\mathbf{M}(\mathbf{q}) = \begin{bmatrix} m_1 + m_2 & 0 & m_2l_3 \cos(\theta) \\ 0 & m_1 + m_2 & m_2l_3 \sin(\theta) \\ m_2l_3 \cos(\theta) & m_2l_3 \sin(\theta) & m_2l_3^2 \end{bmatrix}$$

Two IDA-PBC controllers have been designed for SpiderCrane. In [127] merely the potential energy is shaped while in [131] total energy shaping based on the method proposed in [74] is performed such that at first a partial feedback linearization is applied to the system, and then a desired inertia matrix, which is merely a function of θ , is chosen. Notice that it is possible to derive \mathbf{M}_d as a function of θ based on the case1 presented in Section 4.3. However, here the aim is to derive a more general solution such that \mathbf{M}_d may be set as a function of x_r and y_r . Consider \mathbf{M}_d^{-1} in the form of (4.30). One can easily check that necessary condition (4.26) is satisfied if $b_1m_3l_3 + a_2(m_1 + m_2) > 0$. In order to solve matching equation (2.16), the following parameters are derived

$$\det \mathbf{M} = (m_1 + m_2)^2 m_2 l_3^2 - (m_1 + m_2) m_2^2 l_3^2,$$

$$\mathfrak{M} = \begin{bmatrix} (m_1 + m_2)m_2l_3^2 - m_2^2l_3^2 \sin^2(\theta) & m_2^2l_3^2 \sin(\theta) \cos(\theta) & -(m_1 + m_2)m_2l_3 \cos(\theta) \\ m_2^2l_3^2 \sin(\theta) \cos(\theta) & (m_1 + m_2)m_2l_3^2 - m_2^2l_3^2 \cos^2(\theta) & -(m_1 + m_2)m_2l_3 \sin(\theta) \\ -(m_1 + m_2)m_2l_3 \cos(\theta) & -(m_1 + m_2)m_2l_3 \sin(\theta) & (m_1 + m_2)^2 \end{bmatrix},$$

$$\mathcal{M} = \det \mathbf{M} \begin{bmatrix} -2m_2^2l_3^2 \sin(\theta) \cos(\theta) & m_2^2l_3^2 \cos(2\theta) & (m_1 + m_2)m_2l_3 \sin(\theta) \\ m_2^2l_3^2 \cos(2\theta) & m_2^2l_3^2 \sin(2\theta) & -(m_1 + m_2)m_2l_3 \cos(\theta) \\ (m_1 + m_2)m_2l_3 \sin(\theta) & -(m_1 + m_2)m_2l_3 \cos(\theta) & 0 \end{bmatrix},$$

$$\gamma^T = \begin{bmatrix} -a_2b_1(m_1 + m_2)m_2l_3^2 + a_2b_1m_2^2l_3^2 \sin^2(\theta) - a_1b_2m_2^2l_3^2 \sin(\theta) \cos(\theta) - a_1a_2(m_1 + m_2)m_2l_3 \cos(\theta) \\ -a_2b_1m_2^2l_3^2 \sin(\theta) \cos(\theta) - a_1b_2(m_1 + m_2)m_2l_3^2 + a_1b_2m_2^2l_3^2 \cos^2(\theta) - a_1a_2(m_1 + m_2)m_2l_3 \sin(\theta) \\ a_2b_1(m_1 + m_2)m_2l_3 \cos(\theta) + a_1b_2(m_1 + m_2)m_2l_3 \sin(\theta) + a_1a_2(m_1 + m_2)^2 \end{bmatrix}$$

Based on necessary condition and simplifying the corresponding matching equation, we choose $b_1 = b_2 = 0$. By this means, the matrix Ψ in equality (4.37) is in the following form

$$\Psi = \begin{bmatrix} 2a_1 & 0 & 0 & 0 & 0 & 0 \\ 0 & a_1 & 0 & a_2 & 0 & 0 \\ 0 & 0 & a_1 & 0 & 0 & 0 \\ 0 & 0 & 0 & 0 & 2a_2 & 0 \\ 0 & 0 & 0 & 0 & 0 & a_2 \end{bmatrix}$$

This matrix is full row rank, hence $[\alpha_5^T, \alpha_6^T]^T$ is determined by right pseudo-inverse of Ψ . The Pfaffian differential equations of PDE (4.38) for this system is given as follows

$$\frac{dx}{-m_2l_3 \cos(\theta)} = \frac{dy}{-m_2l_3 \sin(\theta)} = \frac{d\theta}{m_1 + m_2} = \frac{da}{0}$$

The solutions to these equations are

$$x + \frac{m_2 l_3}{m_1 + m_2} \sin(\theta) = c_1, \quad y - \frac{m_2 l_3}{m_1 + m_2} \cos(\theta) = c_2,$$

with c_1 and c_2 as free parameters. Hence, $a(q)$ is derived as follows

$$a(\mathbf{q}) = \phi\left(x + \frac{m_2 l_3}{m_1 + m_2} \sin(\theta), y - \frac{m_2 l_3}{m_1 + m_2} \cos(\theta)\right),$$

in which, ϕ is an arbitrary function.

Bibliography

- [1] S. Khalilpour, R. Khorrambakht, M. Harandi, H. Taghirad, and P. Cardou, “Cascade terminal sliding mode control of a deployable cable driven robot,” in *2019 6th International Conference on Control, Instrumentation and Automation (ICCIA)*, pp. 1–6, IEEE, 2019.
- [2] H. D. Taghirad, *Parallel robots: mechanics and control*. CRC press, 2013.
- [3] S. Khalilpour, R. Khorrambakht, H. Taghirad, and P. Cardou, “Robust cascade control of a deployable cable-driven robot,” *Mechanical Systems and Signal Processing*, vol. 127, pp. 513–530, 2019.
- [4] B. Williams, “Introduction to robotics,” *Mechanical Engineering, Ohio University*, January 2019.
- [5] X. Diao, O. Ma, and Q. Lu, “Singularity analysis of planar cable-driven parallel robots,” in *Robotics, Automation and Mechatronics, IEEE Conference on*, pp. 272–277, IEEE, 2008.
- [6] *Robocrane*. <https://www.nist.gov/programs-projects/robocrane>.
- [7] S.-D. Lee and S. Jung, “Analysis of relationship between body and gimbal motion through experiment of a single-wheel robot based on an inverse gyroscopic effect,” *Journal of Institute of Control, Robotics and Systems*, vol. 21, no. 11, pp. 1064–1069, 2015.
- [8] *Spidercam*. <https://www.spidercam.tv/pictures>.
- [9] R. Olfati-Saber, *Nonlinear control of underactuated mechanical systems with application to robotics and aerospace vehicles*. PhD thesis, Massachusetts Institute of Technology, 2001.
- [10] I. Tortopidis and E. Papadopoulos, “On point-to-point motion planning for underactuated space manipulator systems,” *Robotics and Autonomous Systems*, vol. 55, no. 2, pp. 122–131, 2007.
- [11] M. W. Spong, “The swing up control problem for the acrobat,” *IEEE control systems*, vol. 15, no. 1, pp. 49–55, 1995.
- [12] W. Zhong and H. Rock, “Energy and passivity based control of the double inverted pendulum on a cart,” in *Control Applications, (CCA’01). Proceedings of the IEEE International Conference on*, pp. 896–901, IEEE, 2001.
- [13] R. Ortega, A. Van Der Schaft, B. ke, and G. Escobar, “Interconnection and damping assignment passivity-based control of port-controlled hamiltonian systems,” *Automatica*, vol. 38, no. 4, pp. 585–596, 2002.
- [14] R. Ortega, M. W. Spong, F. Gómez-Estern, and G. Blankenstein, “Stabilization of a class of underactuated mechanical systems via interconnection and damping assignment,” *IEEE transactions on automatic control*, vol. 47, no. 8, pp. 1218–1233, 2002.
- [15] N. Zoso and C. Gosselin, “Point-to-point motion planning of a parallel 3-dof underactuated cable-suspended robot,” in *Robotics and Automation (ICRA), IEEE International Conference on*, pp. 2325–2330, IEEE, 2012.
- [16] E. Idá, A. Berti, T. Bruckmann, and M. Carricato, “Rest-to-rest trajectory planning for planar underactuated cable-driven parallel robots,” in *Cable-Driven Parallel Robots*, pp. 207–218, Springer, 2018.

- [17] E. Idà, T. Bruckmann, and M. Carricato, “Rest-to-rest trajectory planning for underactuated cable-driven parallel robots,” *IEEE Transactions on Robotics*, vol. 35, no. 6, pp. 1338–1351, 2019.
- [18] L. Barbazza, D. Zanutto, G. Rosati, and S. K. Agrawal, “Design and optimal control of an underactuated cable-driven micro–macro robot,” *IEEE Robotics and Automation Letters*, vol. 2, no. 2, pp. 896–903, 2017.
- [19] I. N. Sneddon, *Elements of partial differential equations*. Courier Corporation, 2006.
- [20] H.-D. Do, J.-H. Seo, J.-O. Park, and K.-S. Park, “Wrench-feasible workspace analysis considering aerodynamics of aerial robotic camera under high speed,” *Microsystem Technologies*, vol. 23, no. 11, pp. 5257–5269, 2017.
- [21] A. T. Riechel and I. Ebert-Uphoff, “Force-feasible workspace analysis for underconstrained, point-mass cable robots,” in *IEEE International Conference on Robotics and Automation. Proceedings.*, vol. 5, pp. 4956–4962, IEEE, 2004.
- [22] M. Gouttefarde and C. M. Gosselin, “Analysis of the wrench-closure workspace of planar parallel cable-driven mechanisms,” *IEEE Transactions on Robotics*, vol. 22, no. 3, pp. 434–445, 2006.
- [23] C. B. Pham, S. H. Yeo, G. Yang, M. S. Kurbanhusen, and I.-M. Chen, “Force-closure workspace analysis of cable-driven parallel mechanisms,” *Mechanism and Machine Theory*, vol. 41, no. 1, pp. 53–69, 2006.
- [24] J. Pusey, A. Fattah, S. Agrawal, and E. Messina, “Design and workspace analysis of a 6–6 cable-suspended parallel robot,” *Mechanism and machine theory*, vol. 39, no. 7, pp. 761–778, 2004.
- [25] A. Pott, “Workspace,” in *Cable-Driven Parallel Robots*, pp. 157–227, Springer, 2018.
- [26] G. Barrette and C. M. Gosselin, “Determination of the dynamic workspace of cable-driven planar parallel mechanisms,” *Journal of mechanical design*, vol. 127, no. 2, pp. 242–248, 2005.
- [27] G. Barette and C. Gosselin, “Kinematic analysis and design of planar parallel mechanisms actuated with cables,” in *Proceedings of ASME Design Engineering Technical Conference*, pp. 391–399, 2000.
- [28] A. Pott, “An improved force distribution algorithm for over-constrained cable-driven parallel robots,” in *Computational Kinematics*, pp. 139–146, Springer, 2014.
- [29] S.-R. Oh and S. K. Agrawal, “Cable suspended planar robots with redundant cables: Controllers with positive tensions,” *IEEE Transactions on Robotics*, vol. 21, no. 3, pp. 457–465, 2005.
- [30] A. Trevisani, “Underconstrained planar cable-direct-driven robots: A trajectory planning method ensuring positive and bounded cable tensions,” *Mechatronics*, vol. 20, no. 1, pp. 113–127, 2010.
- [31] C. Gosselin, P. Ren, and S. Foucault, “Dynamic trajectory planning of a two-dof cable-suspended parallel robot,” in *Robotics and Automation (ICRA), IEEE International Conference on*, pp. 1476–1481, IEEE, 2012.
- [32] C. Gosselin and S. Foucault, “Dynamic point-to-point trajectory planning of a two-dof cable-suspended parallel robot,” *IEEE Transactions on Robotics*, vol. 30, no. 3, pp. 728–736, 2014.
- [33] S. Fang, *Design, modeling and motion control of tendon based parallel manipulators*. VDI-Verlag, 2005.
- [34] G. El-Ghazaly, M. Gouttefarde, and V. Creuze, “Adaptive terminal sliding mode control of a redundantly-actuated cable-driven parallel manipulator: cogiro,” in *Cable-Driven Parallel Robots*, pp. 179–200, Springer, 2015.

- [35] M. I. Hosseini, M. J. Harandi, S. A. K. Seyedi, *et al.*, “Adaptive fast terminal sliding mode control of a suspended cable-driven robot,” in *2019 27th Iranian Conference on Electrical Engineering (ICEE)*, pp. 985–990, IEEE, 2019.
- [36] M. I. Hosseini, M. Jafari Harandi, S. Khalilpour Seyedi, and H. Taghirad, “Experimental performance of adaptive fast terminal sliding mode control on a suspended cable robot,” *Journal of Electrical and Computer Engineering Innovations (JECEI)*, vol. 7, no. 1, pp. 59–67, 2018.
- [37] M. A. Khosravi and H. D. Taghirad, “Robust pid control of fully-constrained cable driven parallel robots,” *Mechatronics*, vol. 24, no. 2, pp. 87–97, 2014.
- [38] R. Babaghasabha, M. A. Khosravi, and H. D. Taghirad, “Adaptive robust control of fully constrained cable robots: singular perturbation approach,” *Nonlinear Dynamics*, vol. 85, no. 1, pp. 607–620, 2016.
- [39] M. R. J. Harandi, S. Khalilpour, H. D. Taghirad, and J. G. Romero, “Adaptive control of parallel robots with uncertain kinematics and dynamics,” *Mechanical Systems and Signal Processing*, vol. 157, p. 107693, 2021.
- [40] J. Begey, L. Cuvillon, M. Lesellier, M. Gouttefarde, and J. Gangloff, “Dynamic control of parallel robots driven by flexible cables and actuated by position-controlled winches,” *IEEE Transactions on Robotics*, 2018.
- [41] M. Guerrero, D. Mercado, R. Lozano, and C. García, “Ida-pbc methodology for a quadrotor uav transporting a cable-suspended payload,” in *Unmanned Aircraft Systems (ICUAS), 2015 International Conference on*, pp. 470–476, IEEE, 2015.
- [42] C. Meissen, K. Klausen, M. Arcak, T. I. Fossen, and A. Packard, “Passivity-based formation control for uavs with a suspended load,” *IFAC-PapersOnLine*, vol. 50, no. 1, pp. 13150–13155, 2017.
- [43] R. J. Caverly and J. R. Forbes, “Dynamic modeling and noncollocated control of a flexible planar cable-driven manipulator,” *IEEE Trans. Robotics*, vol. 30, no. 6, pp. 1386–1397, 2014.
- [44] R. J. Caverly, J. R. Forbes, and D. Mohammadshahi, “Dynamic modeling and passivity-based control of a single degree of freedom cable-actuated system,” *IEEE Transactions on Control Systems Technology*, vol. 23, no. 3, pp. 898–909, 2015.
- [45] R. J. Caverly and J. R. Forbes, “Flexible cable-driven parallel manipulator control: Maintaining positive cable tensions,” *IEEE Transactions on Control Systems Technology*, vol. 26, no. 5, pp. 1874–1883, 2018.
- [46] H. Choi, J. Piao, E.-S. Kim, J. Jung, E. Choi, J.-O. Park, and C.-S. Kim, “Intuitive bilateral teleoperation of a cable-driven parallel robot controlled by a cable-driven parallel robot,” *International Journal of Control, Automation and Systems*, pp. 1–14, 2020.
- [47] Y. Wang, K. Wang, Z. Zhang, and Z. Mo, “Control strategy and experimental research of a cable-driven lower limb rehabilitation robot,” *Proceedings of the Institution of Mechanical Engineers, Part C: Journal of Mechanical Engineering Science*, p. 0954406220952510, 2020.
- [48] J. Li, J. Lam, M. Liu, and Z. Wang, “Compliant control and compensation for a compact cable-driven robotic manipulator,” *IEEE Robotics and Automation Letters*, vol. 5, no. 4, pp. 5417–5424, 2020.
- [49] S. Khalilpour, R. Khorrambakht, H. Damirchi, H. Taghirad, and P. Cardou, “Tip-trajectory tracking control of a deployable cable-driven robot via output redefinition,” *Multibody System Dynamics*, vol. 52, no. 1, pp. 31–58, 2021.
- [50] I. Fantoni, R. Lozano, and M. W. Spong, “Energy based control of the pendubot,” *IEEE Transactions on Automatic Control*, vol. 45, no. 4, pp. 725–729, 2000.
- [51] Y. Liu and X. Xin, “Global motion analysis of energy-based control for 3-link planar robot with a single actuator at the first joint,” *Nonlinear Dynamics*, vol. 88, no. 3, pp. 1749–1768, 2017.

- [52] J. M. Avis, S. G. Nersesov, and R. Nathan, "Energy-based hybrid control for the rtac system: Experimental results," in *American Control Conference, 2008*, pp. 3331–3336, IEEE, 2008.
- [53] H.-h. Yuan, Y.-m. Ge, and C.-b. Gan, "A novel hybrid control strategy for an underactuated 3-d biped with asymmetric structure," *Journal of Electrical Engineering & Technology*, vol. 14, no. 3, pp. 1375–1384, 2019.
- [54] L. Chen and M. Van, "Sliding mode control of a class of underactuated system with non-integrable momentum," *Journal of the Franklin Institute*, vol. 357, no. 14, pp. 9484–9504, 2020.
- [55] W. Liu, S.-y. Chen, and H.-x. Huang, "Double closed-loop integral terminal sliding mode for a class of underactuated systems based on sliding mode observer," *International Journal of Control, Automation and Systems*, vol. 18, no. 2, pp. 339–350, 2020.
- [56] S. Mobayen, "Design of lmi-based sliding mode controller with an exponential policy for a class of underactuated systems," *Complexity*, vol. 21, no. 5, pp. 117–124, 2016.
- [57] J. Wang, J. Wang, and Q.-L. Han, "Neurodynamics-based model predictive control of continuous-time under-actuated mechatronic systems," *IEEE/ASME Transactions on Mechatronics*, 2020.
- [58] R. Ortega and E. Garcia-Canseco, "Interconnection and damping assignment passivity-based control: A survey," *European Journal of control*, vol. 10, no. 5, pp. 432–450, 2004.
- [59] R. Ortega and M. W. Spong, "Adaptive motion control of rigid robots: A tutorial," *Automatica*, vol. 25, no. 6, pp. 877–888, 1989.
- [60] R. Ortega, A. J. Van Der Schaft, I. Mareels, and B. Maschke, "Putting energy back in control," *IEEE Control Systems*, vol. 21, no. 2, pp. 18–33, 2001.
- [61] R. Ortega, J. A. L. Perez, P. J. Nicklasson, and H. J. Sira-Ramirez, *Passivity-based control of Euler-Lagrange systems: mechanical, electrical and electromechanical applications*. Springer Science & Business Media, 2013.
- [62] A. M. Bloch, N. E. Leonard, and J. E. Marsden, "Controlled lagrangians and the stabilization of mechanical systems. i. the first matching theorem," *IEEE Transactions on automatic control*, vol. 45, no. 12, pp. 2253–2270, 2000.
- [63] A. M. Bloch, D. E. Chang, N. E. Leonard, and J. E. Marsden, "Controlled lagrangians and the stabilization of mechanical systems. ii. potential shaping," *IEEE Transactions on Automatic Control*, vol. 46, no. 10, pp. 1556–1571, 2001.
- [64] R. Ortega, A. Van der Schaft, B. Maschke, and G. Escobar, "Energy-shaping of port-controlled hamiltonian systems by interconnection," in *Decision and Control. Proceedings of the 38th IEEE Conference on*, vol. 2, pp. 1646–1651, IEEE, 1999.
- [65] G. Blankenstein, R. Ortega, and A. J. Van Der Schaft, "The matching conditions of controlled lagrangians and ida-passivity based control," *International Journal of Control*, vol. 75, no. 9, pp. 645–665, 2002.
- [66] F. M. Serra and C. H. De Angelo, "Ida-pbc controller design for grid connected front end converters under non-ideal grid conditions," *Electric Power Systems Research*, vol. 142, pp. 12–19, 2017.
- [67] D. Garcia, J. Sandoval, J. Gutiérrez-Jagüey, and E. Bugarin, "Ida-pbc control of an underactuated underwater vehicle," *Revista Iberoamericana de Automática e Informática Industrial RIAI*, vol. 15, no. 1, pp. 36–45, 2017.
- [68] H. Hichem, M. Abdellah, T. A. Abderrazak, B. Abdelkader, and S. Ramzi, "A wind turbine sensorless automatic control systems, analysis, modelling and development of ida-pbc method," *International Journal of Power Electronics and Drive Systems*, vol. 11, no. 1, p. 45, 2020.

- [69] E. J. Vidal, O. B. Cieza, and J. Reger, “Explicit and implicit ida-pbc design and implementation for a portal crane,” *IFAC-PapersOnLine*, vol. 53, no. 2, pp. 5592–5597, 2020.
- [70] K. Fujimoto and T. Sugie, “Canonical transformation and stabilization of generalized hamiltonian systems,” *Systems & Control Letters*, vol. 42, no. 3, pp. 217–227, 2001.
- [71] A. D. Lewis, “Notes on energy shaping,” in *Decision and Control, 2004. CDC. 43rd IEEE Conference on*, vol. 5, pp. 4818–4823, IEEE, 2004.
- [72] A. J. van der Schaft and A. Van Der Schaft, *L2-gain and passivity techniques in nonlinear control*, vol. 2. Springer, 2000.
- [73] F. Gómez-Estern and A. J. Van der Schaft, “Physical damping in ida-pbc controlled underactuated mechanical systems,” *European Journal of Control*, vol. 10, no. 5, pp. 451–468, 2004.
- [74] J. A. Acosta, R. Ortega, A. Astolfi, and A. D. Mahindrakar, “Interconnection and damping assignment passivity-based control of mechanical systems with underactuation degree one,” *IEEE Transactions on Automatic Control*, vol. 50, no. 12, pp. 1936–1955, 2005.
- [75] J. Á. Acosta and A. Astolfi, “On the pdes arising in ida-pbc,” in *Proceedings of the 48th IEEE Conference on Decision and Control (CDC) held jointly with 28th Chinese Control Conference*, pp. 2132–2137, IEEE, 2009.
- [76] K. Nunna, M. Sassano, and A. Astolfi, “Constructive interconnection and damping assignment for port-controlled hamiltonian systems,” *IEEE Transactions on Automatic Control*, vol. 60, no. 9, pp. 2350–2361, 2015.
- [77] G. Viola, R. Ortega, R. Banavar, J. Á. Acosta, and A. Astolfi, “Total energy shaping control of mechanical systems: simplifying the matching equations via coordinate changes,” *IEEE Transactions on Automatic Control*, vol. 52, no. 6, pp. 1093–1099, 2007.
- [78] M. Ryalat and D. S. Laila, “A simplified ida-pbc design for underactuated mechanical systems with applications,” *European Journal of Control*, vol. 27, pp. 1–16, 2016.
- [79] A. Donaire, R. Mehra, R. Ortega, S. Satpute, J. G. Romero, F. Kazi, and N. M. Singh, “Shaping the energy of mechanical systems without solving partial differential equations,” in *American Control Conference (ACC)*, pp. 1351–1356, IEEE, 2015.
- [80] P. Borja, R. Cisneros, and R. Ortega, “Shaping the energy of port-hamiltonian systems without solving pde’s,” in *Decision and Control (CDC), IEEE 54th Annual Conference on*, pp. 5713–5718, IEEE, 2015.
- [81] J. G. Romero, R. Ortega, and A. Donaire, “Energy shaping of mechanical systems via pid control and extension to constant speed tracking,” *IEEE Transactions on Automatic Control*, vol. 61, no. 11, pp. 3551–3556, 2016.
- [82] J. G. Romero, A. Donaire, R. Ortega, and P. Borja, “Global stabilisation of underactuated mechanical systems via pid passivity-based control,” *Automatica*, vol. 96, pp. 178–185, 2018.
- [83] A. D. Mahindrakar, A. Astolfi, R. Ortega, and G. Viola, “Further constructive results on interconnection and damping assignment control of mechanical systems: The acrobot example,” *International Journal of Robust and Nonlinear Control: IFAC-Affiliated Journal*, vol. 16, no. 14, pp. 671–685, 2006.
- [84] J. Sandoval, R. Ortega, and R. Kelly, “Interconnection and damping assignment passivity—based control of the pendubot,” *IFAC Proceedings Volumes*, vol. 41, no. 2, pp. 7700–7704, 2008.
- [85] V. de León-Gómez, V. Santibañez, and J. Sandoval, “Interconnection and damping assignment passivity-based control for a compass-like biped robot,” *International Journal of Advanced Robotic Systems*, vol. 14, no. 4, p. 1729881417716593, 2017.
- [86] C. Batlle, A. Dòria-Cerezo, G. Espinosa-Pérez, and R. Ortega, “Simultaneous interconnection and damping assignment passivity-based control: the induction machine case study,” *International Journal of control*, vol. 82, no. 2, pp. 241–255, 2009.

- [87] D. E. Chang, “On the method of interconnection and damping assignment passivity-based control for the stabilization of mechanical systems,” *Regular and Chaotic Dynamics*, vol. 19, no. 5, pp. 556–575, 2014.
- [88] N. Crasta, R. Ortega, and H. K. Pillai, “On the matching equations of energy shaping controllers for mechanical systems,” *International Journal of Control*, vol. 88, no. 9, pp. 1757–1765, 2015.
- [89] A. Donaire, R. Ortega, and J. G. Romero, “Simultaneous interconnection and damping assignment passivity-based control of mechanical systems using dissipative forces,” *Systems & Control Letters*, vol. 94, pp. 118–126, 2016.
- [90] E. Zergeroglu, W. Dixon, A. Behal, and D. Dawson, “Adaptive set-point control of robotic manipulators with amplitude-limited control inputs,” *Robotica*, vol. 18, no. 2, pp. 171–181, 2000.
- [91] A. Loria, R. Kelly, R. Ortega, and V. Santibanez, “On global output feedback regulation of euler-lagrange systems with bounded inputs,” *IEEE Transactions on Automatic Control*, vol. 42, no. 8, pp. 1138–1143, 1997.
- [92] W. E. Dixon, “Adaptive regulation of amplitude limited robot manipulators with uncertain kinematics and dynamics,” *IEEE Transactions on Automatic Control*, vol. 52, no. 3, pp. 488–493, 2007.
- [93] A. Zavala-Rio and V. Santibanez, “A natural saturating extension of the pd-with-desired-gravity-compensation control law for robot manipulators with bounded inputs,” *IEEE Transactions on Robotics*, vol. 23, no. 2, pp. 386–391, 2007.
- [94] V. Santibanez, R. Kelly, and J. Sandoval, “Control of the inertia wheel pendulum by bounded torques,” in *Proceedings of the 44th IEEE Conference on Decision and Control*, pp. 8266–8270, IEEE, 2005.
- [95] J. G. Romero, A. Donaire, and R. Ortega, “Robust energy shaping control of mechanical systems,” *Systems & Control Letters*, vol. 62, no. 9, pp. 770–780, 2013.
- [96] A. Donaire, J. G. Romero, R. Ortega, B. Siciliano, and M. Crespo, “Robust ida-pbc for underactuated mechanical systems subject to matched disturbances,” *International Journal of Robust and Nonlinear Control*, vol. 27, no. 6, pp. 1000–1016, 2017.
- [97] J. Ferguson, A. Donaire, R. Ortega, and R. H. Middleton, “Matched disturbance rejection for a class of nonlinear systems,” *IEEE Transactions on Automatic Control*, vol. 65, no. 4, pp. 1710–1715, 2019.
- [98] J. Ferguson, D. Wu, and R. Ortega, “On matched disturbance suppression for port-hamiltonian systems,” *IEEE Control Systems Letters*, vol. 4, no. 4, pp. 892–897, 2020.
- [99] M. Ryalat and D. S. Laila, “A robust ida-pbc approach for handling uncertainties in underactuated mechanical systems,” *IEEE Transactions on Automatic Control*, vol. 63, no. 10, pp. 3495–3502, 2018.
- [100] A. Donaire, J. G. Romero, and R. Ortega, “Correction to the paper “a robust ida-pbc approach for handling uncertainties in underactuated mechanical systems” [oct 18 3495–3502],” *IEEE Transactions on Automatic Control*, vol. 65, no. 7, pp. 3223–3226, 2020.
- [101] E. Franco, “Adaptive ida-pbc for underactuated mechanical systems with constant disturbances,” *International Journal of Adaptive Control and Signal Processing*, vol. 33, no. 1, pp. 1–15, 2019.
- [102] E. Franco, F. Rodriguez y Baena, and A. Astolfi, “Robust dynamic state feedback for underactuated systems with linearly parameterized disturbances,” *International Journal of Robust and Nonlinear Control*, vol. 30, no. 10, pp. 4112–4128, 2020.
- [103] E. Franco, “Ida-pbc with adaptive friction compensation for underactuated mechanical systems,” *International Journal of Control*, pp. 1–11, 2019.

- [104] M. Ryalat, D. S. Laila, and H. ElMoaqet, “Adaptive interconnection and damping assignment passivity based control for underactuated mechanical systems,” *International Journal of Control, Automation and Systems*, pp. 1–14, 2020.
- [105] R. Colbaugh, E. Barany, and K. Glass, “Global regulation of uncertain manipulators using bounded controls,” in *Proceedings of International Conference on Robotics and Automation*, vol. 2, pp. 1148–1155, IEEE, 1997.
- [106] D. Karagiannis, A. Astolfi, and R. Ortega, “Nonlinear stabilization via system immersion and manifold invariance: Survey and new results,” *Multiscale Modeling & Simulation*, vol. 3, no. 4, pp. 801–817, 2005.
- [107] A. Venkatraman, R. Ortega, I. Sarras, and A. van der Schaft, “Speed observation and position feedback stabilization of partially linearizable mechanical systems,” *IEEE Transactions on Automatic Control*, vol. 55, no. 5, pp. 1059–1074, 2010.
- [108] S. Lefrançois and C. Gosselin, “Point-to-point motion control of a pendulum-like 3-dof underactuated cable-driven robot,” in *Robotics and Automation (ICRA), IEEE International Conference on*, pp. 5187–5193, IEEE, 2010.
- [109] L. Scalera, A. Gasparetto, and D. Zanotto, “Design and experimental validation of a 3-dof underactuated pendulum-like robot,” *IEEE/ASME Transactions on Mechatronics*, vol. 25, no. 1, pp. 217–228, 2019.
- [110] D. Cunningham and H. H. Asada, “The winch-bot: A cable-suspended, under-actuated robot utilizing parametric self-excitation,” in *2009 IEEE International Conference on Robotics and Automation*, pp. 1844–1850, IEEE, 2009.
- [111] J. Park, O. Kwon, and J. H. Park, “Anti-sway trajectory generation of incompletely restrained wire-suspended system,” *Journal of Mechanical Science and Technology*, vol. 27, no. 10, pp. 3171–3176, 2013.
- [112] S. W. Hwang, J.-H. Bak, J. Yoon, J. H. Park, and J.-O. Park, “Trajectory generation to suppress oscillations in under-constrained cable-driven parallel robots,” *Journal of Mechanical Science and Technology*, vol. 30, no. 12, pp. 5689–5697, 2016.
- [113] S. W. Hwang, J.-H. Bak, J. Yoon, and J. H. Park, “Oscillation reduction and frequency analysis of under-constrained cable-driven parallel robot with three cables,” *Robotica*, vol. 38, no. 3, pp. 375–395, 2020.
- [114] E. Idá, S. Briot, and M. Carricato, “Robust trajectory planning of under-actuated cable-driven parallel robot with 3 cables,” in *International Symposium on Advances in Robot Kinematics*, pp. 65–72, Springer, 2020.
- [115] R. Ozawa, H. Kobayashi, and K. Hashirii, “Analysis, classification, and design of tendon-driven mechanisms,” *IEEE transactions on robotics*, vol. 30, no. 2, pp. 396–410, 2014.
- [116] X. Lv, S. Qiao, Y. Shi, and R. Liu, “Characteristics research of an underactuated manipulator basing on the statics and dynamics analysis,” in *Mechatronics and Automation (ICMA), IEEE International Conference on*, pp. 772–776, IEEE, 2016.
- [117] Y. Liu, Y. Gao, F. Xiao, and J. Zhao, “Research on the cable-pulley underactuated lower limb exoskeleton,” in *Mechatronics and Automation (ICMA), IEEE International Conference on*, pp. 577–583, IEEE, 2017.
- [118] R. de Rijk, M. Rushton, and A. Khajepour, “Out-of-plane vibration control of a planar cable-driven parallel robot,” *IEEE/ASME Transactions on Mechatronics*, vol. 23, no. 4, pp. 1684–1692, 2018.
- [119] G. Abbasnejad and M. Carricato, “Direct geometrico-static problem of underconstrained cable-driven parallel robots with n cables,” *IEEE Transactions on Robotics*, vol. 31, no. 2, pp. 468–478, 2015.

- [120] A. Berti, J.-P. Merlet, and M. Carricato, "Solving the direct geometrico-static problem of underconstrained cable-driven parallel robots by interval analysis," *The International Journal of Robotics Research*, vol. 35, no. 6, pp. 723–739, 2016.
- [121] M. Carricato and J.-P. Merlet, "Stability analysis of underconstrained cable-driven parallel robots," *IEEE Transactions on Robotics*, vol. 29, no. 1, pp. 288–296, 2012.
- [122] E. Idá, J.-P. Merlet, and M. Carricato, "Automatic self-calibration of suspended under-actuated cable-driven parallel robot using incremental measurements," in *International Conference on Cable-Driven Parallel Robots*, pp. 333–344, Springer, 2019.
- [123] M. R. J. Harandi, H. Damirchi, H. D. Taghirad, *et al.*, "Point-to-point motion control of an underactuated planar cable driven robot," in *2019 27th Iranian Conference on Electrical Engineering (ICEE)*, pp. 979–984, IEEE, 2019.
- [124] X. Diao and O. Ma, "Workspace analysis of a 6-dof cable robot for hardware-in-the-loop dynamic simulation," in *2006 IEEE/RSJ International Conference on Intelligent Robots and Systems*, pp. 4103–4108, IEEE, 2006.
- [125] M. Harandi, S. Khalilpour, H. Damirchi, and H. D. Taghirad, "Stabilization of cable driven robots using interconnection matrix: Ensuring positive tension," in *2019 7th International Conference on Robotics and Mechatronics (ICRoM)*, pp. 235–240, IEEE, 2019.
- [126] M. R. Harandi and H. Taghirad, "Solution of matching equations of ida-pbc by pfaffian differential equations," *International Journal of Control*, no. just-accepted, pp. 1–21, 2021.
- [127] F. Kazi, R. N. Banavar, P. Mullhaupt, and D. Bonvin, "Stabilization of a 2d-spidercrane mechanism using damping assignment passivity-based control," *IFAC Proceedings Volumes*, vol. 41, no. 2, pp. 3155–3160, 2008.
- [128] M. R. J. Harandi and H. D. Taghirad, "On the matching equations of kinetic energy shaping in ida-pbc," *Journal of the Franklin Institute*, 2021.
- [129] F. Gomez-Estern, R. Ortega, F. R. Rubio, and J. Aracil, "Stabilization of a class of underactuated mechanical systems via total energy shaping," in *Proceedings of the 40th IEEE Conference on Decision and Control (Cat. No. 01CH37228)*, vol. 2, pp. 1137–1143, IEEE, 2001.
- [130] C. Aguiar, D. Leite, D. Pereira, G. Andonovski, and I. Škrjanc, "Nonlinear modeling and robust lmi fuzzy control of overhead crane systems," *Journal of the Franklin Institute*, 2020.
- [131] I. Sarras, F. Kazi, R. Ortega, and R. Banavar, "Total energy-shaping ida-pbc control of the 2d-spidercrane," in *49th IEEE Conference on Decision and Control (CDC)*, pp. 1122–1127, IEEE, 2010.
- [132] D. E. Chang, A. M. Bloch, N. E. Leonard, J. E. Marsden, and C. A. Woolsey, "The equivalence of controlled lagrangian and controlled hamiltonian systems," *ESAIM: Control, Optimisation and Calculus of Variations*, vol. 8, pp. 393–422, 2002.
- [133] C. Aguilar-Ibanez, "The lyapunov direct method for the stabilisation of the ball on the actuated beam," *International Journal of Control*, vol. 82, no. 12, pp. 2169–2178, 2009.
- [134] M. R. J. Harandi, H. D. Taghirad, A. Molaei, and J. Guadalupe Romero, "Bounded inputs total energy shaping for a class of underactuated mechanical systems," *International Journal of Robust and Nonlinear Control*, 2021.
- [135] R. W. Brockett *et al.*, "Asymptotic stability and feedback stabilization," *Differential geometric control theory*, vol. 27, no. 1, pp. 181–191, 1983.
- [136] H. K. Khalil and J. Grizzle, *Nonlinear systems*, vol. 3. Prentice hall Upper Saddle River, NJ, 2002.
- [137] M. R. J. Harandi and H. D. Taghirad, "Motion control of an underactuated parallel robot with first order nonholonomic constraint," in *2017 5th RSI International Conference on Robotics and Mechatronics (ICRoM)*, pp. 582–587, IEEE, 2017.

- [138] S. Khalilpour, R. Khorrambakht, M. Harandi, H. Taghirad, and P. Cardou, "Robust dynamic sliding mode control of a deployable cable driven robot," in *Electrical Engineering (ICEE), Iranian Conference on*, pp. 863–868, IEEE, 2018.
- [139] M. W. Spong, "Energy based control of a class of underactuated mechanical systems," *IFAC Proceedings Volumes*, vol. 29, no. 1, pp. 2828–2832, 1996.
- [140] H. Li, W. Yan, and Y. Shi, "Continuous-time model predictive control of under-actuated spacecraft with bounded control torques," *Automatica*, vol. 75, pp. 144–153, 2017.
- [141] D. Qian and J. Yi, "Hierarchical sliding mode control for under-actuated cranes," *Heidelberg, Ber: Springer*, 2016.
- [142] Z. Qu, "Global stability of trajectory tracking of robot underpd control," *Dynamics and Control*, vol. 4, no. 1, pp. 59–71, 1994.
- [143] D. J. López-Araujo, A. Zavala-Río, V. Santibáñez, and F. Reyes, "Output-feedback adaptive control for the global regulation of robot manipulators with bounded inputs," *International Journal of Control, Automation and Systems*, vol. 11, no. 1, pp. 105–115, 2013.
- [144] M. R. J. Harandi and H. D. Taghirad, "Adaptive interconnection and damping assignment passivity-based control for an underactuated cable-driven robot," *International Journal of Adaptive Control and Signal Processing*, 2021.
- [145] G. H. Golub and C. F. Van Loan, *Matrix computations*, vol. 3. JHU press, 2013.
- [146] M. R. J. Harandi, S. A. Khalilpour, and H. D. Taghirad, "Adaptive dynamic feedback control of parallel robots with unknown kinematic and dynamic properties," *ISA transactions*, 2021.
- [147] M. R. J. Harandi, S. A. Khalilpour, and H. Taghirad, "Robust ida-pbc for a spatial underactuated cable driven robot with bounded inputs," in *2021 29th Iranian Conference on Electrical Engineering (ICEE)*, pp. 689–694, IEEE, 2021.
- [148] R. Kelly, "Pd control with desired gravity compensation of robotic manipulators: a review," *The International Journal of Robotics Research*, vol. 16, no. 5, pp. 660–672, 1997.
- [149] F. Paccot, N. Andreff, and P. Martinet, "A review on the dynamic control of parallel kinematic machines: Theory and experiments," *The International Journal of Robotics Research*, vol. 28, no. 3, pp. 395–416, 2009.
- [150] K. P. Tee, S. S. Ge, and E. H. Tay, "Barrier lyapunov functions for the control of output-constrained nonlinear systems," *Automatica*, vol. 45, no. 4, pp. 918–927, 2009.
- [151] B. Borovic, C. Hong, A. Liu, L. Xie, and F. Lewis, "Control of a mems optical switch," in *2004 43rd IEEE Conference on Decision and Control (CDC)(IEEE Cat. No. 04CH37601)*, vol. 3, pp. 3039–3044, IEEE, 2004.
- [152] R. Ortega, M. W. Spong, F. Gomez-Estern, and G. Blankenstein, "Stabilization of underactuated mechanical systems via interconnection and damping assignment," *IEEE Trans. Aut. Control*, 2000.
- [153] R. Mehra, S. G. Satpute, F. Kazi, and N. M. Singh, "Control of a class of underactuated mechanical systems obviating matching conditions," *Automatica*, vol. 86, pp. 98–103, 2017.